Early Mesozoic extensional tectonics in the northern North China Craton and its geodynamic implications

Huabiao Qiu

ÉCOLE DOCTORALE
ENERGIE, MATERIAUX, SCIENCES DE LA TERRE ET DE L'UNIVERS

Institut des Sciences de la Terre d'Orléans

Institut de Géologie et de Géophysique de l 'Académie des Sciences de Chine

THÈSE EN COTUTELLE INTERNATIONALE présentée par :

Huabiao QIU

soutenue le : 21 Décembre 2020

pour obtenir le grade de :
Docteur de Université d'Orléans et de l'Institut de Géologie et de Géophysique de l 'Académie des Sciences de Chine

Discipline/ Spécialité : Sciences de la Terre / Géodynamique

Early Mesozoic extensional tectonics in the northern North China Craton and its geodynamic implications

THÈSE dirigée par :

Yan CHEN	Professeur, Université d'Orléans
Michel FAURE	Professeur, Université d'Orléans
Wei LIN	Professeur, Institute of Geology and Geophysics, CAS

RAPPORTEURS :

Guang ZHU	Professeur, Hefei University of Technology
Yueqiao ZHANG	Professeur, Nanjing University

JURY :

Jinhui YANG	Professeur, Institute of Geology and Geophysics, CAS
Guang ZHU	Professeur, Hefei University of Technology
Yueqiao ZHANG	Professeur, Nanjing University
Sanzhong LI	Professeur, Ocean University of China
Junlai LIU	Professeur, China University of Geosciences (Beijing)
Michel FAURE	Professeur, Université d'Orléans
Wei LIN	Professeur, Institute of Geology and Geophysics, CAS
Yan CHEN	Professeur, Université d'Orléans

Résumé étendu

Le bloc de Chine du Nord (North China Block ou NCB) est une des grandes masses continentales qui composent l'est du continent asiatique. Il est séparé du craton sibérien au nord par l'orogène d'Asie Centrale (Central Asian Orogenic Belt ou CAOB) au nord, et par la chaîne Qinling-Dabie-Sulu au sud (Figure Ib). Depuis sa formation au Paléoprotérozoïque par le rassemblement des blocs « orientaux », « intermédiaires » et « occidentaux » vers ~1.8-1.9 Ga (Zhao et al., 1998, 2001; Faure et al., 2007; Li & Zhao et al., 2007; Li et al., 2012; Trap et al., 2012), le craton de Chine du Nord est resté stable du Mesoprotérozoïque au Paléozoïque. Le substratum gneissique et migmatitique a été ensuite recouvert par une couverture sédimentaire du Mesoproterozoïque au Permien, avec toutesfois une discordance régionale entre l'Ordovicien moyen et le Carbonifère supérieur-Permien (Li et al. 2016). Le craton stable de Chine du nord a commencé sa transformation au Mésozoïque. Une décratonisation, une destruction cratonique et un amincissement lithosphérique se sont produits au Crétacé inférieur. L'épais (~200 km) manteau lithosphérique situé sous la partie orientale du NCB a été remplacée par un manteau mince (<80 km) et juvénile (Fan and Menzies, 1992; Griffin et al., 1992, 1998; Menzies et al., 1993; Zhu et al., 2012; Wu et al., 2019). Bien que la destruction se soit produite au Crétacé, son commencement, c'est à dire au Trias supérieur (Han et al., 2004; Yang et al., 2007, 2010b, 2012), ou au Jurassique supérieur (Gao et al., 2004), est controversé selon le contexte temporel et spatial et les caractéristiques géochimiques acceptées pour les roches ignées du Mésozoïque inférieur.

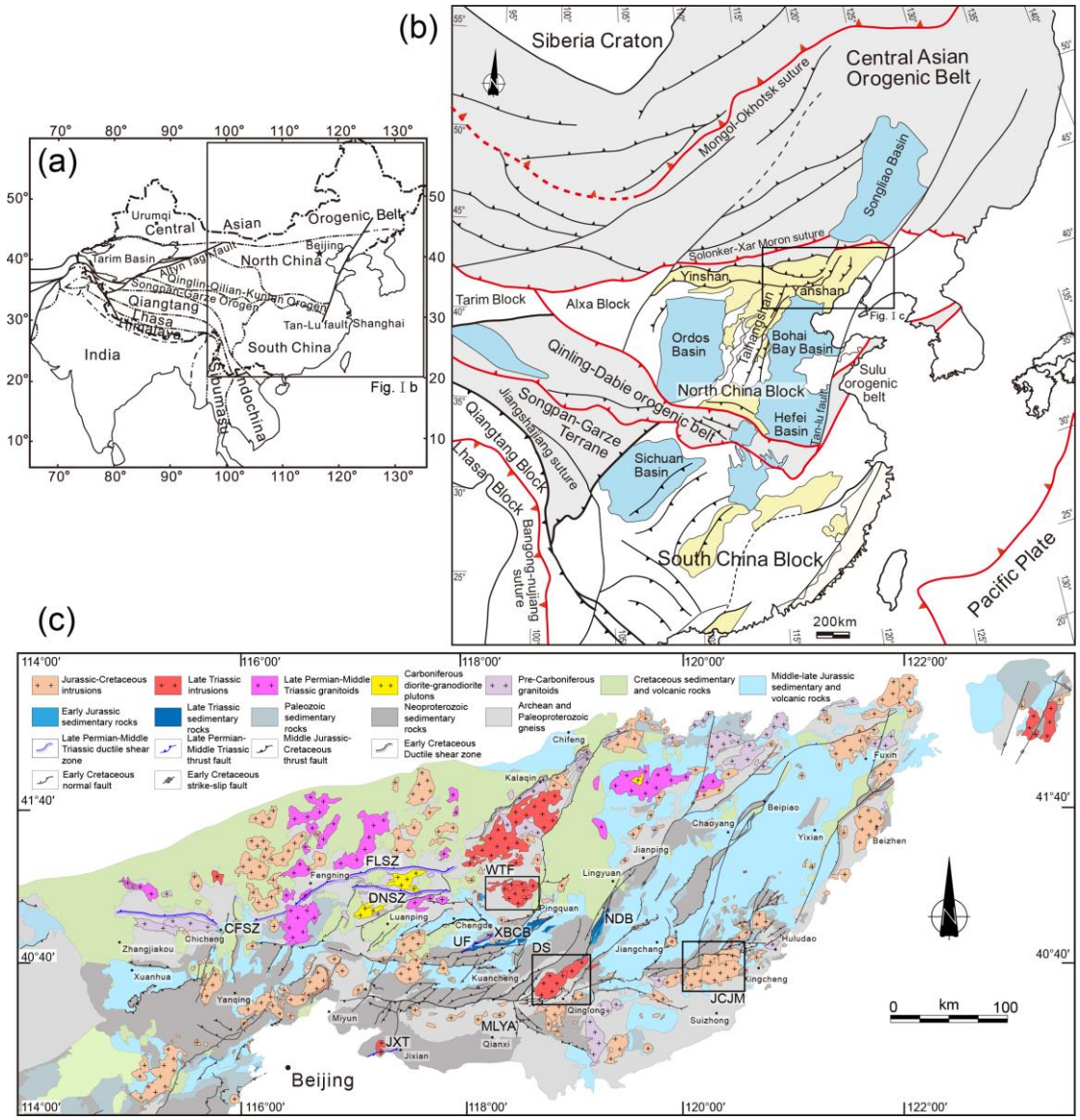

Figure I. Cartes générales de la zone de plis et chevauchements yanshanienne et de ses environs. (a) Carte tectonique simplifiée de l'Asie de l'Est. (b) Cadre tectonique de la Chine orientale. (c) Carte géologique simplifiée de la zone de plis et chevauchements yanshanienne. CFSZ: zone de cisaillement ductile Chicheng-Fengning, FLSZ: zone de cisaillement ductile Fengning-Longhua, DNSZ: zone de cisaillement ductile Damiao-Niangniangmiao, UF: faille sans nom, JXT: chevauchement Jixian, MLYA: anticlinal Malanyu, XBCB: bassin de Xiabancheng, YZB: bassin de Yingzi, NDB: bassin de Niuying-Dengzhangzi, DS: pluton de Dushan; WTF: pluton de Wangtufang; JCJM: pluton de Jianchang-Jiumen.

Avant sa destruction au Crétacé, le craton de Chine du Nord a connu deux cycles orogéniques, notamment des collisions paléozoïques avec les arcs mongols et le bloc de Chine du Sud sur ses marges et au Jurassique-Crétacé inférieur, une orogenèse intracontinentale, aussi appelée orogenèse Yanshanienne. Ceci a donné lieu à un ensemble compliqué de plis, chevauchements, failles inverses et d'intrusions produits par des déformations polyphasées (Figure Ib). Le raccourcissement polyphasé comprend des événements au Trias inférieur-moyen (~255-241 Ma), Jurassique moyen terminal (~172-164 Ma) et fini Jurassique supérieur-éo Crétacé (~152-135 Ma) qui sont bien reconnus. Cependant, les âges précis et la durée des événements reste débattu (Davis et al., 2001; Faure et al., 2012; Wan et al., 2012; Dong et al., 2015; C. Li et al., 2016). A cause des modifications tectoniques, seuls quelques fragments de ces épisodes se retrouvent dans de petits bassins du Mésozoïque inférieur distribués en Chine du Nord. Cependant, quelques indices d'épisodes extensifs, contemporains de roches ignées, et impliquant le début de la destruction du craton de Chine du Nord, se rencontrent dans quelques petits bassins bordés par des failles normales (Darby et al., 2001; Davis et al., 2001, 2009; Ritts et al., 2001; Zhang et al., 2011; Meng et al., 2014, 2019; Li et al., 2015; Qi et al., 2015). Ainsi, la tectonique extensive et les mecanismes géodynamiques associés restent mal contraints à cause du rare enregistrement géologique.

Les problèmes existants

1. Pendant le Trias supérieur, les complexes intrusifs alcalins orientés E-W (p. ex.

syénite néphélinique, syénite quartzeuse, granite de type A) et les roches basiques associées, très développées en Chine du Nord se sont mises en place en contexte extensif (Yang et al., 2012; Zhang et al., 2012). Pendant les décades précédentes, les travaux géochronologiques et géochimiques ont suggéré que les complexes intrusifs alcalins étaient principalement issus de magmas formés par la fusion de manteau lithosphérique enrichi modifié par la subduction et d'une croûte inférieure ancienne avec quelques composants de manteau asthénosphérique appauvris engendrés pendant une tectonique intracontinentale extensive (Yang et al., 2012; Zhang et al., 2014). Cette observation indique une remontée asthénosphérique pendant l'amincissement et la modification du NCB. Toutefois, les formations du trias ne sont exposées que dans quelques petits bassins relictuels (Xiabancheng and Niuyingzi-Dengzhangzi basins; Figure 3.1). La datation de zircons détritiques et les études sédimentologiques des bassins reliques du Trias supérieur montre une évolution décroissante vers le haut de la taille des grains, un approfondissement du système de dépôt dans le bassin et l'abondance de roches vocani-clastiques entre le Trias supérieur et le Jurassique inférieur suggérant un contexte extensif (Davis et al., 2009; Meng et al., 2014). Un extension NE-SW dans le nord du NCB a été documenté dans le « metamorphic core complex » de Sonid Zuoqi près de la zone de Solonker (Davis et al., 2004). Cependant, une tectonique extensive d'âge Trias supérieur-Jurassique inférieur a été proposée sur la base de la discordance entre le trias et le Jurassique inférieur, et les conglomérats syntectoniques du Jurassique inférieur (Zhao, 1990; Liu et al., 2012). Ainsi, le régime tectonique du trias supérieur reste mal contraint du fait des difficulté des recherches

tectonique dans les petites bassins relictuels.

2. L'orogenèse du Jurassique-Crétacé inférieur (aussi appelée orogenèse Yanshan par Wong, 1929), est très répandue dans le craton de Chine du Nord (Davis et al., 2001). Elle a donné lieu à un ensemble complexe de plis, chevauchements, failles inverses et de plutons en Chine du Nord. L'alternance de déformations compressives et extensives ont été reconnues dans la zone de plis et chevauchements yanshanienne (Davis et al., 2001; Faure et al., 2012). Deux phases de raccourcissement, incluant le Jurassique moyen supérieur (172-164 Ma) etFini Jurassique supérieur-Crétacé inférieur (152-135 Ma) sont évidentes même si leur âge et durée restent discutés (Davis et al., 2001; Dong et al., 2015; Faure et al., 2012; C. Li et al., 2016). Cependant, les déformations extensives du Jurassique ne sont pas bien contraintes, contrairement à celles du Crétacé inférieur (Lin & Wei, 2018; Wang et al., 2011). Seuls quelques grabens ou demi-grabens sporadiques sont documentés pour le jurassique en Chine du Nord (Darby et al., 2001; Li et al., 2015; Qi et al., 2015; Ritts et al., 2001; Zhang et al., 2011; Davis et al., 2001, 2009; Qi et al., 2015). En particulier, les tectoniques compressives du Jurassique inférieur sont proposées sur la base de la discordance entre le Trias-Jurassique inférieur et les conglomérats syn-tectoniques du Jurassique inférieur (Zhao, 1990; Liu et al., 2012). Ainsi, la tectonique extensive du Jurassique en Chine du Nord reste ambigue.

3. les roches ignées du Triass-Jurassique sont très répandues en Chine du Nord. D'après les datations isotopiques, quatre stades sont identifiés : Permien-Trias moyen (262–236 Ma),Trias supérieur (231–199 Ma),Jurassique inférieur moyen (189–176 Ma), Jurassique supérieur (155–145 Ma). Les mécanismes de mise en place des plutons du

Mésozoïque inférieur ne sont pas clairs. Jusqu'à présent aucun travail ne s'est intéressé à cette question qui peut cependant apporter un nouveau regard sur l'évolution du NCB.

4. L'évolution du NCB, est un élément clé dans l'histoire tectonique de l'Asie de l'Est. Après l'amalgamation du NCB avec les autres plaques continentale et microcontinents, le continent est-asiatique était bordé par l'océan Mongol-Okhotsk au nord et Bangong-Nujiang au sud-ouest et le Paléo-Pacifique au SE. Ainsi, toute compréhension de la tectonique mésozoïque de l'Asie de l'Est demande une bonne connaissance de l'évolution du NBC. En particulier, l'orogenèse Jurassique-Crétacé inférieur Yanshanienne, a été diversement interprétée comme due à : i) la fermeture de l'océan Mongol-Okhotsk (Yin and Nie, 1996; Davis et al., 2001), ii) la subduction de la plaque paléo-Pacifique (G. Zhu et al., 2011; R. Zhu et al., 2011; Xu and Wang, 1983), iii) les interactions entre la déformation N-S de l'Eurasie et la subduction vers le NW du Paléo-Pacifique (Davis et al., 2001), ou iv) des convergences de plaques multiples entre les océans Mongol-Okhotsk, Bangong–Nujiang, et Paléo-Pacifique (Dong et al., 2015). A cause de la mauvaise compréhension des déformations polyphasées, et particulièrement de la tectonique extensive, le moteur de la déformation du Mésozoïque inférieur en Chine de l'Est demeure controversée.

Seulement les petit grabens du Mésozoïque inférieur sont connus en Chine du Nord, les structures extensives et les mécanismes géodynamiques du Trias et Jurassique ne sont pas bien connus. Pour mieux comprendre cette évolution, il est crucial de clarifier la tectonique en extension du NCB et ses relations avec la dynamique des plaques (subduction/collision) sur les bordures.

Les processus de mise en place des plutons contient potentiellement des informations significatives à la fois sur la dynamique des plutons et le champ de déformation régional (p. ex., Bouchez, et al., 1997; Paterson et al., 1998). L'étude structurale des plutons est une manière efficace est assez simple pour déchiffrer les processus de mise en place (e.g., Bouchez, et al., 1997; De Saint Blanquat et al., 2011; Lin et al., 2013). Dans cette thèse, pour mieuc comprendre le context tectonique et la géodynamique du Mésozoïque inférieur de Chine du Sud, un étude multidisciplinaire intégrée, incluant la géologie structurale, la géochronologie, la géochimie, l'ASM et la modélisation gravimétrique a été conduite sur le pluton de Dushan d'âge Trias supérieur dans l'est Hebei, le pluton Triassique supérieur de Wangtufang, dans le N Hebei, et le pluton jurassique de Jianchang-Jiumen dans l'ouest Liaoning (Figure Ic). En outre, en prenant en compte les autres éléments structuraux de Chine du Sud, au Mésozoïque inférieur, un cadre tectonique détaillé du bloc de Chine du Nord peut être établi pour mieux comprendre l'évolution géodynamique du NCB.

Mise en place et déformation extensive associée au Trias inférieur : Nouvelles données issues d'une étude pluridiscipinaire des plutons de Dushan et Wangtufang.

1. Etude pluridisciplinaire du pluton de Dushan

Le pluton de Dushan est composé de monzogranite avec une bordure de granite à biotite. Le passage entre les deux faciès est progressif, sans contact précis. Structuralement, le pluton varie depuis un monzogranite isotrope au NE à une roche foliée et localement

mylonitique sur la bordure SW. Les foliations minérales macroscopiques et magnétiques (ASM) définissent une forme en dôme ellpitique avec un grand axe NE-SW, mais les foliations pendent vers l'intérieur sur la bordure SE du pluton. La combinaison avec les données gravimétriques montrent que le pluton présente globalement une forme tabulaire ou en forme de langue avec une racine au NE. Les linéations magnétiques sont dans l'ensemble orientées NE-SW, globalement en accord avec les linéations minérales observées dans les zones mylonitiques. Si on considère l'absence de déformation ductile dans l'encaissant, et les variations continues des fabriques dans le pluton depuis un état magmatique à un état solide, il est probable que celles-ci aient été acquises pendant la mise en place du pluton. Nous proposons que le pluton de dushan s'est mis en place vers le SW à partir d'une zone d'alimentation située au NE, bébutant probablement par un sill puis évoluant par gonflement de bouffées de magma. Les injections successives de magma ont poussé les roches encaissantes vers le haut, vers le bas et aussi latéralement pour produire la forme finale du pluton. Ce gonflement a pu localement déformer les injections antérieures déjà refroidies pour produire la foliation mylonitique qui enveloppe la bordure sud-ouest du pluton. A la fois les fabriques minérales mésoscopiques et magnétiques sont donc liées à la mise en place du pluton plutôt qu'à la déformation régionale. sud-ouest. Pour clarifier la tectonique du Trias supérieur et le contexte géodynamique du NCB, plus d'études structurales sonr nécessaires.

2. Pour mieux connaître le cadre tectonique du nord du NCB, le mécanisme de mise en place du pluton de Wangtufang a été étudié. Les datations U/Pb sur zircon, les

mesures isotopiques Hf et les données géochimiques sur roche totale du pluton de Wangtufang montrent que ce pluton est composé de syénogranite et de diorite dérivés de la fusion partielle de la croûte inférieure avec quelques composants de manteau appauvri. Le syénogranite et la diorite sont isotropes. L'anisotrpie de suceptibilité magnétique et les études gravimétriques ont été entreprises pour caractériser la fabrique interne et la forme du pluton. La diorite forme seulement des reliques au- dessus du syénogranite. Des filons (dykes) de syénogranite recoupent la diorite et sont encaissant. Dans le syénogranite, les foliations magmatiques sont subhorizontales ou à faible pendage, avec une direction proche de la limite du pluton. Les linéations magnétiques sont à faible pendage et orientées NE-SW.

La combinaison de la forme allongée NE-SW avec une racine centrale, un plancher bombé et des bordures pendant vers l'intérieur avec un pendage fort ou modéré, ce pluton de syénogranite peut être considéré comme un lopolithe. Le syénogranite s'est vraisemblablement mis en place par gonflement avec plusieurs pulsations de magma à partir d'un conduit central et une dépression du plancher. Le mise en place est considéré en contexte extensif, si on prend en compte : 1) l'orientation NE-SW de la linéation magnétique, 2) la forme allongée NE-SW du pluton, 3) les filons NW-SE de syénogranite interprétés comme des fentes de tension pendant une extension régionale NE-SW. Les datations des zircons détritiques dans les bassins du Trias supérieur-Jurassique inférieur montrent une granulométrie décroissante vers le haut, ainsi qu'un approfondissement du bassin et l'abondance de formations volcanoclastiques. Ceci s'accorde avec un contexte extensif (Davis et al., 2009; Meng et al., 2014). En outre,

l'extension NE-SW dans le N du NCB a été documentée dans le « metamorphic core complex » de Sonid Zhoqi en Mongolie intérieure (Davis et al., 2004). Le pluton de Wangtufang apporte un argument en faveur d'une extension intracontinentale au Trias supérieur en Chine du Nord.

Les complexes alcalins et les roches basiques associés, allongés E-W, se développent vers 231-215 Ma (Yang, 2012, Zhang et al., 2012, 2014). Ils dérivent de la fusion partielle de croûte inférieure et d'une partie de manteau lithosphérique enrichi, ainsi que de quelques matériels de manteau asthénosphériques enrichis (Yang et al., 2012; Zhang et al., 2012; Zhang et al., 2014; Zhu et al., 2012), indiquant une remontée de manteau asthénosphérique et une interaction de manteau asthénosphérique et lithosphérique lors de l'amincissement de la lithosphère de Chine du Nord et de l'étirement crustal contemporain (e.g., Han et al., 2004).

Ainsi, le Trias supérieur était une période d'extension continentale liée à des processus profonds après la fermeture de l'océan Paléo-asiatique or après la compression intracontinentale, même si les mécanismes déclenchants restent débattus : extension intraplaque (Yang et al., 2012), délamination post-orogénique ou post-collisionnelle (Zhang et al. 2012), remontée du manteau au front du panneau subduit de la plaque Mongol-Okhotsk (Meng et al., 2020).

Mise en place de plutons jurassiques, extensions NE-SW au Jurassique inférieur et et NE-SW au début du Jurassique supérieur : données de l'étude pluridisciplinaire du pluton de Jianchang-Jiumen.

L'orogenèse intracontinentale du Jurassique supérieur-Crétacé inférieur d'Asie orientale se manifeste par des structures complexes dans le NCB. En particulier, la tectonique extensive de Chine du Nord reste ambigüe. Une étude pluridisciplinaire du pluton Jurassique de Jianchang-Jiumen a été entreprise pour apporter des éléments de réponse sur la tectonique extensive.

Dans le NCB, les bassins sédimentaires du Jurassique inférieur-début du Jurassique moyen contenant des roches volcaniques basiques et des dépôts charbonneux (Figure 6.1) sont interprétés comme des bassins extensifs (Zhang et al., 2014; Meng et al., 2019; Hao et al., 2020). Dans le bassin de l'Ordos et sa périphérie, à l'ouest du NCB, l'extension est marquée par des failles normales Est-Ouest (Darby et al., 2001; Ritts et al., 2001; Zhang et al., 2011) ? Ceci est également observé dans le Taihangshan (Li et al., 2015) et le Daqingshan (Darby et al., 2001; Ritts et al., 2001). Cependant, dans l'Est du NCB, seulement un rift NE-SW est documenté dans les collines de l'ouest de Beijing. Dans cette étude, le pluton phacolithique de Jiumen (190 Ma) montre des foliations parallèles à ses bordures formées par le gonflement du magma dans le cœur d'un anticlinal. Les linéations magnétiques ont enregistrées l'extension Jujrassique NW-SE.

Dand le NCB, les volcanites et pyroclastites de la formation Tiaojishan/Lanqi et les plutons granitiques contemporains (164-155 Ma) sont uniquement distribués dans la partie est du NCB, dans les péninsules de Liaodong et Jiaodong et le terminaison orientale du YFTB.

Une extension au début du Jurassique supérieur se produit dans l'Est du NCB,

comme le suggèrent le « Metamorphic core complex » de Kalaqin avec une faille de détachement vers le NE (156-150 Ma; Lin et al., 2014), et plusieurs grabens ou hémi-grabens, par exemple, Diaoe et Houcheng (Qi et al., 2015); Chengde (Davis et al., 2001); Guojiadian (Davis et al., 2009). Par conséquent, le pluton tabulaire de Jianchang (~158 Ma) avec des foliations parallèles à ses marges, s'est mis en place par gonflement sous les pluton de Jiumen. Les linéations magmatiques ont enregistré une extension NE-SW. Des extensions d'arrière arc, orientées NW-SE au Jurassique inférieur-début du Jurassique moyen et NE-SW au début du Jurassique supérieur sont caussées par la subduction de la plaque Paléo-Pacifique. Si on considère que les granitoïdes Jurassiques et les roches volcaniques contemporaines distribuées le long de la marge est du continent asiatique, il semble que le pluton de Jianchang-Jiumen e enregistré deux stades d'extension arrière arc dus à cette subduction.

Trois stages d'extension, Trias supérieur, Jurassique inférieur-début du Jurassique moyen, et début du Jurassique supérieur contraignent le cadre tectonique du NCB et du mécanisme géodynamique associé.

Grace à l'étude de la mise en place de trois plutons, trois stades d'extension sont reconnus au Trias supérieur, Jurassique inférieur-début du Jurassique moyen, et début du Jurassique supérieur dans le NCB. Le bloc de Chine du Nord a connu une extension NE-SW au Trias, liée à des processus profonds après la fermeture de l'océan paléo-asiatique. Cette extension a influencé plus du tiers du craton et indique le début de sa destruction. Pendant le Jurassique inférieur et le début du Jurassique moyen, l'extension

est N-S, tandis qu'au début du Jurassique supérieur, l'extension est ENE-WSW contemporaine d'un important magmatisme. La subduction de l'océan Paléo-Pacifique a eu un impact sur la lithosphère de l'est NCB, jusqu'à sa destruction au Crétacé inférieur vers 126 Ma. L'extension a été interrompue à la fin du Jurassique Moyen par une compression N-s liée à la fermeture de l'océan mongol-okhotsk, suivie par une extension à grande échelle à la fin du Jurassique supérieur début du Crétacé liée à la subduction et au retrait par « roll-back » de l'océan Paléopacifique.

En résumé

Dans cette thèse, l'étude pluridisciplinaire de trois plutons apporte de nouvelles données sur les mécanismes de mise en place des plutons du Mésozoïque inférieur et sur la tectonique extensive associée. Qutre conclusions principales peuvent être tirées.

1. Le pluton du Trias supérieur de Dushan s'est mis en place vers le sud à partir d'une zone d'alimentation située au nord. Au début, elle commence probablement par un filon plat (sill) puis évolue par l'injection de plusieurs venus magmatiques. Le gonflement a déformé et recristallisé le magma déjà refroidi produisant une foliation courbée et m^me des mylonites sur la bordure SW du pluton. Les fabriques mésoscopiques et magnétiques du pluton de Dushan sont liées à son édification plutôt qu'à la tectonique régionale du Trias.

2. Au GTrias supérieur, dans le pluton de Wangtufang, la diorite forme une mince enveloppe résiduelle au-dessus du syéno-granite. Des dykes de syéno-granites orientés NW-SE intrudent la diorite et les roches encaissantes. Ce syéno-granite est un intrusion

lopolithique probablement mis en place par gonflement au cours de plusieurs pulsations magmatiques issues d'un conduit central. Il se construit par une dépression du plancher au cours d'une tectonique extensive en accord avec 1) le linéation magnétique NE-SW, 2) l'allongement NE-SW du pluton et 3) les filons de syéno-granite perpendiculaires, interprétés comme des fentes de tension.

3. Dans le pluton Jurassique de Jianchang-Jiumen, le phacolite de Jiumen (~190 Ma) avec des foliations parallèles aux bordures s'est mis en place par gonflement dans le cœur d'un anticlinal, tandis que le pluton tabulaire de Jianchang (~158 Ma) avec ses foliations concentriques, s'est mis en place par injection et gonflement des magmas sous jacents. Les linéations magnétiques enregistrent les deux régimes extensifs NW-SE au Jurassique inférieur et NE-SW au début du Jurassique supérieur connus dans le NCB.

4. La mise en place du pluton de Wangtufang apporte des informations importantes pour la tectonique extensive du Trias supérieur, après la fin de la tectonique compressive de la ceinture orogénique d'Asie centrale. Le pluton de Jianchang-Jiumen a enregisté les deux stades de tectonique extensives dans l'est du NCB. Au Jurassique inférieur-début du Jurassique moyen, une extension N-S de développe dans la partie ouest du NCB, tandis que les extensions d'arrière arc NW-SE du Jurassique inférieur-début du Jurassique moyen et celle NE-SW du début du jurassique supérieur sont liées à la subduction de la plaque Paléo-Pacifique. Ces deux stades extensifs sont interrompus par une compression N-S à la fin du Jurassique moyen dus à la fermeture de l'océan Mongol-Okhotsk. Par conséquent, la tectonique intracontinentale du

Jurassique-Crétacé de Chine du Nord est dominée par le régime tectonique du Paléo-Pacifique interrompue par les effets à grande distance de la compresion Mongol-Okhotsk.

Perspectives

L'évolution phanérozoïque du bloc de Chine du Nord est liée à deux cycles orogéniques comprenant 1) les collisions paléozoïques avec les arc mongols et le bloc de Chine du Sud, respectivement au N et au S du bloc et 2) la tectonique intracontinentale Yanshan du Jurassique-Crétacé. L'évolution Mésozoïque inférieur du NCB est exprimée par des structures complexes polydéformées. En particulier, l'extension du Mésozoïque inférieur est ambigüe. Mieux comprendre cette évolution polyphasée et ses relations géodynamiques avec les plaques environnantes est cruciale, mais les enregistrements géologiques sédimentaires sont rares. Dans cette thèse, grâce à une approche pluridisciplinaire de trois plutons, l'auteur apporte des arguments en faveur des épisodes extensifs du Mésozoïque inférieur. L'étude structurale des plutons est une manière efficace de comprendre la tectonique régionale et les modalités de leur mise en place (e.g., Bouchez & Gleizes, 1995; Bouchez, et al., 1997; Sant'Ovaia et al., 2000; De Saint Blanquat et al., 2011; Lin et al., 2013). Mais il n'existe pas nécessairement de corrélation unique entre le mécanismes de mise en place et le contexte tectonique (compression, extension, coulissage). De plus, le lien avec le contexte géodynamique (convergence, divergence, intraplaque) et le régime tectonique n'est pas direct non plus. Ainsi pour mieux comprendre la tectonique régionale du

bloc de Chine du Nord, d'avantage d'études pluridisciplinaires sont nécessaires. Par exemple, la reconstruction des bassins du Trias supérieur, et l'étude d'autres plutons et de leur encaissant.

Mots clés: Bloc de Chine du Nord, pluton de Dushan, pluton de Wangtufang, pluton de Jianchang-Jiumen, Trias Jurassique, Tectonique extensive, Mécanismes géodynamiques

Abstract

The North China Block (NCB) is one of the important continental terranes that form the East Asian continent. It is separated from the Siberia Craton in the north by the Central Asian Orogenic Belt and from the South China Block in the south by the Qinling-Dabie-Sulu orogen (Figure Ib). The North China Craton formed a stable craton from Mesoproterozoic to Paleozoic, after its assembly through the collision of the Eastern, Intermediate (or Fuping), and Western blocks during the Paleoproterozoic (~1.8-1.9 Ga; Zhao et al., 1998, 2001; Faure et al., 2007; Li & Zhao et al., 2007; Li et al., 2012; Trap et al., 2012). The basement of the stable craton was overlain by a Mesoproterozoic to Permian sedimentary cover, separated by a regional unconformity between the Middle Ordovician and Upper Carboniferous–Permian strata (Li et al., 2016). The stable North China Craton began to transform in the Mesozoic, and cratonic destruction, coeval with lithospheric thinning occurred during Early Cretaceous. The thick (~200 km) Archean lithosphere mantle beneath the eastern NCB was replaced by a thin (<80 km) juvenile one (Fan and Menzies, 1992; Griffin et al., 1992, 1998; Menzies et al., 1993; Zhu et al., 2012; Wu et al., 2019). Although the destruction of the North China Craton occurred in the Cretaceous, this is controversial with various estimates as to the onset of destruction, i.e., Late Triassic (Han et al., 2004; Yang et al., 2007, 2010b, 2012), or Late Jurassic (Gao et al., 2004), according to the temporal and spatial framework and geochemical characteristics of the Early Mesozoic igneous rocks in the NCB.

Before the Cretaceous destruction of the North China Craton, it has undergone two

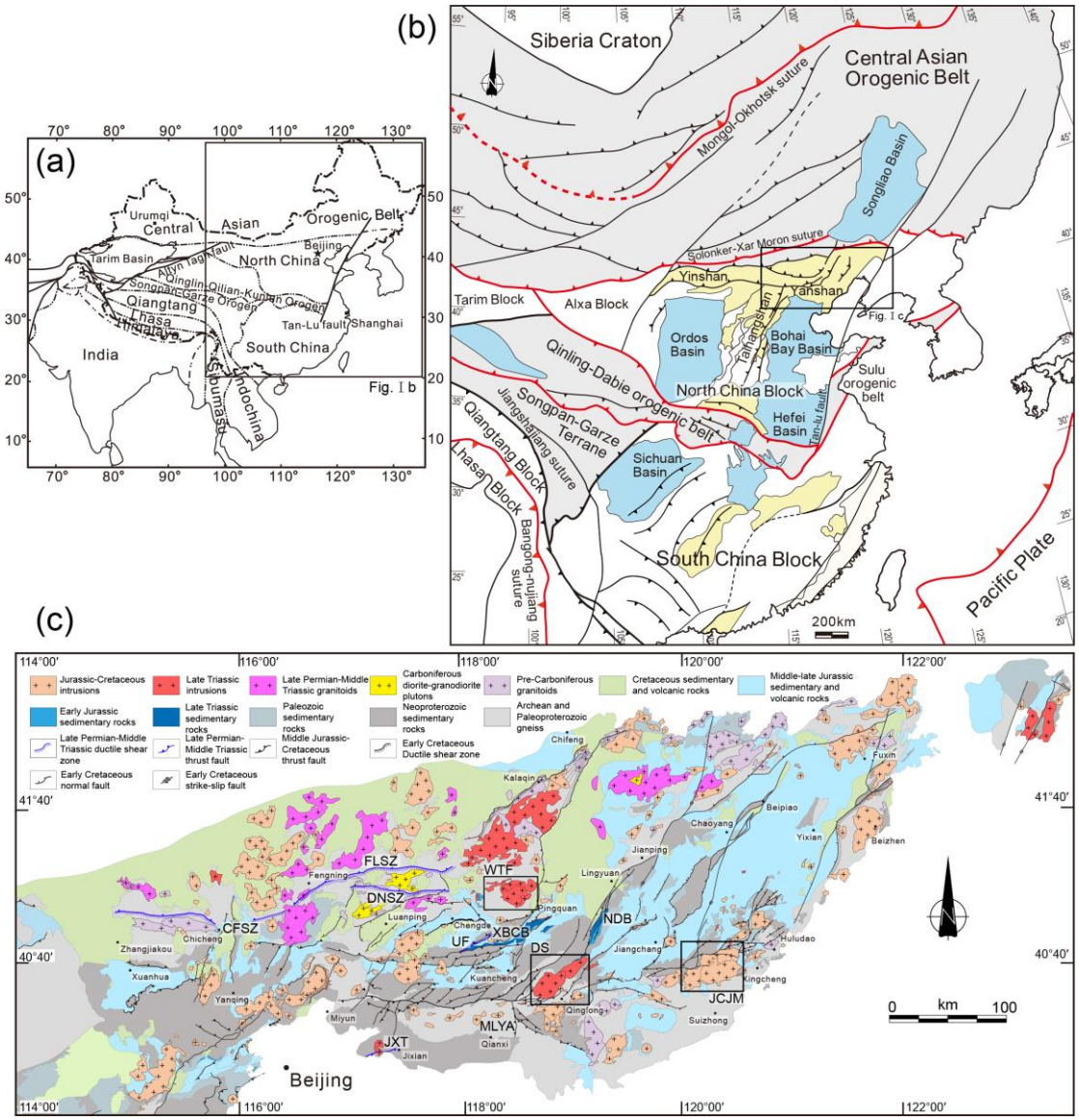

Figure I. Overview maps of the Yanshan fold and thrust belt and its surrounding area. (a) Simplified tectonic map of East Asia. (b) Tectonic framework of East China. (c) Simplified geological map of the Yanshan fold and thrust belt. CFSZ: Chicheng-Fengning ductile shear zone, FLSZ: Fengning-Longhua, ductile shear zone, DNSZ: Damiao-Niangniangmiao ductile shear zone, UF: Unamed fault, JXT: Jixian thrust, MLYA: Malanyu anticline, XBCB: Xiabancheng basin, YZB: Yingzi basin, NDB: Niuying-Dengzhangzi basin, DS: Dushan pluton; WTF: Wangtufang pluton; JCJM: Jianchang-Jiumen pluton.

orogenic events, including Paleozoic continental collisions with Mongolian arc terranes

and South China Block at block boundaries, and Jurassic-Early Cretaceous intracontinental orogeny (also called Yanshanian Orogeny). Furthermore, Triassic deformations and magmatism are also recognized. The Jurassic-Early Cretaceous intracontinental orogeny gave rise to a complicated assemblage of folds and thrusts (Figure Ic). Contemporaneous plutonic intrusions and lava flows are widespread in the NCB during these deformation events. Multiple-phase shortening, including Early-Middle Triassic (~255-241 Ma), late Middle Jurassic (~172-164 Ma) and late Late Jurassic-earliest Cretaceous (~152-135 Ma) are quite evident, albeit timing and duration of these events remain debated (Davis et al., 2001; Faure et al., 2012; Wan et al., 2012; Dong et al., 2015; C. Li et al., 2016). Due to modification by multiphase deformations, only few remnants of Early Mesozoic sedimentary basins are presently distributed in the NCB. However, some clues of extensional episodes, coeval with the igneous rocks possibly implying the onset of the destruction of the North China Craton, can be documented by sporadic small grabens or normal faults (Darby et al., 2001; Davis et al., 2001, 2009; Ritts et al., 2001; Zhang et al., 2011; Meng et al., 2014, 2019; Li et al., 2015; Qi et al., 2015). Therefore, the extensional tectonics and associated geodynamic mechanisms remain poorly constrained due to rare geological records.

Existing problems

1. During the Late Triassic, the EW-trending alkaline intrusive complexes (e.g., nepheline syenite, quartz syenite, and A-type granite) and associated mafic rocks were widely developed along the northern NCB. The emplacement tectonic setting of these

magmatic rocks is interpreted as extensional (Yang et al., 2012; Zhang et al., 2012). During the past decades, isotope chronology and geochemical works suggested that the Late Triassic alkaline intrusive complexes were mainly derived from the melts of subduction-modified enriched lithospheric mantle and ancient lower crust with some depleted asthenospheric mantle components during an intracontinental extensional setting (Yang et al., 2012; Zhang et al., 2014). It points to an upwelling of the asthenospheric mantle during the early lithospheric thinning or modification of the northern NCB. Nevertheless, the Triassic strata in the northern NCB are only exposed in few small remnant basins (i.e., Xiabancheng and Niuyingzi-Dengzhangzi basins). Detrital zircon dating and sedimentological studies of the Late Triassic basin remnants showed a fining and deepening upward depositional system as well as abundant volcaniclastic rocks from the conformable Upper Triassic to Lower Jurassic strata, suggesting a Late Triassic extensional tectonic setting (Davis et al., 2009; Meng et al., 2014). A NE–SW trending regional extension in the northern NCB has been documented by the Sonid Zuoqi MCC in the vicinity of the Solonker zone (Davis et al., 2004). However, Late Triassic-Early Jurassic contractional tectonics was also proposed according to the unconformity between Triassic and Lower Jurassic strata, and Lower Jurassic syntectonic conglomerate (Zhao, 1990; Liu et al., 2012). Therefore, the Late Triassic tectonic regime remains poorly constrained due to the difficulty of structural investigation in few small remnant basins.

2. Jurassic-Early Cretaceous intracontinental orogeny, also termed the Yanshanian Orogeny (Wong, 1929), was widespread and intense in the North China Craton (Davis

et al., 2001). It gave rise to a succession of folds, thrusts, high-angle faults, normal faults, and Mesozoic plutons in the NCB. Alternating contractional and extensional deformations have been recognized in the Yanshan fold-and-thrust belt (Davis et al., 2001; Faure et al., 2012). Two phases of shortening, including late Middle Jurassic (172-164 Ma) and late Late Jurassic-earliest Cretaceous (152-135 Ma) are identified, albeit timing and duration of these events remain debated (Davis et al., 2001; Dong et al., 2015; Faure et al., 2012; C. Li et al., 2016). However, Jurassic extensional deformations have not widely constrained except Early Cretaceous large-scale crustal extension implying the destruction of the North China Craton (Lin & Wei, 2018; Wang et al., 2011). Only sporadic grabens or half-grabens have been documented in the NCB during the Jurassic (Darby et al., 2001; Li et al., 2015; Qi et al., 2015; Ritts et al., 2001; Zhang et al., 2011; Davis et al., 2001, 2009; Qi et al., 2015). Particularly, Early Jurassic contractional tectonics were also proposed according to the unconformity between Triassic and Lower Jurassic strata, and Lower Jurassic syntectonic conglomerate (Zhao, 1990; Liu et al., 2012). Therefore, Jurassic extensional tectonics of the NCB remains ambiguous.

3. The Triassic-Jurassic igneous rocks are widely distributed in the NCB. According to the isotope chronology, four stages of magmatism have been identified, i.e., Late Permian to Middle Triassic (262–236 Ma), Late Triassic (231–199 Ma), Early to Middle Jurassic (189–176 Ma), and Late Jurassic (155–145 Ma). The emplacement mechanism of the Early Mesozoic granitic plutons keeps unclear. However, so far, nobody paid attention to the emplacement mechanism of the Early Mesozoic magma,

which can provide new insight into the evolution of the NCB. Therefore, the study of the emplacement mechanisms of the Early Mesozoic granitic plutons in the NCB would be beneficial to understand the evolution of the NCB.

4. The evolution of the NCB is a key element of the East Asian tectonics. After the Paleozoic amalgamation of the NCB with other continental plates (or microcontinents), the welded East Asian continent was bounded by the Mongol-Okhotsk Ocean in the north, Bangong–Nujiang Ocean in the southwest, and the Paleo-Pacific Ocean in the southeast. As such, any proper understanding of the Mesozoic East Asian tectonics requires a clear vision of the evolution of the NCB during the Mesozoic. Particularly, the Jurassic–Early Cretaceous intracontinental orogeny in the NCB, named the Yanshanian Orogeny, was variously interpreted to be related to i) the closure of the Mongol–Okhotsk Ocean (Yin and Nie, 1996; Davis et al., 2001), ii) the subduction of the Paleo-Pacific plate (G. Zhu et al., 2011; R. Zhu et al., 2011; Xu and Wang, 1983), iii) the interactions of north-south Eurasian intraplate deformation and northwestward Pacific Paleo-Pacific plate (Davis et al., 2001) or iv) multiple plate convergence of the Mongolo-Okhotsk Ocean, Bangong–Nujiang Ocean, and the Paleo-Pacific Ocean (Dong et al., 2015). Due to poor understanding of multiphase deformation events, especially extensional tectonics, the external driving force for the Early Mesozoic of East China continent remains controversial.

Only small Early Mesozoic grabens and half grabens have been reported in the NCB, the Triassic and Jurassic extensional structures and dynamic mechanism in the NCB have not been well constrained due to rare geological records. To better

understand the Early Mesozoic evolution of the NCB, it is crucial to clarify Early Mesozoic extensional tectonics and its relationship to the dynamics of plate subduction/collision along plate boundaries. Pluton emplacement processes potentially contain significant information on both magma internal dynamics and external strain fields to which the magma was subjected (e.g., Bouchez, et al., 1997; Paterson et al., 1998). The structural study of plutons is an effective and practical way to unveil regional tectonic setting coeval with the emplacement process (e.g., Bouchez, et al., 1997; De Saint Blanquat et al., 2011; Lin et al., 2013). In this thesis, to better understand the tectonic setting and dynamic mechanism during the early Mesozoic in the northern NCB, an integrated multidisciplinary investigation, including structural geology, geochronology, geochemistry, AMS, and gravity modeling, has been conducted in the Late Triassic Dushan pluton in Eastern Hebei, the Late Triassic Wangtufang pluton in northern Hebei and Jurassic Jianchang-Jiumen pluton in western Liaoning (Figure Ic). Furthermore, integrating previous studies concerning other structural elements in North China during Early Mesozoic, an improved and more detailed tectonic framework of the NCB was established for understanding the evolution of the NCB and associated geodynamic mechanism.

Late Triassic pluton emplacement and associated extensional tectonic setting: insight from the multidisciplinary studies of the Dushan pluton and the Wangtufang pluton.

1. A multidisciplinary investigation has been carried out in the Dushan pluton. The Dushan pluton consists of monzogranite and biotite-rich marginal facies without sharp

contact between them. The pluton varies southwestwards from isotropic monzogranite in the northeast to arc-shaped gneissosity with locally mylonitic structures in the southwestern margin. The compatible outward dipping mesoscopic and magnetic foliations define an elliptic dome-like pattern with a NE-SW oriented long axis, despite the foliations dip inwards in the southeastern margin of the pluton. Combining gravity modeling, the Dushan pluton with the structural data show that presents an overall tabular or tongue-like shape with a northeastern root. The magnetic lineations generally strike NE-SW, concordant with the stretching lineations observed in the mylonitic zones. Considering the absence of contemporaneous ductile shearing in the country rocks, we argue that a continuum of fabric variation within pluton from magmatic to solid-state conditions probably occurred during pluton emplacement. We propose an emplacement model in which the Dushan pluton emplaced southwards through a northeastern feeder zone, beginning probably with a sill then evolving into the inflation of magma batches. The following successive magma batches inflated the country rocks upward, downward, and also laterally, giving rise to the final pluton. This inflation deformed, and even recrystallized the former cool-down magma, forming a curved gneissic to mylonitic foliation delineating the pluton southwestern margin. Both mesoscopic and magnetic fabrics in the Dushan pluton were rather related to its building than the Late Triassic regional tectonics. To clarify the Late Triassic tectonic and geodynamic setting of the NCB, more detailed structural studies are needed.

2. To better understand Late Triassic tectonic setting in the northern NCB, the emplacement mechanism of the Wangtufang pluton, which recorded the synmagmatic

regional tectonic signature, has been investigated. Zircon U-Pb ages, and Hf isotopic data, and whole-rock geochemical analyses suggest that the Late Triassic Wangtufang pluton composed of syenogranite and diorite is derived from partial melting of lower crust with some depleted mantle components. Both the syenogranite and diorite appear isotropic. Anisotropy of magnetic susceptibility and gravity studies have been carried out to characterize internal fabrics and shape of the pluton. The diorite forms just thin remnants above the syenogranite. The syenogranite with a series of NW-SE trending dykes intruded into the diorite and its country rocks. In the syenogranite, the gently dipping magnetic foliations strike nearly parallel to the pluton border. The shallow plunging magnetic lineations mainly strike NE–SW. Combining NE-SW trending elongated subsurface shape with central root, unflat bottom, and moderate- to high-inward dipping sidewalls, the syenogranite could be considered as a lopolith-like intrusion. The syenogranite was likely emplaced by inflation of magma pulses from its central conduit and built up by floor depression. Emplacement of the syenogranite was in an extensional setting, considering: (1) the NE–SW striking magnetic lineation, (2) the NE–SW trending elongated subsurface pluton shape, and (3) the orthogonal NW–SE striking syenogranitic dykes considered as tension gashes during the NE–SW trending extension. Detrital zircon dating and sedimentological studies of these basin remnants showed a fining and deepening upward depositional system as well as abundant volcaniclastic rocks from the conformable Upper Triassic to Lower Jurassic strata, suggesting a Late Triassic extensional tectonic setting (Davis et al., 2009; Meng et al., 2014). Besides, a NE–SW trending regional extension in the northern NCB has

been documented in the Sonid Zuoqi MCC in the vicinity of the Solonker zone (Davis et al., 2004). The Wangtufang pluton provides reliable arguments to the Late Triassic intracontinental extensional setting already suggested in the northern NCB.

An E-W trending Late Triassic alkaline intrusive complexes and associated mafic rocks widely occurred at around 231–215 Ma in the northern NCB (Yang, 2012, Zhang et al., 2012, 2014). They were derived from partial melting of lower crust and metasomatized enriched lithospheric mantle with some materials from the depleted asthenospheric mantle (Yang et al., 2012; Zhang et al., 2012; Zhang et al., 2014; Zhu et al., 2012), indicating the upwelling of the asthenospheric mantle and the asthenosphere-lithospheric mantle interaction during the early lithospheric thinning or modification of the North China Craton (e.g., Han et al., 2004). Contemporaneous surface uplift and supracrustal stretching also occurred in the northern NCB. Therefore, the Late Triassic was in a NE-SW intracontinental extensional setting, related to the deep process after the final closure of Paleo-Asian Ocean or subsequent intracontinental compression, despite the trigger mechanism remains debated, e.g., intraplate extension (Yang et al., 2012), post-collisional or post-orogenic lithospheric delamination (Zhang et al., 2012), and mantle upwelling in front of the subducting slab of Mongol-Okhotsk plate (Meng et al., 2020).

Jurassic pluton emplacement and Early Jurassic NW-SE and early Late Jurassic NE-SW extensional tectonic setting: insight from a multidisciplinary study of the Jianchang-Jiumen pluton.

The Jurassic-Early Cretaceous intracontinental orogeny in East Asia is expressed by a complicated structural feature in the NCB with multiphase deformations that timing and kinematics are crucial to decipher the geodynamics of the NCB. Particularly, Jurassic extensional tectonics in North China remains ambiguous due to rare geological records. A multidisciplinary investigation on the Jurassic Jianchang-Jiumen pluton has been performed to provide tectonic information for Jurassic extensional episodes. In the NCB, the Early Jurassic-early Middle Jurassic infill contains mafic volcanic rocks in the eastern NCB and widespread coal-bearing sequence in the whole NCB (Figure 6.1), which were considered to take place in an extensional setting (Zhang et al., 2014; Meng et al., 2019; Hao et al., 2020). In the western NCB, the N-S extension is well recorded by nearly E-W trending brittle normal faults in the Ordos Basin and its periphery (Darby et al., 2001; Ritts et al., 2001; Zhang et al., 2011), the Taihangshan (Li et al., 2015) and the Daqingshan (Darby et al., 2001; Ritts et al., 2001). However, in the eastern NCB, only a NE trending rift was documented in the Western Hill of Beijing. In this study, the phacolith-like Jiumen pluton (~190 Ma) reveals margin-parallel foliations produced by magma inflation in the anticlinal core. The magnetic lineations recorded the Early Jurassic NW-SE extension.

In the NCB, the early Late Jurassic volcanic and pyroclastic rocks of the Tiaojishan/Lanqi Formation, and concomitant granite plutons (164-155 Ma) are only distributed in the eastern NCB (i.e., the Liaodong and Jiaodong peninsulas and the eastern YFTB). An early Late Jurassic extension occurred in the eastern NCB, suggested by the Kalaqin metamorphic core complex with a top-to-the-NE detachment

(156-150 Ma; Lin et al., 2014), and several grabens or half-grabens, e.g., Diaoe graben and Houcheng half-graben, (Qi et al., 2015); Chengde graben, (Davis et al., 2001); Guojiadian half-graben, (Davis et al., 2009). Therefore, the tabular-like Jianchang pluton (~158 Ma) with margin-parallel foliations, intruded by magma inflation, underlay the Jiumen pluton. The magnetic lineations recorded an early Late Jurassic NE-SW extension in the eastern NCB. The Early Jurassic-early Middle Jurassic NW-SE striking and early Late Jurassic NE-SW striking backarc extensions, related to the Paleo-Pacific Plate subduction, occurred in the eastern NCB. Considering that the Jurassic granitoid and coeval volcanic rocks were all distributed along the eastern margin of the East Asian continent, it seems that the Jianchang-Jiumen pluton recorded two-stage backarc extension in the eastern NCB, related to the Paleo-Pacific Plate subduction beneath the NCB.

Three extensional stages, including Late Triassic, Early Jurassic-early Middle Jurassic, and early Late Jurassic further constrain the regional tectonic framework of the NCB and associated geodynamic mechanism during Early Mesozoic.

Through the emplacement of three plutons, three extensional stages, including Late Triassic, Early Jurassic-early Middle Jurassic, and early Late Jurassic occurred in the NCB. It further constrains regional tectonic framework of the NCB during Early Mesozoic. The NCB experienced Late Triassic intracontinental NE-SW extension related to deep-seated tectonic process, following the closure of Paleo-Asian Ocean. Large-scale Late Triassic extensional structures in the northern NCB influenced one-

third of the craton, indicating the beginning of craton destruction. During the Jurassic, the Early Jurassic-early Middle Jurassic N-S post-collisional extension occurred in the western NCB after the amalgamation between North China and South China, whereas Early Jurassic-early Middle Jurassic NW-SE trending and early Late Jurassic ENE-WSW extension and associated magmatism occurred in the eastern NCB. The subduction of the Paleo-Pacific plate had an impact on lithosphere of the eastern NCB until the cratonic destruction during Early Cretaceous (126 Ma). The two-stage extension was interrupted by late Middle Jurassic N-S compression related to the closure of Mongol–Okhotsk Ocean, followed by large-scale late Late Jurassic-Early Cretaceous NW-SE compression and extension related to the subduction and rollback of the Paleo-Pacific Plate, respectively.

Summary

In this thesis, through the multidisciplinary studies of three plutons, it provides new insights into the emplacement mechanism of the Early Mesozoic granitic pluton and associated extensional tectonic setting, from which we draw four main conclusions.

1. The Late Triassic Dushan pluton emplaced southwards through a northeastern feeder zone, beginning probably with a sill then evolving into the inflation of magma batches. This inflation deformed, and even recrystallized the former cool-down magma, forming a curved gneissic to mylonitic foliation delineating the pluton southwestern margin. Both mesoscopic and magnetic fabrics in the Dushan pluton were rather related to its building than the Late Triassic regional tectonics.

2. In the Late Triassic Wangtufang pluton, the diorite forms just thin remnants above the syenogranite. The syenogranite with a series of NW-SE trending dykes intruded into the diorite and its country rocks. The syenogranite, a lopolith-like intrusion, was likely emplaced by inflation of magma pulses from its central conduit and built up by floor depression under an extensional setting, considering: (1) the NE–SW striking magnetic lineation, (2) the NE–SW trending elongated subsurface pluton shape, and (3) the orthogonal NW–SE striking syenogranitic dykes considered as tension gashes during the NE–SW trending extension.

3. In the Jurassic Jianchang-Jiumen pluton, the phacolith-like Jiumen pluton (~190 Ma) with margin-parallel foliations emplaced by magma inflation in the anticlinal core, while the tabular-like Jianchang pluton (~158 Ma) with concentric foliations underlay the Jiumen pluton by inflation of conduit-fed magma from its feeder zone. Two patterns of magnetic lineations recorded Early Jurassic NW-SE extension and early Late Jurassic NE-SW extension in the eastern NCB, respectively.

4. The emplacement of the Wangtufang pluton provides reliable arguments to the Late Triassic intracontinental extensional setting after the final formation of the Central Asian Orogenic Belt. The Jianchang-Jiumen pluton recorded the Jurassic two-stage extension in the eastern NCB. The Early Jurassic-early Middle Jurassic post-collisional N-S extension occurred in the western NCB after the collision between the North and South China Blocks, whereas the Early Jurassic-early Middle Jurassic NW-SE striking and early Late Jurassic NE-SW striking backarc extensions, related to the Paleo-Pacific Plate subduction, occurred in the eastern NCB. The two-stage extension was interrupted

by late Middle Jurassic N-S compression related to the closure of Mongol–Okhotsk Ocean, followed by large-scale late Late Jurassic-Early Cretaceous NW-SE compression and extension related to the subduction and rollback of the Paleo-Pacific Plate, respectively. Accordingly, Jurassic-Early Cretaceous intracontinental orogeny in North China was dominated by the Paleo-Pacific tectonic regime, interrupted by far-field compression of the Mongol–Okhotsk tectonic regime.

Perspectives

The Phanerozoic tectonic evolution of the NCB is related to two orogenic cycles, including Paleozoic continental collisions with Mongolian arc terranes and South China Block at block boundaries, and Jurassic-Early Cretaceous intracontinental orogeny (Yanshanian Orogeny). The Early Mesozoic tectonic evolution of the NCB is expressed by a complicated structural feature in the NCB with multiphase deformations that timing and kinematics are crucial to decipher the geodynamics of the NCB. Particularly, Early Mesozoic extensional tectonics in North China remains ambiguous due to sporadic geological records. To understand multiphase evolution of the NCB, it is crucial to clarify Early Mesozoic extensional tectonics and its relationship to the dynamics of plate subduction/collision along active boundaries. Indeed, due to rare geological records, it is difficult to recognize the regional tectonic framework from few small remnant basins. In this thesis, through the multidisciplinary studies of three plutons, the author provides some arguments for the Early Mesozoic extensional episodes. The structural study of plutons is an effective and practical way to unravel

regional tectonic setting coeval with the emplacement process (e.g., Bouchez & Gleizes, 1995; Bouchez, et al., 1997; Sant'Ovaia et al., 2000; De Saint Blanquat et al., 2011; Lin et al., 2013). However, there is not necessary and unique correlation between emplacement mechanism with tectonic setting (i.e. compressive, extensive, strike-slip). Moreover, the link with geodynamic context (i.e. plate convergence, plate divergence, intraplate) is not directly corresponding. Thus, to provide reliable arguments for the Early Mesozoic extensional tectonics, more multidisciplinary studies are needed, such as structural reconstruction of basins and investigations on the magmatic plutons and their adjacent areas.

Key Words: North China Block, Dushan pluton, Wangtufang pluton, Jianchang-Jiumen pluton, Triassic-Jurassic, Extensional tectonics, Regional tectonic framework, Dynamic mechanism

Table of Contents

Chapter 1. General introduction

1.1. Background and scientific issues

After its assembly through the collision of the Eastern, Intermediate (or Fuping), and Western blocks during the Paleoproterozoic (~1.8-1.9 Ga; Zhao et al., 1998, 2001; Faure et al., 2007; Li & Zhao et al., 2007; Li et al., 2012; Trap et al., 2012), the North China Craton formed a stable craton from Mesoproterozoic to Paleozoic. During the Cretaceous, the destruction of the craton or the large-scale lithosphere thinning occurred in the North China Craton. The thick (~200 km) Archean lithosphere mantle beneath the eastern NCB was replaced by a thin (<80 km) juvenile one (Fan and Menzies, 1992; Griffin et al., 1992, 1998; Menzies et al., 1993; Zhu et al., 2012; Wu et al., 2019). The destruction of the North China Craton has become a hot issue of international geoscientific research today and considerable progress has been made during the past two decades.

Before the destruction of the North China Craton in the Cretaceous, the North China Craton has undergone two orogenic cycles, including Paleozoic-Triassic continental collisions with Mongolian arc terranes and South China Block at block boundaries (Hacker et al., 2000; Mattauer et al., 1985; Meng & Zhang, 1999; Windley et al. 2007; Xiao et al., 2003, 2015; Z. Xu et al., 1986; B. Xu et al., 2013; Figure 1.1), and Jurassic-Early Cretaceous intracontinental orogeny (also called Yanshanian Orogeny, Davis et al., 2001; Dong et al., 2015; Faure et al., 2012; Figure 1.1). Since the early 1900s, the Phanerozoic NCB has been studied from the standpoint of both structure and stratigraphy (e.g., Wong, 1929; Davis et al., 2001). Especially in the Yinshan-Yanshan fold and thrust belt in the north, the alternating compressional and extensional deformations during the Mesozoic have been identified (Davis et al., 2001;

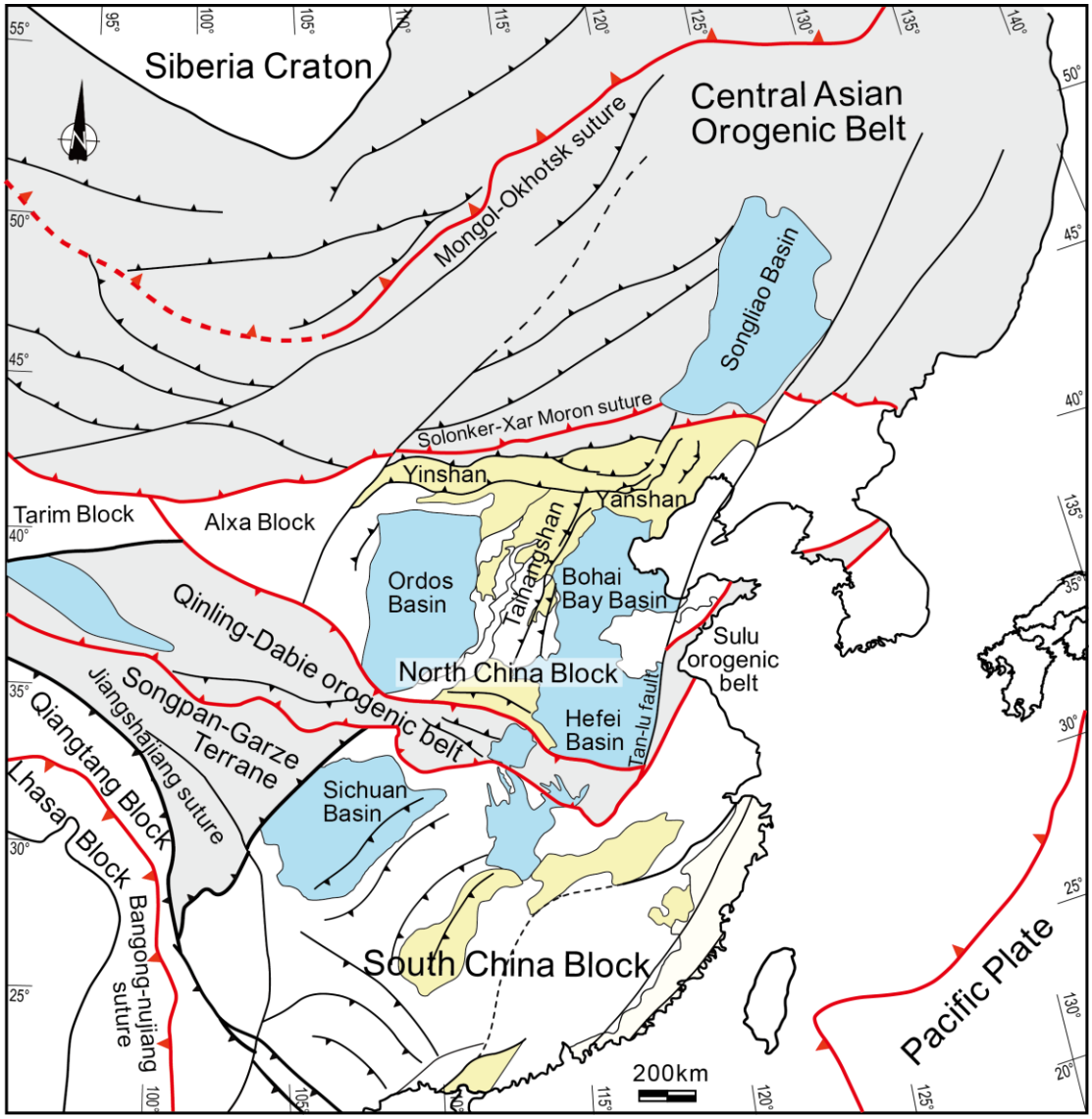

Figure 1.1 Simplified geological sketch map of the East Asian continent (Modified from Lin & Wei, 2018).

Faure et al., 2012; Li et al., 2016; Figure 1.2). Although the destruction of the North China Craton occurred in the Cretaceous, this is controversial with various estimates as to the onset of destruction (Figure 1.3), i.e., Late Triassic (Han et al., 2004; Yang et al., 2007, 2010b, 2012), or Late Jurassic (Gao et al., 2004).

During the Late Triassic, the EW-trending alkaline intrusive complexes (e.g., nepheline syenite, quartz syenite, and A-type granite) and associated mafic rocks were widely developed along the northern NCB in an extensional setting (Yang et al., 2012; Zhang et al., 2012). Detrital zircon dating and sedimentological studies of

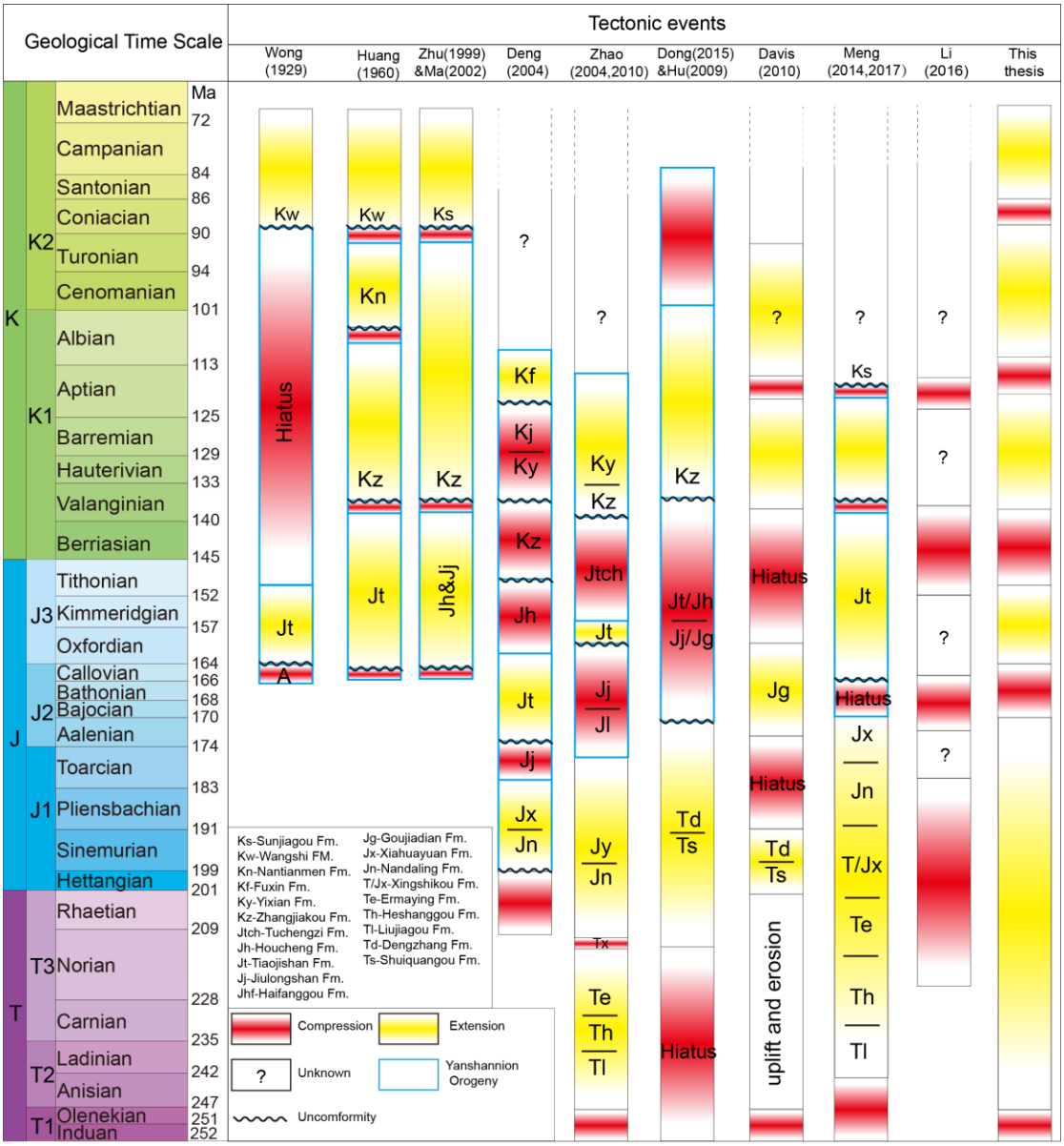

Figure 1.2 Regional structural framework of the Yanshan fold and thrust belt (Zeng, Unpublished)

the Late Triassic basin remnants showed a fining and deepening upward depositional system as well as abundant volcaniclastic rocks from the conformable Upper Triassic to Lower Jurassic strata, suggesting a Late Triassic extensional tectonic setting (Davis et al., 2009; Meng et al., 2014). A NE–SW trending regional extension in the northern NCB has been documented in the Sonid Zuoqi MCC in the vicinity of the Solonker zone (Davis et al., 2004). During the Jurassic, two stages of magmatism have been identified, i.e., Early Jurassic-early Middle Jurassic (199-174 Ma) and Early Jurassic

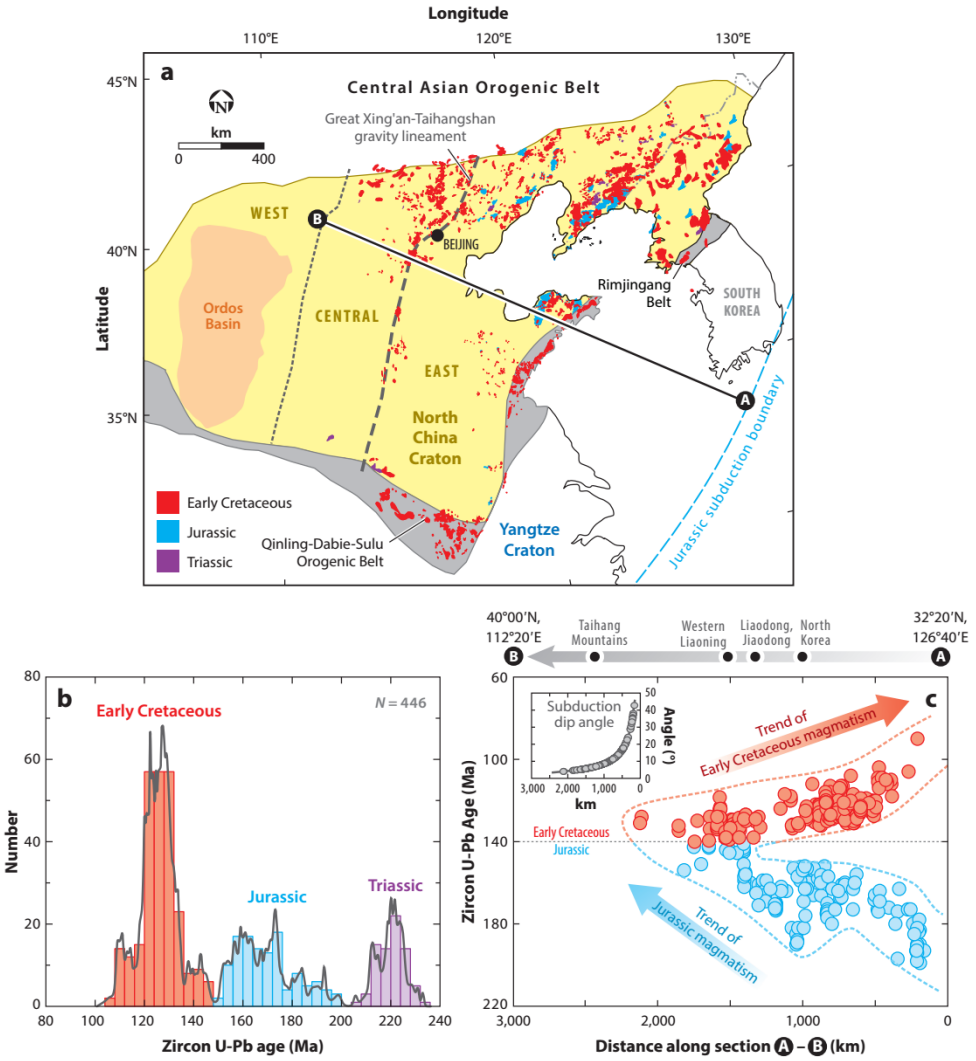

Figure 1.3 (a) Distribution of Mesozoic intrusive rocks in the NCB. (b) Histogram of zircon U-Pb ages of Mesozoic igneous rocks in the NCB. (c) Projection of zircon U-Pb ages along the AB line perpendicular to the Mesozoic structural strike of the NCB in panel a, showing a younging trend from east to west for the Jurassic igneous rocks, but a reverse trend for the Cretaceous rocks. (Inset) Graphical representation of a function controlling distance from trench to magma arc with subduction zone dip angles (from Wu et al., 2019).

(161-155 Ma) (Zhu et al., 2012; Zhang et al., 2014). During the Early Jurassic-early Middle Jurassic, the E-W trending extensional basins or normal faults were widely in the western NCB, e.g., the Ordos basin and its periphery (Zhang et al., 2011), the Daqingshan (Darby et al., 2001; Ritts et al., 2001), and the Taihangshan (Li et al., 2015). Meanwhile, the eruption of basalt (the Nadaling or Xinglonggou Formations) in the

eastern NCB and the coal-bearing basins have been considered to occur in a backarc extensional setting (Meng et al., 2019; Hao et al., 2020). During the early Late Jurassic, an early Late Jurassic extension was recorded by Kalaqin metamorphic core complex with top-to-the-NE shearing (156-150 Ma; Lin et al., 2014), nearly N-S or NE trending Diaoe graben and Houcheng half-graben (Qi et al., 2015), Chengde graben (Davis et al., 2001), and Guojiadian half-graben (Davis et al., 2009). However, Late Triassic-Early Jurassic contractional tectonics was also proposed according to the unconformity between Triassic and Lower Jurassic strata, and Lower Jurassic syntectonic conglomerate (Zhao, 1990; Liu et al., 2012). Therefore, the tectonic evolution of the NCB during early Mesozoic remains debated. Particularly, the extensional tectonics were almost documented in several basin remnants. The timing and duration of these extensional tectonics remain ambiguous (Figure 1.3).

Deciphering the interplay existing between tectonics and granitic pluton emplacement mechanisms is of fundamental importance for the understanding of the evolution of the continental crust (e.g., Bouchez & Gleizes, 1995; Gleizes et al., 1997; De Saint Blanquat et al., 2011; Žák et al., 2013). The structural study of plutons is an effective and practical way to unravel regional tectonic setting coeval with the emplacement process (e.g., Bouchez & Gleizes, 1995; Bouchez, et al., 1997; Sant'Ovaia et al., 2000; De Saint Blanquat et al., 2011; Lin et al., 2013). The early Mesozoic magmatism is conspicuous in the NCB, represented by E–W trending Late Triassic alkaline intrusive complexes in the northern NCB and Jurassic granites in the Liaodong and Jiaodong peninsulas and the eastern Yanshan Fold and Thrust Belt. The Late Triassic and Jurassic granitic plutons from the NCB present good opportunities to realize the tectonic regimes during the early Mesozoic. In this thesis, Late Triassic Dushan-Dashizhu pluton and Wangtufang pluton, and Jurassic Jianchang-Jiumen

pluton were selected to provide regional tectonic information for the extensional episodes through an integrated multidisciplinary investigation (including structural geology, isotope chronology, geochemistry, Anisotropy of magnetic susceptibility (AMS), and gravity modeling). Then, the geodynamics of the NCB during the early Mesozoic was discussed.

1.2. Research contents and methodology

As the research targets, three representative plutons (Dushan-Dashizhu pluton, Wangtufang pluton, and Jianchang-Jiumen pluton) were chosen to clarify the extensional tectonics through an integrated multidisciplinary investigation (including structural geology, isotope chronology, geochemistry, Anisotropy of magnetic susceptibility (AMS), and gravity modeling).

1.2.1. Research purpose and contents

In the northern NCB, the Triassic strata are only exposed in few small remnant basins (i.e., Xiabancheng and Niuyingzi-Dengzhangzi basins). Detrital zircon dating and sedimentary studies suggest that the conformable Upper Triassic to Lower Jurassic strata were deposited in an extensional setting (Davis et al., 2009; Meng et al., 2014). The Late Triassic tectonic regime remains poorly constrained due to the difficulty of structural investigation in few small remnant basins. Therefore, two Late Triassic plutons (Dushan-Dashizhu pluton and Wangtufang pluton) as good targets were chosen to clarify Late Triassic tectonic regime.

Jurassic-Early Cretaceous intracontinental orogeny, also termed the Yanshanian Movement in the Chinese literature (Wong, 1929), was widespread and intense in the North China Craton (Davis et al., 2001). Albeit alternating contractional and extensional deformations have been recognized in the Yanshan fold-and-thrust belt,

timing and duration of these events remain debated (Davis et al., 2001; Dong et al., 2015; Faure et al., 2012; C. Li et al., 2016). Particularly, Jurassic extensional deformations have not firmly constrained. Only sporadic grabens or half-grabens have been documented in the NCB during Early Jurassic-early Middle Jurassic (Darby et al., 2001; Li et al., 2015; Qi et al., 2015; Ritts et al., 2001; Zhang et al., 2011) and early Late Jurassic (Davis et al., 2001, 2009; Qi et al., 2015). Therefore, Jurassic plutons from the NCB present good opportunities to realize this purpose, and, accordingly, the Jianchang-Jiumen pluton was chosen for this study.

Early Mesozoic tectonic evolution is a key element of the East Asian tectonics. After the amalgamation of Paleo-Asian ocean, the Late Triassic tectonic regime in the northern NCB remains controversial. After the Paleozoic-Triassic amalgamation, multiphase deformation events in the welded East Asian continent related to Jurassic-Early Cretaceous intracontinental orogeny remain poorly constrained. It is crucial to clarify Early Mesozoic extensional tectonics in the NCB for establishing the detailed structural framework of the NCB and understanding the geodynamic mechanism of Early Mesozoic tectonics in East Asia.

1.2.2. Methodology

Three granite plutons were selected as the targets to decipher the unclarified scientific problems, some methods have been utilized as follows:

(1) Detailed field observations in three areas, including Dushan-Dashizhu, Wangtufang, and Jianchang-Jiumen, to investigate the deformations of the plutons and their country rocks.

(2) Geochemical investigation of the Wangtufang pluton, which lack of geochemical data, aiming to reveal its origin and tectonic setting.

(3) Isotope chronology analysis on three granite plutons to constrain precise age

of magmatism by a Cameca IMS 1280 large-radius SIMS (SIMS zircon U-Pb Dating).

(4) Measurement of the Anisotropy of Magnetic Susceptibility (AMS), to determine the fabrics of the plutons and the tectonic setting of pluton emplacement.

(5) Gravity modelling, to constrain the deep structures of the plutons (the geometry and possible feeder zones of pluton).

1.3. Workload of the study

Detailed workload can be listed in Table 1.1

1.4. Major findings and innovations

1. The Late Triassic Dushan pluton emplaced southwards through a northeastern feeder zone, beginning probably with a sill then evolving into the inflation of magma batches. This inflation deformed, and even recrystallized the former cool-down magma, forming a curved gneissic to mylonitic foliation delineating the pluton southwestern margin. Both mesoscopic and magnetic fabrics in the Dushan pluton were rather related to its building than the Late Triassic regional tectonics.

2. In the Late Triassic Wangtufang pluton, the diorite forms just thin remnants above the syenogranite. The syenogranite with a series of NW-SE trending dykes intruded into the diorite and its country rocks. The syenogranite, a lopolith-like intrusion, was likely emplaced by inflation of magma pulses from its central conduit and built up by floor depression under an extensional setting, considering: (1) the NE–SW striking magnetic lineation, (2) the NE–SW trending elongated subsurface pluton shape, and (3) the orthogonal NW–SE striking syenogranitic dykes considered as tension gashes during the NE–SW trending extension.

3. In the Jurassic Jianchang-Jiumen pluton, the phacolith-like Jiumen pluton (~190

Table 1.1 Physical workload of the thesis

Content	*Unit*	*Number*
Field observation	day	43
	site	367
Samples	piece	52
Photos	piece	1250
Thin section	piece	320
Oriented thin section	piece	68
Major elements	sample	9
Trace elements	sample	11
Cathodoluminescence	grain	8
Zircon U-Pb SIMS dating	sample	8
In-situ zircon Hf isotopes	sample	2
AMS samples	site	167
AMS measurment	core	943
Magnetic mineralogical analysis	sample	39
Gravity modeling	profile	12

Ma) with margin-parallel foliations emplaced by magma inflation in the anticlinal core, while the tabular-like Jianchang pluton (~158 Ma) with concentric foliations underlay the Jiumen pluton by inflation of conduit-fed magma from its feeder zone. Two patterns of magnetic lineations recorded Early Jurassic NW-SE extension and early Late Jurassic NE-SW extension in the eastern NCB, respectively.

4. Pluton emplacement provides reliable arguments to the Late Triassic intracontinental extensional setting after the final formation of the Central Asian Orogenic Belt.

5. The Early Jurassic-early Middle Jurassic post-collisional N-S extension occurred in the western NCB after the collision between the North and South China Blocks, whereas the Early Jurassic-early Middle Jurassic NW-SE striking and early

Late Jurassic NE-SW striking backarc extensions, related to the Paleo-Pacific Plate subduction, occurred in the eastern NCB. The two-stage extension was interrupted by late Middle Jurassic N-S compression related to the closure of Mongol–Okhotsk Ocean, followed by large-scale late Late Jurassic-Early Cretaceous NW-SE compression and extension related to the subduction and rollback of the Paleo-Pacific Plate, respectively. Accordingly, Jurassic-Early Cretaceous intracontinental orogeny in North China was dominated by the Paleo-Pacific tectonic regime, interrupted by far-field compression of the Mongol–Okhotsk tectonic regime.

Chapter 2. Regional geological outline of North China

2.1. Tectonic setting of the North China Block and its adjacent area

The NCB is one of the most important continental terranes that form the East Asian continent (e.g. Davis et al., 2001; Yin and Nie, 1996). It is separated from the Siberia Craton in the north by the Central Asian Orogenic Belt and from the South China Block in the south by the Qinling-Dabie-Sulu orogen, respectively (Figure 1.1). The North China Craton formed a stable craton from Mesoproterozoic to Paleozoic, after its assembly through the collision of the Eastern, Intermediate (or Fuping), and Western blocks during the Paleoproterozoic (Zhao et al., 2001; Faure et al., 2007; Li and Zhao, 2007; Li et al., 2012). The basement of the stable craton was overlain by a Mesoproterozoic to Permian sedimentary cover, separated by a regional unconformity between the Middle Ordovician and Upper Carboniferous–Permian strata (Li et al., 2016). The northern NCB is located to the south of the eastern segment of the CAOB (Figure 1.1). The evolution of the eastern segment of the CAOB is dominated by the late Paleozoic Paleo-Asian Ocean domain in the south and Mesozoic Mongol-Okhotsk Ocean domain in the north (Wang and Liu, 1986; Sengör and Natal'in, 1996; Xu and Chen, 1997; Davis et al., 2001; Xiao et al., 2003; Donskaya et al., 2013). The eastern segment of the CAOB is the result of a complex multi-period tectonic evolution during late Paleozoic to Mesozoic, with the subduction and closure of the Paleo-Asian Ocean and the Mongol-Okhotsk Ocean (Zonenshain et al., 1990; Sengor and Natal'in, 1996; Yin and Nie, 1996; Kravchinsky et al., 2002; Xiao et al., 2003; Windley et al., 2007;

Zhang et al., 2007; Xiao and Kusky, 2009; Zhang et al., 2009; Han et al., 2012; Zhang et al., 2012; Zhang et al., 2014). In the south, it is characterized by the amalgamation of several microcontinents including, from west to east, the Erguna, Xing'an, Songnen, Jiamusi, and Khanka massifs (Sengör et al., 1993; Xu et al., 2013). Timing and process of the closure of the Paleo-Asian Ocean are still debated, 1) the late Devonian closure of the Paleo-Asian ocean occurred during the middle Paleozoic, with two opposite subductions and collisions along Ondor Sum in the south and Sunid Zuoqi in the north (Xu and Chen, 1997; Xu et al., 2013), 2) a Late Permian to Early Triassic collision, between the Tuva-Mongolia microcontinent and NCB, occurred with long-lived multiple southward and northward subductions from 530 to 250 Ma (Chen et al. 2000, 2009), 3) the final amalgamation of the CAOB occurred during latest Permian to mid-Triassic by termination of the accretionary processes (Xiao et al., 2003, 2015), and 4) an early to mid-Paleozoic paired orogens with a Permian intra-oceanic arc trench system and a sequence of tectono-magmatic events from 299 Ma to 260 Ma were responsible for the CAOB accretion (Jian et al. 2008, 2010). Numerous authors suggested the final closure of the Paleo-Asian Ocean was along the Solonker-Xra Moron-Changchun suture during Permian-Early Triassic (Sengör et al., 1993; Yin and Nie, 1996; Chen et al., 2000; Xiao et al., 2003; Shang, 2004; Li, 2006; Lin et al., 2008; Jian et al., 2010; Eizenhöfer et al., 2014; Li et al., 2014).

In the eastern CAOB, it is closely related to the closure of the Mongol-Okhotsk Ocean in the north (Xu et al., 2009; Wu et al., 2011; Xiao et al., 2015). The Mongol-Okhotsk Ocean subducted northward beneath the Siberia Craton, resulting in the

collision between the Siberia Craton and the Amurian supertarrane (Vander Voo et al., 1999). The suture extends from the middle Mongolia to the Mongol-Okhotsk Sea (Tomurtogoo et al., 2005). This is controversial with various estimates as to the timing of its closure, i.e., Middle Jurassic (Zorin, 1999; Yarmolyuk et al., 2000; Tomurtogoo et al., 2005; Sun et al., 2013), Late Jurassic (Zonenshain et al., 1990), and Late Jurassic-Early Cretaceous (Parfenov et al., 2001; Kravchinsky et al., 2002; Cogné et al., 2005; Metelkin et al., 2010; Pei et al., 2011). However, the collision between the Siberia Craton and the Amurian supertarrane occurred after the Middle Jurassic, evidenced by the Triassic-Middle Jurassic marine deposits (Enkin et al., 1992). The majority of scholars suggested that the closure of the Mongol-Okhotsk Ocean was diachronous but generally became younger eastward (Zonenshain et al., 1990; Yin and Nie, 1996; Kravchinsky et al., 2002; Xiao and Kusky, 2009; Berzina et al., 2014), for instance, the Middle Jurassic in the west (Zorin, 1999; Parfenov et al., 2001) and the Late Jurassic or the Early Cretaceous in the east (Yarmolyuk et al., 2000; Daoudene et al., 2013). Paleomagnetic studies suggested that the Mongol-Okhotsk Ocean subducted southward and collided with the Amurian supertarrane (Enkin et al., 1992).

In the south of the NCB, it is separated the South China Block by the Qinglin-Dabie-Sulu Orogenic belt (Figure 1.1), which underwent a complex multi-period tectonic evolution related to the Proto-Tethys Ocean and the Paleo-Tethys Ocean (e.g., Mattauer et al. 1985; Hacker et al., 1995, 1996, 1998, 2000; Wang et al., 1995; Faure et al., 1999, 2003; Meng and Zhang 2000; Ratschbacher et al., 2003, 2006; Lin et al., 2005, 2009; Dong et al. 2011; Wu and Zheng 2013; Dong and Santosh 2016). Generally,

the amalgamation of the South Qinling and the NCB occurred in the middle Paleozoic, forming the North Qinling (e.g., Mattauer et al. 1985; Meng and Zhang 2000). In the Late Triassic, the final amalgamation of the North and South China Blocks was along the Mianlue suture (e.g., Mattauer et al. 1985; Hacker et al., 1995, 1996, 1998, 2000; Wang et al., 1995; Meng and Zhang 2000; Ratschbacher et al., 2003, 2006). The continental deep subduction of the Yangtze Block occurred beneath the NCB, forming the HP–UHP Dabie-Sulu orogenic belt (Okay et al. 1989; Wang et al. 1989; Xu et al. 1992; Faure et al., 1999, 2003; Lin et al., 2005, 2009; Dong et al., 2011; Wu and Zheng, 2013; Dong and Santosh, 2016).

During the late Mesozoic, it transited to the Pacific tectonic regime from the Paleo-Tethys tectonic regime in eastern China, corresponding to the evolution of the Paleo-Pacific Plate (Izanagi Plate). However, timing and process of the subduction beneath the East Asian continent remain controversial. The borehole encountered the early Early Jurassic volcanics on the continental shelf of the East China Sea. Due to the nature of continental margin arc, the volcanics were considered to be related to the onset of the Paleo-Pacific Plate subduction beneath the South China Block (198-195Ma; Xu et al., 2017). In the Korean Peninsula, the Early Jurassic synorogenic foreland deposits and high-k calc-alkaline volcanic rocks were supposed to a result of the Paleo-Pacific Plate subduction in the active continental margin (184~167 Ma; Han et al., 2006; Kim et al., 2011). The Early Jurassic volcanics in the Yanshan belt of the NCB recorded the onset of the Paleo-Pacific Plate subduction (Hao et al., 2020). The Middle-Late Jurassic fold and thrust belt, and extensive Jurassic magmatism was also considered as a result of the

Paleo-Pacific Plate subduction (Zhou and Li, 2000; Li and Li, 2007; Li et al., 2018).

2.2. Tectonic evolution of the Triassic-earliest Cretacous basins

2.2.1. Triassic

In the NCB, the Triassic strata are mainly distributed in the Ordos Basin, e.g., the Helanshan, the Liupanshan, and the Alxa Block in its west (Deng and Li, 1998). The Ordos Basin was a cratonic basin with convergence plate margins during the late Paleozoic-Early Triassic (Yang et al., 2015). In the Early Triassic, sand and mudstone in fluvial and lacustrine facies were deposited in the Ordos Basin. During the Middle Triassic, red conglomerate and mudstone were deposited in its eastern margin, and gray green mudstone with intercalated coal seams was deposited in the middle. The Triassic structural deformation was sporadically documented in the Yanshan belt. In the Yanshan belt, the ductile shear zone concerns the E-W trending Chicheng-Fengning, Fengning-Longhua, and Damiao-Niangniangmiao ductile shear zones in the north (Wang et al., 2013; Zhang et al., 2014; Figure 2.1), and the E-W trending folds and thrusts include the Unnamed fault, Malanyu anticline, and Jixian thrust fault in the south (Davis et al., 2001; Ma et al., 2007).

During the Late Triassic, the Ordos Basin was generally a cratonic basin, characterized by the nature of the foreland depression in its southwest and rift in its northwest (Li et al., 2012). Several small-sized half-grabens were documented in the Helanshan and Zhuozishan to the southwest of the Ordos basin (Darby and Ritts, 2002; Ritts et al., 2004; Figure 2.1). Besides, only few small remnants of Late Triassic

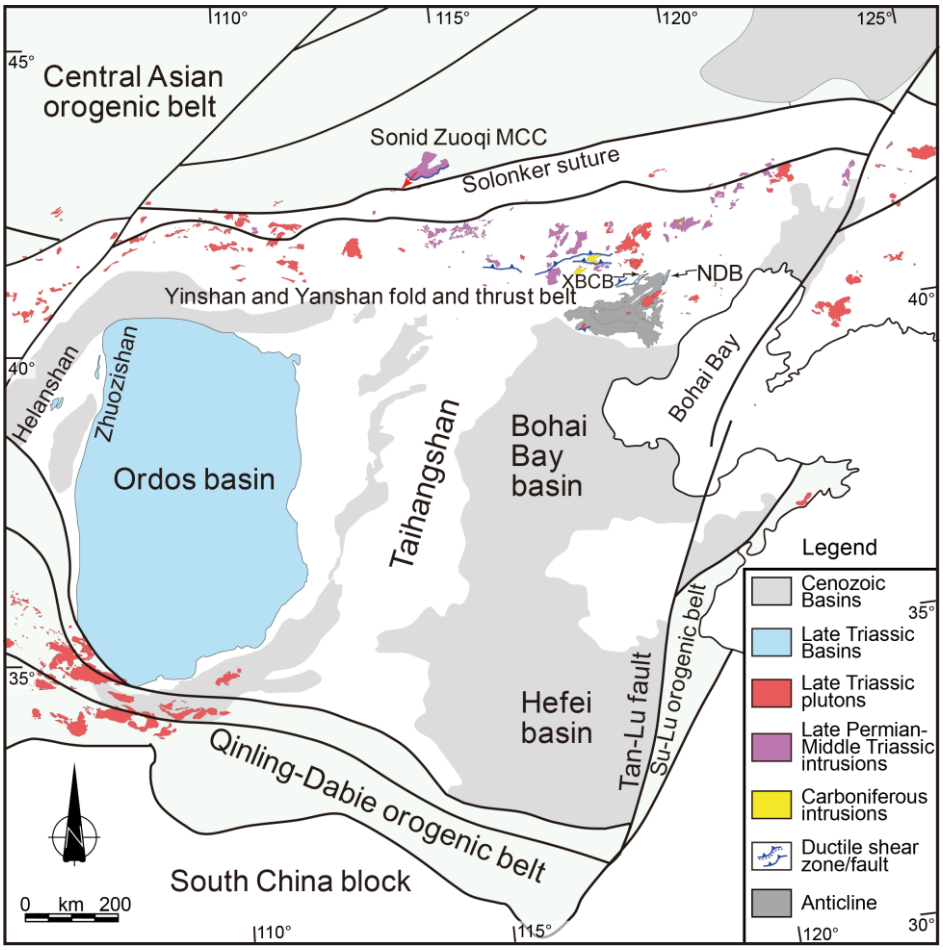

Figure 2.1 Triassic tectonic framework of the North China Craton

CFDS: Chicheng-Fengning ductile shear zone, FLDS: Fengning-Longhua, ductile shear zone, DNDS: Damiao-Niangniangmiao ductile shear zone

sedimentary basins can be observed in the northern NCB (i.e., Xiabancheng basin and Niuyingzi-Dengzhangzi basin in the Yanshan belt and Shiguai basin in the Yinshan belt; Davis et al., 2009; Meng et al., 2014; Meng et al., 2019). In the Xiabancheng basin, it was usually considered as a contractional tectonic setting during the Late Triassic-Early Jurassic according to the unconformity between Triassic and Lower Jurassic strata, and Lower Jurassic syntectonic conglomerate (Zhao, 1990; Liu et al., 2012). Detrital zircon dating and sedimentary studies suggest that the conformable Upper Triassic strata were

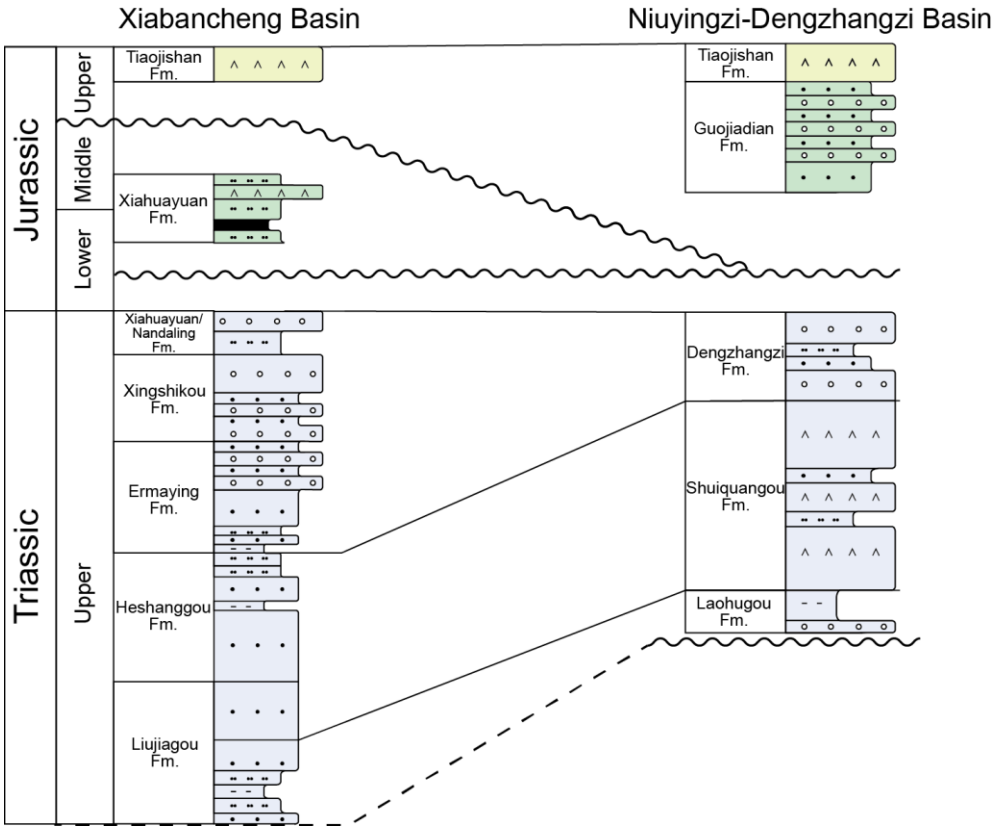

Figure 2.2 Stratigraphic correlation of the Triassic strata (Data from: Meng et al., 2019; Zhang et al., 2019)

deposited in an extensional setting (Davis et al., 2009; Meng et al., 2014; Meng et al., 2019). In addition, both the Shuiquangou Formation and Dengzhangzi Formation belong actually to the Upper Triassic strata (Zhang et al., 2019; Figure 2.2). The Shuiquangou Formation and Dengzhangzi Formation are controlled by the boundary normal faults (Davis et al., 2009). The gravity slide collapse deposits related to the extensional deformation was extensively identified in these areas (e.g., Davis et al., 2009; Hu et al., 2010).

2.2.2. Early-Middle Jurassic

The Upper-Lower Jurassic strata were distributed in the Ordos Basin, the Taihangshan, the Helanshan-zhuozishan, the Yinshan-Yanshan fold and thrust belt

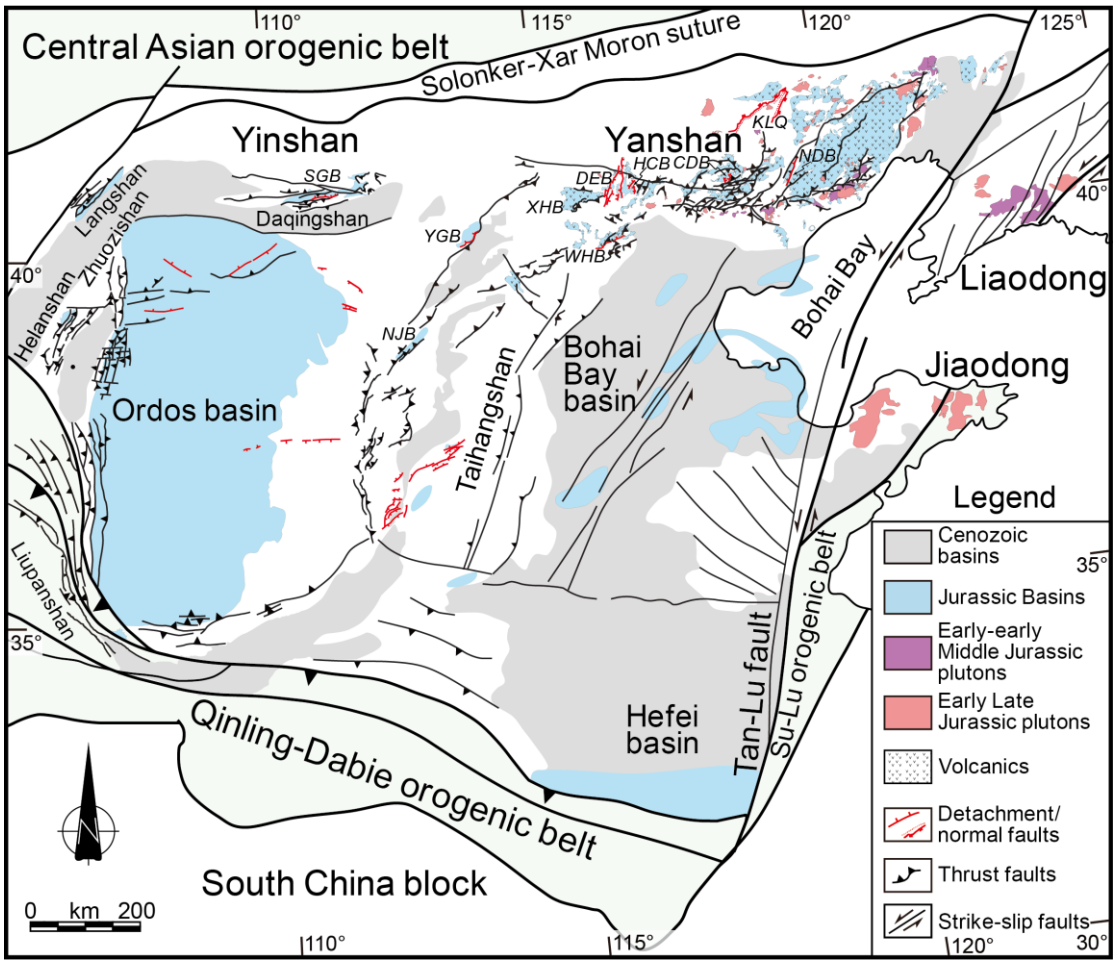

Figure 2.3 Jurassic-earliest Cretaceous tectonic framework of the North China Craton showing the Jurassic structures and magmatic rocks in the NCB (Modified from Zhang et al., 2007). SGB: Shiguai basin; YGB: Yungang basin; NJB: Ningwu-Jingle basin; XHB: Xuanhua basin; WHB: Western Hill basin; DEB: Diaoe basin; HCB: Houcheng basin; CDB: Chengde basin; NDB: Niuyingzi-Dengzhangzi basin; KLQ: Kalaqin metamorphic core complex. See Figure 1 for location. (Modified from Zhang et al., 2011)

(Figure 2.3). Regionally, the Lower Jurassic strata unconformably overlay the Upper Triassic (Meng et al., 2019). The Lower Jurassic strata were extensively distributed in areas mentioned above, e.g., the Fuxian and Yanan Formiations in the Ordos Basin its west, the Yongdingzhuang and Datong Formations in the Taihangshan, the Wudanggou

and Zhaogou Formations in the Daqingshan, the Nandaling and Yaopo Formations in the Western Hill of Beijing, the Xingshikou, Nandaling, and Xiahuayuan Formations in the Chengde-Xuanhua area, the Xinglonggou and Beipiao Formations in the western Liaoning (Figures 2.3-2.4). The Lower Jurassic strata contain abundant volcanic rock or pyroclastic rock in the Yanshan belt, and coal-bearing series in the whole North China (Figure 2.4). The structural and sedimentary studies suggested that the North China Craton was in an extensional setting during the Early-early Middle Jurassic (Darby et al., 2001; Ritts et al., 2001; Meng et al., 2019). The NNE-SSW or nearly N-S extensional normal faults were identified in the Upper Triassic-Lower Jurassic strata in the central and northeastern Ordos Basin (Zhang et al., 2011; Figure 2.3). In the Yungang and Guangling Basins, the normal faults cut the conglomerates in the lower Lower Jurassic, covered by the upper Lower Jurassic strata (Li et al., 2015; Figure 2.3). The sedimentary studies showed a fining and deepening upward depositional system from the Upper Triassic to Lower Jurassic strata, suggesting a Late Triassic extensional tectonic setting in the Lingwu-Jingle Basin (Meng et al., 2014; Li et al., 2015). In the southwestern Daqingshan, the E-W trending normal faults cut the unconformity between the Lower Jurassic and Archeozoic (Darby et al., 2001; Figure 2.4). The small-sized grabens were developed, dominated by the growth normal faults.

2.2.3. Event A of the Yanshanian Orogeny

Wong (1927) suggested that the unconformity at the bottom of Jurassic Tiaojishan Formation in Western Hill of Beijing is of regional tectonic significance, named

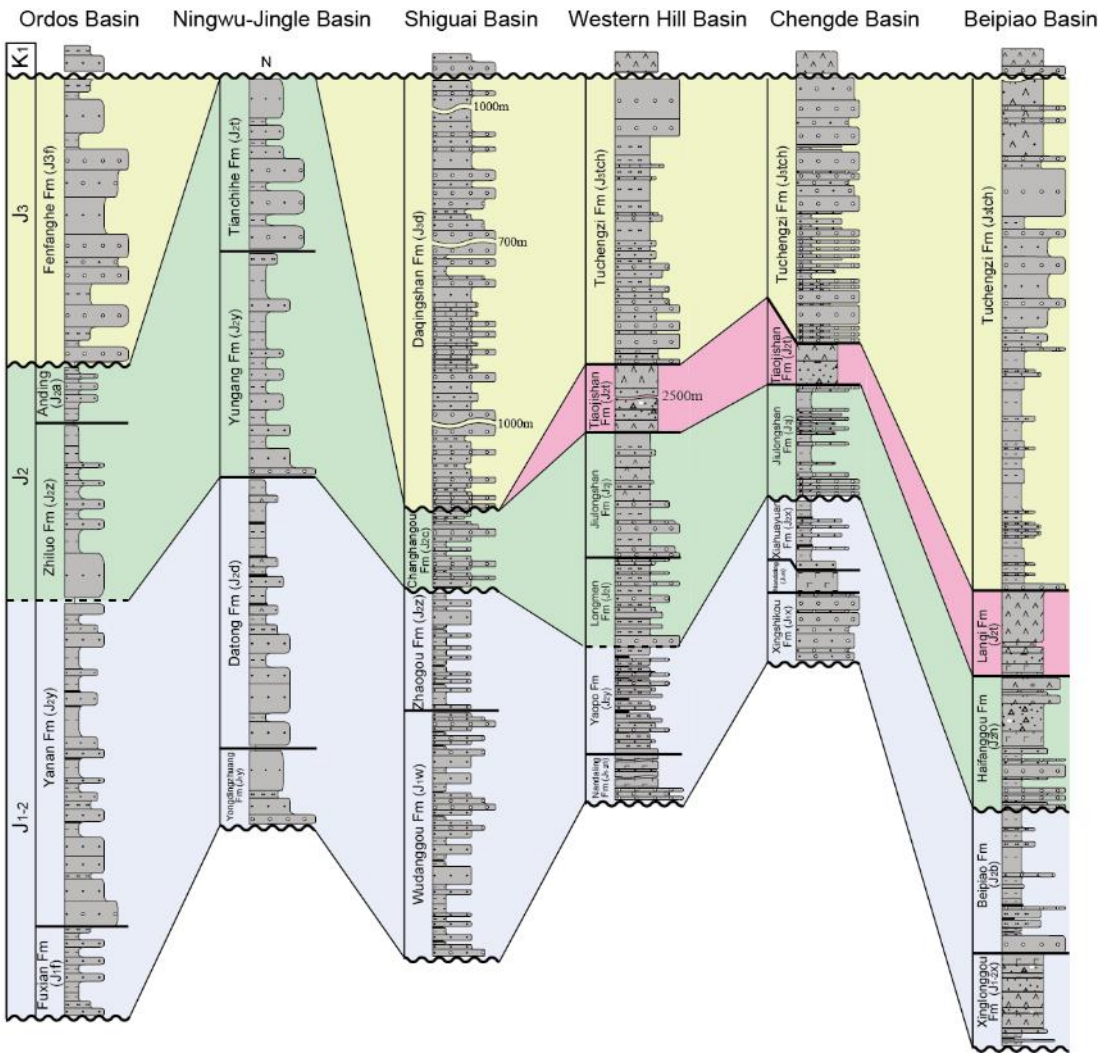

Figure 2.4 Stratigraphic correlation of the Jurassic-lowest Cretaceous strata (Modified from Darby et al., 2001)

"Yanshanian Orogeny". The Yanshanian Orogeny was divided into Event A, Intermediate phase, and Event B (Wong, 1929). The Event A, namely onset of the Yanshanian Orogeny, originated from the unconformity between the Tiaojishan Formation and the Jiulongshan Formation, presented as open folds (Figure 2.4). Afterward, Previous studies suggested that it is comformable between the Tiaojishan Formation and the Jiulongshan Formation in large area of the North China (Li et al., 2014). Recently, the prospecting trench and drilling indicated that the Tiaojishan

Formation, the Jiulongshan Formation, and the Longmen Formation all converge to an unconformity in space (Li et al., 2014). The Jiulongshan-Longmen Formations are a set of conglomerates as a molasse below the volcanics in the Tiaojishan Formation (Zhao et al., 1990), corresponding to the Haifanggou Formation in the western Liaoning (Figure 2.4). The Jiuongshan Formation consists of the thick terrestrial clastic rocks intercalated with the volcanic rocks, and conglomerates and tuff at the bottom (Figure 2.4). The Longmen Formation is absent in the Chengde area. Previous studies suggested there is no distinction between the Longmen Formation and the Jiulongshan Formation in the lithology (Li et al., 2014). It exists obvious sedimentary discontinuity between the Yaopo Formation and the Longmen Formation (Zhao, 1990; Li et al., 2014). The Event A is indicated by the parallel unconformity between the conglomerates in the Longmen Formation and the coal-bearing series in the Yaopo Formation in the Western Hill of Beijing (Li et al., 2014; Hao et al., 2019; Figure 2.4). The volcanics in the Tiaojishan Formation was only distributed in the Yanshan belt. However, the conglomerates below the volcanics in the Tiaojishan Formation were widely distributed in the North China (Figure 2.4), e.g., the Yungang Formation and the Tianchihe Formation in the Ningwu-Jingle Basin, Taihanshan (Li et al., 2015), the Changhangou Formation in the Shiguai Basin, Yanshan belt (Wang et al., 2017), and the Zhiluo Formation in the Ordos Basin (Zhang et al., 2011). Therefore, the Event A is presented by the unconformity between the conglomerates below the volcanics and underlying coal-bearing series (Figure 2.4).

Due to the discontinuous distribution of the conglomerates, the Event A was

presented as different contact relationships in different areas (Figure 2.4), e.g., parallel unconformity between the Longmen Formation and the Yaopo Formationin the Western Hill (Li et al., 2014; Hao et al., 2019), angular unconformity between the Jiulongshan Formation and the Xiahuayuan Formation (Liu et al., 2018), and angular unconformity between the Haifanggou Formation and the Beipiao Formation (Meng et al., 2019). In the Shiguai Basin, Yinshan, the Event A is suggested by the angular unconformity between the Changhangou Formation and the underlying Zhaogou Formation (Wang et al., 2017). The intense fold and thrust deformations in the coal-bearing series in the Wudanggou and Zhaogou Formations was covered by the growth strata in the Changhangou Formation (Wang et al., 2017). In the Yungang Basin, Taihangshan, it is angular unconformity between the Permian Shanxi Formation and the overlying Jurassic Tiaojishan Formation (Li et al., 2015). It is it is angular unconformity between the Tianchihe Formation and the underlying Datong Formation in the Ningwu-Jingle Basin, Taihangshan, presenting as the great changes in the Lithology, heavy minerals, sediment source and detrital zircon (Li et al., 2015).

However, Wong (1927) suggested that the volcanics in the Tiaojishan Formation overlay the different strata, indicating the intense deformation and erosion before the deposition of the the Tiaojishan Formation (Figure 2.3). The conglomerates below the Tiaojishan Formation are locally distributed in the Yanshan belt. In fact, the Event A was presented as the unconformity between the volcanics in the Tiaojishan Formation and the different underlying strata (Faure et al., 2012). The extensive deformations related to Event A have been overlaid by the volcanics in the Tiaojishan Formation. For

instance, the fold and thrust belt in the Proterozoic-Paleozoic strata were covered by the he volcanics in the Tiaojishan Formation, e.g., Mengjiazhuang anticline and Duanshuao-Jianbaoshan thrust fault (Li et al., 2016), Miyun-Xifengkou fault, Zhujiagou fault, Qingshuihu fault, Xinglong fault, Gaobanhe fault, Sanpo fault, Banbishan fault, and Lengkou fault (Chen, 1998, Davis et al., 2001; Zhang et al., 2004). This event was considered as northward thrust that occurred during post-161 Ma, pre-148 Ma?, pre-131 Ma according to the isotope chronology (Davis et al., 2001). Faure et al. (2012) and Li et al. (2016) suggested the Event A was related to the unconformity below the volcanics in the Tiaojishan Formation (172-164 Ma).

2.2.4. Intermediate phase of the Yanshanian Orogeny

Wong (1928) firstly described “Intermediate phase” as the volcanism stage, characterized by the volcanics in the upper and the conglomerates in the lower (Figure 2.4). As mentioned above, the Longmen Formation and Jiulongshan Formation, distributed locally in the Yanshan belt, might be the molasse after the Event A of the Yanshanian Orogeny. Alternatively, both the Longmen Formation and the Jiulongshan Formation belong to one set of conglomerates beneath the volcanics (Zhang et al., 2013). The Intermediate phase has been defined as the volcanism stage of the Tiaojishan Formation. The Tiaojishan Formation consists of dark purple, purple-brown, and gray-green andesite, amphibole andesite, pyroxene andesite, andesitic lava breccia, andesitic breccia, andesite agglomerate with purplish red, grayish brown and grayish-green sandstone, conglomerate, siltstone and mudstone (Li et al., 2014). Several rifts have been distinguished in the Yanshan belt, e.g., Diaoe graben and Houcheng half-graben

(Qi et al., 2015). A N-S striking graben was developed in the Jurassic strata in the hanging wall of the Chengde thrust (Davis et al., 2001). In the Niuyingzi-Dengzhangzi basin, the Middle Jurassic Guojiadian half-graben was dominated by the normal fault (Davis et al., 2009). Besides, the top-to-the NE detachment fault was developed in the Kalaqin MCC (156-150 Ma; Lin et al., 2014). However, the volcanics of the Tiaojiashan Formation are only distributed in the Yanshan belt and the north of the Taihangshan (Figure 2.3). In the western Liaoning, it corresponds to the Lanqi Formation (Figure 2.4). The coeval extensional basins are also distributed in the Yanshan belt (Figure 2.3). As mentioned above, the conglomerates below the volcanics are widely distributed in other areas (Figure 2.4). In the Shiguai basin of the Daqingshan, the Event A of the Yanshanian orogeny is characterized by the unconformity between the Zhaogou Formation and the Changhangou Formation (Figure 2.4), and the growth strata of the Changhangou Formation. Above it, the growth strata of the Daqingshan Formation overlie the Changhangou Formation (Wang et al., 2017; Figure 2.4). Therefore, the volcanism and coeval extensional basins in the intermediate phase could only occur in the eastern NCB (Figure 2.3).

2.2.5. Event B of the Yanshanian Orogeny

The Event B of the Yanshanian Orogeny occurred after the volcanism of the Tiaojishan Formation, characterized by the large-scale fold-and-thrust belts (Wong, 1928). In the Yanshan belt, the widely distributed conglomerates in the Tuchengzi/Houcheng Formation overlie the volcanics (Zhao et al., 1990; Cope et al., 2007; Li et al., 2016; Figure 2.4). The Event B corresponds to the unconformity between

the Tuchengzi/Houcheng Formation and the overlying Zhangjiakou Formation (Figure 2.4). The growth strata of Tuchengzi/Houcheng Formation consist of syn-tectonic conglomerates during the Event B of the Yanshanian orogeny (Fu et al., 2018; Liu et al., 2018).

The deformation of the Event B was widely distributed in the Yanshan belt. E-W striking fold and thrust belts were widely developed in the middle and western segments of the Yanshan belt, for instances, the Xuanhua fault, the Xiahuayuan fault, and the Jimingshan fault in the Xiaohuayuan basin (Zhang et al., 2006), the Xiaosuangou-Jiuchaigou fault and the Shangyi fault in the southeastern Shangyi basin (He et al., 1999), the Qianjiadian fault, the Shaliangzi fault, and the Tanghekou fault (<158Ma), the thrust nappe in the Shisanling (151-127Ma; Davis et al., 2001), the Sihetang thrust (151-143Ma) and Shanggu-pingquan fault (145-135Ma) and the Gubeikou fault (148-132Ma) (Davis et al., 2001). The paleostress along the dextral strike-slip faults is NW-SE direction (Lin et al., 2020). It is characterized by NE or NNE striking thrust and fold belts in the western Liaoning, e.g., the Lingyuan-Dongguanyingzi fault, the Nangongyingzi-Beipiao fault, the Jianchang-chaoyang fault and the Jingzhougou fault. These faults thrust onto the Lanqi/Tuchengqi Formation, and were overlaid by the Early Cretaceous Yixian Formation (Zhang et al., 2002; Davis et al., 2009; Hu et al., 2010).

Although the Tiaojishan/Lanqi Formation was only distributed in the Yanshan belt, the conglomerates in the Tuchengzi/Houcheng Formation and their counterparts were distributed in the whole NCB (Figure 2.4). In the Shiguai basin of the

Daqingshan, the Late Jurassic Daqingshan Formation, synchronous with the NW–SE compression, underlay the growth strata of the Changhangou Formation related to the Event A (Wang et al., 2017). In the western margin of the Ordos basin, the Middle Jurassic Anding Formation, involved in fold and thrust belt, was covered by the syn-tectonic conglomerates in the Fenfanghe Formation (Zhang et al., 2011). In the northern segment of the Taihangshan, the syn-tectonic conglomerates were developed in the footwall of the NNE striking Nanyangzhai-Heishiling fault (Wang et al., 2016). The unconformity between the Upper Jurassic Tuchengzi Formation and the lower Cretaceous Zhangjiakou Formation was developed in the Hunyuan basin (Li et al., 2015).

2.3. Triassic-Jurassic magmatism

The Triassic-Jurassic igneous rocks were widely distributed in the NCB. According to the isotope chronology, four stages of magmatism have been identified, i.e., Late Permian to Middle Triassic (262–236 Ma), Late Triassic (231–199 Ma), Early to Middle Jurassic (189–176 Ma), and Late Jurassic (155–145 Ma) (Figures 2.1and 2.3).

The Late Permian to Middle Triassic intrusive rocks (262–236 Ma) were mainly distributed in the Yinshan-Yanshan fold and thrust belt. These intrusive rocks are mainly composed of monzogranite, syenogranite and monzonite, with minor mafic rocks and granodiorite (Zhang et al., 2014). Some volcanics were developed in the Yanshan belt, e.g., the andesitic volcanic rocks in the Shuiquangou Formation. Late Permian–Middle Triassic intrusive rocks were derived from mixing of coeval mantle-

and crust-derived melts, linked to the postcollisional/postorogenic lithospheric extension and asthenospheric upwelling after the final collision of the Mongolian arc terranes with the North China craton (e.g., Zhang et al., 2009; Zhang et al., 2012).

The EW-trending Late Triassic alkaline intrusive complexes (e.g., nepheline syenite, quartz syenite, and A-type granite) and associated mafic rocks were widely developed along the northern NCB (Zhang et al., 2012). The Late Triassic alkaline intrusive complexes were mainly derived from the melts of subduction-modified enriched lithospheric mantle and ancient lower crust with some depleted asthenospheric mantle components during an intracontinental extensional setting (Yang et al., 2012; Zhang et al., 2014). It points to an upwelling of the asthenospheric mantle during the early lithospheric thinning or modification of the northern NCB. In the southern NCB, the Late Triassic igneous rocks, including Hornblende monzonite, quartz monzonite, quartz diorite, syenite and monzogranite, are mainly distributed in the Xiaoqingling area (Ding et al., 2011; Zhang et al., 2014). These rocks were originated from the partial melting of thickened lower crust, suggesting the postcollisional lithospheric extension after the collision of the South and North China blocks.

Early Jurassic–earliest Middle Jurassic igneous rocks are mainly distributed in the eastern NCB, including the Liaodong and Jiaodong peninsulas and the eastern Yanshan belt (Wu et al., 2005, 2011; Figure 2.3). The main rock types include granite, monzodiorite, monzonite, and syenite, as well as the volcanics in the Nandaling/Xinglonggou Formation. The volcanics are composed of basalt, andesite, andesite, dacite and a small amount of trachyte. The intrusive rocks were mainly

produced by partial melting of the ancient lower crust, whereas the volcanics were derived mainly from the ancient enriched lithospheric mantle (Wu et al., 2005; Yang et al., 2010). One group of researchers considers that the Early Jurassic–earliest Middle Jurassic igneous rocks are related to the subduction of the Paleo-Pacific plate, and the volcanic rocks are originated from the back-arc extension (Wu et al., 2005; Gao et al., 2004; Yang et al, 2010). Some scholars believe that it is an ongoing postcollisional lithospheric extension after the Mongolia arc terranes and the NCB (e.g., Zhang et al., 2014).

The Late Jurassic intrusive rocks are widely distributed in the Yanshan belt, the Liaodong area and Jiaodong Peninsulas in the eastern NCB, and the southern Yanbian–Liaobei area in the northeastern NCB and the northern North Korea (Wu et al., 2011; Figure 2.3). These intrusive rocks include monzogranite, syenite, diorite, monzonite and granite. The simultaneous volcanics are composed of the Tiaojishan Formation in the mid-western Yanshan belt and the Lanqi Formation in the eastern Yanshan belt, including andesite, basaltic andesite, andesitic tuff and trachyandesite, and minor rhyolite. Both the intrusive rocks and the volcanics were derived from partial melting of the ancient lower crust (e.g., Zhang et al., 2014). It was considered that the Late Jurassic igneous rocks are related to the subduction of the Paleo-Pacific plate (e.g., Wu et al., 2019).

Chapter 3. Emplacement of the Late Triassic granitic Dushan pluton

3.1. Introduction

The NCB is located on the southern border of the longest Paleozoic Central Orogenic Belt (CAOB), and this latter has been the target of numerous studies over the past decades, however, no common consensus has been reached on its time of formation among the geologists. One opinion considers that the Paleo-Asian Ocean had closed since the Devonian to form the CAOB (e.g., Xu & Chen, 1997; Xu et al., 2013; Zhao et al., 2013). Another argues that this event occurred along the Solonker zone during the Permo-Triassic time (e.g., Chen et al., 2000; Xiao et al., 2003; Jian et al., 2010; Eizenhöfer et al., 2014; Xiao et al., 2015; Figure 3.1). Therefore, the recognition of the Late Triassic tectonic context in the northern part of the NCB becomes essential to understand the evolution of the CAOB. Meanwhile, the North China Craton is often considered to be destroyed during the Late Mesozoic when it experienced extensive magmatism and deformation, characterized by metamorphic core complexes, detachment faults, fault-bounded half-grabens and a general thinning of the cratonic lithospheric mantle (e.g., Zhu et al., 2012; Wu et al., 2019). However, the onset of cratonic modification was considered to occur in an early time, for instance, in the Late Triassic (e.g., Han et al., 2004; Yang et al., 2010) or the Late Jurassic (e.g., Gao et al., 2004). Consequently, the Late Triassic tectonic setting is also crucial to improve our understanding of the evolution of the NCB.

In the Late Triassic, the EW-trending alkaline intrusive complexes (e.g., nepheline syenite, quartz syenite, and A-type granite) and associated mafic rocks were widely developed along the northern NCB (Zhang et al., 2012; Figure 3.1). Over the past decades, isotope chronology and geochemical works suggested that the Late Triassic alkaline intrusive complexes were mainly derived from the melts of subduction-modified enriched lithospheric

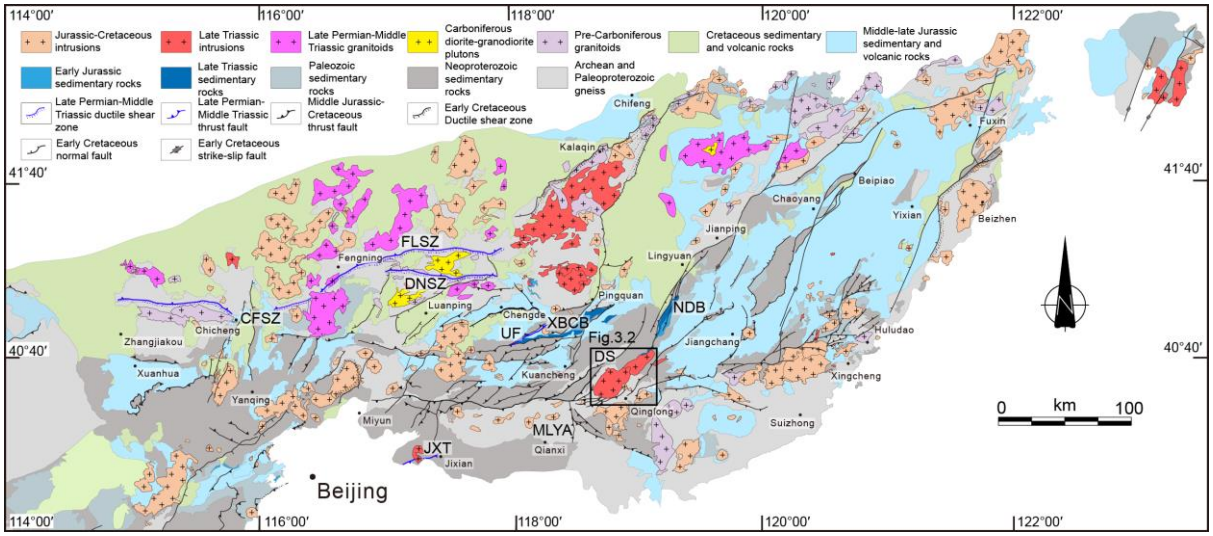

Figure 3.1 Simplified geological map of the Yanshan fold and thrust belt. CFSZ: Chicheng-Fengning ductile shear zone, FLSZ: Fengning-Longhua, ductile shear zone, DNSZ: Damiao-Niangniangmiao ductile shear zone, UF: Unamed fault, JXT: Jixian thrust, MLYA: Malanyu anticline, XBCB: Xiabancheng basin, YZB: Yingzi basin, NDB: Niuying-Dengzhangzi basin, DS: Dushan pluton.

mantle and ancient lower crust with some depleted asthenospheric mantle components during an intracontinental extensional setting (Yang et al., 2012; Zhang et al., 2014). It points to an upwelling of the asthenospheric mantle during the early lithospheric thinning or modification of the northern NCB. Nevertheless, the Triassic strata in the northern NCB are only exposed in few small remnant basins (i.e., Xiabancheng and Niuyingzi-Dengzhangzi basins; Figure 3.1). Detrital zircon dating and sedimentary studies suggest that the conformable Upper Triassic to Lower Jurassic strata were deposited in an extensional setting (Davis et al., 2009; Meng et al., 2014). The Late Triassic tectonic regime remains poorly constrained due to the difficulty of structural investigation in few small remnant basins.

Deciphering the interplay existing between tectonics and granitic pluton emplacement mechanisms is of fundamental importance for the understanding of the evolution of the continental crust (e.g., Bouchez & Gleizes, 1995; Gleizes et al., 1997; De Saint Blanquat et al., 2011; Žák et al., 2011). During the emplacement of granitic plutons, magmatic fabrics

could not only record mineral shape preferred orientation in the magma flow but also retain information on strain field to which the magma was subjected (Paterson et al., 1989; Bouchez et al., 1997; Žák et al., 2012; 2013). The solid-state fabrics record structural deformation after complete crystallization of the magma (Paterson et al., 1989). Consequently, structural studies of granite plutons have been used for their potential in recording the tectonic regime coeval with their emplacement (e.g., Bouchez & Gleizes, 1995; Žák et al., 2008; Lin et al., 2013). Up to now, the Late Triassic plutons in the northern NCB have not been the subject of structural studies that would shed light on Late Triassic tectonic regime. To offer direct structural evidence on the Late Triassic granite emplacement, the Dushan pluton in the Yanshan fold-and-thrust belt (YFTB) was chosen for this study. On the basis of a multidisciplinary investigation, including structural geology, isotope chronology, AMS measurement, and gravity modeling, this study reveals the emplacement mechanism of the Late Triassic Dushan pluton and coeval tectonic regime.

3.2. Geological overview of the YFTB

After its cratonization during the Paleoproterozoic (Zhao et al., 2001), the NCB was overlain by a Mesoproterozoic to Permian sedimentary cover, separated by a regional unconformity between the Middle Ordovician and Upper Carboniferous–Permian strata (Li et al., 2016). The geological evolution of the YFTB began in the Late Paleozoic–Early Mesozoic, resulting possibly from the closure of the Paleo-Asian Ocean (Davis et al., 2001; Xiao et al., 2003; Xu et al., 2013). The related deformation was featured by the E–W trending ductile shear zones (e.g., Chicheng-Fengning, Fengning-Longhua, and Damiao-Niangniangmiao ductile shear zones) and thick- and thin-skinned folds and faults (e.g., Unnamed fault, Malanyu anticline, and Jixian thrust) (Wang et al., 2013; Figure 3.1). The Late Paleozoic–Early Mesozoic magmatism is widely developed in the YFTB (Zhang et al., 2014; Figure 3.1c).

The intra-continental deformation and magmatism, traditionally referred to as the Yanshanian movement, occurred during the Jurassic to Cretaceous. The NE- and E–W-trending thrust faults are distributed throughout the YFTB (e.g. Davis et al., 2001; Faure et al., 2012; Figure 3.1). The YFTB generally trends E–Wwards, but NE–SWwards in the east. Several generations of out-of-sequence thrusts took place during the Middle Jurassic to Cretaceous and crosscut preexisting southward verging E–W trending fold-and-thrust belt (Li et al., 2016). Several Jurassic to Cretaceous fault-bounded basins, related to multi-phase thrusting events, are widely distributed in the YFTB, whereas the Triassic strata are only exposed in few small remnant basins as mentioned above (Figure 3.1).

During the Early Cretaceous, extensional tectonics became prevalent in the NCB and superimposed on the YFTB. Early Cretaceous magmatism, rift basins, and metamorphic core complexes are widely developed in the NCB and its adjacent regions (Lin & Wei, 2018; Figure 3.1c).

3.3. Field Observations in the Dushan pluton

3.3.1. Lithological Units and Bulk Architecture

The Dushan pluton intrudes into the northeast part of the E–W trending Malanyu anticline (Figure 3.1). To the northeast of the Dushan pluton, the Dashizhu pluton consists mainly of granite and granodiorite (Ye et al. 2014; Xiong et al., 2017; Figure 3.2). The country rocks, composed of Archaean gneiss (Qianxi Group) and Proterozoic unmetamorphosed carbonates (Changcheng group and Jixian group), are deformed by NE–SW striking fold-and-thrust belts (Figure 3.2). Around the Dushan pluton, the contact with the country rocks is sharp with a regular elliptical shape (Figures 3.2 and 3.3a). The foliation in the gneiss dips mainly at moderate to high angles to the NNW or SSE (Figure 3.3b). Some post-folial folds can be observed (Figure 3.3c). Close to the contact, the foliation of the gneiss is roughly parallel to

the border of the Dushan pluton (Figure 3.2). The arc-shaped fold-and-thrust belt appears on the northwestern side of the Dushan pluton (Figure 3.3d). The planar structures of the country rocks unwrap along the elliptical contact of the pluton. It seems that country-rock structures were deflected by the Dushan pluton.

3.3.2. Fabric and Structure of the Dushan Pluton

The Dushan pluton, which extends ~30 km along a NE-SW long axis, consists of monzogranite with a biotite-rich marginal facies (Figure 3.2; Ye et al. 2014; Jiang et al., 2018). There is no clear contact between them. Mineral fabrics are well developed in the southwest

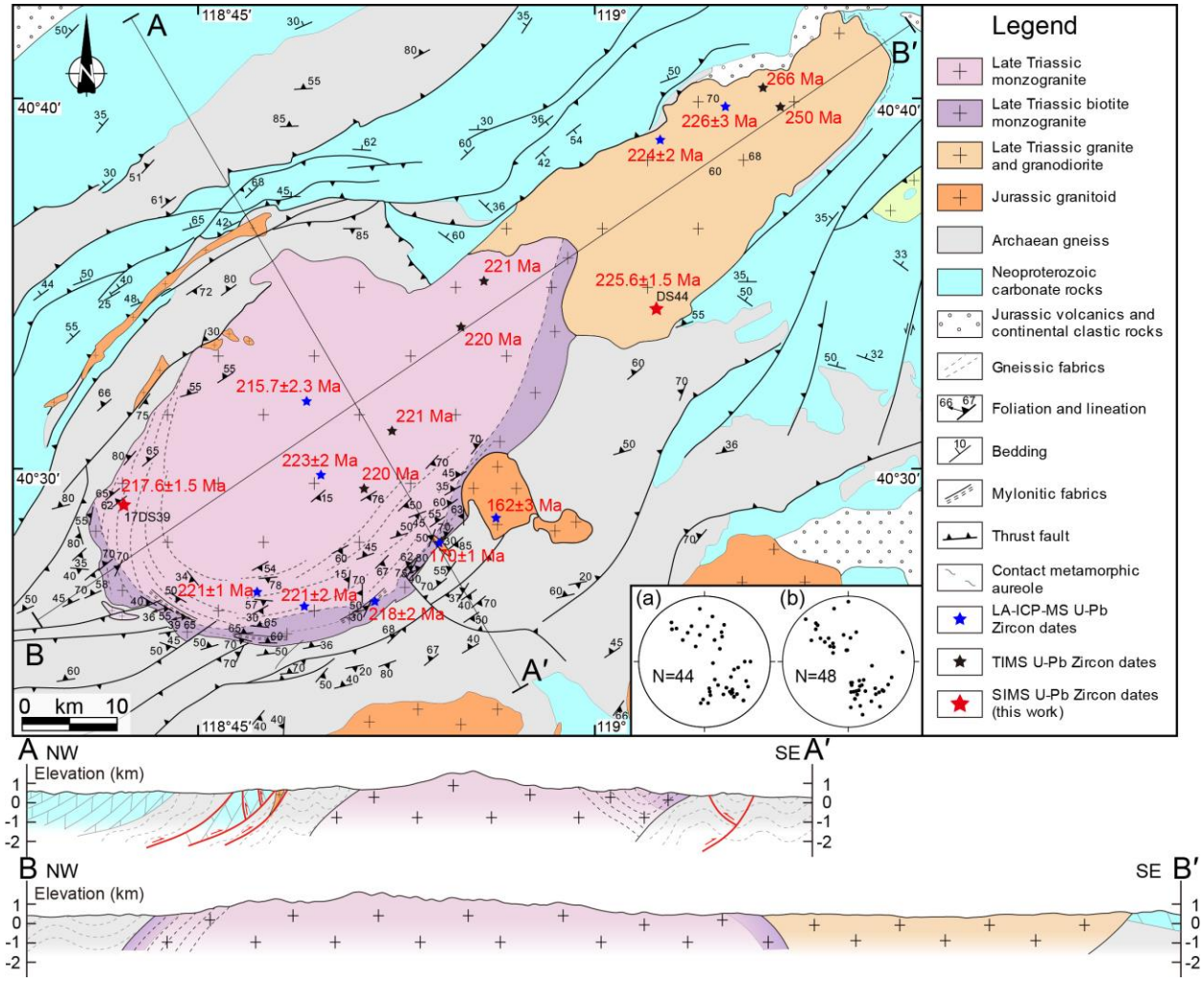

Figure 3.2 Structural geological map of the Dushan pluton and adjacent area. U–Pb zircon data from: Jiang et al. (2018); Luo et al. (2003); Xu et al. (2016); Ye et al. (2014); Xiong et al. (2017). (a) Stereonet for foliations in the Dushan pluton; (b) Stereonet for foliations in the country rocks.

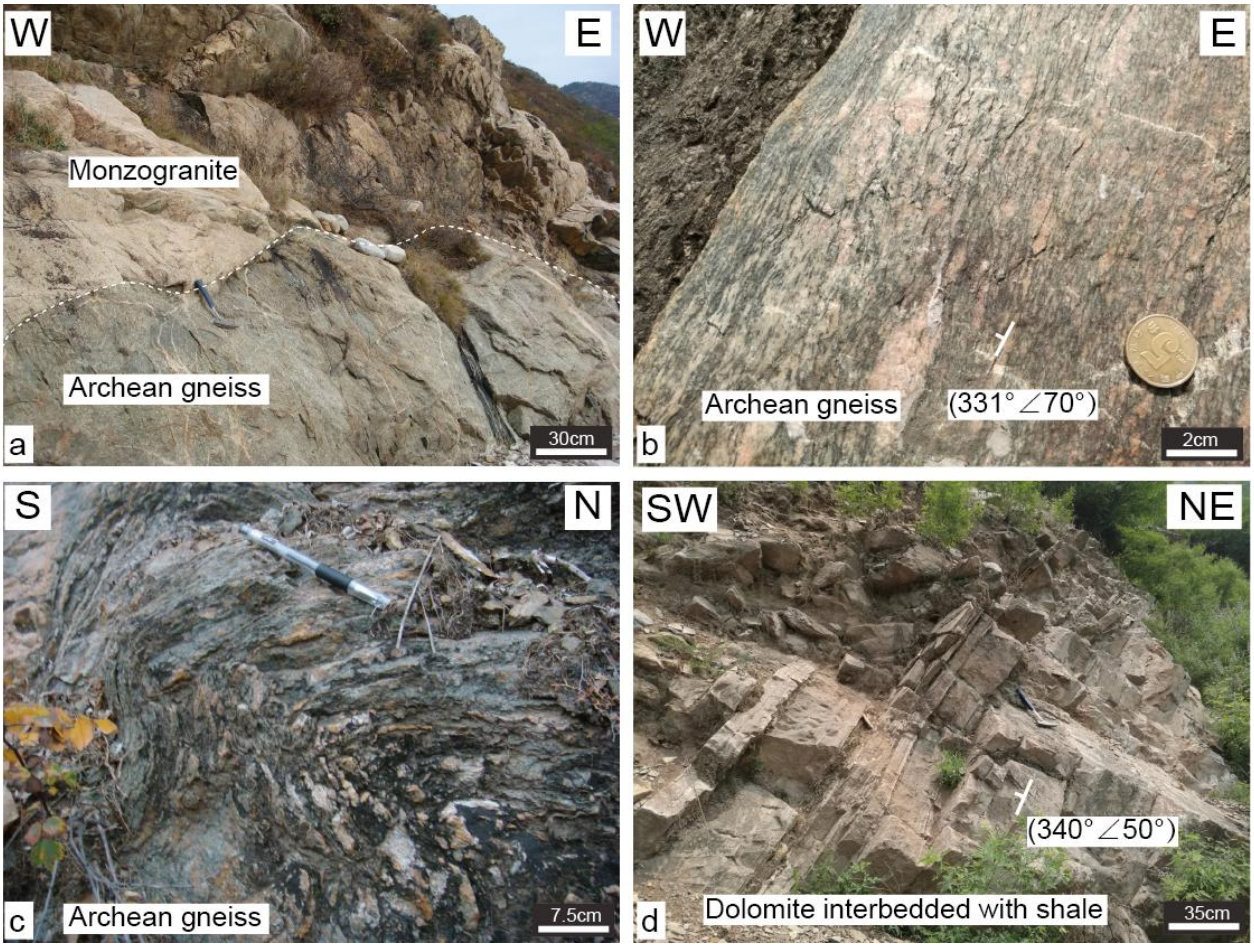

Figure 3.3 Field photographs of the country rocks. (a) Western contact between the Dushan pluton and its country rocks. (b) Country rocks in the southeast of the Dushan pluton. (c) Folded gneiss to the south of the Dushan pluton. (d) Country rocks in the north of the Dushan pluton.

part of the Dushan pluton, whereas its central and northeastern parts display only weak planar fabrics or appear isotropic (Figure 3.2 and 4a-4b). The plagioclase, K-feldspar, and quartz crystal have euhedral to sub-euhedral habitus, biotite and amphibole are randomly distributed without any preferred orientation. The pluton varies from isotropic monzogranite in its northeast to arc-shaped gneissosity, with locally mylonitic zones in its southwestern margin (Figure 3.2). The transition between the gneissic, up to mylonitic fabrics and the isotropic fabrics is gradational without sharp contacts. The southward increase of deformation toward the pluton border is illustrated by a fabric evolution, ranging from a poorly-defined foliation to a gneissic foliation striking parallel to the pluton margin (Figures 3.2 and 3.4c-3.4d). The

gneissosity is marked by oriented K-feldspar megacrysts and biotite platelets (Figures 3.2 and 3.4c-3.4d). Strongly flattened xenoliths, parallel to the gneissosity, are common in the

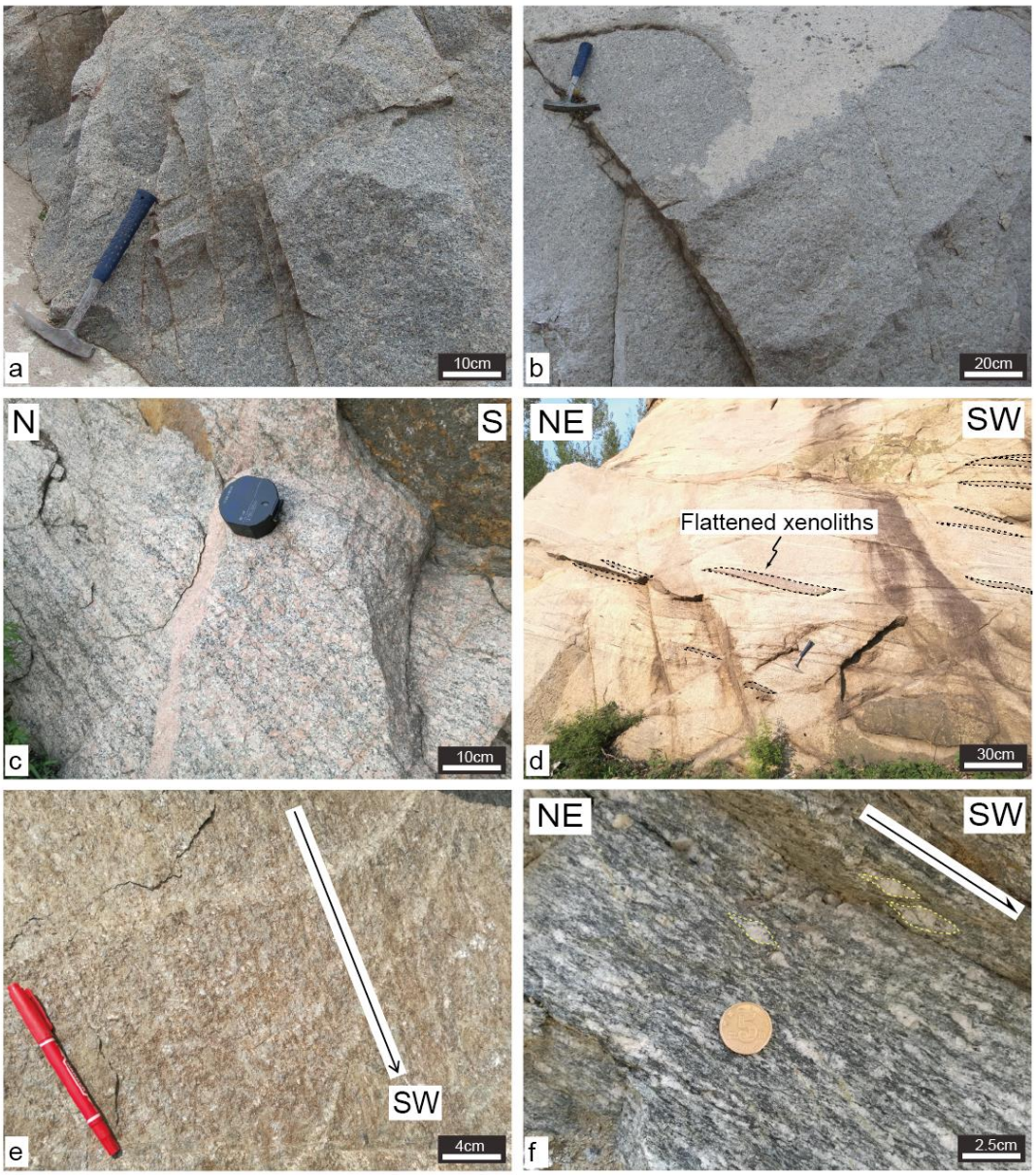

Figure 3.4 Field observations of the Dushan pluton. (a) Isotropic monzogranite in the northeastern part of the Dushan pluton. (b) Isotropic monzogranite in the central part of the Dushan pluton. (c) Foliation defined by biotite flakes and K-feldspar (southwest of the Dushan pluton). (d) Flattened xenoliths (southwest of the Dushan pluton). (e) NE-SW trending mineral lineations in mylonitic monzogranite of the Dushan pluton. (f) Sigmoidal feldspar porphyroclasts in mylonitic monzogranite in the Dushan pluton, showing a top-to-the-SW shearing (The section is parallel to lineation and perpendicular to foliation).

southwestern border of the Dushan pluton (Figure 3.4d), without evident stretching lineations. Close to the southeastern contact with the country rocks, the foliation dips toward the interior of the pluton (Figure 3.2). This southwestern part of the pluton also reveals a mylonitic fabric with a well-defined lineation that locally develops (Figures 3.2 and 3.4e-3.4f). The mylonite exhibits a margin-parallel foliation with NE-SW trending lineation outlined by plagioclase and K-feldspar crystals that consistently plunge 30°–40° to the southwest. Along the SW-plunging (N210°E) lineation (Figure 3.4e), Sigmoidal shaped K-feldspars indicated a top-to-the-SW shearing (Figure 3.4f). Note that similar mylonitic fabrics are not present in the country rocks close to the pluton.

3.4. Microscopic Observation

Microstructural investigations of the plutons provide insights into the crystallization-deformation relationships from magma cooling to post-solidus fabrics (Paterson et al., 1989). Magmatic fabric is recorded when the pluton does not suffer solid-state deformation, whereas a solid-state fabric characterizes a deformation after magma full crystallization (e.g., Talbot et al., 2004). In the Dushan pluton, microscopic observations were performed to establish the relationships between the minerals and magnetic fabrics. Through observations of more than sixty thin-sections, three microscopic fabric types can be distinguished in the Dushan pluton (Figure 3.5).

(1) Magmatic fabrics and weak solid-state fabrics. The magmatic fabrics concern the northeastern Dushan pluton (Figures 3.5a and 3.5g). Quartz crystals are anhedral, non-deformed, and do not exhibit obvious shape preferred orientation. Joints in quartz grains are planar or weakly lobate (Figure 3.5a). However, a weak solid-state overprint is also commonly present in the Dushan pluton (Figures 3.5b and 3.5g). Millimeter-sized quartz grains show a weak undulose extinction. Sometimes, small well-individualized quartz

grains occur at the border of the coarse grains (Figure 3.5b) suggesting that they underwent slight dynamic recrystallization. The euhedral biotite flakes have a sharp extinction and are neither kinked nor bent. Significant solid-state deformation has not been observed. Hence, these weak solid-state fabrics are probably acquired mainly under high-temperature subsolidus conditions, indicative of submagmatic to solid-state flow.

(2) Moderate solid-state fabrics. Many samples from the southwestern part and local areas of the northeastern part of the Dushan pluton exhibit moderate solid-state fabrics. Quartz grains display intensive dynamic recrystallization and are replaced by aggregates of newly formed grains (Figures 3.5c-3.5d and 3.5g). Numerous subgrains with serrated boundaries display a conspicuous undulose extinction. The biotite grains are kinked and bent. The quartz grains are organized into ribbons and form a gneissosity. At this stage, the plagioclase and K-feldspars do not display any recrystallization or deformation suggesting low-grade temperature conditions during deformation (300–400°C; Passchier & Trouw, 2005).

(3) Strong solid-state microstructures. Approaching the southern border of the Dushan pluton, the monzogranite is locally mylonitized (Figures 3.5e-3.5g). Quartz aggregates with irregular grain boundaries record widespread recrystallization by subgrain rotation. The biotite flakes are commonly elongate, kinked and bent but plagioclase grains and K-feldspars are devoid of ductile deformation. Extremely fine-grained quartz and feldspar sigma-type tails occur on K-feldspar and plagioclase residual phenoclasts, suggesting temperature conditions between 300 and 400°C (Passchier & Trouw, 2005) and pointing to a top-to-the-SW sense of ductile shearing in the locally mylonitic structures (Figure 3.5f). In short, an increase intensity of solid-state fabrics is observed in the Dushan pluton from the northeast to the southwest (Figure 3.5g), without sharp boundaries between fabric types. Mylonitic fabrics develop in the southernmost part of the pluton, close to the

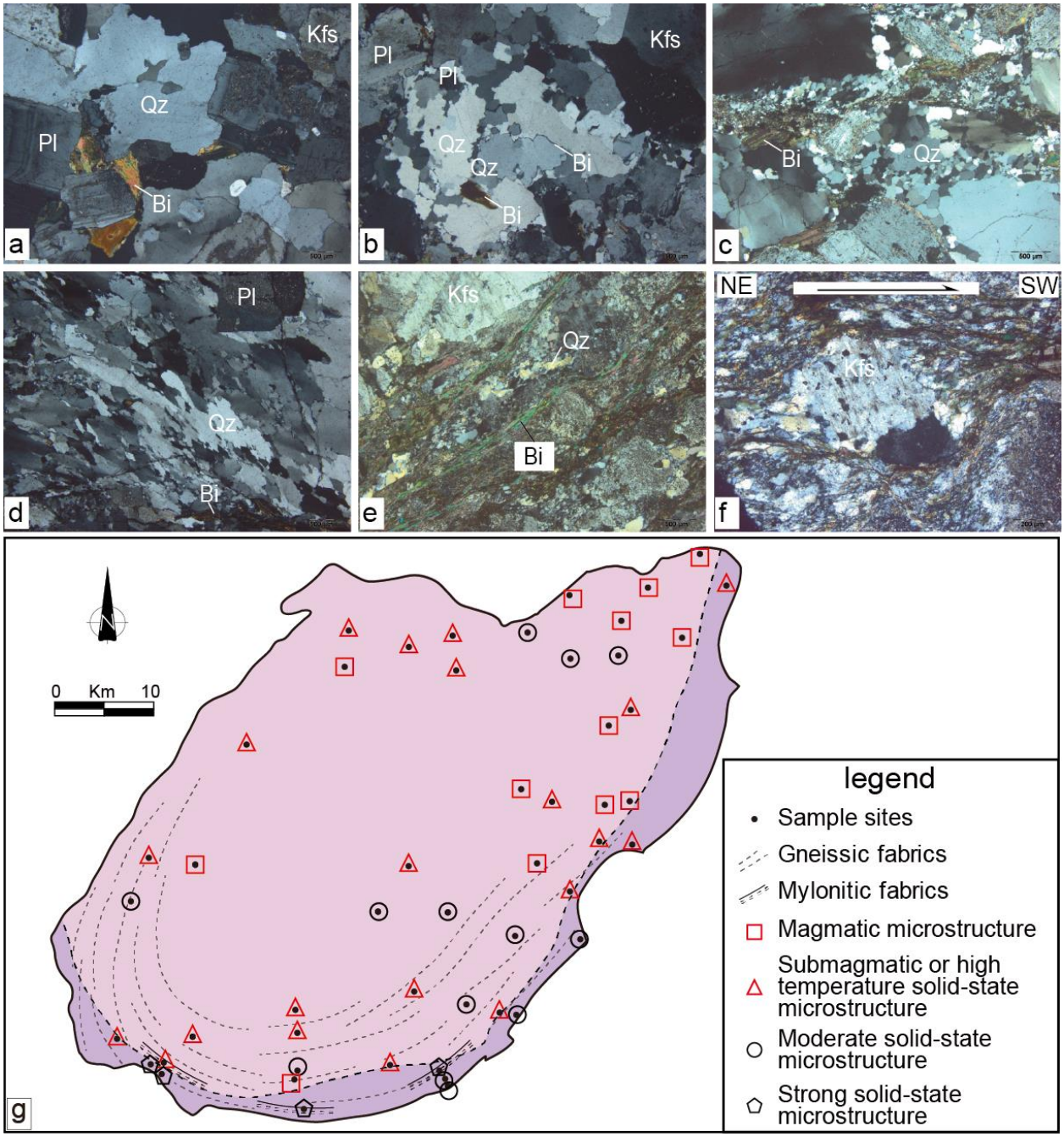

Figure 3.5 Microstructures of typical investigated samples in the Dushan pluton. (a) Magmatic microstructures in the northeastern part of the Dushan pluton. (b) Submagmatic or high temperature solid-state microstructures in the northern Dushan pluton. (c) Moderate solid-state microstructures in the central Dushan pluton. (c) Moderate solid-state microstructures in the southern Dushan pluton. (e) Strong solid-state microstructures in the southern Dushan pluton. (f) Strong solid-state microstructures in mylonitic monzogranite of the Dushan pluton. (g) Distribution map of the different types of microstructures. Bi = biotite, Kfs = K-feldspar, Pl = Plagioclase, Qz = quartz.

contact with the country rocks.

3.5. New Dating Results

Several isotope chronology data have been documented in the Dushan pluton and its neighboring Dashizhu pluton (Figure 3.2). Late Triassic ages are rather consistent for the Dushan pluton (223–215 Ma; Luo et al., 2003; Ye et al., 2014; Xu et al., 2016; Jiang et al., 2018), and they are relatively close to those of the Dashizhu pluton ranging from 266 to 224 Ma (Ye et al., 2014; Xiong et al., 2017). To clarify temporal precedence between two plutons, new zircon U-Pb dating was performed by a Cameca IMS 1280 large-radius SIMS at IGGCAS. Samples 17DS39 and DS44 are collected from the monzogranite in the western Dushan pluton and the granodiorite in the southern Dashizhu pluton, respectively (Figure 3.2).

The zircon grains from these two samples are subhedral, transparent, and 50–150 μm in length with aspect ratios between 1:1 and 3:1. CL images show clear oscillatory zoning (Figure 3.6a). Th/U ratios of Sample 17DS39 vary from 0.14 to 1.21. Twenty-one analyses of the $^{206}Pb/^{238}U$ and $^{207}Pb/^{235}U$ results plotted on a Concordia diagram are relatively consistent, yielding a Concordia age of 217.6±1.5 Ma, interpreted as the Late Triassic crystallization age of the Dushan pluton (Figure 3.6b, Table 3.1). Th/U ratios of Sample DS44 range from 0.71 to 1.66. Twenty-one analyses of the $^{206}Pb/^{238}U$ and $^{207}Pb/^{235}U$ results, excluding one inherited grain at 2437 Ma, show a Concordia age of 225.6±1.5 Ma (Figure 3.6b, Table 3.1). It corresponds to the Late Triassic emplacement age of the Dashizhu pluton.

3.6. Measurement of Anisotropy of Magnetic Susceptibility

Planar fabrics are hardly observable in the northeastern and central parts of the Dushan pluton, and when a planar fabric can be observed, the mineral lineation never shows up, except within the mylonites. It is well-established that magnetic fabrics record the fabric elements of

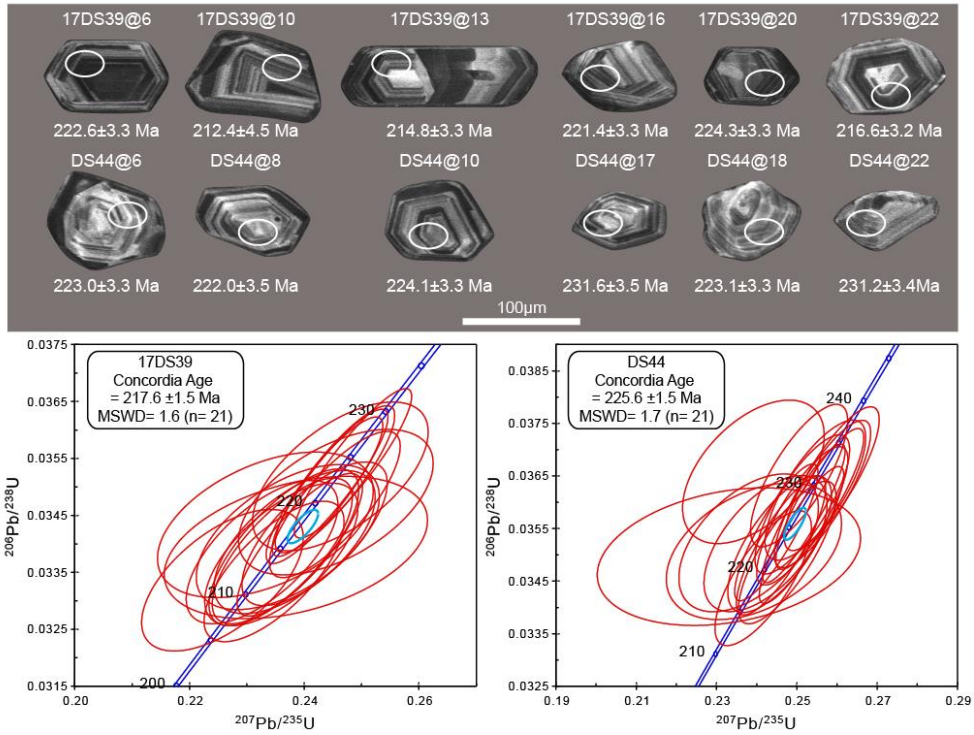

Figure 3.6 Cathodoluminescence (CL) images and U-Pb diagrams of Concordia age of representative zircons from collected samples. White elliptical circles are Secondary Ion Mass Spectrometer (SIMS) analysis locations; the numbers are ages. MSWD: mean square of weighted deviates.

anisotropic rocks where macro and microscopic features cannot be observed (Archanjo et al., 1994; Bouchez & Gleizes, 1995; Bouchez et al., 1997; Benn et al., 2001). An AMS study has been therefore carried out on the Dushan pluton in order to reveal its magnetic fabrics and set up the surface structure of the pluton. It is worthy to notice that the AMS study has not been performed in the neighboring coeval Dashizhu pluton due to the poor outcrop conditions.

3.6.1. Sampling and Measurements

A total of 252 cores from 41 sampling sites have been collected in the Dushan pluton. Five to eight cores of 2.5 cm in diameter have been sampled from each site. In the laboratory, each core was cut into cylindrical specimens of 2.2 cm in length. A KLY4 susceptometer was used to measure both the anisotropy magnetic susceptibility and the bulk susceptibility (Figure 3.7). The statistical analysis of the AMS data was carried out using the ANISOFT package (Jelinek, 1981) that calculates the mean orientation of three principal axes of the AMS ellipsoid ($K_1 \geq$

Table 3.1 SIMS zircon U-Pb data of the collected samples in the Dushan pluton.

Sample spot	U (ppm)	Th (ppm)	Th/U	f_{206} (%)	$^{207}Pb/^{206}Pb$	±σ (%)	$^{207}Pb/^{235}U$	±σ (%)	$^{206}Pb/^{238}U$	±σ (%)	$t_{207/206}$(Ma)	±σ (Ma)	$t_{207/235}$(Ma)	±σ (Ma)	$t_{206/238}$(Ma)	±σ (Ma)
17DS39@01	458	384	0.838	0.54	0.05127	2.39	0.24552	2.82	0.0347	1.50	252.9	54.0	222.9	5.7	220.1	3.2
17DS39@02	400	350	0.875	0.05	0.05129	1.15	0.24534	1.90	0.0347	1.51	253.9	26.2	222.8	3.8	219.8	3.3
17DS39@03	802	312	0.390	0.27	0.05056	0.76	0.24451	1.69	0.0351	1.50	221.0	17.6	222.1	3.4	222.2	3.3
17DS39@04	783	107	0.136	1.60	0.05041	2.29	0.23715	2.75	0.0341	1.52	214.0	52.2	216.1	5.4	216.3	3.2
17DS39@05	191	67	0.351	0.29	0.05053	1.53	0.23646	2.26	0.0339	1.66	219.4	35.1	215.5	4.4	215.2	3.5
17DS39@06	2441	1537	0.630	0.53	0.05065	0.87	0.24537	1.73	0.0351	1.50	224.9	19.9	222.8	3.5	222.6	3.3
17DS39@07	147	178	1.214	0.17	0.05077	2.04	0.24631	2.54	0.0352	1.52	230.5	46.3	223.6	5.1	222.9	3.3
17DS39@08	534	94	0.175	0.15	0.05106	1.10	0.23923	1.87	0.0340	1.51	243.3	25.2	217.8	3.7	215.4	3.2
17DS39@09	143	47	0.328	0.08	0.05079	1.87	0.23834	2.41	0.0340	1.51	231.5	42.7	217.1	4.7	215.7	3.2
17DS39@10	617	299	0.484	0.42	0.04984	1.76	0.23266	2.32	0.0339	1.52	187.6	40.4	212.4	4.5	214.6	3.2
17DS39@11	106	66	0.622	0.33	0.05098	3.63	0.23855	3.93	0.0339	1.50	240.0	81.7	217.2	7.7	215.1	3.2
17DS39@12	406	92	0.227	0.09	0.05080	1.50	0.23475	2.12	0.0335	1.50	231.7	34.3	214.1	4.1	212.5	3.1
17DS39@13	386	327	0.845	0.13	0.05057	1.44	0.23618	2.11	0.0339	1.54	221.1	33.0	215.3	4.1	214.8	3.3
17DS39@14	322	279	0.867	0.11	0.05132	1.52	0.24182	2.14	0.0342	1.51	255.1	34.5	219.9	4.2	216.6	3.2
17DS39@15	294	213	0.724	0.26	0.04908	2.05	0.22575	2.55	0.0334	1.52	151.5	47.3	206.7	4.8	211.6	3.2
17DS39@16	1105	625	0.566	0.15	0.05055	0.81	0.24353	1.71	0.0349	1.50	220.3	18.6	221.3	3.4	221.4	3.3
17DS39@17	165	112	0.677	0.30	0.04927	2.92	0.23323	3.30	0.0343	1.52	160.6	67.0	212.9	6.3	217.6	3.3
17DS39@18	460	193	0.420	1.95	0.03938	3.98	0.18873	4.25	0.0348	1.50	-391.6	100.5	175.5	6.9	220.3	3.2
17DS39@19	489	83	0.170	3.21	0.03629	5.20	0.17597	5.41	0.0352	1.51	-608.9	136.0	164.6	8.3	222.8	3.3
17DS39@20	1017	668	0.657	0.17	0.05089	0.74	0.24850	1.68	0.0354	1.51	235.9	16.9	225.4	3.4	224.3	3.3
17DS39@21	329	122	0.372	0.26	0.05062	1.75	0.23601	2.31	0.0338	1.51	223.6	39.9	215.2	4.5	214.4	3.2
DS44@01	312	275	0.881	1.25	0.04591	3.65	0.21627	3.97	0.0342	1.56	-7.0	85.8	198.8	7.2	216.6	3.3
DS44@02	989	878	0.888	0.05	0.05102	0.72	0.25174	1.67	0.0358	1.50	241.5	16.6	228.0	3.4	226.7	3.4
DS44@03	408	678	1.659	2.13	0.04835	5.54	0.23308	5.75	0.0350	1.53	116.3	125.7	212.7	11.1	221.6	3.3
DS44@04	448	394	0.878	1.51	0.04388	3.33	0.22084	3.65	0.0365	1.51	-117.6	80.1	202.6	6.7	231.1	3.4
DS44@05	232	170	0.735	0.01	0.16591	1.20	10.51154	2.09	0.4595	1.71	2516.8	20.0	2480.9	19.6	2437.3	34.9
DS44@06	477	404	0.848	0.04	0.05062	1.53	0.24573	2.15	0.0352	1.51	223.7	34.9	223.1	4.3	223.0	3.3
DS44@07	424	304	0.717	0.29	0.05073	1.03	0.24606	1.84	0.0352	1.53	228.8	23.6	223.4	3.7	222.9	3.4
DS44@08	294	209	0.710	0.25	0.05124	1.23	0.24760	2.01	0.0350	1.58	251.8	28.1	224.6	4.0	222.0	3.5
DS44@09	592	452	0.764	0.00	0.05014	0.87	0.24491	1.73	0.0354	1.50	201.4	20.0	222.4	3.5	224.4	3.3
DS44@10	870	829	0.953	0.05	0.05149	0.82	0.25116	1.71	0.0354	1.50	262.9	18.7	227.5	3.5	224.1	3.3
DS44@11	597	598	1.001	0.81	0.04949	3.41	0.23931	3.73	0.0351	1.51	171.3	77.6	217.9	7.3	222.2	3.3
DS44@12	840	790	0.941	0.24	0.05097	1.33	0.25461	2.01	0.0362	1.50	239.4	30.5	230.3	4.1	229.4	3.4
DS44@13	692	1036	1.498	0.13	0.05100	1.07	0.25134	1.85	0.0357	1.50	240.9	24.5	227.7	3.8	226.4	3.3
DS44@14	631	455	0.721	0.06	0.05071	1.35	0.24163	2.03	0.0346	1.52	227.8	31.0	219.8	4.0	219.0	3.3
DS44@15	367	285	0.777	0.86	0.04900	2.57	0.23800	2.98	0.0352	1.52	147.8	59.1	216.8	5.8	223.2	3.3
DS44@16	599	533	0.890	0.10	0.05070	1.18	0.25136	1.91	0.0360	1.50	227.0	27.1	227.7	3.9	227.7	3.4
DS44@17	477	374	0.784	1.17	0.04743	2.60	0.23919	3.01	0.0366	1.52	70.7	60.7	217.8	5.9	231.6	3.5
DS44@18	407	395	0.971	0.08	0.04989	2.11	0.24221	2.59	0.0352	1.50	189.6	48.3	220.2	5.1	223.1	3.3
DS44@19	386	328	0.851	0.19	0.05143	1.07	0.25639	1.91	0.0362	1.58	260.1	24.3	231.8	4.0	229.0	3.6
DS44@20	1439	2154	1.497	0.28	0.05147	1.07	0.25868	1.87	0.0364	1.53	262.0	24.3	233.6	3.9	230.8	3.5
DS44@21	615	499	0.812	0.03	0.05143	0.87	0.25571	1.75	0.0361	1.52	260.0	19.9	231.2	3.6	228.4	3.4
DS44@22	574	468	0.815	0.49	0.04978	1.26	0.25056	1.97	0.0365	1.52	184.6	29.1	227.0	4.0	231.2	3.4

f_{206} (%) is the percentage of common ^{206}Pb in total ^{206}Pb

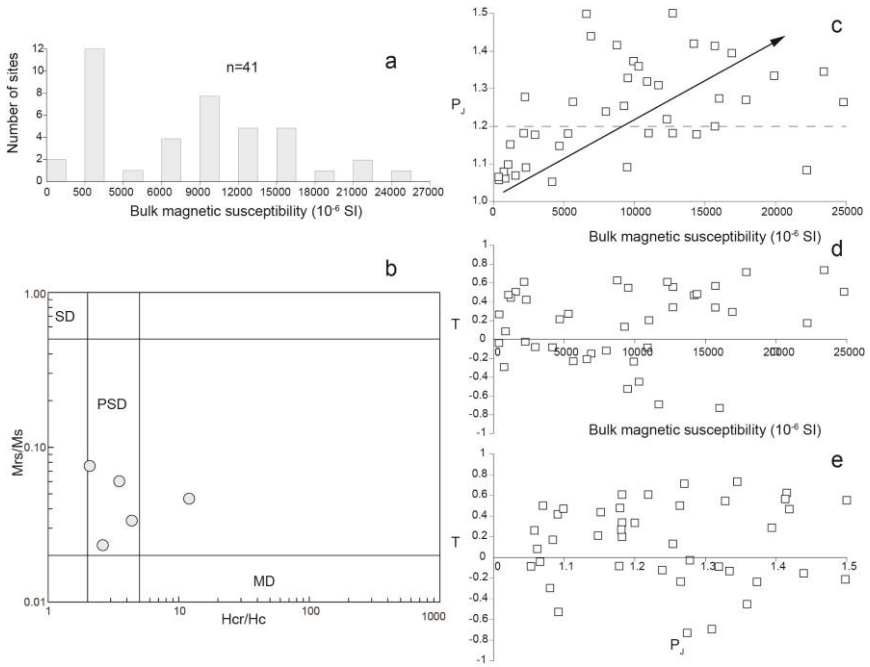

Figure 3.7 AMS scalar parameters of the Dushan pluton. (a) Histogram of site mean magnetic susceptibility (K_m). (b) Day plot of hysteresis parameters. Mrs: saturation of magnetic remanence, Ms: saturation of induced magnetization, Hcr: coercivity of magnetic remanence, Hr: coercivity of the measured sample. SD: single domain, PSD: pseudo-singledomain, MD: multidomain. (c) Shape parameter T versus anisotropy degree P_J value. (d) Bulk magnetic susceptibility K_m versus shape parameter T. (e) Anisotropy degree P_J value versus K_m.

$K_2 \geq K_3$), the shape parameter (T), and the anisotropy degree (P_J). To identify the magnetic carriers, the magnetic mineralogy was investigated with the following measurements (Figure 3.8): (1) Isothermal Remanent Magnetization (IRM); (2) thermomagnetic (K-T) curves, and (3) hysteresis loops. The measurements are performed in the Laboratory of Paleomagnetism and Chronology of IGGCAS, Beijing.

3.6.2. Magnetic Susceptibility Carrier

The mean magnetic susceptibility, $K_m = (K_1 + K_2 + K_3)/3$, of 41 sampling sites displays a rather large range of values in the Dushan pluton, from 397 to 25,800×10^{-6} SI (Figure 3.7a and Table 3.2). 27 out of 41 AMS (more than 66%) sites reveal high K_m values (> 500×10^{-6} SI), indicating that ferromagnetic minerals are the principal magnetic carriers (Figure 3.7a, Table

Table 3.2 The results of AMS measurements for the Dushan pluton. Lat: latitude, Long: longitude, N: the number of cylinders measured in each site, Km: mean magnetic susceptibility, P_J and T: anisotropy degree and shape parameter, respectively, K_1 and K_3: magnetic lineation and pole of magnetic foliation, respectively, Inc: inclination, and Dec: declination, α_{95max} and α_{95min}: Jelinek's statistic confidence at 95% level (Jelinek, 1981) in degrees, respectively.

site	Coordinates		N	K_m	P_J	T	K_1				K_3			
	Long(°E)	Lat(°N)		(10^{-6}SI)			Dec(°)	Inc(°)	α_{95max}(°)	α_{95min}(°)	Dec(°)	Inc(°)	α_{95max}(°)	α_{95min}(°)
DS1	118.843	40.460	6	9930	1.373	-0.236	241.6	9.4	7.0	3.1	335.5	22.1	11.1	7.0
DS2	118.866	40.456	5	852	1.062	0.084	86.6	41.2	34.2	5.7	352.1	5.1	26.3	8.5
DS3	118.884	40.452	5	1610	1.07	0.518	241.6	28.0	24.7	3.3	136.0	26.8	10	4.6
DS4	118.919	40.476	6	2320	1.091	0.418	230.4	15.0	81.8	28.3	127.4	40.0	30.5	14.4
DS5	118.934	40.582	5	15700	1.2	0.336	115.1	14.5	9.6	8.6	25.0	0.6	8.6	4.6
DS6	118.888	40.478	7	6920	1.439	-0.152	59.2	28.1	5.2	2.1	304.9	37.6	4.5	2.5
DS7	118.859	40.486	6	6600	1.498	-0.211	71.6	27.0	8.9	4.8	332.5	17.3	22.3	4.4
DS8	118.841	40.501	5	9530	1.322	-0.28	70.7	10.6	10.4	0.3	328.4	48.7	16.8	6.5
DS9	118.827	40.486	9	7980	1.239	-0.121	44.0	3.0	13.8	8.9	307.5	65.1	14.8	10.2
DS10	118.897	40.502	5	4810	1.238	-0.205	42.7	25.2	6.6	4.2	309.6	6.6	13.3	5.7
DS11	118.938	40.506	5	4280	1.055	-0.074	39.0	24.0	19.9	9.6	159.8	49.0	24.4	10.8
DS12	118.832	40.436	7	757	1.08	-0.295	70.9	9.1	9.6	4.7	332.9	40.9	23.8	5.8
DS13	118.791	40.454	7	9270	1.254	0.132	72.7	21.7	6.5	3.9	325.7	36.4	15.1	5.9
DS14	118.791	40.431	6	2960	1.178	-0.083	83.0	22.1	7.9	3.5	313.6	57.4	9.4	5.3
DS15	118.746	40.445	7	1220	1.152	0.439	250.5	14.1	8.6	6.0	355.4	45.7	10.2	7.3
DS16	118.731	40.436	5	11000	1.182	0.201	248.2	5.4	22.3	6.3	350.4	66.0	21.8	6.4
DS17	118.712	40.444	5	411	1.048	0.199	111.0	6.0	24.6	15.5	12.4	54.7	15.6	9.5
DS18	118.702	40.490	5	2220	1.335	-0.122	246.0	13.6	13.3	9.5	134.3	56.8	21.1	3.5
DS19	118.746	40.502	8	9490	1.092	-0.525	274.1	27.0	8.4	3.3	48.4	53.9	7.5	3.3
DS20	118.708	40.505	7	397	1.066	-0.04	223.3	32.0	13.7	6.5	113.8	28.1	11.4	5.6
DS21	118.769	40.542	7	8760	1.415	0.624	54.8	18.5	12.1	4.7	152.8	22.7	9.5	5.0
DS22	118.812	40.567	5	1770	1.182	0.645	33.3	58.6	23.3	5.1	175.4	25.7	9.4	5.2
DS23	118.814	40.579	6	12700	1.5	0.553	86.4	9.1	5.2	3.7	181.9	31.1	6.8	3.9
DS24	118.841	40.573	8	15700	1.413	0.565	97.2	52.8	4.8	3.6	233.4	28.7	7.2	1.5
DS25	118.860	40.578	7	24800	1.264	0.502	87.8	67.8	10.9	4.3	244.1	20.5	10.6	3.2
DS26	118.925	40.510	5	13800	1.178	0.368	45.7	7.7	24.9	2.1	313.6	15.2	15.4	2.4
DS27	118.927	40.522	6	19900	1.334	-0.13	42.0	26.9	14.0	4.3	283.7	43.0	9.9	3.0
DS28	118.904	40.523	6	10900	1.319	-0.088	55.0	49.3	7.3	4.0	268.9	35.5	6.2	4.5
DS29	118.890	40.526	7	11700	1.309	-0.691	65.7	44.7	9.3	3.5	316.7	18.2	7.7	4.2
DS30	118.937	40.523	5	16200	1.287	-0.744	10.9	48.5	4.4	1.0	103.3	2.1	20.6	2.2
DS31	118.929	40.548	6	9540	1.328	0.546	1.7	71.0	12.6	8.0	264.3	2.5	14.2	10.2
DS32	118.938	40.552	6	1060	1.099	0.471	147.4	11.1	45.3	8.6	241.6	20.6	9.2	4.4
DS33	118.932	40.568	5	5360	1.164	0.202	146.9	34.4	19.5	1.6	54.8	3.0	10.5	2.5
DS34	118.912	40.569	7	14200	1.419	0.468	64.1	71.4	5.6	3.2	245.6	18.6	4.3	3.1
DS35	118.911	40.591	5	9100	1.202	0.585	245.4	66.4	22	4.4	22.6	17.7	7.7	4.6
DS36	118.862	40.566	7	16900	1.394	0.289	64.7	47.4	8.7	5	269.1	39.9	8.2	3.5
DS37	118.894	40.578	8	4690	1.148	0.212	359.4	74.5	14.3	3.8	248.9	5.6	12.5	3.3
DS38	118.970	40.607	8	22200	1.084	0.172	25.0	59.2	10.1	7.5	205.3	30.8	16.7	6.7
DS39	118.982	40.594	7	17900	1.27	0.713	168.4	10.3	1.03	1.8	272.3	52.9	4.4	2.2
DS40	118.947	40.593	5	14400	1.179	0.479	122.5	8.1	9.7	3.0	213.8	9.5	7.5	1.2
DS41	118.961	40.576	5	23400	1.345	0.733	28.7	18.3	7.6	3.1	284.5	36.6	7.9	0.9

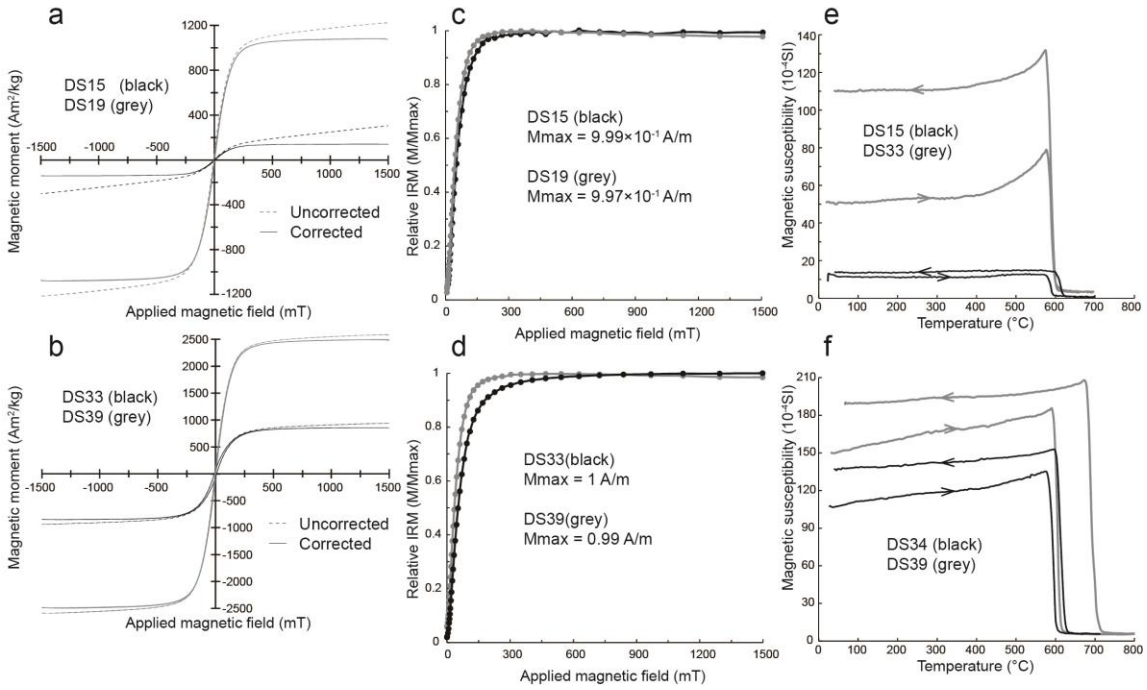

Figure 3.8 Magnetic mineralogy investigations of representative specimens from the Dushan pluton. (a–c) hysteresis loops, (d–f) acquisition of isothermal remanent magnetization (IRM), and (g–i) thermomagnetic curves (K (T) curves).

3.2; Bouchez, 2000). Only 2 AMS sites (DS17 and DS20) display the K_m values less than 500×10^{-6} SI, usually attributed to an exclusively paramagnetic contribution. A broad correlation between petrographic facies type and K_m variations can be observed, with lower K_m values for the biotite monzogranite marginal facies and higher ones for other facies (Figure 3.9a).

The hysteresis loops of six representative samples display nonlinear variations of hysteresis curves, indicating a dominance of the ferromagnetic minerals (Figures 3.8a-3.8b). All IRM acquisition curves show a sudden saturation below 300 mT (Figures 3.8c-3.8d). All thermomagnetic measurements display sharp drops of magnetic susceptibility at 550-600°C, suggesting the presence of magnetite as the principal susceptibility carrier (Figures 3.8e-3.8f). According to the ratios of hysteresis parameters Mr/Ms and Hcr/Hc, the mean grain size of the magnetite is within the pseudo-single domain (PSD) range (Dunlop, 2002; Figure 3.7b).

In conclusion, despite the presence of abundant biotite, the magnetite is likely the

dominant contributor to the magnetic susceptibility of more than 96% AMS sites in the Dushan pluton. For 2 sites (DS17 and DS20), biotite may be a significant magnetic susceptibility carrier. The magnetic susceptibility seems to vary according to petrofacies type and the relative contents of magnetite. Moreover, the paramagnetic and ferromagnetic minerals often carry compatible magnetic fabrics (Archanjo et al., 1994; Martín-Hernández & Hirt, 2003). Since there is no magnetite in single-domain (SD) that could bring inverse fabrics, the principal axis of the magnetic susceptibility ellipsoid (i.e., K_1 and K_3 axes) can be correlated to the lineation and the pole of foliation, respectively (e.g. Hargraves et al., 1991; Tarling & Hrouda, 1993).

3.6.3. Anisotropy Degree and Shape Parameter

Figure 3.7c shows that more than 58% of sampled sites in the Dushan pluton display an anisotropy degree higher than 1.2 with a positive correlation between P_J and K_m. In the arc-shaped gneissic and locally mylonitic zones where moderate to strong solid-state deformation occurred, the P_J values are not higher than elsewhere (Figure 3.9b). Therefore, it seems that the higher P_J values have no correlation with strain intensity. The shape parameter T varies from -0.728 to 0.733 (Figures 3.7d-3.7e). The shape parameters with both negative and positive T values occupy mainly the southwest of the Dushan pluton that essentially belongs to arc-shaped gneissic and locally developed mylonitic zone (Figure 3.9c). It seems that P_J and T parameters, usually used to describe the degree of AMS and the shape of the AMS ellipsoid, respectively

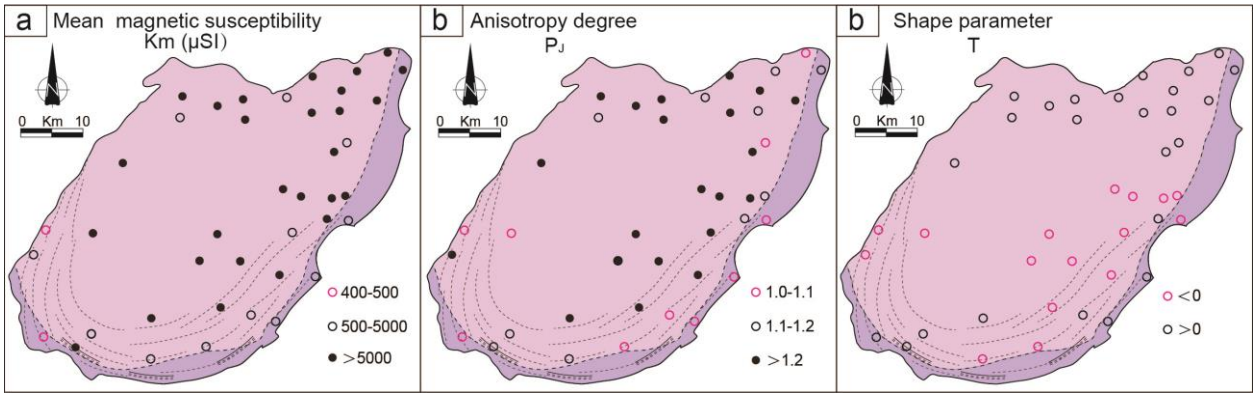

Figure 3.9 AMS maps of the Dushan pluton (a) Mean magnetic susceptibility map, (b) Anisotropy degree map, and (c) Shape parameter map in the Dushan pluton.

(Jelinek, 1981), cannot constrain strain patterns in this study.

3.6.4. Fabric Pattern and Comparison with Mesoscopic Fabric

For each site, the site-average orientation with corresponding 95% confidence level (α_{95max} and α_{95min}) was calculated for K_1 and K_3 axes (Jelinek, 1978; Figure 3.10). Note that for a confidence level larger than 25°, the direction of corresponding magnetic axis is considered as poorly defined; when lower than 25°, it is considered as well-defined or reliable. The latter is the case for more than 74% of the AMS sites for both K_1 and K_3. Figure 3.11 shows that the magnetic foliations measured in the laboratory are rather consistent with the mesoscopic fabrics observed in the field.

In the Dushan pluton, both mesoscopic and magnetic foliations with moderate to steep outward dipping display a well-defined elliptic pattern with a NE-SW oriented long axis (Figure 3.11a). In the northeastern part of the pluton, the foliations are sub-vertical and close to the southeastern border, they dip inward and strike sub-parallel to the contact with the country rocks. The magnetic lineations display gentle to moderate NE-SW plunging throughout the pluton except in its northeastern part where they become more scattered in trends and locally steeper dipping (Figure 3.11b).

3.7. Gravity Modeling

Gravity modeling has been proved its efficiency to depict the architecture of deep structures, especially for granitic plutons (Améglio & Vigneresse, 1999; Vigneresse, 1990). In order to constrain the geometry of the Dushan pluton, its shape, and possible feeder zones, a gravity modeling study has been performed. Meanwhile, the Dashizhu pluton has also taken into account to clarify its relationship with the Dushan pluton in the gravity modeling study. The available Bouguer anomaly map (1: 200,000) was derived from the Chinese regional gravity survey. The short wavelengths of the gravity anomaly originate from the upper crust

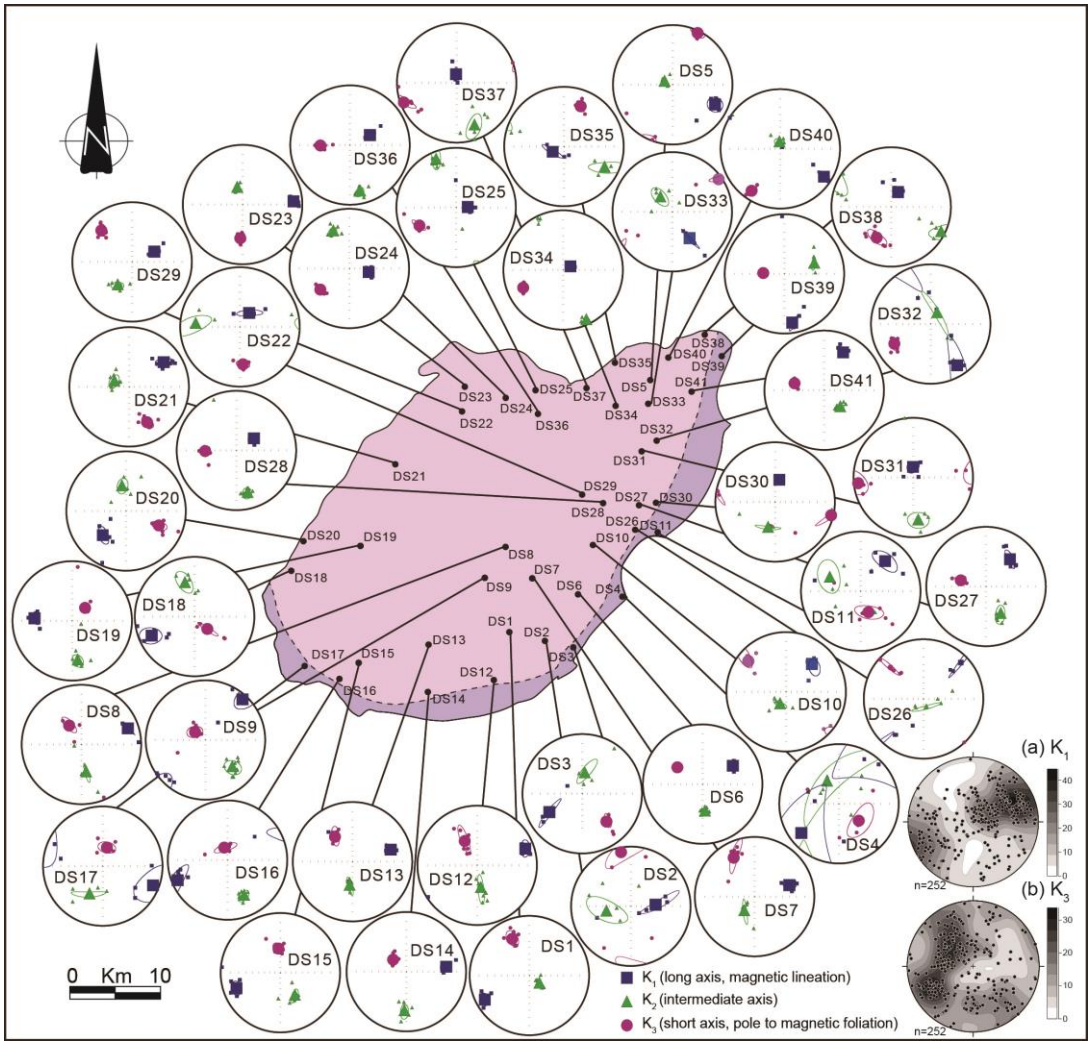

Figure 3.10 Equal-area projections (lower hemisphere) of AMS results for each sampling site. Confidence ellipses at 95% level are drawn around each average orientation direction. (a) K_1, long axis or magnetic lineation; K_3, short axis or pole to magnetic foliation.

(down to a few kilometers). The long wavelengths of the gravity anomaly, due to deeper structures, must be removed from the complete Bouguer anomaly to highlight the Dushan pluton related anomalies. The filtered regional Bouguer anomaly has been computed from a lower-resolution (2′×2′) Bouguer grid, which was acquired from the International Gravimetric Bureau database (Bonvalot et al., 2012). The long wavelengths of the gravity anomaly were extracted using a 380 km low-pass Butterworth filter after several attempts. The residual Bouguer anomaly map was obtained by subtracting the filtered regional Bouguer anomaly (Figure 3.12a).

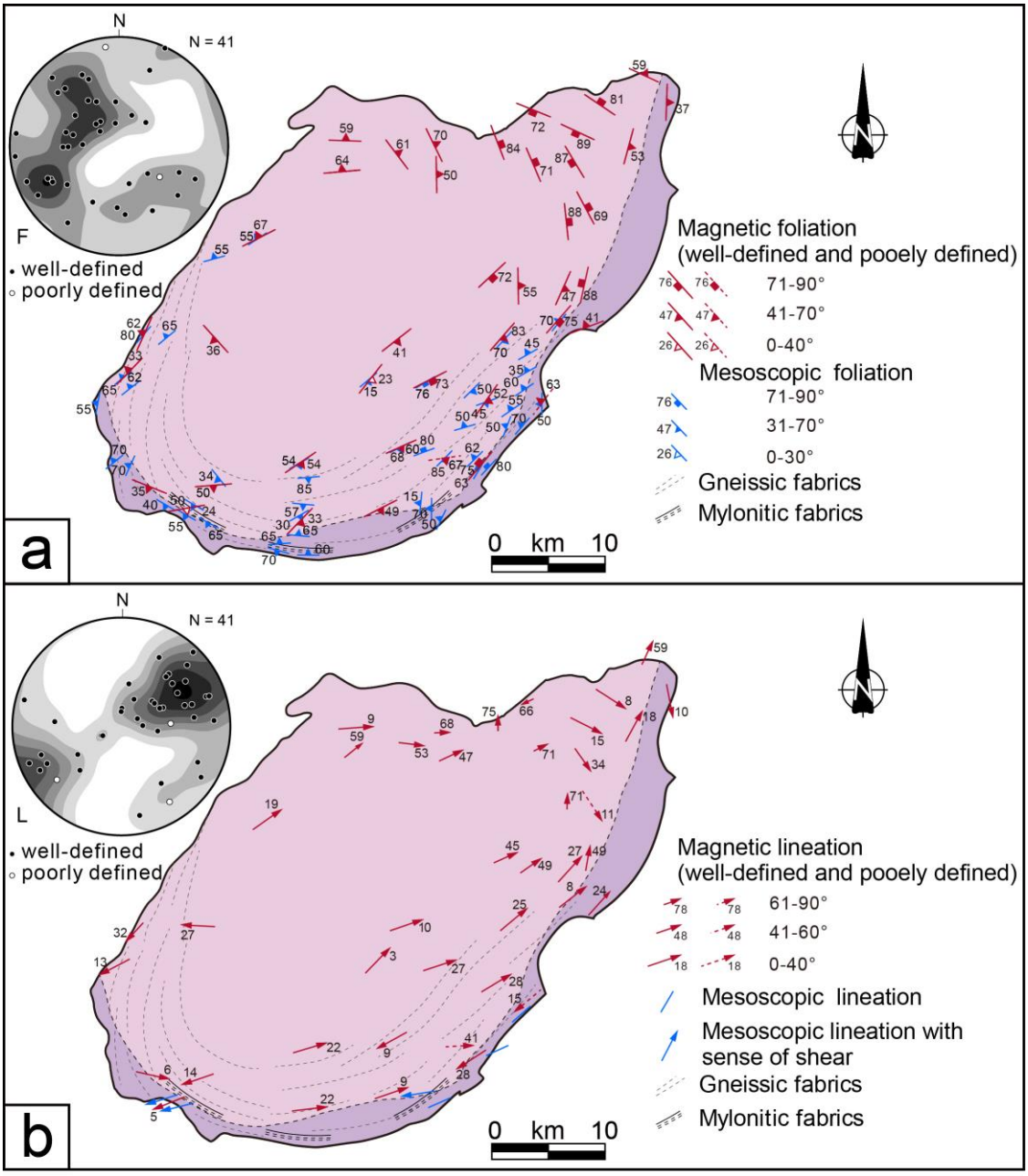

Figure 3.11 Mesoscopic and magnetic fabric patterns and orientation diagrams of K_3 and K_1. (a) Foliations. (b) Lineations.

According to the residual Bouguer anomaly map that reflects the density heterogeneities of the first kilometers below the surface, 2-D gravity modeling is also performed to characterize the geometry of the Dushan pluton at depth along four cross-sections, perpendicular to the long and short axes of the pluton (Figure 3.12b). Several constraints have been taken into account in modeling, mainly including geological contacts, lithological units, structural data and

density of lithological units. In our modeling, all available information from geological maps and field observations have been taken into account, namely that the Neoproterozoic carbonate rocks overlie the Archaean gneiss, and that granite was emplaced into the Malanyu anticline. Densities of these lithologies have been determined by the laboratory measurements (Lin et al., 2013) and summarized in Figure 3.12b.

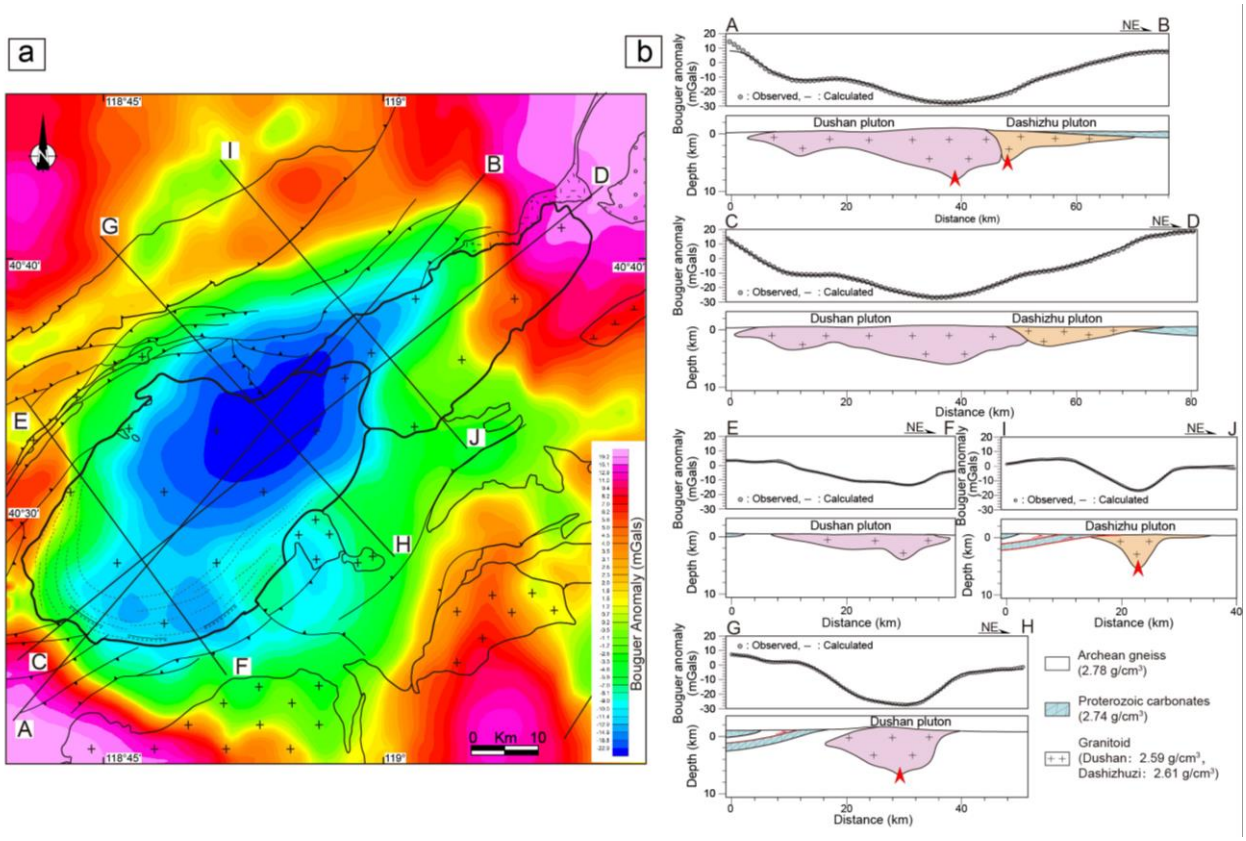

Figure 3.12 Gravity modeling. (a) Residual Bouguer gravity anomaly of the Dushan pluton and adjacent areas after subtraction of a 380 km wavelength regional trend from the complete Bouguer anomaly. Symbols and captions are the same as in Figure 2. (b) 2-D gravity modeling across the Dushan pluton. Note that the arrows show the possible feeder zones for the pluton.

The negative anomalies show a NE-SW trending elliptical shape that more or less correlates with the main geological boundary of the Dushan pluton (Figure 3.12a). The Dushan pluton shows a negative anomaly with an anomaly center in its northeastern part, suggesting corresponds to the root of the pluton. In its north, the negative anomaly beyond the contact is

likely related to the outward extension of the pluton below its country rocks. A maximal thickness of ~7 km in the southeastern part progressively decreases southwestward to a minimum of ~1 km. However, it exists a higher negative anomaly close to the southwestern border, indicating local thickening of the pluton. The Dushan pluton presents an overall southwestward thinning tabular or tongue-like shape with a feeder zone in its northeast. In the Dashizhu pluton, the negative anomaly, located in the west of the current exposure, is beyond the contact with cover rocks. The NE trending highest negative anomaly, that likely represents its root, is located in the western corner of the current exposure. In its current exposure, it changes into a positive anomaly away from the western corner. It seems that the Dashizhu pluton presents a funnel shape that sharply thins outward from a feeder zone in its western corner.

3.8. Discussion

3.8.1. A continuum of fabric variation from magmatic to solid-state conditions in the Dushan pluton

The central and northeastern parts of the Dushan pluton display weak or invisible mineral preferred orientation (Figures 3.4a-3.4b), and in the southwestern part of the pluton a gneissosity, even with locally developed mylonitic structures, defines the pluton margin (Figures 3.2 and 3.4c-3.4f). However, no sharp boundaries between these magmatic and solid-state fabrics can be observed across the pluton (Figure 3.5). The strong solid-state fabrics are only developed in the mylonitic zones in the southernmost part of the pluton (Figure 3.5g). The pervasive gneissosity develops southwards, and the mylonitic fabric is only exposed when approaching the margin. However, the country rocks never present such a similar penetrative fabric that appears to be restricted in the granite. Strongly flattened xenoliths without any stretching lineation are distributed in the gneissic monzogranite (Figure 3.4d). In locally the

mylonitic zones, the fabrics are associated with a top-to-the-SW ductile shearing (Figures 3.5f and 3.11b). These structural data suggest that the Dushan pluton underwent a southwestward increasing strain gradient of solid-state deformation. Magmatic fabrics extensively remain preserved in the northeast part of the Dushan pluton (Figure 3.5g). Moreover, the mesoscopic planar fabrics (i.e. gneissic and mylonitic foliations) are geometrically compatible with the magnetic foliations that strike parallel to the pluton contact (Figure 3.11a). The cartographic elliptic dome-like pattern with a NE-SW striking long axis is in good agreement with both mesoscopic and magnetic foliations, despite the fabrics dip inwards close to the southeastern border of the pluton. The stretching lineations observed in the mylonitic zones strike NE-SW, and are also concordant with the magnetic lineations measured in the pluton (Figure 3.11b). Combining this dome geometry with the absence of top-to-the-SW ductile shearing in the country rocks, it undoubtedly argues for the contemporaneity between the pluton emplacement and solid-state deformation. Our field and microscopic observations, together with AMS data, allow us to recognize a continuum of fabric variation from magmatic to solid-state conditions during the pluton emplacement.

3.8.2. Emplacement mode

The Dashizhu pluton presents a funnel-shaped architecture with a feeder zone in the northwestern corner of its current exposure (Figures 3.12b and 3.13). The funnel-shaped Dashizhu pluton sharply thins away from the feeder zone, implying that the current exposure may be also close to the root of the Dashizhu pluton. According to the geochronological results from both plutons, the Dashizhu pluton firstly intruded into Malanyu anticline at ca. 225 Ma, then the Dushan pluton intruded against the southwestern sidewall of the Dashizhu pluton at ca. 220 Ma.

The Dushan pluton has a NE-SW trending tabular or tongue-like shape with a feeder zone in its northeast. The roof is estimated as a dome-like structure due to the moderate to high

outward dipping foliations parallel to the border (Figure 3.12a), except that the biotite-rich marginal facies. Close to the southeastern border, the foliations present inward dipping and strike sub-parallel to the contact with the country rocks. These foliations roughly conform to the overall attitude of the country rocks near the pluton (Figure 3.2). Taking the geochronological uncertainties into account, it seems that the biotite-rich magma batch probably firstly made it ascent via the feeder zone and injected as a sill into the Malanyu anticline (Figure 3.13). Following monzogranite magma may relatively upwell to inflate and push aside the country rocks to build the Dushan pluton. No internal petrographic zoning of pluton with sharp facies boundaries can be observed, although a progressive mineral fabric change is observed. As no related ductile deformation has been observed in the country rocks along the contact between the pluton and the country rocks, it seems that the emplacement of the Dushan pluton could not be interpreted as a nested diapir of expanded plutons that implies rising of large magma batches, but inflation of small conduit-fed magma batches (Paterson & Vernon, 1995).

The following lines of evidence suggest that the inflation occurred not only upwards and downwards, but also laterally: (1) a dome-like roof, confined by outward dipping foliations; (2) an unflat floor and inward dipping sidewalls; (3) the strongly flattened xenoliths without stretching lineations in the gneissic monzogranite; (4) the deflection of country-rock structures; and (5) the arc-shaped fold-and-thrust belt unwrapping along the Dushan pluton in the northwest. The dominant NE-SW lineations may reflect main southwestward intrusion, due possibly to the blocking of the Dashizhu pluton to the northeast (Figure 3.11b). The latter arrivals of magma might inflate, deform and even recrystallize the former cooled-down magma.

The magma spreads southwestwards from the feeder zone until loss of heat and its crystallization, while the later magma continues to expand the already crystallized

southwestern margin. This inflation formed an arc-shaped, gneissic to mylonitic foliation in

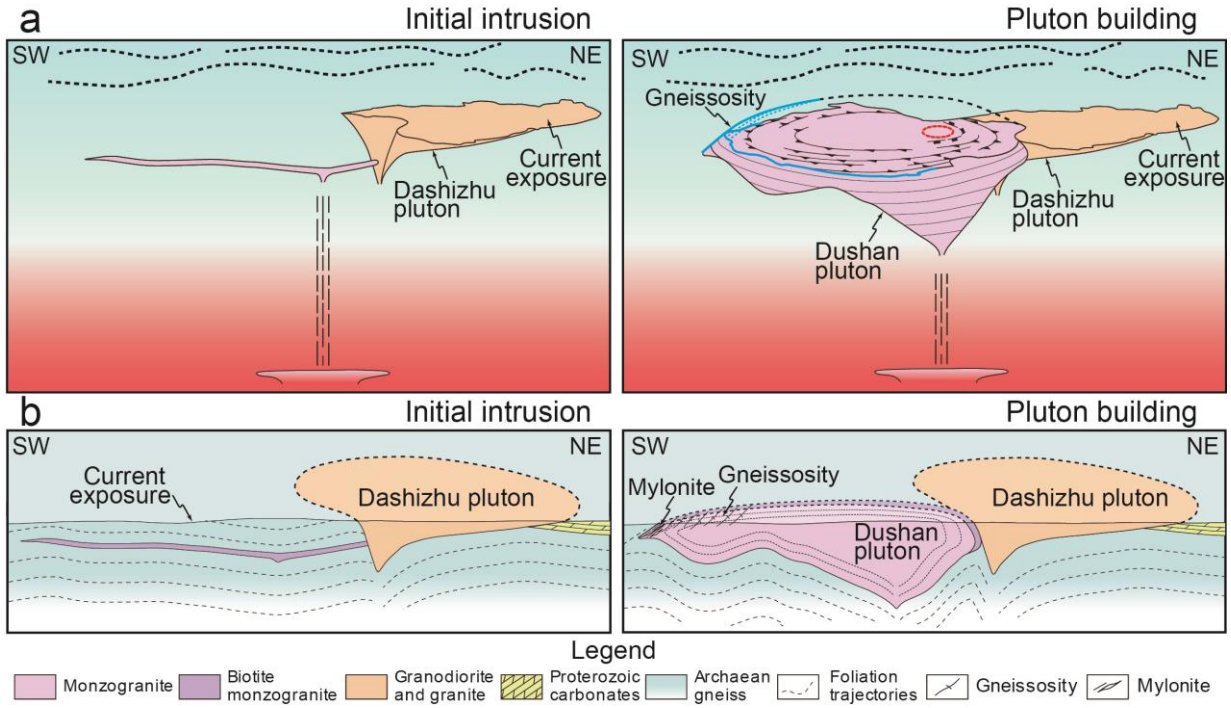

Figure 3.13 Scenarios for multiple emplacement of the Dushan pluton and ductile shear zone nucleation. (a) 3-D schematic sketch summarizing emplacement of the Dushan pluton. (b) Cross sections of the Dushan pluton showing its emplacement. The overlying rocks above the current exposure are not considered, and the shape of the plutons at depth is inferred from gravity data.

the southwestern margin of the pluton by means of subsolidus deformation (Figure 3.13). It seems that it occurred in a relatively continuous process of the pluton emplacement as the magmatic to post-solidus fabrics do not present a sharp contact. Numerous xenoliths with flattened shapes are aligned parallel to magmatic foliations in the southwestern margin, presenting as strain markers or indicators of the expansion (Figure 3.4d). In brief, the building of the Dushan pluton probably began with a sill then evolved into the inflation of small magma batches. The dome-like roof with outward dipping foliations was eroded during its exhumation, leaving preserved biotite-rich marginal facies (Figure 3.13). In the biotite-rich marginal facies, the foliations remain original inward dipping in the southeast but outward dipping elsewhere due to the pluton inflation (Figure 3.11b).

3.8.3. Tectonic implication

The fabrics of the Dushan pluton may be mainly explained by magma intrusion, pluton inflation, and syn-emplacement solid-state deformation. The fabrics recorded a continuum of fabric variation from magmatic to solid-state conditions during the pluton emplacement. In the study area, a syn-magmatic ductile shearing coeval with the fabrics observed within the Dushan pluton is absent in the country rocks. Moreover, in the regional scale, no syn-magmatic tectonic phenomenon can be documented. Therefore, the pluton emplacement was probably mainly driven by magma buoyancy without significant influence of regional tectonics. In other words, both mesoscopic and magnetic fabrics in the Dushan pluton were rather related to its building than the Late Triassic regional tectonics, if there existed any. Alternatively, the Late Triassic was a period of relative "tectonic quiescence" in the northern NCB after the final formation of the CAOB.

However, a Late Triassic extensional setting for the northern NCB has been proposed according to the geochemistry of the E-W trending alkaline intrusive complexes (Yang et al., 2012; Zhang et al., 2012). The geochemistry of the Dushan pluton, similar to the Late Triassic alkaline intrusive complexes, indicates that it originated from partial melting of the lower crust with a contribution of mantle-derived materials during an extensional setting (Ye et al. 2014; Jiang et al., 2018). Fining and deepening upward depositional system and abundant volcaniclastic rocks in the remnant basins suggest a Late Triassic extensional setting in the northern NCB (Davis et al., 2009; Meng et al., 2014; Figure 3.1). In the south of Sonid Zuoqi in the vicinity of the Solonker zone, a NE-SW trending extension has been also documented in a Late Triassic metamorphic core complex (Davis et al., 2004; Figure 3.1b). Nevertheless, the Dushan pluton did not record any regional extension feature, coeval with its emplacement process. To clarify the Late Triassic tectonic and geodynamic setting of the NCB, more detailed structural studies are needed.

Chapter 4. Emplacement of the Late Triassic granitic Wangtufang pluton

4.1. Introduction

The early Mesozoic magmatism, represented by E–W trending Late Triassic alkaline intrusive complexes, is conspicuous in the northern NCB. However, their tectonic and geodynamic settings are still debated (Yang et al., 2012; Zhang et al., 2012; Zhao et al., 2015). Based on structural observations and paleomagnetic studies, one group of researchers considers that these Late Triassic granitic and syenitic plutons were due to large-scale Triassic thrusting and strike-slip faulting in the northern margin of the NCB and produced in the local extensional areas by the pull-apart of the strike-slip faults (e.g., Zhao et al., 2015). According to geochemical studies, another group proposes that the Late Triassic alkaline complexes in the northern NCB, especially silica-undersaturated syenites, occurred in an intracontinental extensional tectonic setting (e.g., Yang et al., 2012; Zhang et al., 2012), implying the early timing of cratonic destruction during the Late Triassic (Han et al., 2004). The Late Triassic tectonic regime is important to understand the tectonic and geodynamic evolution of the NCB. However, only few small remnants of Late Triassic sedimentary basins can be observed and offer little coeval structural information in the northern NCB due to the intense post-Triassic tectonics (i.e., Xiabancheng basin and Niuyingzi-Dengzhangzi basin in the Yanshan Fold-and-Thrust Belt (YFTB); Figure 4.1; Davis et al., 2009; Meng et al., 2014). Moreover, it is difficult to recognize the regional tectonic framework from these few small remnant basins. Due to less impressive and controversial evidence, the nature of the Triassic regime is in debate since long time with different hypotheses. Late Triassic contractional tectonics was proposed according to the unconformity between Triassic and Lower Jurassic strata, and Lower Jurassic syntectonic conglomerate (Zhao, 1990; Liu et al., 2012). Detrital zircon dating and sedimentary studies suggest that the conformable Upper Triassic strata were deposited in an extensional setting

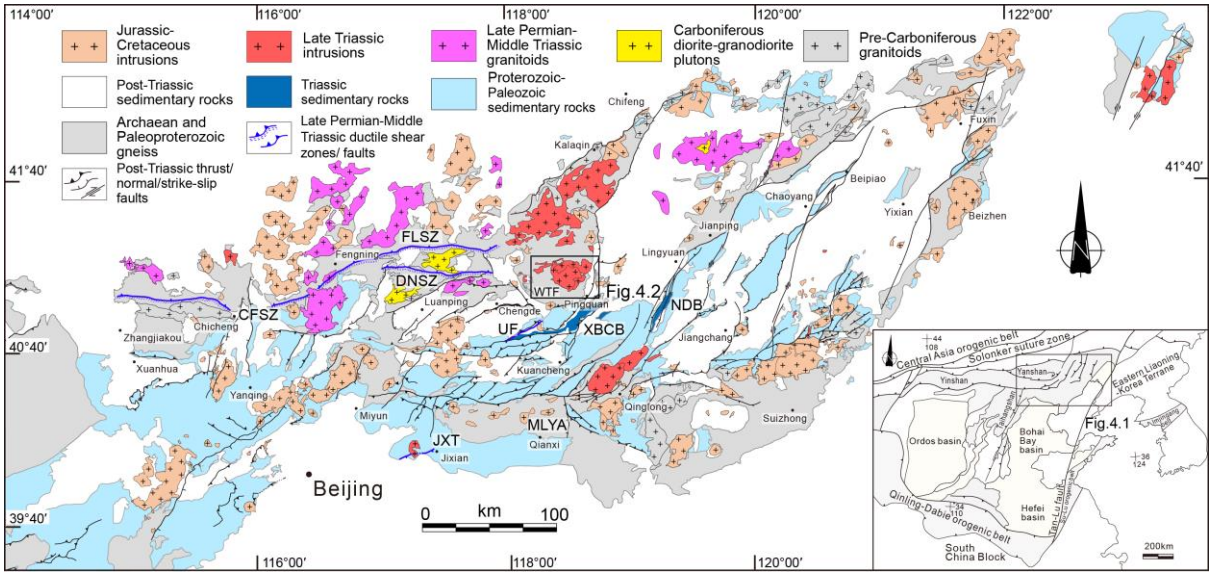

Figure. 4.1 Simplified geological map of the Yanshan fold and thrust belt and location of the Wangtufang pluton. CFSZ: Chicheng-Fengning ductile shear zone, FLSZ: Fengning-Longhua, ductile shear zone, DNSZ: Damiao-Niangniangmiao ductile shear zone, UF: Unnamed fault, JXT: Jixian thrust, MLYA: Malanyu anticline, XBCB: Xiabancheng basin, NDB: Niuying-Dengzhangzi basin, WTF: Wangtufang pluton.

(Davis et al., 2009; Meng et al., 2014; Meng et al., 2019). Consequently, the paucity of structural data makes difficult to assess the Late Triassic tectonic regime.

During pluton emplacement, magma fabrics can potentially record information on both magma dynamics and regional strain fields to which the magma was subjected (e.g., Bouchez, et al., 1997; Paterson et al., 1998; Sant'Ovaia et al., 2000). The solid-state fabrics present structural deformation after magma full crystallization (Paterson et al., 1989). Therefore, the fabric pattern and shape of pluton are crucial to decipher the pluton emplacement process. The structural study of plutons is an effective and practical way to unravel regional tectonic setting coeval with the emplacement process (e.g., Bouchez, et al., 1997; De Saint Blanquat et al., 2011). Numerous studies have proven that the fabrics of granitic plutons may provide signatures of the local and regional constraints on the pluton emplacement (e.g., Paterson et al., 1998; De Saint Blanquat et al., 2011; Lin et al., 2013b). Therefore, Late Triassic plutons from the NCB present good opportunities to realize this purpose, and, accordingly, the Wangtufang

pluton was chosen for this study (Figure 4.1). Indeed, such studies have been rarely performed on Late Triassic plutons of the northern NCB. An integrated multidisciplinary investigation, including structural geology, geochronology, geochemistry, Anisotropy of magnetic susceptibility (AMS), and gravity modeling, has been conducted to decipher the Late Triassic tectono-magmatic setting in the northern NCB. Given the correlation with other contemporaneous plutons or tectonics, the proposed model may have regional implications for the Late Triassic tectonic setting in the northern NCB.

4.2. Geological setting

After its assembly through the collision of the Eastern, Intermediate (or Fuping), and Western blocks during the Paleoproterozoic (Zhao et al., 2001; Faure et al., 2007; Li and Zhao et al., 2007; Li et al., 2012), the NCB formed a stable craton from Mesoproterozoic to Paleozoic. Archaean and Paleoproterozoic gneiss, migmatites and granites were overlain by a Mesoproterozoic to Permian sedimentary cover, separated by a widespread disconformity between the Middle Ordovician and Upper Carboniferous sequences (Li et al., 2016). The closure time of the Paleo-Asian Ocean to the north of the NCB is still controversial. Some authors argue for a Late Permian to the Early Triassic age (e.g., Windley et al. 2007; Xiao et al., 2015), whereas others propose the Paleo-Asian Ocean closed during the Late Devonian, followed by the Late Carboniferous–Triassic intracontinental tectonics (Xu et al., 2013; Zhao et al., 2013). In the south, the NCB collided with the South China Block before the Middle Devonian (e.g., Mattauer et al., 1985; Xu et al., 1986) or in the Triassic (e.g., Meng and Zhang, 1999; Hacker et al., 2000; Li et al., 2010, 2011, 2017, 2018). In the YFTB, the E-W trending ductile shear zone and thick- and thin-skinned folds and faults occurred progressively from the northern margin toward the interior (Wang et al., 2013). The ductile shear zone concerns the E-W trending Chicheng - Fengning, Fengning - Longhua, and Damiao – Niangniangmiao

ductile shear zones in the north (Wang et al., 2013; Zhang et al., 2014; Figure 4.1), and the E-W trending folds and thrusts include the Unnamed fault, Malanyu anticline, and Jixian thrust fault in the south (Davis et al., 2001; Ma et al., 2007). Few Triassic remnant basins and a large number of contemporaneous plutons are exposed in the northern NCB (Davis et al., 2009; Zhang et al., 2012; Meng et al., 2014).

During the Jurassic to earliest Cretaceous, the Mongol-Okhotsk Ocean closed progressively from west to east in the north of the East Asian continent (Zorin, 1999; Daoudene et al., 2013). Meanwhile, the subduction of the Paleo-Pacific Ocean plate occurred in the southeast of the East Asian continent (Davis et al., 2001). A large scale intra-continental deformation and magmatism, traditionally referred to as the Yanshanian movement, occurred in the NCB (Davis et al., 2001; Faure et al., 2012; Zhang et al., 2014; Dong et al., 2015). The YFTB is a typical intracontinental orogen, formed in the northern part of the NCB (Davis et al., 2001). The thrust faults, which strike E–W in the west and NE–SW in the east, are distributed throughout the YFTB (e.g., Davis et al., 2001; Faure et al., 2012; Figure 4.1). As mentioned above, due to the intense deformation during the Jurassic Yanshanian contractional events, only few pre-Jurassic structures could be surely recognized in the YFTB (e.g., Davis et al., 2009; Zhang et al., 2012; Meng et al., 2014; Zhang et al., 2014; Figure 4.1). In the Early Cretaceous, the NCB was dominated by extensional tectonics (i.e., metamorphic core complexes (MCCs), A-type magmatism, graben or half-graben basins; Li et al., 2012; Zhang et al., 2014, Lin et al., 2018).

4.3. Structural observations

4.3.1. Field observations

The Wangtufang pluton has a subcircular surface exposure with a radius of about 12 km. It mainly consists of syenogranite in the southwest and diorite in the northeast (Figure

4.2).Macroscopically, these two types of rocks (i.e., pale red syenogranite and dark gray diorite) appear totally isotropic, lacking of any planar and linear structures at outcrops (Figures 4.3a and 4.3b). The main rock-forming minerals, namely, quartz, K-feldspar, plagioclase, amphibole, and biotite, are generally euhedral to subhedral without obvious preferred orientation. The Wangtufang pluton intrudes into foliated, even mylonitic Archaean gneiss and undeformed migmatitic granite (Lin et al., 2013a; Figure 4.2). In the gneiss, in spite of the strike variation of foliation, the mineral and stretching lineations are consistently oriented along a NW–SE direction (Figures 4.2 and 4.3c–3d). A top-to-the SE sense of shear is indicated by sigmoidal K-feldspar porphyroclasts (Figure 4.3e). The gneiss is pervasively folded by the top-to-the SE shearing, indicative of strong deformation before pluton emplacement. In the

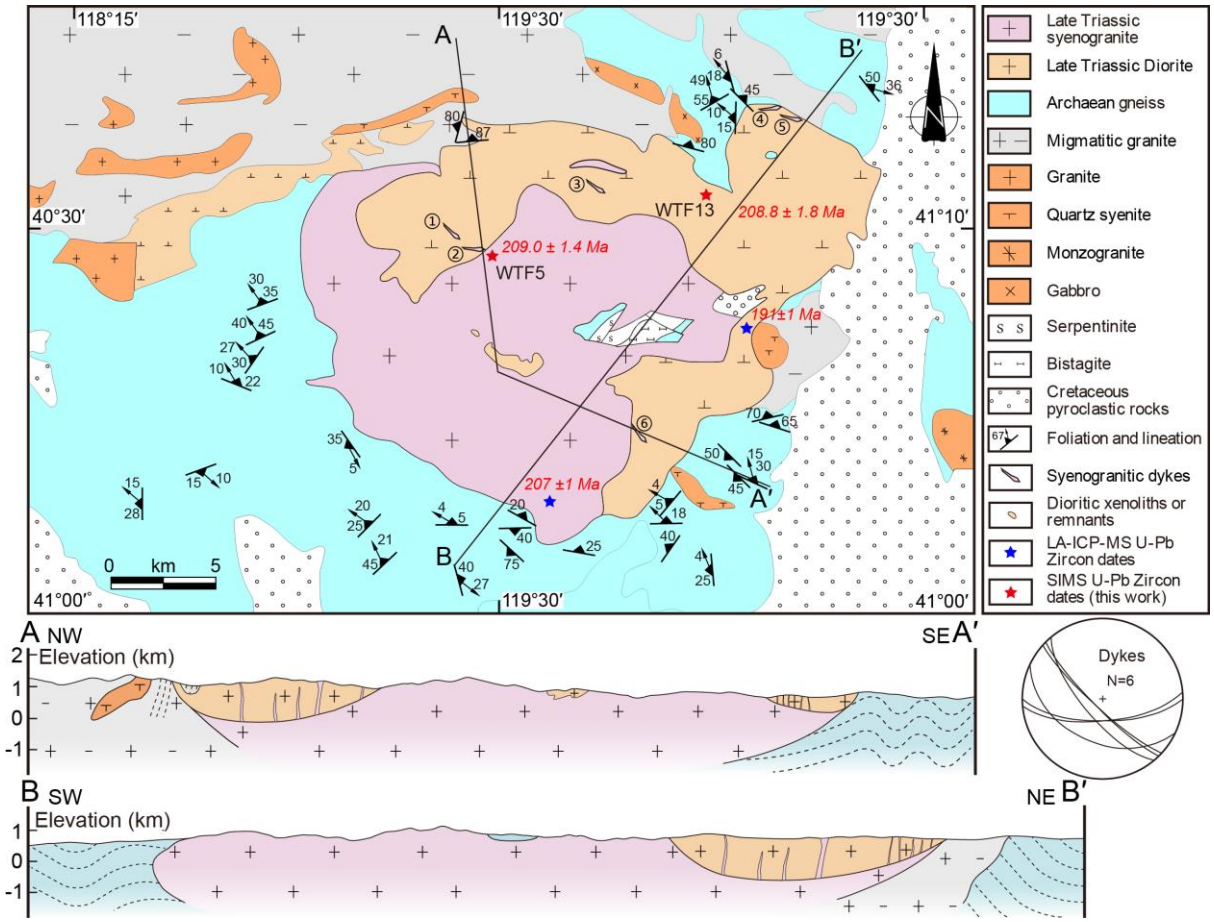

Figure. 4.2 Geological map and cross-sections in the Wangtufang pluton and its adjacent area. Numbers in circles and stereonet show the locations and attitudes of the measured dykes, respectively. U–Pb zircon data from Liu et al. (2012). See Figure 4.1 for location.

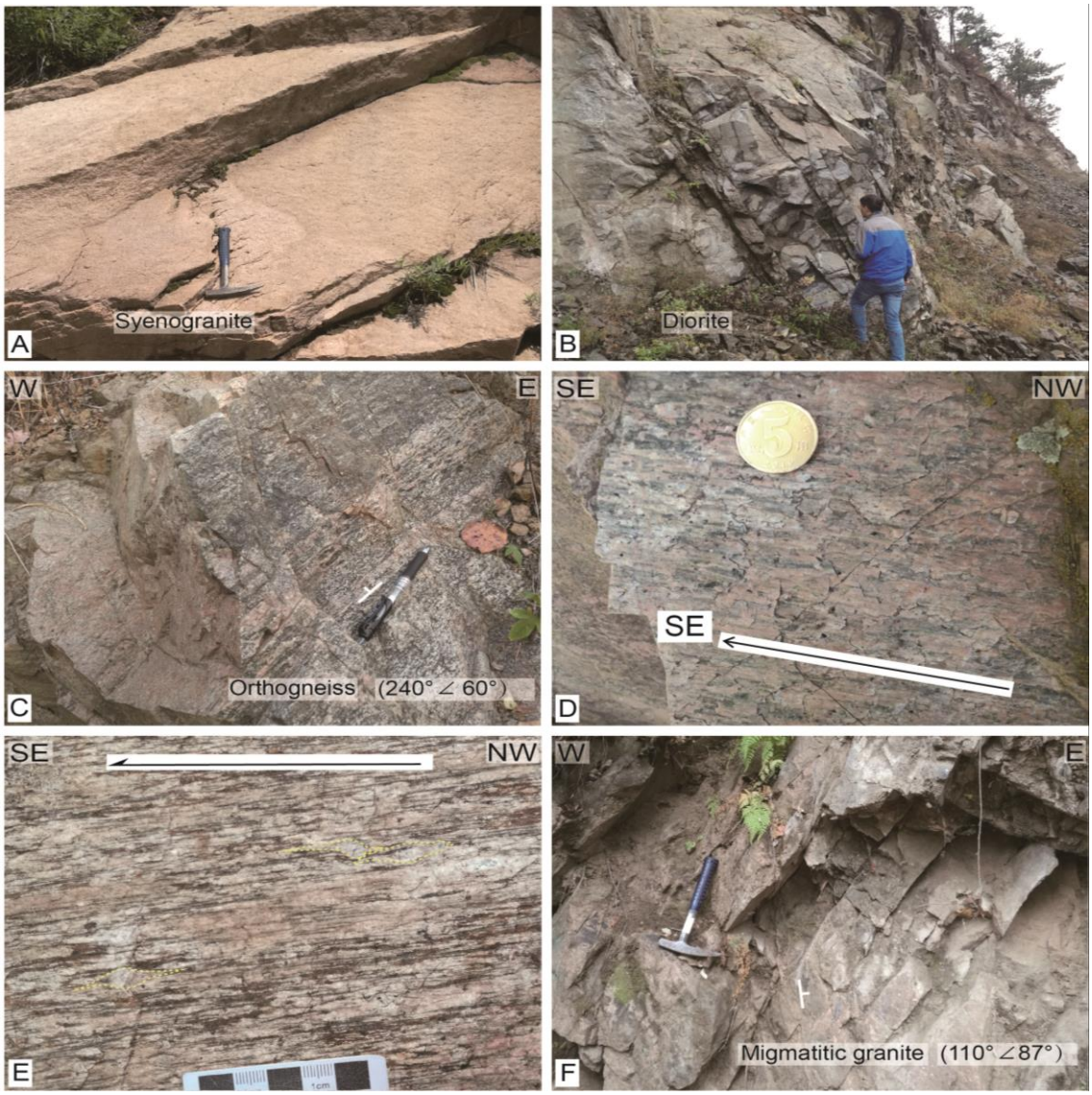

Figure 4.3 Field photographs of the Wangtufang pluton and its country rocks. (a) Syenogranite in the south of the Wangtufang pluton. (b) Diorite in the north of the Wangtufang pluton. (c) Archaean gneiss in the south of the Wangtufang pluton. (d) NW–SE trending lineation in Archaean gneiss. (e) Sigmoidal K-feldspar porphyroclast in Archaean gneiss, indicating a top-to-the-SE sense of shearing. (f) Migmatitic granite in the north of the Wangtufang pluton.

northwest, steep and weak foliations are developed in the migmatitic granite near the contact with the diorite (Figures 4.2 and 4.3f). A remnant of the country rocks is preserved in the southeast of the syenogranite (Figure 4.2). The pluton is overlain by Cretaceous pyroclastic rocks in its east (Figure 4.2).

In the Wangtufang pluton, centimeter to ten-meter wide syenogranitic dykes extensively intrude in the diorite (Figure 4.2). Meter-scale dykes intruded into the diorite near the contact between the syenogranite and diorite (Figure 4.4a). Locally, diorite blocks are included in syenogranite dykes (Figure 4.4b). The contact between syenogranite and drop blocks of diorite is sharp. It can be observed that numerous dykes of the syenogranite intruded into the diorite in its northeasternmost (Figure 4.4c). Furthermore, all dykes are steep and strike consistently NW–SE direction (Figure 4.2). In the syenogranite, several ten-meter xenoliths in diameter of the diorite are scattered in the syenogranite (Figure 4.4d). A remnant of diorite remains in the center of the syenogranite (Figure 4.2). These phenomena show that the diorite was dismembered by the intrusion of the syenogranite with a series of dykes after the diorite had fully crystallized.

Figure 4.4 Field photographs of the dykes and xenoliths in the Wangtufang pluton. (a) Syenogranitic dykes near the contact between the syenogranite and the diorite. (b) Dioritic xenoliths in the syenogranitic dykes. (c) Syenogranitic dykes near the northeastern border of the Wangtufang pluton. (d) Dioritic xenolith in the syenogranite.

4.3.2. Microscopic observations

To determine the relationships between the minerals and magnetic fabrics, microstructures are investigated in 36 sampling sites of the Wangtufang pluton (Figure 4.5a). Under the microscope, two textural types can be distinguished in the Wangtufang pluton. At most sites (67%), the Wangtufang pluton presents magmatic fabrics without any evidence of deformation (Figures 4.5a–4.5c). Quartz crystals are anhedral, non-deformed, and do not show signs of undulose extinction or dynamic recrystallization. K-feldspars present Carlsbad twinning and marginal replacement by myrmekite (Figure 4.5b). The euhedral biotite flakes have a sharp extinction and are neither kinked nor bent (Figure 4.5c). Plagioclase grains are euhedral and exhibit Carlsbad-albite compound twinning and polysynthetic twinning (Figure 4.5c). Besides, at some sites (33%), submagmatic fabrics can be also observed (Figure 4.5a). Millimeter-sized quartz grains show an undulose extinction, and small well-individualized quartz grains occur at the border of the coarse grains (Figures 4.5d and 4.5e). Generally, significant solid-state deformation has not been observed. The fabrics are mostly acquired in magmatic state but record some submagmatic deformation.

4.4. Geochronology and geochemistry

4.4.1. Zircon U–Pb geochronology

Considering the paucity of available dating in this pluton, new zircon U-Pb dating of two samples WTF5 and WTF13 was performed by a Cameca IMS 1280 large-radius SIMS at the Institute of Geology and Geophysics, Chinese Academy of Sciences (IGGCAS), Beijing (Figure 4.2; Table 4.1). The zircon grains from these two samples are subhedral, transparent, and 50–150 μm in length with aspect ratios between 1:1 and 3:1. CL images show clear oscillatory zoning (Figure 4.6). Th/U ratios of Sample WTF5 vary from 0.42 to 1.12. Twenty analyses of $^{206}Pb/^{238}U$ and $^{207}Pb/^{235}U$ results plotted on a Concordia diagram are relatively

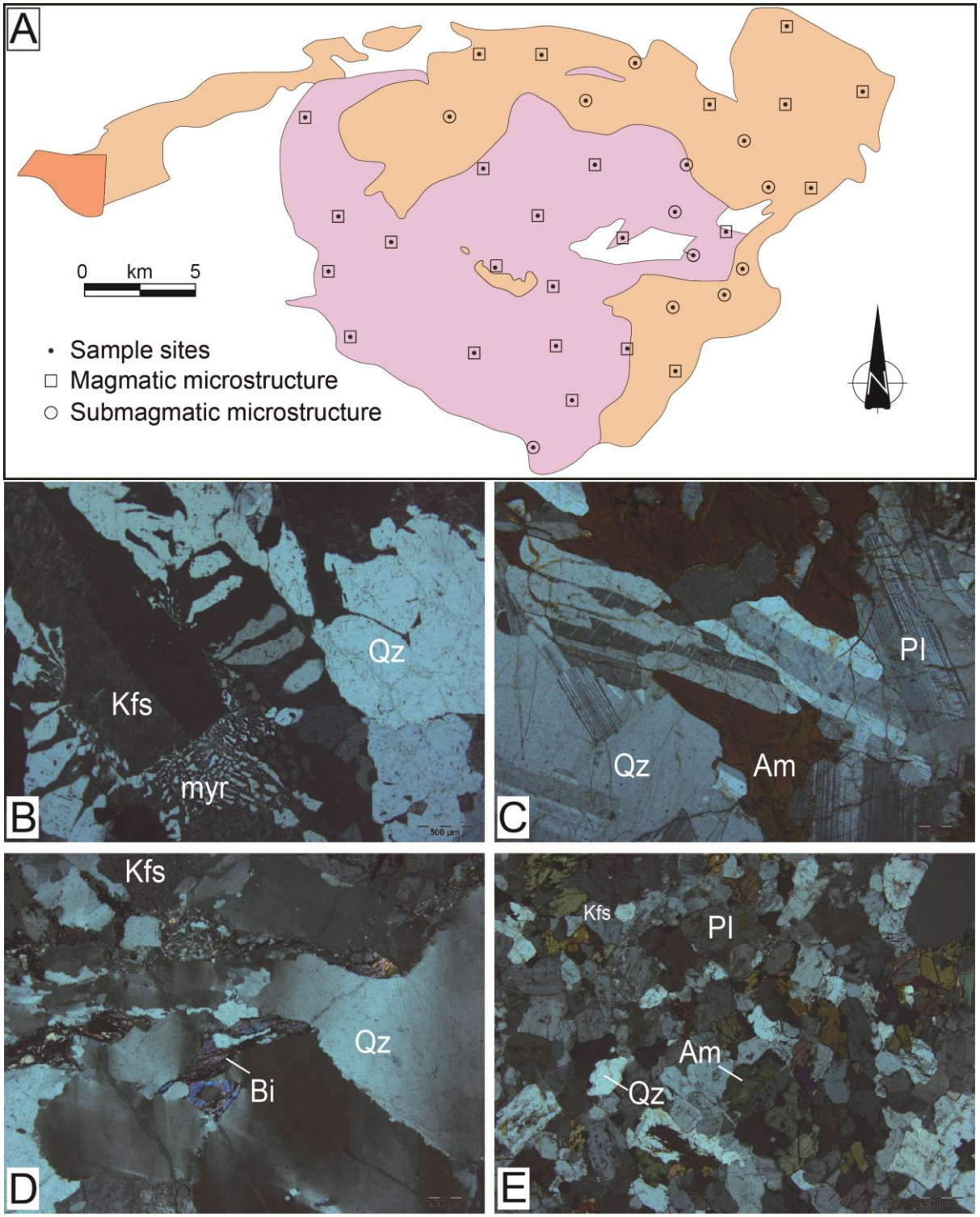

Figure 4.5 Microstructures of typical investigated samples in the Wangtufang pluton. (a) Distribution map of the different types of microstructures. (b) and (c) Magmatic microstructures in the syenogranite and the diorite, respectively. (d) and (e) Submagmatic microstructures in the syenogranite and the diorite, respectively.

consistent, yielding a Concordia age of 209.0 ± 1.4 Ma, interpreted as the Late Triassic crystallization age of the syenogranite (Figure 4.6, Table 4.1). This age is in agreement with previous age at 207 ± 1 Ma (Liu et al., 2012; Figure 4.2). Th/U ratios of Sample WTF13 range from 0.38 to 1.50. Nineteen analyses of $^{206}Pb/^{238}U$ and $^{207}Pb/^{235}U$ results show a Concordia age of 208.8 ± 1.8 Ma (Figure 4.6, Table 4.1). It corresponds to the Late Triassic emplacement age of the diorite, older than a previous age at 191 ± 1 Ma (Liu et al., 2012; Figure 4.2). The ages of the syenogranite and diorite are the same within errors.

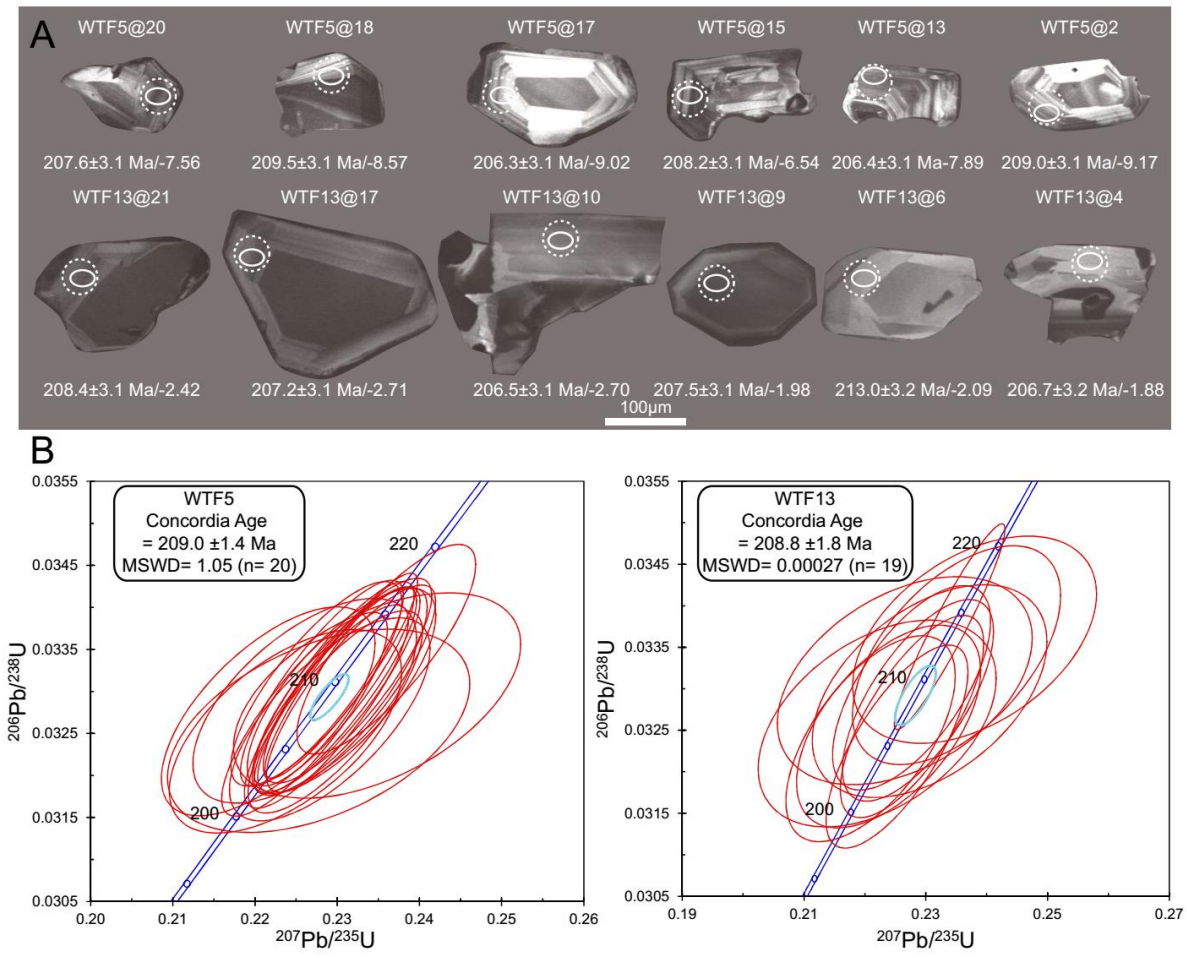

Fig 4.6 Cathodoluminescence (CL) images and U-Pb diagrams of Concordia age of representative zircons from collected samples. White solid ellipses are Secondary Ion Mass Spectrometer (SIMS) U-Pb analysis locations. White dashed circles are locations of LA-MC-ICPMS Hf analyses. Age and εHf(t) data are listed under individual zircons with ages ahead. MSWD: mean square of weighted deviates.

4.4.2. Major and trace elements analyses

Analyses of whole-rock major and trace elements were carried out at the IGGCAS. Major elements were analysed by X-ray spectrometry. Analytical precision is estimated at 1–5% for major elements. Trace elements were determined by inductively coupled plasma mass spectrometry (ICP-MS). The major- and trace-element data are documented in Table 4.2. The syenogranite samples have high SiO_2 contents ranging from 75.05 to 77.01 wt %. All samples are relatively high in Al_2O_3 (12.44–13.34 wt %), Na_2O (3.51– 4.06 wt %) and total alkalis (K_2O+ Na_2O, 8.42–8.91 wt %), with Na_2O/K_2O ratios of 0.71–0.84. They are low in P_2O_5 (0.02–0.04 wt %) and TiO_2 (0.12–0.19 wt %) abundances, and have Mg number # of 6.76–17.73. In the total alkali versus silica diagram (Figure 4.7a), all samples plot in granite field. The diorite displays a SiO_2 abundance of 51.88–56.31 wt %. It is characterized by a high Al_2O_3 content (15.78–19.66 wt %), a wide K_2O range of 1.46–3.50 wt % and total alkalis (K_2O+ Na_2O, 6.68–8.16 wt %), with Na_2O/K_2O ratios of 1.33–2.97. They have relatively high $Fe_2O_3^T$ (7.77–9.14 wt %) and low MgO (2.52–3.63 wt %) contents, with Mg # of 30.67–51.97. The samples plot in the monzodiorite and monzonite fields in the total alkali versus silica diagram (Figure 4.7a). Both the syenogranite and the diorite are peraluminous (Figure 4.7b) and can be categorized as high-K calc-alkaline series rocks (Figure 4.7c).

4.4.3. *In-situ* zircon Hf isotopes

Previously analyzed zircon grains for U-Pb isotopes were chosen for *In-situ* zircon Hf isotopic analyses. It was carried out in situ on a Neptune multi-collector ICP-MS equipped with a Geolas-193 laser ablation system at IGGCAS. Results for in situ Hf isotope analyses of zircons are shown in Figure 4.9 and Table 4.3. Zircons from the syenogranite (WTF5) have variable Hf isotopic compositions, $^{176}Hf/^{177}Hf$ ratios between 0.282377015 and 0.282469207, εHf(t) values between –9.78 and –6.54, and two-stage depleted mantle Hf model (t_{DM2}) ages

Table 4.1 SIMS zircon U-Pb data of the collected samples in the Wangtufang pluton.

Sample spot	U (ppm)	Th (ppm)	Th/U	f_{206} (%)	$^{207}Pb/^{206}Pb$	±σ (%)	$^{207}Pb/^{235}U$	±σ (%)	$^{206}Pb/^{238}U$	±σ (%)	$t_{207/206}$(Ma)	±σ (Ma)	$t_{207/235}$(Ma)	±σ (Ma)	$t_{206/238}$(Ma)	±σ (Ma)
WTF5@01	322	271	14	0.11	0.05066	1.36	0.23053	2.03	0.0330	1.51	225.2	31.2	210.6	3.9	209.3	3.1
WTF5@02	233	110	9	0.50	0.05169	2.63	0.23485	3.04	0.0330	1.51	271.8	59.3	214.2	5.9	209.0	3.1
WTF5@03	1061	1183	49	0.02	0.05037	0.68	0.23049	1.65	0.0332	1.50	212.0	15.7	210.6	3.1	210.5	3.1
WTF5@04	644	517	28	0.08	0.05048	0.87	0.22979	1.76	0.0330	1.52	217.3	20.1	210.0	3.3	209.4	3.1
WTF5@05	651	530	28	0.02	0.05032	0.87	0.22960	1.74	0.0331	1.50	209.9	20.1	209.9	3.3	209.9	3.1
WTF5@06	281	212	12	0.31	0.04985	1.94	0.22605	2.46	0.0329	1.51	188.0	44.5	206.9	4.6	208.6	3.1
WTF5@07	287	220	12	0.13	0.04906	1.83	0.22160	2.40	0.0328	1.55	150.5	42.3	203.2	4.4	207.8	3.2
WTF5@08	789	828	36	0.10	0.04999	0.93	0.22814	1.77	0.0331	1.51	194.6	21.5	208.7	3.4	209.9	3.1
WTF5@09	402	251	17	0.80	0.05108	1.11	0.23597	1.88	0.0335	1.52	244.6	25.4	215.1	3.7	212.4	3.2
WTF5@10	583	540	26	0.10	0.05055	0.90	0.23020	1.75	0.0330	1.50	220.6	20.7	210.4	3.3	209.5	3.1
WTF5@11	843	788	37	0.02	0.05087	1.14	0.22976	1.89	0.0328	1.50	235.0	26.2	210.0	3.6	207.8	3.1
WTF5@12	564	528	25	0.02	0.05063	1.01	0.23125	1.81	0.0331	1.50	223.9	23.2	211.2	3.5	210.1	3.1
WTF5@13	192	191	9	0.66	0.05077	2.93	0.22774	3.30	0.0325	1.52	230.5	66.2	208.3	6.2	206.4	3.1
WTF5@14	530	403	22	0.02	0.05086	1.57	0.22910	2.18	0.0327	1.51	234.6	35.8	209.5	4.1	207.2	3.1
WTF5@15	536	489	24	0.07	0.05054	0.96	0.22868	1.78	0.0328	1.50	219.7	22.0	209.1	3.4	208.2	3.1
WTF5@16	553	422	24	0.04	0.04985	1.11	0.22746	1.87	0.0331	1.50	188.2	25.6	208.1	3.5	209.9	3.1
WTF5@17	115	84	5	0.11	0.04988	2.09	0.22370	2.58	0.0325	1.52	189.5	47.8	205.0	4.8	206.3	3.1
WTF5@18	540	488	24	0.04	0.05087	0.98	0.23168	1.81	0.0330	1.52	234.8	22.5	211.6	3.5	209.5	3.1
WTF5@19	618	260	24	0.15	0.05061	1.11	0.23029	1.89	0.0330	1.53	223.2	25.4	210.4	3.6	209.3	3.2
WTF5@20	535	438	23	0.05	0.05009	1.01	0.22602	1.82	0.0327	1.51	199.0	23.4	206.9	3.4	207.6	3.1
WTF13@01	263	394	1.499	0.17	0.05002	1.76	0.22767	2.33	0.0330	1.52	195.9	40.4	208.3	4.4	209.4	3.1
WTF13@02	44	29	0.666	1.07	0.05302	3.33	0.19579	8.01	0.0319	1.59	-80.0	181.8	181.6	13.4	202.3	3.2
WTF13@03	39	27	0.677	1.16	0.05122	3.51	0.18726	9.02	0.0323	1.57	-223.6	209.8	174.3	14.5	204.9	3.2
WTF13@04	48	30	0.639	0.31	0.04942	3.24	0.22202	3.59	0.0326	1.56	167.9	73.9	203.6	6.7	206.7	3.2
WTF13@05	85	75	0.883	1.18	0.04956	3.03	0.18139	9.77	0.0327	1.64	-338.8	231.4	169.3	15.3	207.6	3.4
WTF13@06	76	65	0.851	0.61	0.05139	3.08	0.23802	3.44	0.0336	1.52	258.4	69.3	216.8	6.7	213.0	3.2
WTF13@07	47	31	0.651	4.83	0.07242	3.08	0.14161	25.79	0.0304	1.80	-812.4	610.4	134.5	33.0	193.3	3.4
WTF13@08	328	355	1.083	0.11	0.05058	1.44	0.22528	2.11	0.0323	1.55	221.7	32.9	206.3	3.9	204.9	3.1
WTF13@09	444	487	1.097	0.05	0.04889	1.07	0.22051	1.84	0.0327	1.50	142.5	24.9	202.3	3.4	207.5	3.1
WTF13@10	94	97	1.038	0.05	0.04990	2.29	0.22390	2.76	0.0325	1.53	190.2	52.5	205.1	5.1	206.5	3.1
WTF13@11	77	29	0.381	0.19	0.05104	2.49	0.23506	2.97	0.0334	1.61	242.4	56.5	214.4	5.8	211.8	3.4
WTF13@12	2313	1678	0.726	0.01	0.05027	0.52	0.23392	1.59	0.0337	1.50	207.6	12.0	213.4	3.1	214.0	3.2
WTF13@13	68	53	0.770	0.18	0.05213	2.58	0.23063	3.41	0.0330	1.59	228.7	68.3	210.7	6.5	209.1	3.3
WTF13@14	49	41	0.837	1.13	0.05274	3.17	0.19235	10.68	0.0319	1.68	-124.2	241.9	178.6	17.7	202.3	3.4
WTF13@15	48	32	0.673	1.68	0.05213	3.26	0.16799	13.77	0.0314	1.96	-434.0	324.8	157.7	20.3	199.6	3.8
WTF13@16	123	139	1.131	0.07	0.04946	2.04	0.22094	2.57	0.0324	1.56	169.7	46.9	202.7	4.7	205.5	3.2
WTF13@17	252	159	0.632	0.05	0.05096	1.40	0.22774	2.11	0.0327	1.52	221.0	33.5	208.3	4.0	207.2	3.1
WTF13@18	63	35	0.550	0.20	0.05121	2.97	0.22655	3.77	0.0331	1.55	178.4	78.3	207.3	7.1	209.9	3.2
WTF13@19	185	129	0.698	0.15	0.05048	1.62	0.22872	2.22	0.0329	1.51	217.2	37.1	209.1	4.2	208.4	3.1

f_{206} (%) is the percentage of common ^{206}Pb in total ^{206}Pb

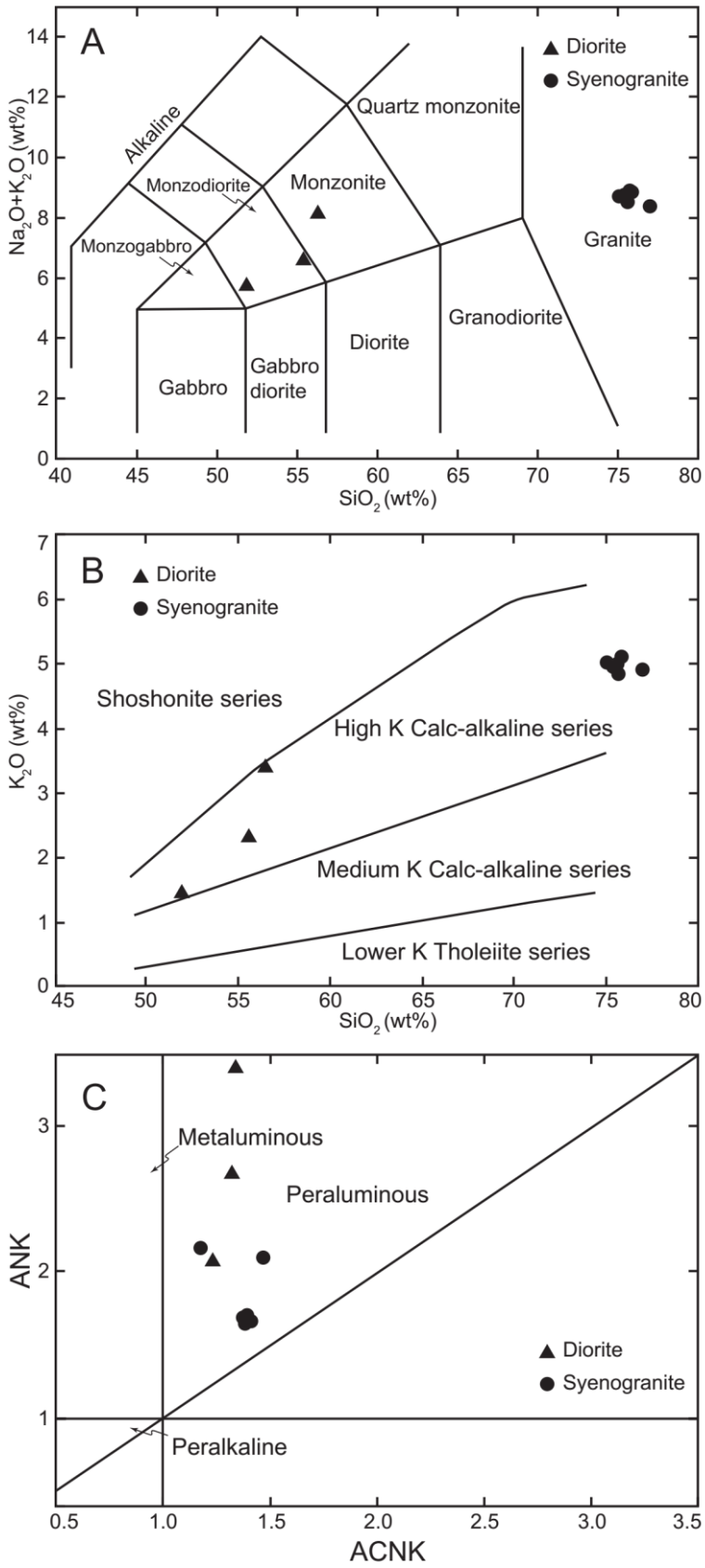

Figure 4.7 Chemical analyses diagrams of major elements for the Wangtufang pluton. (a) SiO_2 vs. Na_2O+K_2O diagram. (b) SiO_2 vs. K_2O diagram. (c) Plot of A/CNK vs. ANK.

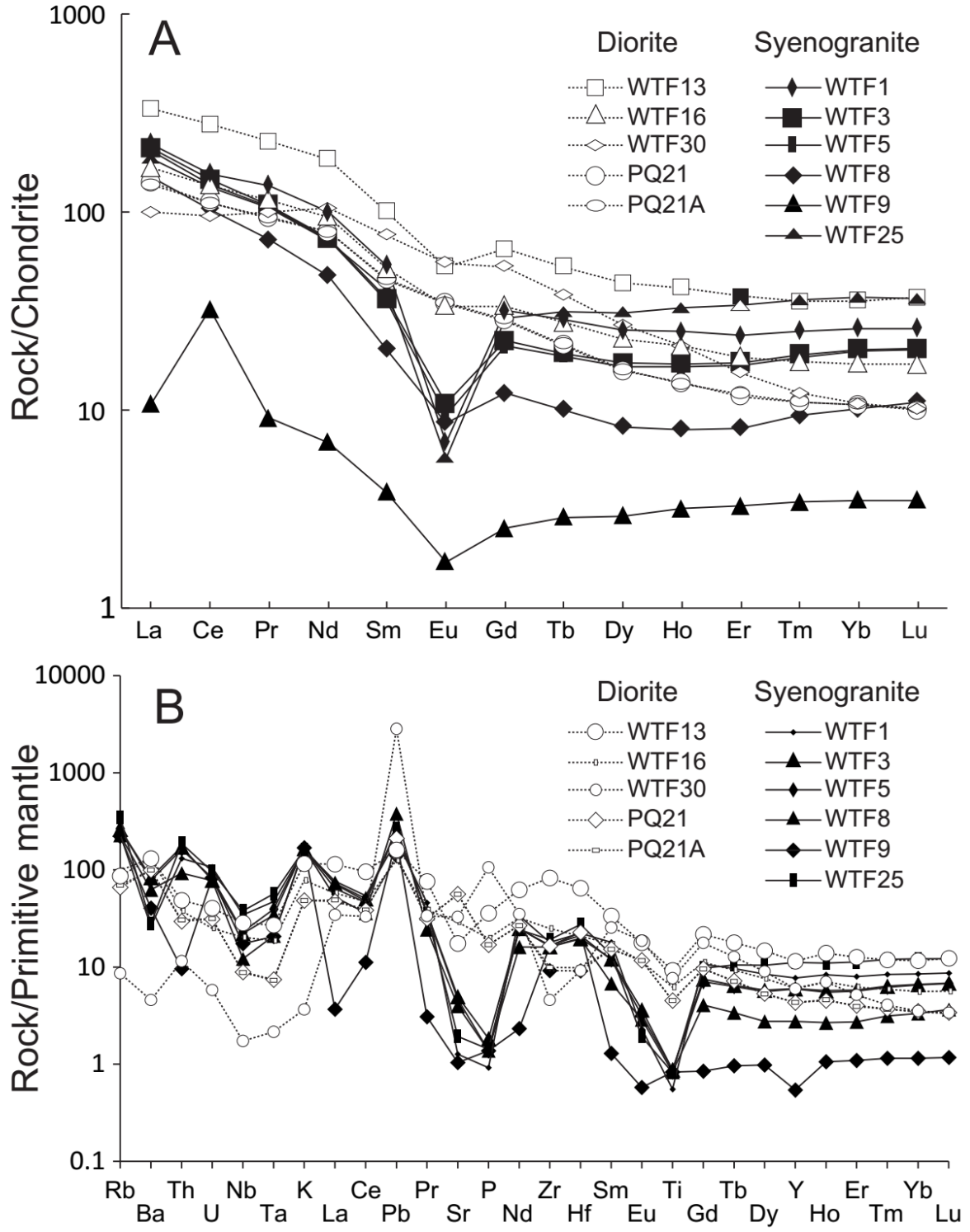

Figure 4.8 Trace elements diagrams for the Wangtufang pluton. (a) Chondrite-normalized REE patterns. (b) Primitive mantle normalized element spider patterns.

Table 4.2 Major- and trace-element concentrations of the Wangtufang pluton.

Samples	Syenogranite						Diorite				
	WTF1	WTF3	WTF5	WTF8	WTF9	WTF25	WTF13	WTF16	WTF30	PQ21	PQ21A
Major elements (wt %)											
SiO_2	75.12	75.05	75.4	75.61	75.84	76.41	56.31	55.52		51.88	
TiO_2	0.12	0.19	0.19	0.18	0.18	0.18	2.01	1.35		0.98	
Al_2O_3	12.99	13.12	13.34	12.78	13.01	12.44	15.78	17.35		19.66	
Fe_2O_3	1.48	1.46	1.49	1.38	1.47	1.29	9.14	7.77		7.79	
MnO	0.02	0.03	0.03	0.02	0.02	0.01	0.16	0.12		0.12	
MgO	0.09	0.23	0.23	0.22	0.18	0.13	2.52	3.63		3.4	
CaO	0.49	0.85	0.8	0.67	0.51	0.4	4.65	6.47		8.91	
Na_2O	4.06	3.69	3.82	3.56	3.77	3.51	4.66	4.33		4.33	
K_2O	4.85	5.03	4.96	5.01	5.11	4.91	3.5	2.35		1.46	
P_2O_5	0.02	0.04	0.03	0.03	0.03	0.03	0.78	0.43		0.37	
LOI	0.9592	0.4598	0.3599	0.4196	0.3999	0.8192	0.4995	0.7594		0.9396	
Total	100.2	100.15	100.65	99.88	100.52	100.13	100	100.08		99.84	
Mg no.	6.76	17.52	17.17	17.73	13.62	11.21	48.55	30.67		51.97	
Trace elements (ppm)											
Li	26.629	57.563	46.212	12.974	33.194	25.598	15.669	30.052	11.118	25.55	25.217
Be	5.165	3.894	4.462	2.822	4.722	9.499	1.919	1.656	0.248	1.54	1.541
Sc	2.241	2.948	2.737	2.289	0.473	2.369	17.782	17.204	36.488	22.105	22.657
V	6.851	11.208	10.163	10.614	2.956	6.081	116.69	150.06	799.62	153.699	149.922
Cr	2.66	12.504	1.943	26.645	0.064	2.004	0.175	45.085	0.424	36.91	30.475
Ni	0.097	20.613	1.699	43.821	0.015	0.075	0.102	49.898	3.375	29.137	23.733
Co	0.995	1.913	1.794	1.951	0.619	1.197	14.889	23.986	104.947	21.255	20.419
Cu	0.008	0.046	0.043	1.585	1.091	0.008	9.221	20.907	388.457	63.363	62.847
Zn	22.416	19.086	19.669	22.216	15.271	26.696	114.56	84.684	248.226	76.473	75.234
Ga	20.344	17.137	17.57	15.854	17.354	21.028	22.171	20.262	19.12	21.68	21.386
Rb	147.715	167.411	169.26	145.081	141.593	220.369	55.117	62.922	5.473	41.992	44.08
Sr	26.72	105.174	98.416	84.152	21.974	40.742	369.718	611.191	691.183	1192.454	1180.872
Y	35.136	27.271	27.023	12.558	2.47	50.738	52.193	27.574	27.282	19.615	19.722
Zr	200.774	182.478	187.2	180.3	185.199	214.669	926.307	279.572	51.377	102.939	111.36
Nb	24.563	15.802	16.483	8.701	12.421	26.982	20.246	14.465	1.235	6.34	6.244
Cs	1.471	1.995	1.717	1.507	1.947	2.704	0.885	1.015	0.638	2.147	2.121
Ba	182.298	585.276	544.673	437.668	281.945	196.154	918.051	924.753	31.966	696.358	697.568
La	52.776	49.954	48.941	36.139	2.532	44.168	78.797	39.691	23.624	32.61	33.606
Ce	96.409	89.543	84.939	63.896	19.878	82.215	170.46	83.865	58.718	68.139	68.503
Pr	12.695	10.101	9.888	6.737	0.848	9.754	21.08	10.74	9.285	8.693	8.708
Nd	45.854	33.809	33.569	21.881	3.144	32.829	84.707	43.415	47.739	36.373	36.246
Sm	7.977	5.403	5.277	3.021	0.573	6.031	14.915	7.69	11.349	6.797	6.755
Eu	0.387	0.61	0.534	0.486	0.097	0.323	2.999	1.9	3.142	1.971	1.955
Gd	6.37	4.479	4.215	2.431	0.504	5.786	12.98	6.694	10.572	5.741	5.675
Tb	1.041	0.702	0.681	0.365	0.104	1.134	1.922	1.005	1.378	0.778	0.769
Dy	6.226	4.271	4.117	2.03	0.723	7.693	10.839	5.642	6.62	3.937	3.886
Ho	1.369	0.939	0.904	0.438	0.174	1.8	2.28	1.156	1.155	0.743	0.753
Er	3.824	2.785	2.706	1.306	0.525	5.407	6.053	2.977	2.477	1.931	1.882
Tm	0.62	0.471	0.458	0.233	0.085	0.891	0.876	0.436	0.301	0.274	0.272
Yb	4.187	3.267	3.229	1.64	0.566	5.984	5.746	2.759	1.737	1.725	1.707
Lu	0.64	0.505	0.499	0.271	0.087	0.899	0.912	0.419	0.251	0.252	0.246
Hf	6.913	6.127	6.544	6.042	7.045	8.448	20.08	6.437	2.838	2.82	3.041
Ta	1.928	1.404	1.619	0.861	0.846	2.329	1.112	0.764	0.088	0.305	0.299
Tl	0.571	0.682	0.729	0.6	0.667	0.954	0.274	0.317	0.109	0.206	0.206
Pb	14.446	17.441	18.217	26.998	15.039	18.975	11.447	8.97	201.832	9.969	9.73
Bi	0.008	0.018	0.008	0.022	0.035	0.072	0.015	0.028	0.025	0.024	0.025
Th	11.154	14.683	13.84	7.894	0.814	15.901	4.127	3.233	0.979	2.506	2.593
U	2.246	1.649	1.739	1.634	1.752	2.02	0.85	0.525	0.122	0.654	0.664
REE	240.375	206.839	199.957	140.874	29.84	204.914	414.566	208.389	178.348	169.964	170.963
$(La/Yb)^N$	9.041	10.968	10.872	15.806	3.209	5.294	9.837	10.319	9.756	13.56	14.122
$(Gd/Yb)^N$	1.259	1.134	1.08	1.226	0.737	0.8	1.869	2.007	5.035	2.753	2.75
δEu	0.161	0.368	0.335	0.531	0.54	0.165	0.644	0.791	0.862	0.939	0.939
Sr/Y	0.76	3.857	3.642	6.701	8.896	0.803	7.084	22.165	25.335	60.793	59.876

between 1840.9 and 1635.3 Ma. Zircons from the diorite (WTF13) have $^{176}Hf/^{177}Hf$ ratios between 0.282555378 and 0.282665470, a range of εHf(t) values varying from –3.42 to –0.01, and two-stage depleted mantle Hf model (t_{DM2}) ages between 1439.9 and 1205.6 Ma. Magmatic zircons from the Wangtufang pluton exhibit similar εHf(t) values from −13.69 to 3.94, and two-stage depleted mantle Hf model (t_{DM2}) ages from 1582 to 950 Ma in the contemporaneous plutons (Yang et al., 2012; Zhang et al., 2012; Ye et al., 2014; Xiong et al., 2017).

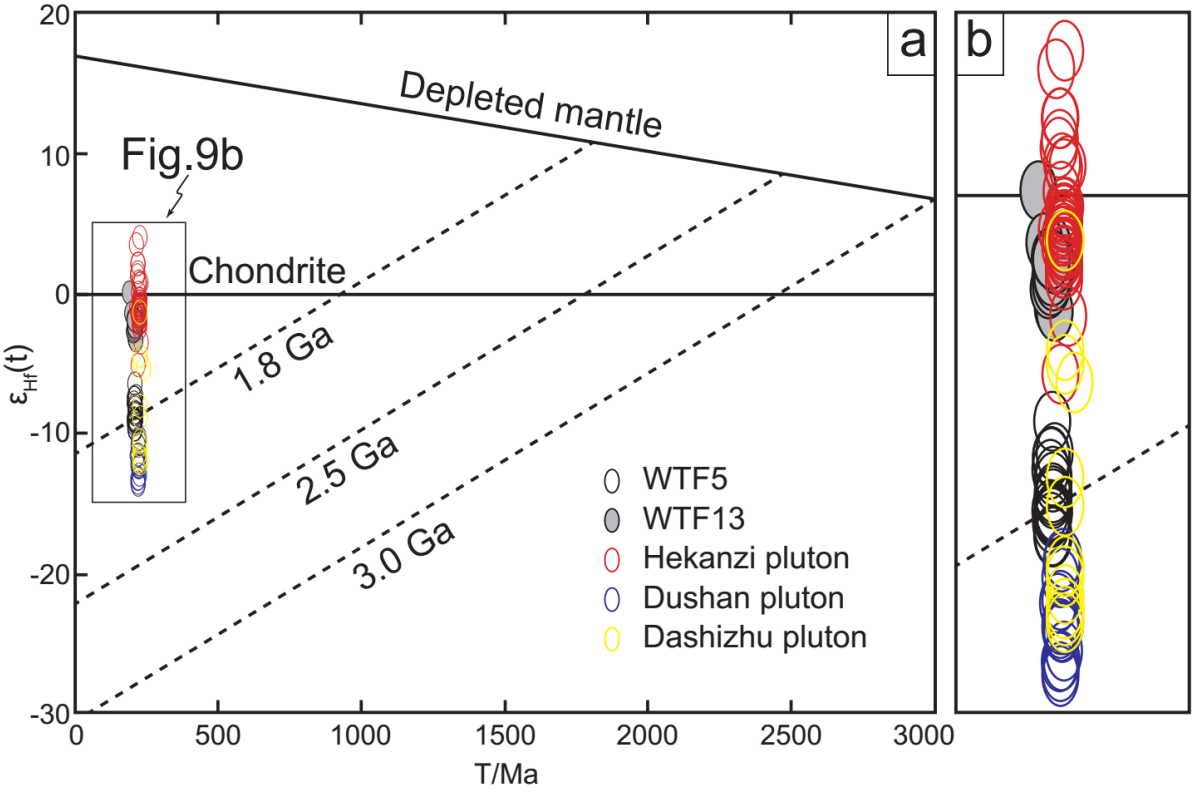

Figure 4.9 Diagram of $\varepsilon_{Hf}(t)$ vs. U-Pb ages Plot of all previously analyzed zircons for U-Pb isotopes in the Wangtufang pluton. Hf isotopic compositions of zircons from the contemporaneous plutons are from: Yang et al. (2012); Ye et al. (2014) and Xiong et al. (2017).

4.5. Anisotropy of magnetic susceptibility

Field and microscopic observations suggest that both planar and linear fabrics cannot be directly observed in the Wangtufang pluton. Magnetic fabrics can often record the fabric elements of anisotropic rocks where macro and microscopic features fail to do it (Archanjo et

al., 1994; Bouchez and Gleizes, 1995; Bouchez et al., 1997). In order to assess the fabric elements, an AMS study has been carried out. Two hundred and four cores from 36 sites have been sampled for AMS measurements in the Wangtufang pluton, 20 in the syenogranite and 16 in the diorite. The measurements are realized in the Laboratory of Paleomagnetism and Chronology of IGGCAS. A total of 204 cores from 36 sampling sites were cut into cylindrical

Table 3. LA-ICP-MS in-situ Hf isotopic analyses of zircons for the Wangtufang pluton.

Spots	$^{176}Yb/^{177}Hf$	2σ	$^{176}Lu/^{177}Hf$	2σ	$^{176}Hf/^{177}Hf$	2σ	Age Ma	Hf(0)	2σ	Hf(t)	2σ	T_{DM2} Ma
WTF5												
WTF5@01	0.061918559	0.000565047	0.002391936	0.000023718	0.282434157	0.000018958	209.2	-12.41	0.67	-8.09	0.67	1733.88
WTF5@02	0.046200317	0.000411638	0.001849648	0.000011237	0.282401908	0.000017648	208.6	-13.55	0.62	-9.17	0.62	1801.85
WTF5@03	0.10015873	0.001722638	0.00380818	0.000059406	0.282410842	0.000016635	210.5	-13.23	0.59	-9.09	0.59	1797.2
WTF5@04	0.043678224	0.000333828	0.001785268	0.000012268	0.282400376	0.000018869	209.3	-13.6	0.67	-9.2	0.67	1804.34
WTF5@05	0.060369462	0.00155435	0.002270177	0.00004654	0.282429433	0.00002053	209.9	-12.57	0.73	-8.23	0.73	1743.05
WTF5@06	0.046368219	0.000476369	0.001881102	0.000016523	0.282399856	0.000017757	208.7	-13.62	0.63	-9.24	0.63	1806.64
WTF5@07	0.063492758	0.001195794	0.002500673	0.000045288	0.28238828	0.000018342	208.1	-14.03	0.65	-9.75	0.65	1837.99
WTF5@08	0.060061948	0.000430011	0.002402079	0.000015585	0.282418168	0.000018773	210	-12.97	0.66	-8.64	0.66	1769.31
WTF5@09	0.061598304	0.000742348	0.002474388	0.000026142	0.282452683	0.000018607	212.2	-11.75	0.66	-7.39	0.66	1691.49
WTF5@10	0.045805925	0.000486004	0.001796017	0.000020742	0.28238405	0.000016971	209.4	-14.18	0.6	-9.78	0.6	1840.89
WTF5@11	0.074213346	0.000499838	0.002906497	0.000018239	0.282452932	0.000016019	207.6	-11.74	0.57	-7.53	0.57	1696.99
WTF5@12	0.054319438	0.000815447	0.002155112	0.00003442	0.282415435	0.000016802	210	-13.07	0.59	-8.7	0.59	1773.36
WTF5@13	0.048023317	0.000522095	0.00190748	0.000019111	0.282439881	0.000019216	206.2	-12.2	0.68	-7.89	0.68	1718.68
WTF5@14	0.086054436	0.002171724	0.003268983	0.000075259	0.282401921	0.000019818	207.1	-13.55	0.7	-9.4	0.7	1814.34
WTF5@15	0.048793311	0.000601951	0.001927492	0.000021159	0.28247671	0.000016599	208.1	-10.9	0.59	-6.54	0.59	1635.28
WTF5@16	0.055291388	0.000872876	0.002195829	0.000031512	0.282403999	0.000015609	210	-13.47	0.55	-9.11	0.55	1799.28
WTF5@17	0.034245856	0.000440947	0.001405436	0.000017472	0.282405618	0.000018208	206.4	-13.42	0.64	-9.02	0.64	1791.13
WTF5@18	0.071680233	0.001317072	0.002836645	0.000047486	0.282422243	0.000017641	209.4	-12.83	0.62	-8.57	0.62	1764.15
WTF5@19	0.064660119	0.001470524	0.0025632	0.000055302	0.282388079	0.000017971	209.2	-14.04	0.64	-9.75	0.64	1838.37
WTF5@20	0.065005412	0.004494199	0.002331459	0.000127921	0.28244977	0.000019249	207.7	-11.85	0.68	-7.56	0.68	1699.23
WTF13												
WTF13@01	0.070887503	0.001712752	0.00268663	0.000068933	0.282570257	0.000018423	209.4	-7.59	0.65	-3.31	0.65	1431.1
WTF13@03	0.029921548	0.001028485	0.001169852	0.000034018	0.282606536	0.000017126	207	-6.31	0.61	-1.87	0.61	1337.94
WTF13@04	0.029388946	0.000721667	0.001145751	0.000027018	0.282606237	0.000018846	206.9	-6.32	0.67	-1.88	0.67	1338.47
WTF13@05	0.021363644	0.000604621	0.000872504	0.000023278	0.282608109	0.000015082	210.3	-6.26	0.53	-1.7	0.53	1329.88
WTF13@06	0.017132269	0.000115249	0.000706643	0.000003246	0.282595116	0.000016763	212.7	-6.71	0.59	-2.09	0.59	1356.21
WTF13@07	0.014886991	0.000613816	0.000627931	0.000023041	0.282621542	0.000019501	197.3	-5.78	0.69	-1.48	0.69	1305.5
WTF13@08	0.036410477	0.000316122	0.00148751	0.000014563	0.282608086	0.000017707	204.9	-6.26	0.63	-1.9	0.63	1338.37
WTF13@09	0.024641399	0.000638458	0.001032268	0.000027792	0.282602484	0.000016474	207.9	-6.45	0.58	-1.98	0.58	1345.35
WTF13@10	0.025008579	0.000030585	0.001019844	0.000001348	0.282582773	0.000015989	206.5	-7.15	0.57	-2.7	0.57	1390.42
WTF13@11	0.024925629	0.000319276	0.001006833	0.000012157	0.282559363	0.000016186	211.6	-7.98	0.57	-3.42	0.57	1439.89
WTF13@12	0.0404143	0.000489241	0.001672372	0.000017644	0.282593622	0.000015717	214	-6.77	0.56	-2.25	0.56	1367.27
WTF13@13	0.023320932	0.000155003	0.000961585	0.000006994	0.282590546	0.000016755	209	-6.88	0.59	-2.37	0.59	1370.94
WTF13@14	0.020683125	0.000504685	0.000842818	0.000018371	0.282581244	0.000015753	203.9	-7.21	0.56	-2.79	0.56	1393.93
WTF13@15	0.015469057	0.00040892	0.000648871	0.000016472	0.282615949	0.000015587	202.5	-5.98	0.55	-1.57	0.55	1315.08
WTF13@16	0.01855407	0.000181344	0.00077223	0.000007187	0.282589274	0.000015173	205.7	-6.92	0.54	-2.46	0.54	1374.19
WTF13@17	0.028404672	0.000414295	0.001211955	0.000017877	0.282582848	0.000015722	207.1	-7.15	0.56	-2.71	0.56	1391.52
WTF13@18	0.010089984	0.000224199	0.000431451	0.000008819	0.282582036	0.000014209	210.1	-7.18	0.5	-2.57	0.5	1384.85
WTF13@19	0.024513621	0.000339898	0.001026578	0.000014811	0.282589553	0.000015794	208.4	-6.91	0.56	-2.42	0.56	1374.09

specimens of 2.2 cm in length and 2.5 cm in diameter. The anisotropy magnetic susceptibility and the bulk susceptibility were measured with a KLY4 susceptometer. The mean orientation of three principal axes of the AMS ellipsoid ($K_1 \geq K_2 \geq K_3$), the shape parameter (T), and

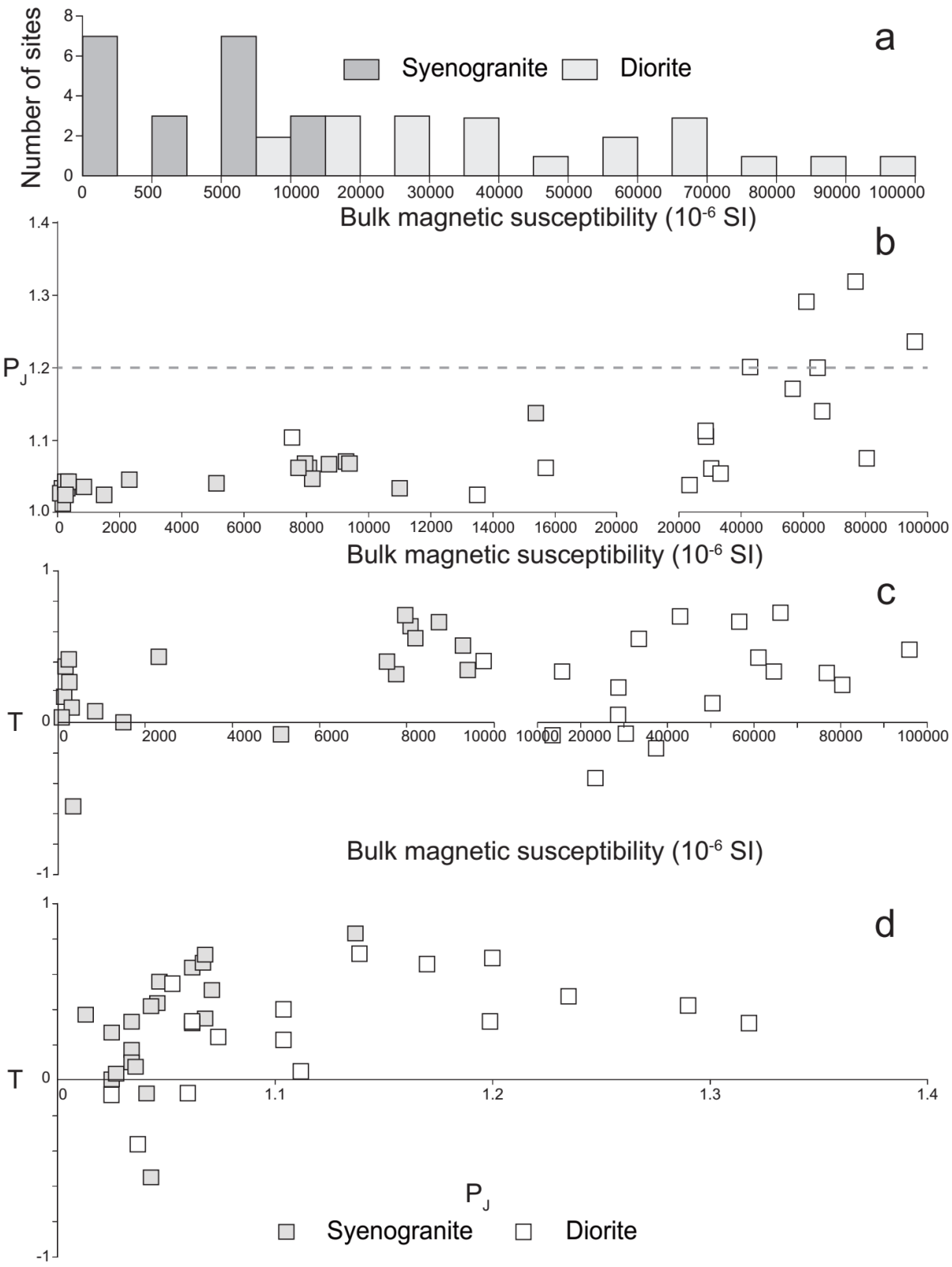

Figure 4.10 AMS scalar parameters of the Wangtufang pluton. (a) Histogram of site mean magnetic susceptibility (K_m). (b) Anisotropy degree P_J value vs. Bulk magnetic susceptibility K_m. (c) Shape parameter T vs. Bulk magnetic susceptibility K_m. (d) Shape parameter T vs. anisotropy degree P_J value.

Table 4.4 The results of AMS measurements for the Wangtufang pluton. Lat: latitude, Long: longitude, N: the number of cylinders measured in each site, Km: mean magnetic susceptibility, P_J and T: anisotropy degree and shape parameter, respectively, K_1 and K_3: magnetic lineation and pole of magnetic foliation, respectively, Inc: inclination, and Dec: declination, α_{95max} and α_{95min}: Jelinek's statistic confidence at 95% level (Jelinek, 1981) in degrees, respectively.

site	Coordinates		N	Km	P_J	T	K_1				K_3			
	Long(°E)	Lat(°N)		(10^{-6}SI)			Dec(°)	Inc(°)	α_{95max}(°)	α_{95min}(°)	Dec(°)	Inc(°)	α_{95max}(°)	α_{95min}(°)
WTF1	118.544	41.060	6	9280	1.071	0.509	232.7	25.7	9.1	3.2	346.1	39.5	3.7	2.5
WTF2	118.490	41.078	5	8080	1.062	0.636	306.8	15.6	23.5	4	56.6	50.5	6.5	2.6
WTF3	118.535	41.081	6	8730	1.067	0.663	241.6	1.7	20	4.2	333.4	46.4	6.6	3.4
WTF4	118.477	41.175	6	23400	1.037	-0.362	220.9	10.4	13	3.3	112.5	59.9	18.1	6.5
WTF5	118.495	41.155	5	7960	1.068	0.709	238.7	12.1	19.4	4.2	110.8	71.1	6.2	3.5
WTF6	118.526	41.136	5	2310	1.046	0.435	226	16.7	13.1	2.2	22.4	71.9	9.9	2.6
WTF7	118.534	41.107	6	15400	1.137	0.829	251.7	6.1	14.6	3.1	6	75.4	19.1	2.3
WTF8	118.502	41.114	5	9390	1.068	0.348	200.4	14.4	29.1	13	315.5	58.9	14.6	4.5
WTF9	118.576	41.080	7	8190	1.047	0.557	194.8	25.2	11.2	3.2	318.2	49.5	3.9	3.9
WTF10	118.601	41.072	5	28700	1.104	0.23	17.2	6.6	17.8	7.3	114.8	48.8	11.2	6.5
WTF11	118.662	41.213	6	95900	1.235	0.477	292.7	51.5	12	4	199.9	2.2	7	4.7
WTF12	118.704	41.187	5	80400	1.074	0.247	173	30.6	22.4	10.9	336.5	58.4	13.8	3.1
WTF13	118.619	41.180	5	30400	1.06	-0.072	203.7	34.1	13.3	2.4	31.2	55.7	10	2.5
WTF14	118.493	41.202	6	64600	1.199	0.334	240.9	86.4	6.5	3.2	122.2	1.7	4.4	2.9
WTF15	118.527	41.201	6	42900	1.2	0.694	168.3	50.3	12	1.6	4.5	38.5	3.5	0.8
WTF16	118.551	41.183	6	33400	1.053	0.548	274	2.5	24.3	3.9	8.1	58.2	9.4	3.1
WTF17	118.579	41.199	5	76800	1.318	0.325	146.6	74.4	32.8	10.4	28.6	7.5	14.8	10.7
WTF18	118.637	41.167	5	15700	1.06	0.334	135.3	21.9	69	5.9	330	67.4	13	4.5
WTF19	118.661	41.181	6	66100	1.139	0.718	99.9	43.5	16	5.5	213.3	22.7	9	2.5
WTF20	118.557	41.156	6	1500	1.025	0.003	104	6.0	15.9	15.9	8.7	40.7	46.4	10.2
WTF21	118.568	41.129	6	146	1.034	0.171	30.8	3.1	38.1	15.7	144.8	82.4	31.1	8.1
WTF22	118.601	41.137	6	318	1.034	0.1	105.8	15.3	19.5	9.2	201	18.3	21.4	1.5
WTF23	118.610	41.157	6	176	1.013	0.37	254.2	29.4	57	13	33.9	53.5	19.9	12.2
WTF24	118.599	41.097	7	28600	1.112	0.051	332.3	63.4	8.2	5	124.4	23.9	18.6	5.9
WTF25	118.611	41.119	6	90	1.027	0.036	273.4	15.1	13.9	9.7	66.1	73.1	22.7	13.5
WTF26	118.627	41.103	6	61000	1.29	0.425	306	66.0	7.1	3.5	118.5	23.8	6.6	3.4
WTF27	118.637	41.114	5	7540	1.104	0.403	303.2	50.1	10.9	5.1	56.4	18.2	24.5	7.8
WTF28	118.629	41.131	6	250	1.043	0.418	17.5	23.3	16.5	2.5	277.4	22	3.9	2.2
WTF29	118.652	41.147	5	13500	1.025	-0.082	171.6	25.1	15.8	1.4	319.4	61	26.3	2.8
WTF30	118.675	41.148	6	56600	1.17	0.659	315.9	78.4	18.8	7.4	137.6	11.6	18.1	7.2
WTF31	118.416	41.134	6	854	1.036	0.075	194.9	19.4	73.4	66	313.8	53.9	77.2	66
WTF32	118.398	41.175	5	352	1.043	-0.551	94.8	8.8	7.1	3.2	217.1	73.8	20.9	2.1
WTF33	118.522	41.037	5	5110	1.041	-0.076	247.3	16.0	7.8	3.1	128	59.6	11.2	5.2
WTF34	118.423	41.086	5	263	1.025	0.268	350.8	0.2	20.4	7.9	85.1	86.7	15.2	7.6
WTF35	118.445	41.125	6	7750	1.062	0.32	248.3	18.2	86.3	3.5	96.5	69.6	10.4	3.4
WTF36	118.410	41.112	6	11000	1.034	0.33	199.1	39.4	57.7	16.7	78.5	31.8	37.6	21.3

the anisotropy degree (P_J) were calculated by the ANISOFT package (Jelinek, 1981). The magnetic mineralogy was investigated to identify the magnetic susceptibility carriers by several methods, including: (1) Isothermal Remanent Magnetization (IRM); (2) thermomagnetic (K-T) curves, and (3) hysteresis loops.

4.5.1. Magnetic mineralogy

The histogram of mean magnetic susceptibility, $K_m = (K_1 + K_2 + K_3)/3$, displays a large range of values in 36 sites, from 90 to 95,900×10^{-6} SI (Figure 4.10a and Table 4.4). In the diorite, all 16 sites exhibit K_m values higher than 7,000×10^{-6} SI (7,540 to 95,900×10^{-6} SI), demonstrating the predominance of ferromagnetic minerals. In the syenogranite, K_m mainly varies from about 90 to 15,400×10^{-6} SI, and 7 out of 20 sites show K_m values lower than 500×10^{-6} SI, implying that the paramagnetic minerals (biotite) may be the main carriers of the magnetic susceptibility (e.g., Tarling and Hrouda, 1993). In 13 out of 20 sites, K_m values are higher than 500×10^{-6} SI, suggesting the presence of ferromagnetic minerals. It seems that both paramagnetic and ferromagnetic minerals are the contributors to the magnetic fabrics in the syenogranite.

All hysteresis curves of six representative samples display nonlinear variations (Figures 4.11a–4.11c). Sudden saturation of the isothermal magnetic remanence below 300 mT occurs in all samples (Figures 4.11d–4.11f). Thermomagnetic measurements show a rapid drop of magnetic susceptibility at ~580°C (Figures 4.11g–4.11i). All these results suggest that magnetite is likely an overwhelming contributor to the magnetic carriers in the Wangtufang pluton despite the presence of biotite. The ratios of hysteresis parameters Mr/Ms and Hcr/Hc display the mean grain size of the magnetite of the analyzed samples is within the pseudo-single domain (PSD) zone (Dunlop, 2002; Figure 4.12), indicating that the principal axes of the magnetic susceptibility ellipsoid (K_1 and K_3 measured in this study) correspond to the major

morphological axes of minerals, representing magnetic lineation and the pole of magnetic foliation, respectively.

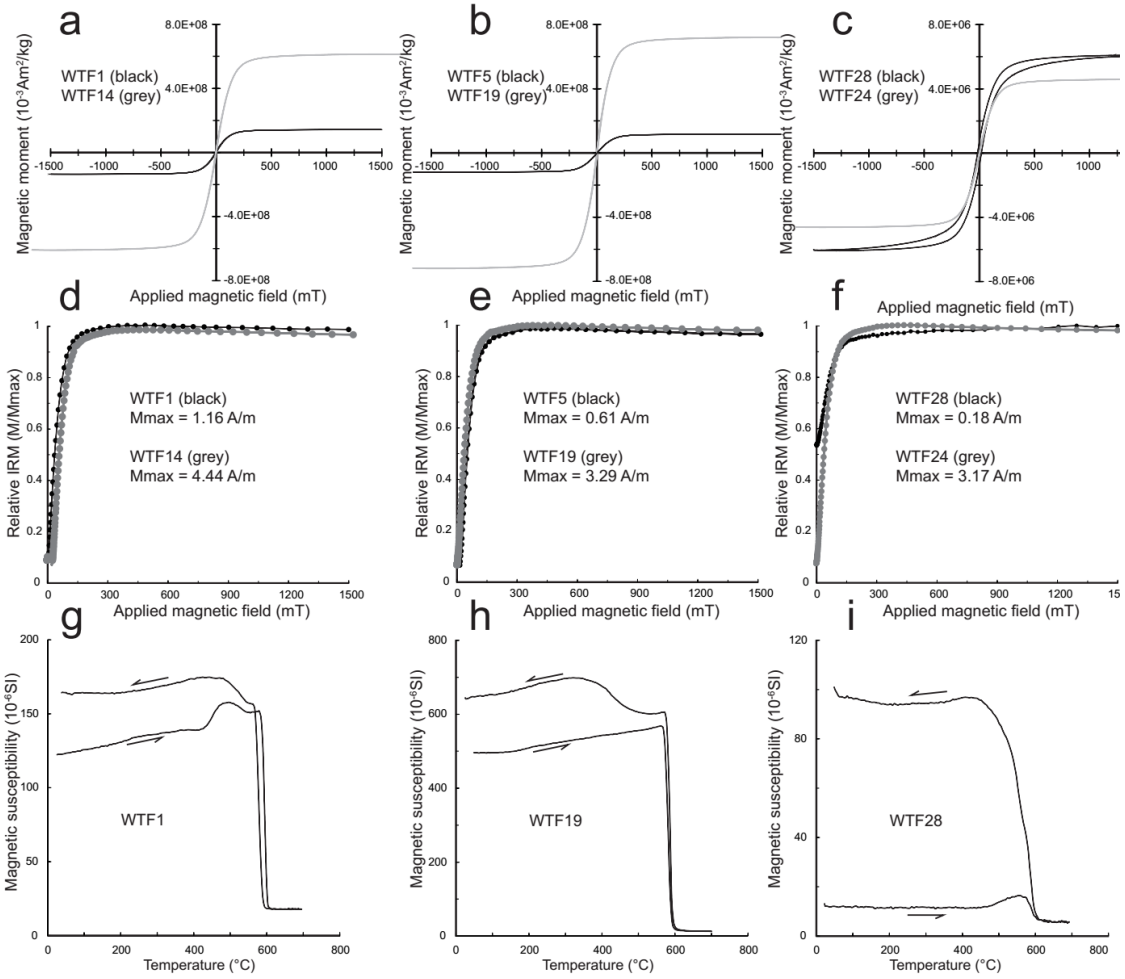

Figure 4.11 Magnetic mineralogy investigations of representative specimens from the Wangtufang pluton. (a–c) hysteresis loops, (d–e) acquisition of isothermal remanent magnetization (IRM), and (g–i) thermomagnetic curves (K (T) curves).

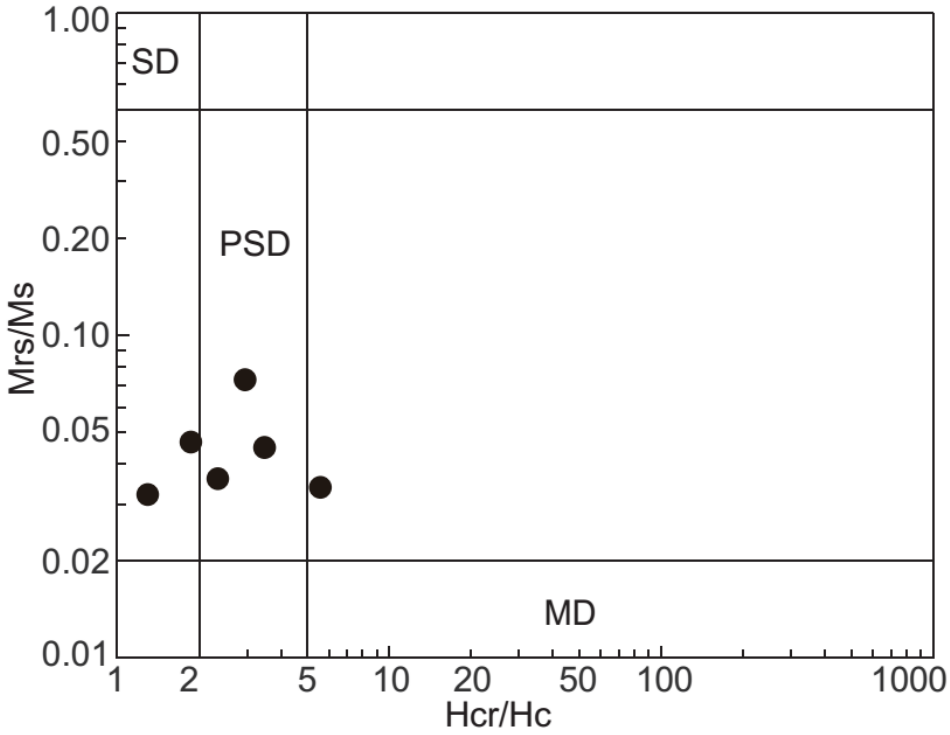

Figure 4.12 Day plot of hysteresis parameters. Mrs: saturation of magnetic remanence, Ms: saturation of induced magnetization, Hcr: coercivity of magnetic remanence, Hr: coercivity of the measured sample. SD: single domain, PSD: pseudo-singledomain, MD: multidomain.

More than 92% of the sampled sites display an anisotropy degree (P_J) lower than 1.2 (Figures 4.10b and 4.10c), concordant with the magmatic fabrics recognized by microscopic observations, and the remaining sites come from the diorite, implying that their higher P_J value may be due to the high concentration of magnetite (Cruden, et al., 1999). The shape parameter (T) mainly ranges between -0.551 and 0.829, showing a dominant oblate shape (~86%) for magnetic fabrics (Figures 4.10c and 4.10d). Obvious correlations between P_J, T, and K_m is lacking, implying that AMS varies independently from the magnetic minerals (Borradaile and Henry, 1997; Figures 4.10b–4.10d).

4.5.2. AMS results

The site-average orientation with corresponding 95% confidence level (α_{95max} and α_{95min}) was calculated for K_1 and K_3 axes of each site (Jelinek, 1978; Figure 4.13). For a confidence level larger than 25°, the direction of the corresponding magnetic axis is considered as poorly

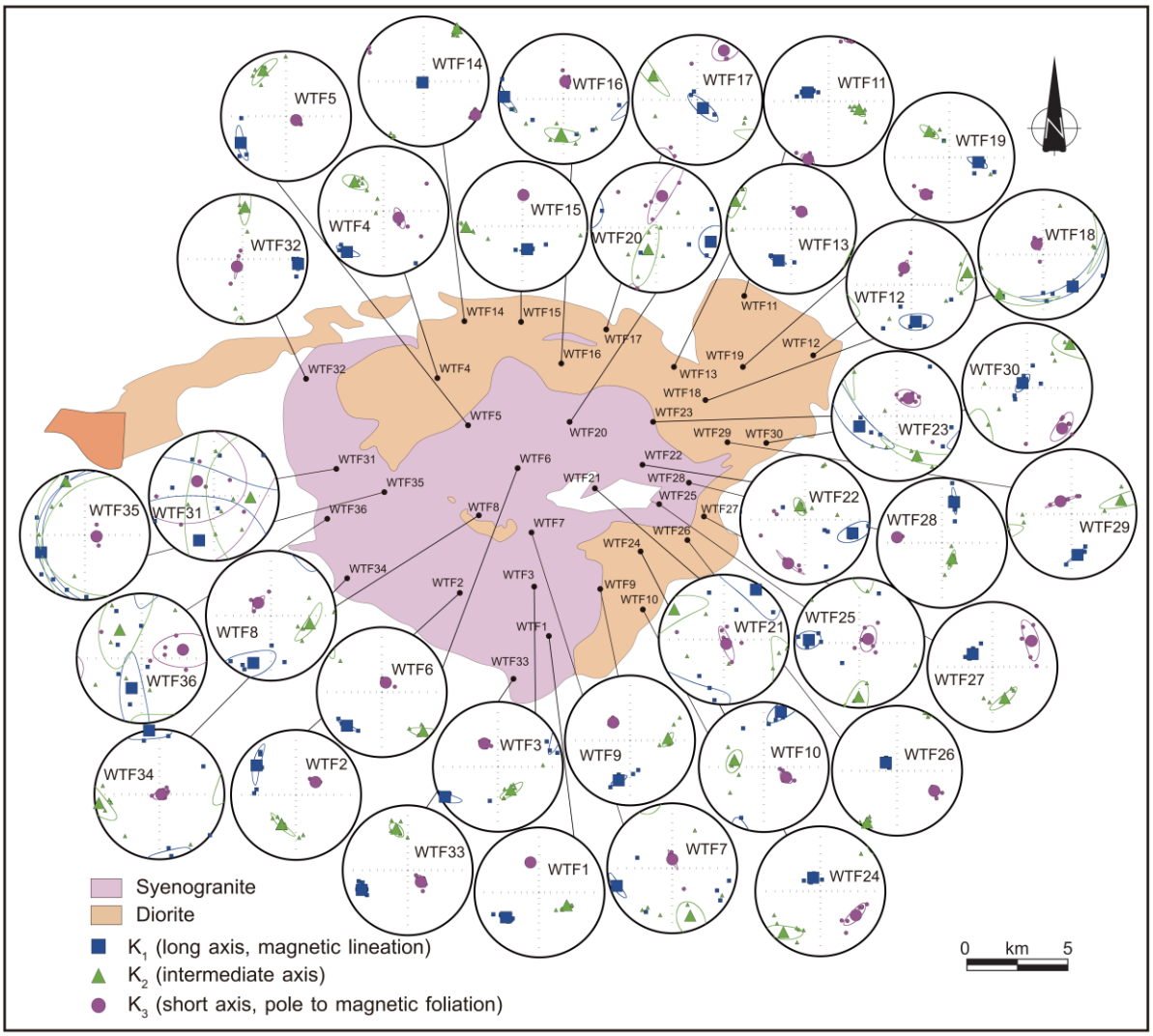

Figure 4.13 Equal-area projections (lower hemisphere) of AMS results for each sampling site. Confidence ellipses at 95% level are drawn around each average orientation direction.

defined, whereas it is considered as well-defined or reliable when lower than 25°. More than 78 % of the AMS sites are well defined for both K_1 and K_3. The magnetic fabrics were mapped throughout the Wangtufang pluton (Figure 4.14).

At the map scale, the magnetic foliations in the diorite strike subparallel to the pluton boundary and dip inward at variable angles (Figure 4.14a). The magnetic lineations are highly scattered with variable dips (Figure 4.14b). This may be due to an overprint by the late-stage tectonomagmatism. Instead, in the syenogranite, both the magnetic foliations and lineations are highly grouped (Figure 4.14a). Magnetic foliations, also parallel to the pluton boundary,

display a concentric arrangement. The majority of specimen (14 out of 20 sites) show subhorizontal foliations with dip angles ranging from 3° to 40°. Specimens from six sites have moderately steep magnetic foliations (dip angles ranging from 45° to 70°). These sites are almost near the contacts with the country rock and the diorite. The magnetic lineations are all horizontal to subhorizontal (mainly ~9° to 29°) and have nearly constant NE–SW plunges (Figure 4.14b).

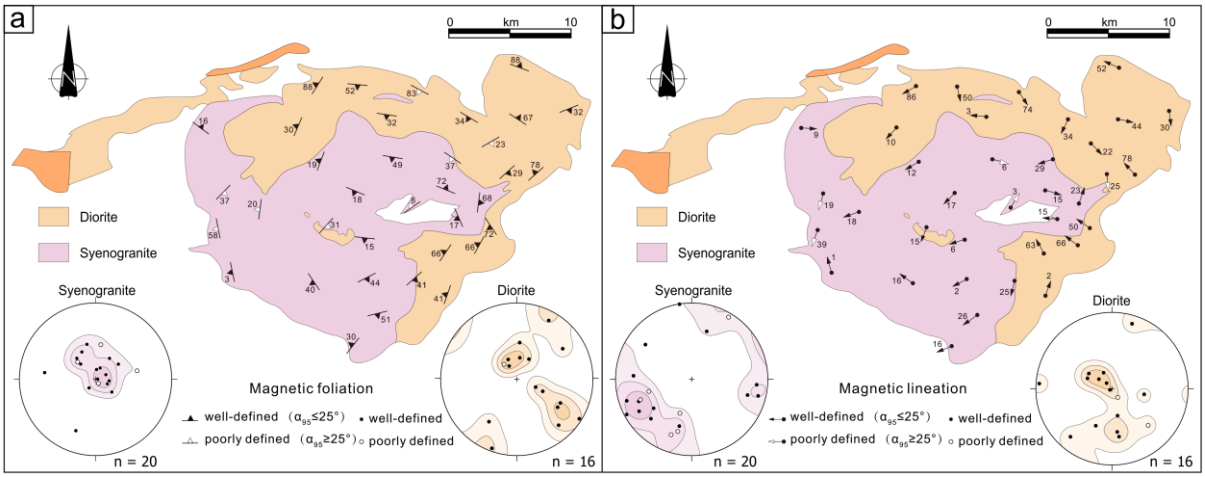

Figure 4.14 Mesoscopic and magnetic fabric patterns and orientation diagrams of K_3 and K_1. (a) Foliations. (b) Lineations.

4.6. Gravity modeling

Gravity modeling has been long proved its efficiency to constrain the geometry and possible feeder zones of pluton (e.g., Vigneresse et al., 1990; Améglio and Vigneresse, 1999; Lin et al., 2013b). We carried out a gravity study to characterize the shape of the Wangtufang pluton at depth.

4.6.1. Residual Bouguer anomaly and 2D modeling

The short wavelengths of the gravity anomaly originate from upper crust (down to a few kilometers). The long wavelengths of the gravity anomaly, which reflect the deep structures, must be removed from the complete Bouguer anomaly to highlight the Wangtufang pluton related anomalies. Available Bouguer anomaly map (1: 200,000) in the Wangtufang

pluton and its surrounding area was derived from the Chinese regional gravity survey. A regional lower-resolution (2′×2′) Bouguer grid acquired from the International Gravimetric Bureau database (Bonvalot et al., 2012). The long wavelengths of the gravity anomaly were extracted using a 200 km low-pass Butterworth filter from a lower-resolution (2′×2′) Bouguer grid after several attempts. The residual Bouguer anomaly map was obtained from the complete Bouguer anomaly by subtracting the filtered regional Bouguer anomaly related to the long wavelengths (Figure 4.15a).

2D gravity modeling was also performed to characterize the geometry of the Wangtufang pluton. To build these models, several constraints have been taken into account, including (1) geological contacts, lithological units, and structural data from geological maps and our field observations; (2) geometrical constraints, derived from indirect analysis of gravity anomaly, and (3) densities of geological units, determined by the laboratory measurements. The residual gravity anomaly has been modelled along three profiles across the center of the pluton (Figure 4.15b).

4.6.2. Results

In the residual Bouguer gravity anomaly map, the Wangtufang pluton displays a NE–SW trending elongated negative anomaly with a highest value in its center (Figure 4.15a). The negative anomalies decrease, even change into positive anomalies outwards. Particularly, the diorite shows a less negative anomaly in its northwest and a higher positive anomaly in its southeast, suggesting its thin thickness. The Wangtufang pluton becomes thinner outwards, presenting an overall funnel-shaped geometry. The country rocks display high positive anomalies in its east. To the southwest, the country rocks show a high negative anomaly, indicating the possible continuity of the pluton underlain the country rocks. The highest negative anomaly is located in its northwest due to a large area of Archaean migmatitic granite. Three 2D modeling profiles image the detailed geometry of the two major intrusions (Figure

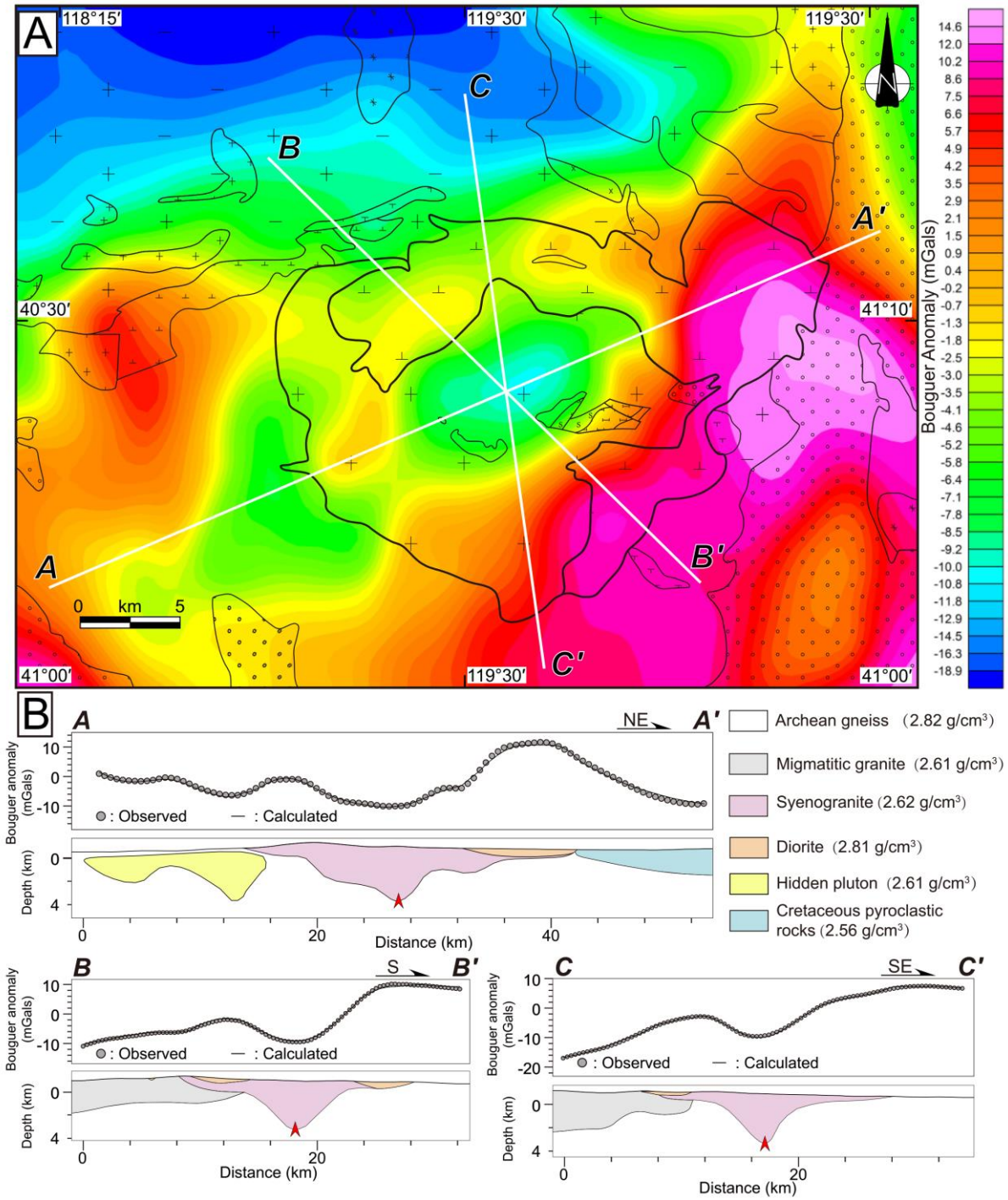

Figure 4.15 Gravity modeling. (a) Residual Bouguer gravity anomaly of the Wangtufang pluton and adjacent areas after subtraction of a 200 km wavelength regional trend from the complete Bouguer anomaly. Symbols and captions are the same as in Fig. 2. (b) 2D gravity modeling across the Wangtufang pluton. Note that the arrows show the possible feeder zones for the pluton.

4.15b), revealing (1) a thin thickness of the diorite that overlies the syenogranite; (2) a maximal thickness of about 4 km in the center of the syenogranite which progressively decreases outwards; (3) a slightly NE–SW trending elongated subsurface shape of the syenogranite with inward dipping sidewalls.

4.7. Discussion

4.7.1. Magma sources of the Wangtufang pluton

Both high SiO_2 syenogranite and relatively low SiO_2 diorite are characterized by low MgO, enrichment in LREE and LILE, and depletion in HREE and HFSE, with negative Eu anomalies (Figures 4.7 and 4.8), suggesting that they mainly derived from partial melting of ancient lower crust. However, their in-situ zircon two-stage depleted mantle Hf model ages (t_{DM2}) are both Proterozoic, ranging from ~1.840 to 1.635 Ga and ~1.439 to 1.205 Ga, respectively (Figure 4.9). Considering that the Wangtufang pluton intrudes into Archaean gneiss and migmatitic granite ($>$2.5 Ga), the sources should be derived from the partial melting of Archean TTG in the lower crust with a contribution from a depleted mantle source. The $\varepsilon_{Hf}(t)$ values for the syenogranite range from –9.78 to –6.54 and those of the diorite from –3.42 to –0.01 (Figure 4.9). Although the diorite was mainly derived from melting of ancient lower crust, $\varepsilon_{Hf}(t)$ values of the diorite are much higher than normal crustal melting (Figure 4.9), requiring some input of depleted asthenospheric mantle components. The $\varepsilon_{Hf}(t)$ values of the syenogranite are higher than those of the Archean lower crust (-28 ~ -13; Jiang et al., 2013). It suggests that the syenogranite has a contribution from an enriched subcontinental lithospheric mantle. Therefore, the Wangtufang pluton was mainly derived from partial melting of the ancient lower crust of the NCB with some involvements of enriched subcontinental lithospheric mantle and depleted asthenospheric mantle components. Coeval with the Wangtufang pluton, Late Triassic silica-undersaturated syenites in the alkaline complexes in

the northern NCB were derived from partial melting of an enriched lithospheric mantle, coupled with crustal assimilation and crystal fractionation in an intracontinental extensional setting (i.e., rift; Yang et al., 2012). Its similarity with the contemporaneous alkaline complexes may indicate an asthenosphere–lithospheric mantle interaction in the northern NCB during the Late Triassic (Yang et al., 2012; Zhang et al., 2012). Briefly, the Wangtufang pluton was derived from the mixing of magmas from asthenospheric upwelling-induced melting of subcontinental lithospheric mantle and ancient lower crust during an intracontinental extensional setting.

4.7.2. Emplacement model

Geochronology data suggest that both the syenogranite and the diorite were emplaced in the Late Triassic (both at ~209 Ma; Figure 4.6). Concerning the fabric pattern of the diorite, magnetic foliations show variable dip angles and scattered magnetic lineations, and this may be due to the later intrusion of the syenogranite (Figure 4.14). The border-parallel magnetic foliations are usually considered as a consequence of magma inflation during the intrusion. Gravity modeling reveals thin remnants of diorite, which are close to the roof of the syenogranite (Figure 4.15). Furthermore, field observations indicate that numerous syenogranite dykes intruded into the diorite with sharp contact and dismembered the diorite after its fully crystallization (Figure 4.4). As the fabric pattern seems to be modified, it is difficult to retrace the emplacement process of the diorite, therefore, we shall focus on the emplacement of the syenogranite.

In the syenogranite, the current exposure is close to the roof of the pluton due to the covering of the diorite remnants (Figure 4.15). The mostly subhorizontal magnetic foliations, roughly parallel to the contact, develop near the roof (Figure 4.14a). Bouguer gravity anomaly reveals a NE-SW trending elongated subsurface shape with an overall funnel-shaped geometry, an unflat bottom, and moderate- to high- inward dipping sidewalls (Figure 4.15). The root of

the syenogranite as a feeder zone is located in its center. Thus, it might be estimated as a lopolith-like intrusion (Figure 4.16). Considering the lack of significant emplacement-related ductile deformation in the country rocks, the syenogranite with a concentric fabric pattern could emplace by the inflation of the magma from its central feeder zone and the pluton is built up by floor depression (Figure 4.16). The subhorizontal magnetic fabrics could have developed by magmatic flow subparallel to a roof, represented by the floor of the diorite (e.g., McNulty et al., 2000). A dominant gentle magnetic fabric could be formed by flattening of magma mush against its roof, driven by later magma pulses (McNulty et al., 2000). The arrivals of later magma batches resulted in downward inflation of magma chamber against the roof. Floor

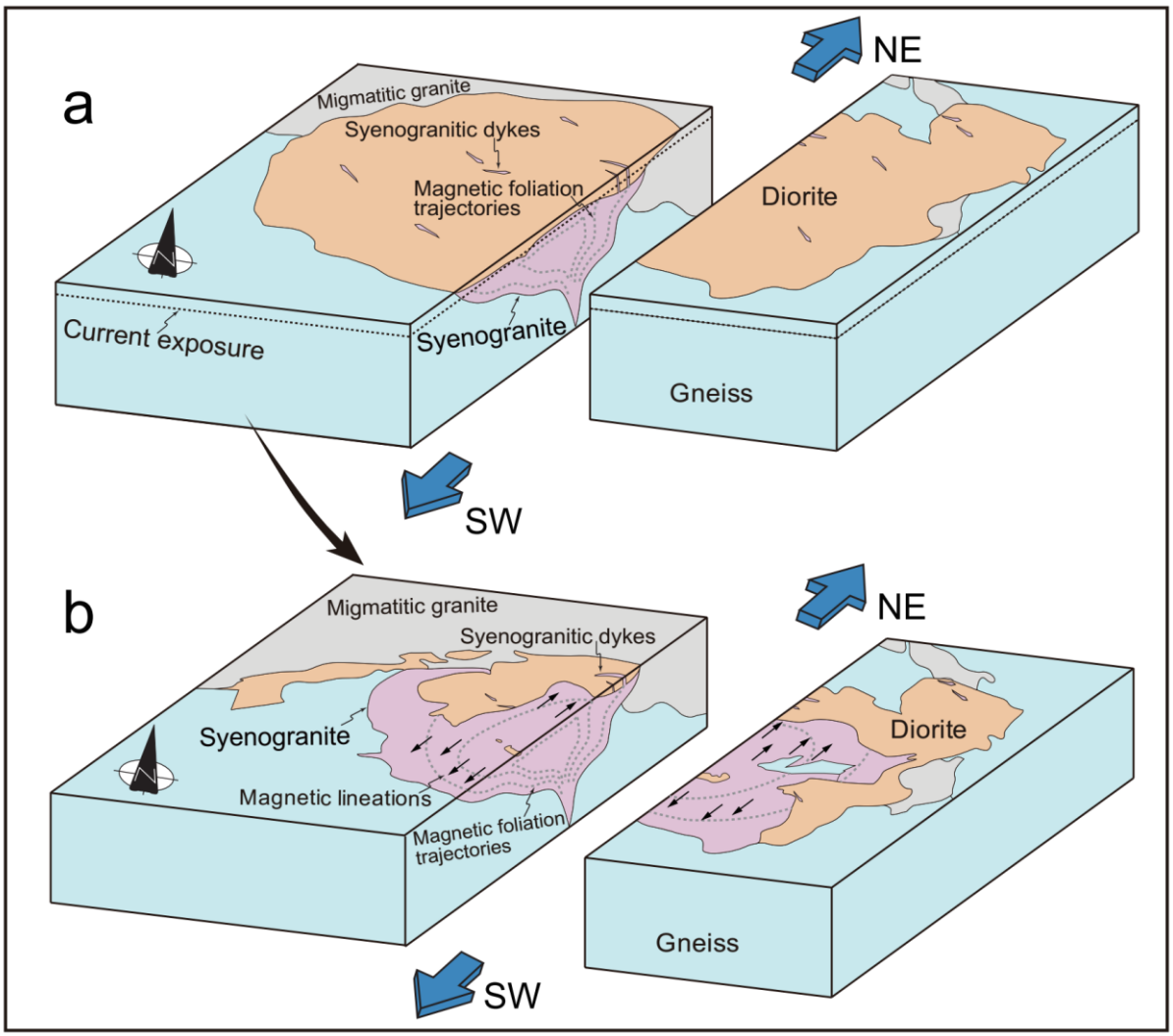

Figure 4.16 Block diagrams of emplacement mode of the Wangtufang pluton.

depression occurred and created space for the pluton building (Figure 4.16). Close to the pluton, the country rocks were pushed aside and it resulted in the border-parallel foliations in the surrounding gneiss (Figure 4.2). We suggest that the diorite made a first intrusion, probably with a thin thickness, and then the syenogranite intruded and possibly dismembered the former with a series of dykes after the diorite had fully crystallized (Figure 4.16).

4.7.3. Relationships between the pluton emplacement and regional tectonics

The microstructures observed in the Wangtufang pluton are typical of magmatic or sub magmatic fabrics that developed during, or just after, the full crystallization of the magma. However, the lack of significant emplacement-related ductile deformation in both the pluton and its country rocks does not preclude that a regional tectonic event, dominated by brittle deformation occurred during the Wangtufang pluton emplacement. The syenogranite intruded the diorite after its full crystallization as shown by the dyke swarm containing diorite xenoliths (Figure 4.4b). All the syenogranitic dykes are steeply dipping and striking NW–SE. We interpret these syenogranite dykes as tension gashes developed in the brittle upper crust, and controlled by a NE–SW stretching. This view implies a possible NE–SW trending regional extension (Figure 4.16).

Moreover, the plutons shape and internal fabric can record some increments of the regional strain to which the magma was subjected (e.g., Paterson et al., 1998; Sant'Ovaia et al., 2000). Because mineral fabrics are easily reset, they reflect only the last strain increment developed in soft material such as magmatic rocks before their full crystallization. Furthermore, without any regional strain or pre-existing structural control, the magmatic lineation that reflects the magma flow within the pluton would have variable orientations and plunges (e.g., Paterson, 1989; Liu et al., 2018). Thus, we argue that the syenogranite, presenting a general NE–SW magnetic lineation, may have recorded a NE–SW trending regional extension (Figure 4.16). Meanwhile, the pluton growth could have been guided by the NE–SW trending regional

tectonic regime, suggested by a NE–SW trending elongated subsurface shape of the pluton (Figure 4.15a).

Geochemical data suggest that the Wangtufang pluton was derived from the partial melting of Archaean TTG in the lower crust with a contribution from a depleted mantle source. This feature is consistent with the geochemical characteristics of the E–W trending alkaline intrusive complexes along the northern NCB (Zhang et al., 2012; Figure 4.17). Especially, the silica-undersaturated syenites comply with a Late Triassic intracontinental extensional setting after the final formation of the Central Asian Orogenic Belt (Yang et al., 2012; Figure 4.17). Besides, a NE–SW trending regional extension in the northern NCB has been documented in the Sonid Zuoqi MCC in the vicinity of the Solonker zone (Davis et al., 2004; Figure 4.17). The $^{40}Ar/^{39}Ar$ ages of muscovite in the detachment fault were 224~208 Ma. Detrital zircon dating and sedimentological studies of these basin remnants showed a fining and deepening upward depositional system as well as abundant volcaniclastic rocks from the conformable Upper Triassic to Lower Jurassic strata, suggesting a Late Triassic extensional tectonic setting (Davis et al., 2009; Meng et al., 2014; Figure 4.1). The emplacement of the Wangtufang pluton provides new structural constraints on the Late Triassic NE–SW trending extensional setting in the northern NCB.

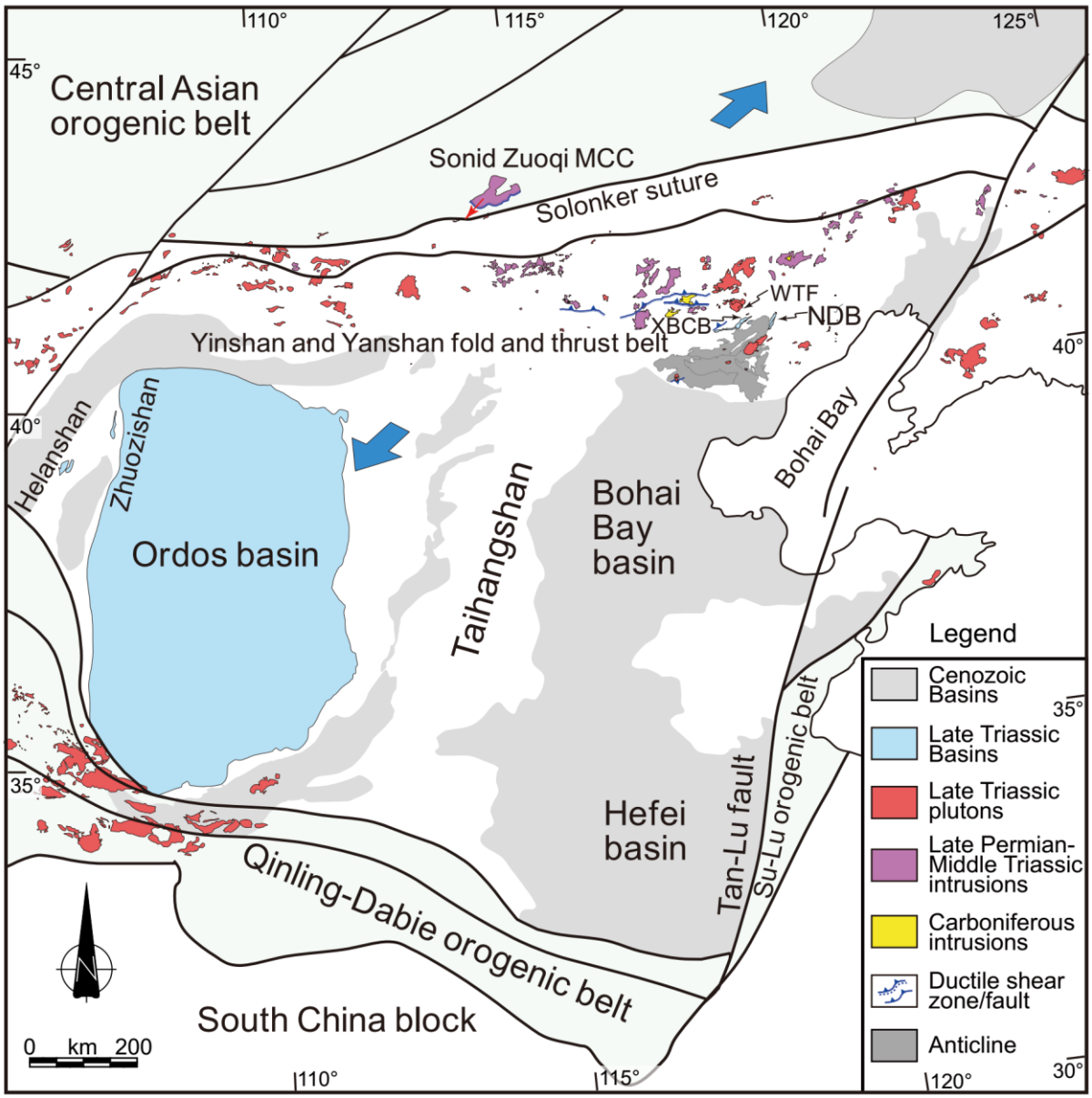

Figure 4.17 Triassic tectonic framework of the NCB showing Late Triassic tectonic setting of the northern NCB. XBCB: Xiabancheng basin, NDB: Niuying-Dengzhangzi basin, WTF: Wangtufang pluton.

Chapter 5. Emplacement of the Jurassic Jianchang-Jiumen pluton

5.1. Introduction

The NCB is one of the most important continental terranes that form the East Asian continent (e.g. Davis et al., 2001; Yin and Nie, 1996). It is separated from the Siberia Craton in the north by the Central Asian Orogenic Belt and from the South China Block in the south by the Qinling-Dabie-Sulu orogen (Figure 5.1). The NCB is considered to be a stable craton after the Paleoproterozoic amalgamation of the Eastern, Intermediate (or Fuping) and Western blocks (Faure et al., 2007; Trap et al., 2012; Zhao et al., 2001). The Phanerozoic tectonic evolution of the NCB is related to two orogenic cycles, including Paleozoic-Triassic continental collisions with Mongolian arc terranes and South China Block at block boundaries (Hacker et al., 2000; Mattauer et al., 1985; Meng & Zhang, 1999; Windley et al. 2007; Xiao et al., 2003, 2015; Z. Xu et al., 1986; B. Xu et al., 2013), and Jurassic-Early Cretaceous intracontinental orogeny (Davis et al., 2001; Dong et al., 2015; Faure et al., 2012).

Jurassic-Early Cretaceous intracontinental orogeny, also termed the Yanshanian Orogeny in the Chinese literature (Wong, 1929), was widespread and intense in the North China Craton (Davis et al., 2001). It gave rise to a complicated assemblage of folds, thrust and reverse faults, normal faults, and Mesozoic plutons in the NCB. Alternating contractional and extensional deformations have been recognized in the Yanshan fold-and-thrust belt (Davis et al., 2001; Faure et al., 2012). Two phases of shortening, including late Middle Jurassic (172-164 Ma) and late Late Jurassic-earliest Cretaceous (152-135 Ma) are quite evident, albeit timing and duration of these events remain debated (Davis et al., 2001; Dong et al., 2015; Faure et al., 2012; C. Li et al., 2016). However, Jurassic extensional deformations have not widely constrained except Early Cretaceous large-scale crustal extension implying the destruction of the North China Craton (Lin & Wei, 2018; Wang et al., 2011). Only sporadic grabens or half-

grabens have been documented in the NCB during Early Jurassic-early Middle Jurassic (Darby et al., 2001; Li et al., 2015; Qi et al., 2015; Ritts et al., 2001; Zhang et al., 2011) and early Late Jurassic (Davis et al., 2001, 2009; Qi et al., 2015). Particularly, Early Jurassic contractional tectonics were also proposed according to the unconformity between Triassic and

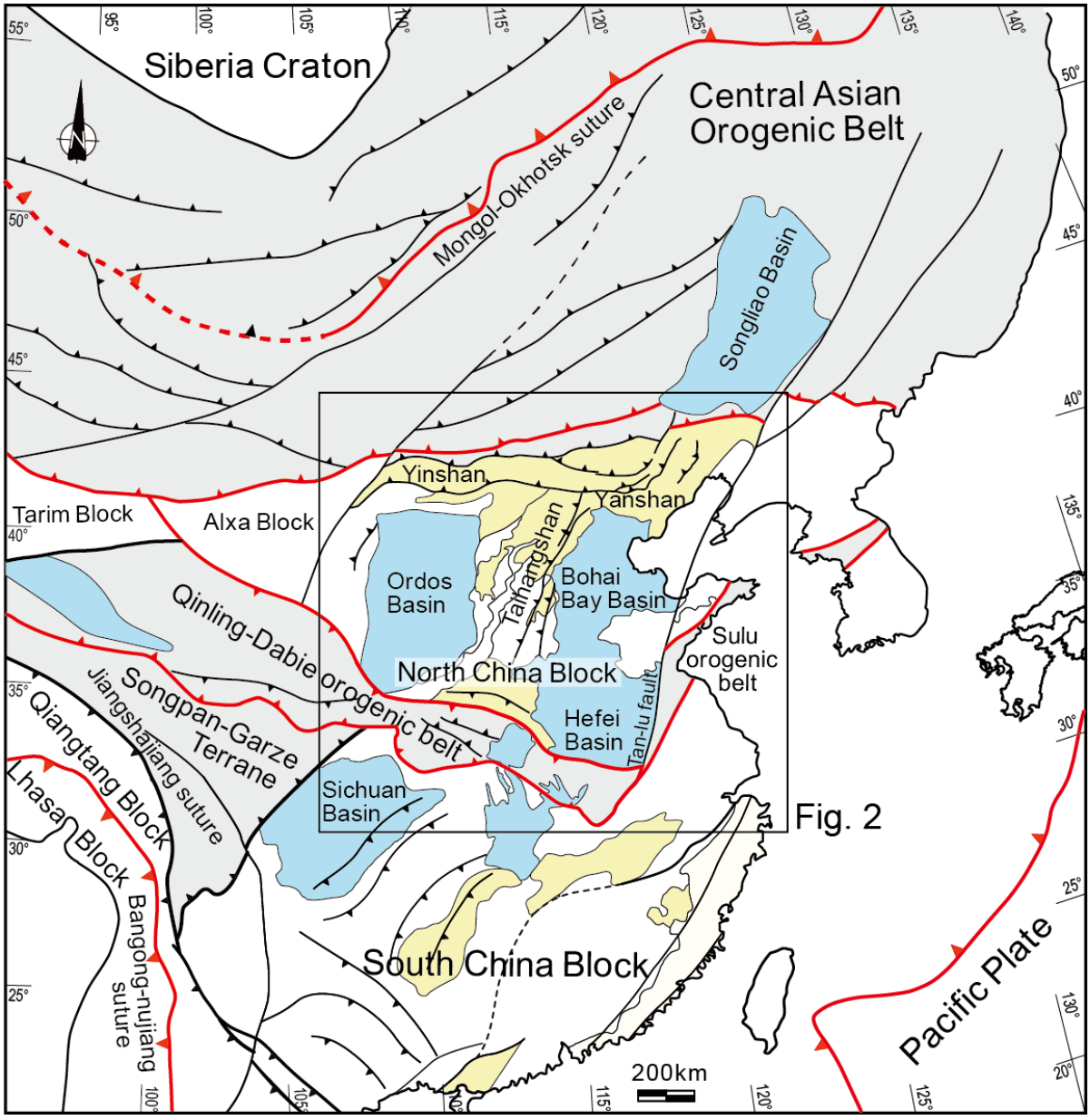

Figure 5.1 Simplified geological sketch map of the East Asian continent (Modified from Lin & Wei, 2018).

Lower Jurassic strata, and Lower Jurassic syntectonic conglomerate (Zhao, 1990; Liu et al., 2012). Therefore, Jurassic extensional tectonics of the NCB remains ambiguous.

Jurassic-Early Cretaceous intracontinental orogeny is a key element of the East Asian tectonics. After Paleozoic-Triassic amalgamation, the welded East Asian continent was bounded by the Mongol-Okhotsk Ocean in the north, Bangong–Nujiang Ocean in the southwest, and the Paleo-Pacific Ocean in the southeast. Jurassic–Early Cretaceous deformations are widespread through East Asia (Figure 5.1; Dong et al., 2015). As such, any proper understanding of the Mesozoic East Asian tectonics requires a clear vision on the Jurassic-Early Cretaceous intracontinental orogeny. The Jurassic–Early Cretaceous intracontinental orogeny in the NCB, named the Yanshanian Orogeny, was variously interpreted to be related to i) the closure of the Mongol–Okhotsk Ocean (Yin and Nie, 1996; Davis et al., 2001), ii) the subduction of the Paleo-Pacific plate (G. Zhu et al., 2011; R. Zhu et al., 2011; Xu and Wang, 1983), iii) the interactions of north-south Eurasian intraplate deformation and northwestward Pacific Paleo-Pacific plate (Davis et al., 2001) or iv) multiple plate convergence of the Mongolo-Okhotsk Ocean, Bangong–Nujiang Ocean, and the Paleo-Pacific Ocean (Dong et al., 2015). Due to poor understanding of multiphase deformation events, especially extensional tectonics, the external driving force for the Jurassic-Early Cretaceous intracontinental orogeny in East China remains controversial.

To understand the Jurassic-Early Cretaceous intracontinental orogeny of the NCB, it is crucial to clarify Jurassic extensional tectonics and its relationship to the dynamics of plate subduction/collision along active boundaries. Pluton emplacement processes potentially contain significant information on both magma internal dynamics and external strain fields to which the magma was subjected (e.g., Bouchez, et al., 1997; Paterson et al., 1998). The structural study of plutons is an effective and practical way to unveil regional tectonic setting coeval with the emplacement process (e.g., Bouchez, et al., 1997; De Saint Blanquat et al.,

2011; Lin et al., 2013). In this study, we selected Jurassic Jianchang-Jiumen pluton in the Yanshan fold-and-thrust belt to provide regional tectonic information for Jurassic extensional episodes through an integrated multidisciplinary investigation (including structural geology, isotope chronology, Anisotropy of magnetic susceptibility (AMS), and gravity modeling). Further, Integrating previous studies concerning other structural elements in North China during Jurassic-Early Cretaceous, an improved and more detailed structural framework of the NCB was established for understanding the Jurassic-Early Cretaceous intracontinental orogeny and associated geodynamic mechanism in East Asia.

5.2. Geological Setting

5.2.1. Tectonic setting

After the cratonization through Paleoproterozoic amalgamation of the Eastern, Intermediate (or Fuping), and Western blocks (Faure et al., 2007; Li et al., 2012; Trap et al., 2012; Zhao et al., 2001), the NCB was surrounded by the Paleo-Asian Ocean in the north (Windley et al. 2007; Xiao et al., 2003, 2015; Xu et al., 2013) and the eastern branches of Paleo-Tethys Ocean in the south (Hacker et al., 2000; Mattauer et al., 1985; Meng and Zhang, 1999; Xu et al., 1986). In the north of the NCB, the closure of the Paleo-Asian Ocean was characterized by the amalgamation of several microcontinental blocks (e.g., the Erguna, Xing'an, Songnen, Jiamusi, and Khanka block; Liu et al., 2017; Sengör et al., 1993; Zhou et al., 2018), albeit the timing of the final closure of the Paleo-Asian Ocean remains debated, i.e., Late Devonian (Xu et al., 2013; Zhao et al., 2013) or Late Permian-Early Triassic (Chen et al., 2000, 2009; Jian et al., 2008, 2010; Li et al., 2006; Lin et al., 2008; Xiao et al., 2003, 2015). In the south, the final amalgamation between the North and South China Blocks occurred in the Triassic through multistage orogeny during the Paleozoic to the Triassic, giving rise to Late Triassic Dabie-Sulu high-pressure and ultrahigh-pressure (HP–UHP) orogenic belt (e.g.,

Mattauer et al. 1985; Faure et al., 1999, 2003; Hacker et al., 2000; Lin et al., 2005, 2009; Li et al., 2017, 2018; Ratschbacher et al., 2003, 2006; Figure 5.1).

During the Jurassic-Cretaceous, the welded East Asian continent was surrounded by the Mongol-Okhotsk Ocean, the Paleo-Pacific Ocean, and the Bangong–Nujiang Ocean. The Mesozoic tectonics of the NCB is mainly related to the spatial-temporal influence of the Paleo-Pacific and Mongol–Okhotsk tectonic regimes (Figure 5.1). The closure time of the Mongol-Okhotsk Ocean between the Siberian Craton and the North China–Mongolian terrane remains controversial, e.g., the Middle Jurassic (Zorin, 1999; Parfenov et al., 2001; Kravchinsky et al., 2002), the Late Jurassic- early Early Cretaceous (Cogné et al., 2005; Metelkin et al., 2010; Pei et al., 2011; Yang et al., 2015), or the Early Cretaceous (Enkin et al., 1992). Generally, it is acknowledged that the Mongol-Okhotsk Ocean closed progressively from west to east in the north of the East Asian continent (Zorin, 1999; Daoudene et al., 2013; Kravchinsky et al., 2002; Metelkin et al., 2010; Dong et al., 2015). The onset of Paleo-Pacific Plate subduction has been considered to occur in the Late Triassic (Sagong et al., 2005; Kim et al., 2015), or Early Jurassic (Wu et al., 2007; Guo et al., 2015; Wang et al., 2019). It is well agreed that the influence of the Paleo-Pacific tectonic regime has extended to the northern and northeastern China from the Early Jurassic (e.g., Hao et al., 2020; Li et al., 2007; Wang et al., 2019; Wu et al., 2007).

5.2.2. Jurassic Geological Overview of the NCB

Due to the intense deformation during the Yanshanian orogeny, Jurassic strata mainly remain in the Ordos basin, the Yinshan-Yanshan fold and thrust belt, as well as Taihangshan, and Bohai Bay-Hefei basins (Figure 5.2). The Lower Jurassic-lower Middle Jurassic strata in the NCB consist of conglomerate, sandstone, and mudstone intercalated with thick coal beds (Figure 5.3). In these strata of the western NCB, the E-W trending normal faults are widely recognized in the Ordos basin and its periphery, such as Daqingshan, and Taihangshan (Figure

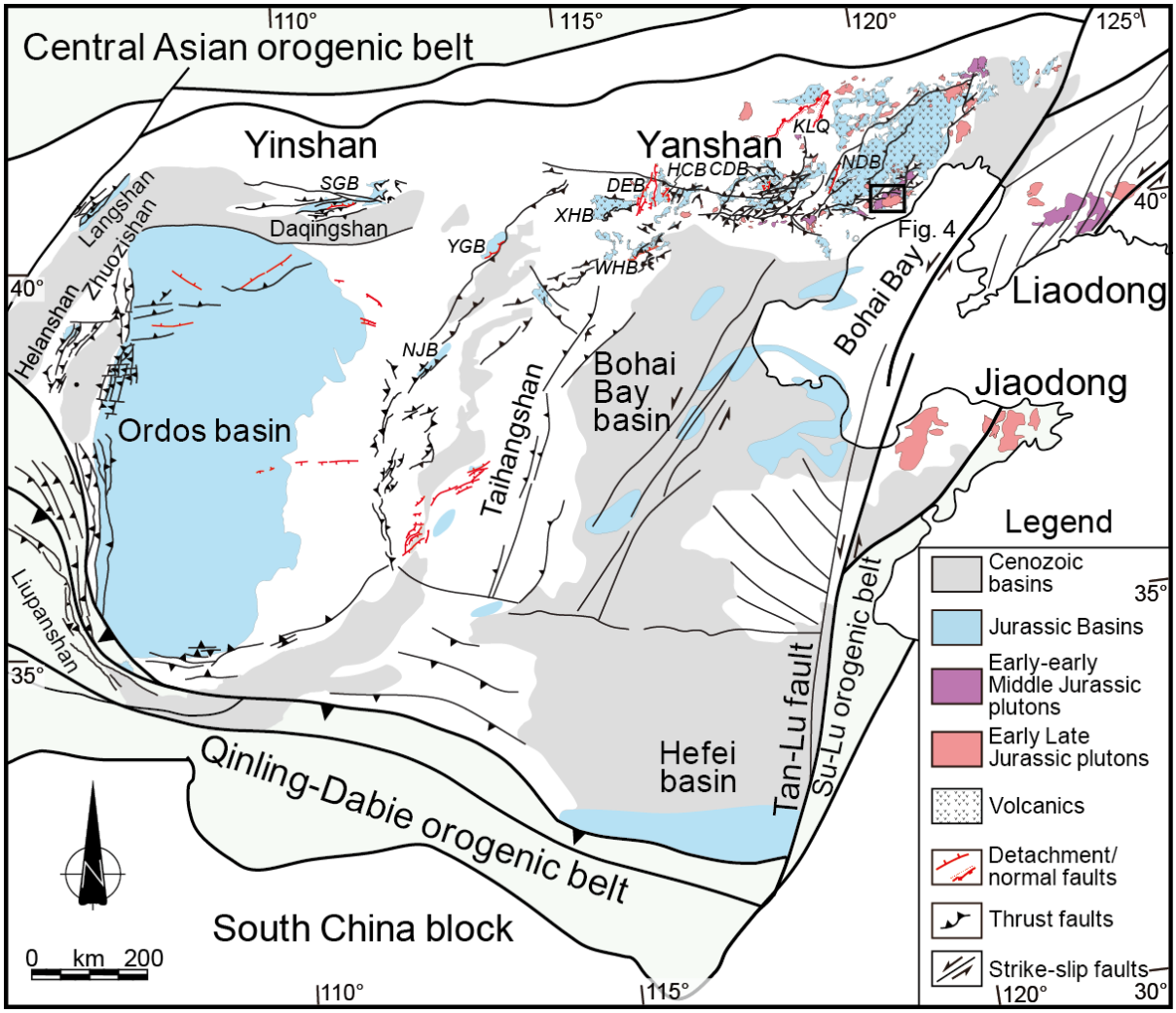

Figure 5.2 Simplified geological map showing the Jurassic structures and magmatic rocks in the NCB (Modified from Zhang et al., 2007). SGB: Shiguai basin; YGB: Yungang basin; NJB: Ningwu-Jingle basin; XHB: Xuanhua basin; WHB: Western Hill basin; DEB: Diaoe basin; HCB: Houcheng basin; CDB: Chengde basin; NDB: Niuyingzi-Dengzhangzi basin; KLQ: Kalaqin metamorphic core complex. See Figure 5.1 for locations.

5.2; Darby et al., 2001; Li et al., 2015; Ritts et al., 2001; Zhang et al., 2011). In the eastern NCB, the Lower Jurassic-lower Middle Jurassic strata contain abundant basalt interlayered with andesite and pyroclastic rocks (e.g., the Nadaling or Xinglonggou Formations; Figure 5.3). Sedimentary studies suggest that these Lower Jurassic-lower Middle Jurassic strata were deposited in an extensional setting (Davis et al., 2009; Meng et al., 2014; Meng et al., 2019). The late Middle Jurassic - Late Jurassic-magmatic rocks are only distributed in the eastern

NCB (e.g., the Liaodong peninsula and the eastern Yanshan fold-and-thrust belt; Figure 5.2). An Early Jurassic NE trending rift basin was recognized in the Western Hill basin in Beijing (Xu and Wu, 1989).

The upper Middle Jurassic strata are separated from the lower Middle Jurassic coal-bearing sequences and older units by an angular unconformity (Figure 5.3). The syntectonic conglomerate and sandstone (i.e., Longmen (J_2l) and Jiulongshan (J_2j) Formations, Li et al., 2014; Xiahuayuan Formation (J_2x), Liu et al., 2018; Changhangou Formation (J_2c), Wang et al., 2017; Yungang Formation (J_2y), Li et al., 2014) overlay this unconformity. The nearly N-S directed thrusts related to this event widely occurred within the Yanshan fold and thrust belt (Figure 5.3; e.g., the Duanshuwa-Jianbaoshan thrust, C. Li et al., 2016; Miyun-Xifengkou fault and secondary faults, Zhujiakou fault, Xinglong fault, Gaobanhe fault, Sanpo fault, and Banbishan fault, Chen, 1998; Lengkou fault, Zhang et al., 2004; Sandaogou fault, Zhao, 2016). The volcanic and pyroclastic rocks of the Tiaojishan/Lanqi Formation cover these N-S directed thrusts. The N–S shortening was synchronous with the syntectonic Changhangou and Yungang growth strata in the western Daqingshan and Taihangshan (Li et al., 2014; Wang et al., 2017). The duration of this event (i.e., Event A of the Yanshanian orogeny) has been well constrained between 172 and 164 Ma (Li et al., 2016).

The volcanic and pyroclastic rocks of the Tiaojishan/Lanqi Formation in lower Upper Jurassic and concomitant granite plutons (164-155 Ma) are only distributed in the eastern NCB (i.e., the Liaodong and Jiaodong peninsulas and the eastern Yanshan fold-and-thrust belt; Figure 5.3). Coeval with this magmatic event, nearly N-S or NE trending grabens or half-grabens were distributed in the Yanshan fold-and-thrust belt (e.g., Diaoe graben and Houcheng half-graben, Qi et al., 2015; Chengde graben, Davis et al., 2001; Guojiadian half-graben, Davis et al., 2009; Figure 5.3). A detachment fault with top-to-the-NW shearing (156-150 Ma) was developed in the Kalaqin metamorphic core complex (Lin et al., 2014; Figure 5.3).

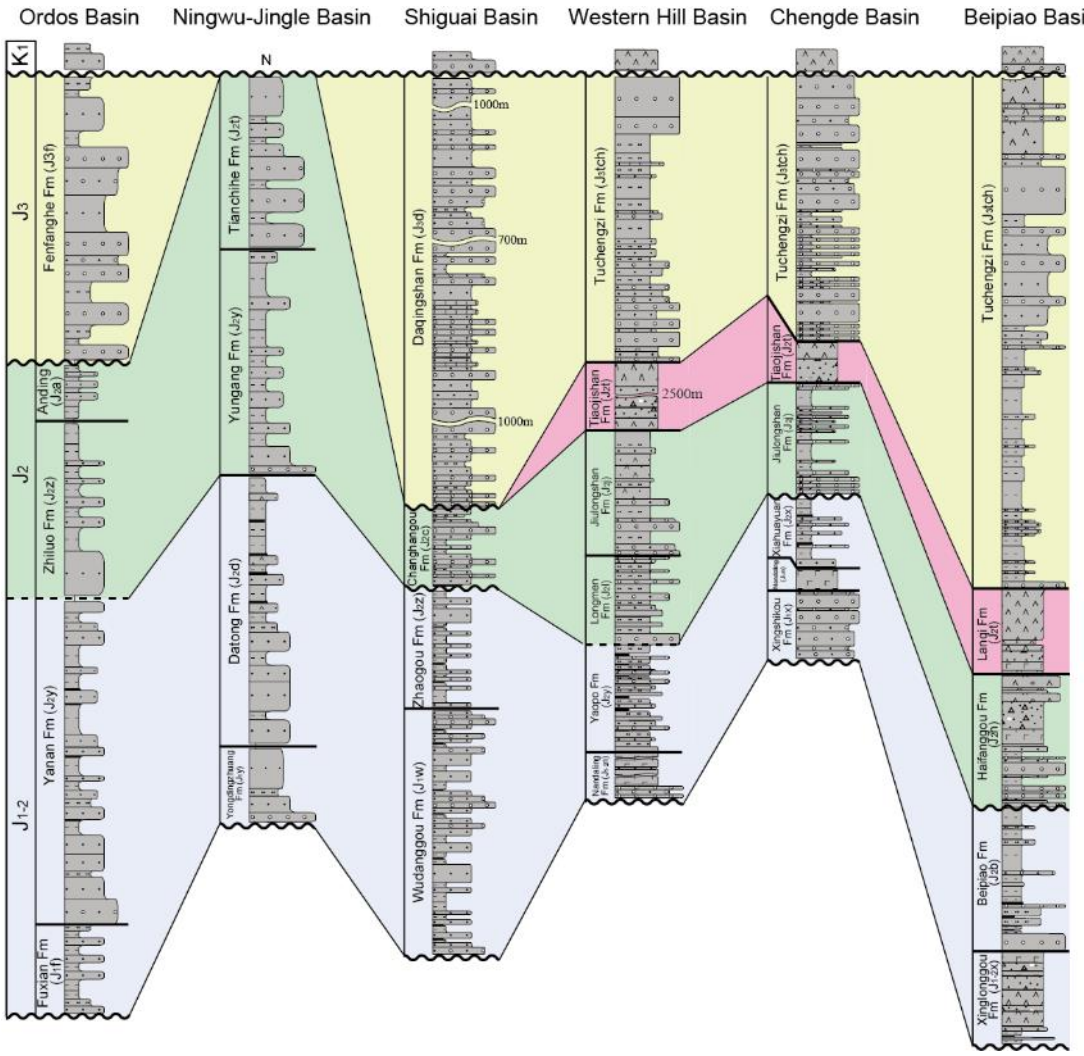

Figure 5.3 Stratigraphic correlation of the Jurassic-lowest Cretaceous strata (Modified from Darby et al., 2001). See Figure 5.2 for locations of the basins.

In the eastern NCB, the syntectonic conglomerate and coarse sandstone in the Upper Jurassic-lowermost Cretaceous Tuchengzi/Houcheng Formation conformably overlay pyroclastic rocks of the Tiaojishan/Lanqi Formation (Fu et al., 2018; C. Li et al., 2016; Liu et al., 2018; Figure 5.3). In the western NCB, however, Upper Jurassic-lowermost Cretaceous syntectonic conglomerate unconformably overlies upper Middle Jurassic syntectonic conglomerate (i.e., the Daqingshan, Wang et al., 2017; the Taihangshan, Li et al., 2015; the Ordos basin and its periphery, Zhang et al., 2011; Figure 5.3). A regional unconformity separates the Upper Jurassic-lowermost Cretaceous syntectonic strata from Lower Cretaceous.

The NE trending thrusts below this unconformity are widely distributed in the central YTFB (Figure 5.2; e.g., Chengde thrust, Davis et al., 2001; Shanggu-Pingquan thrust, Gubeikou thrust, and Dayingzi thrust, C. Li et al., 2016) and the eastern YTFB (Zhang et al., 2004). In the western YTFB, the paleostress along the dextral Shangyi-Chicheng and Pingquan-Gubeikou faults is NW-SE direction (Lin et al., 2019; Figure 5.2). In the western Daqingshan, the N–S thrusts were overprinted by the NW-SE thrusts, indicated by the superimposed striations and syntectonic Daqingshan strata (Wang et al., 2017; Figure 5.2). The NW-SE thrusts are also widely developed in the Taihangshan (Zhang et al., 2020; Figure 5.2). The duration of this event (i.e., Event B of the Yanshanian orogeny) has also been well constrained around 152–135 Ma (C. Li et al, 2016). Afterwards, the North China Craton was destroyed in the Early Cretaceous, characterized by A-type magmatism, metamorphic core complexes (MCCs), and graben or half-graben basins (Wang et al., 2011; Zhang et al., 2014, Lin et al., 2018).

5.2.3. Jianchang-Jiumen pluton

The granitic Jianchang-Jiumen pluton, extending ~50 km along a NE-SW long axis (Figure 5.4), is the largest one and representative for most of the Jurassic granites in North China. It consists of an early-stage medium- to fine-grained monzogranite exposed in the Jiumen pluton and a late-stage monzogranite exposed in the Jianchang pluton. Both these two plutons are metaluminous to weakly peraluminous, with geochemical features of I-type granites (Cui, 2015). According to geochemical analyses and LA-ICP-MS zircon U–Pb dating, both of them were formed by the partial melting of a lower crustal source in a subduction-related setting during 194–176 Ma and 161–153 Ma, respectively (Wu et al., 2006; Cui, 2015).

5.3. Structural Observations

5.3.1. Field observations

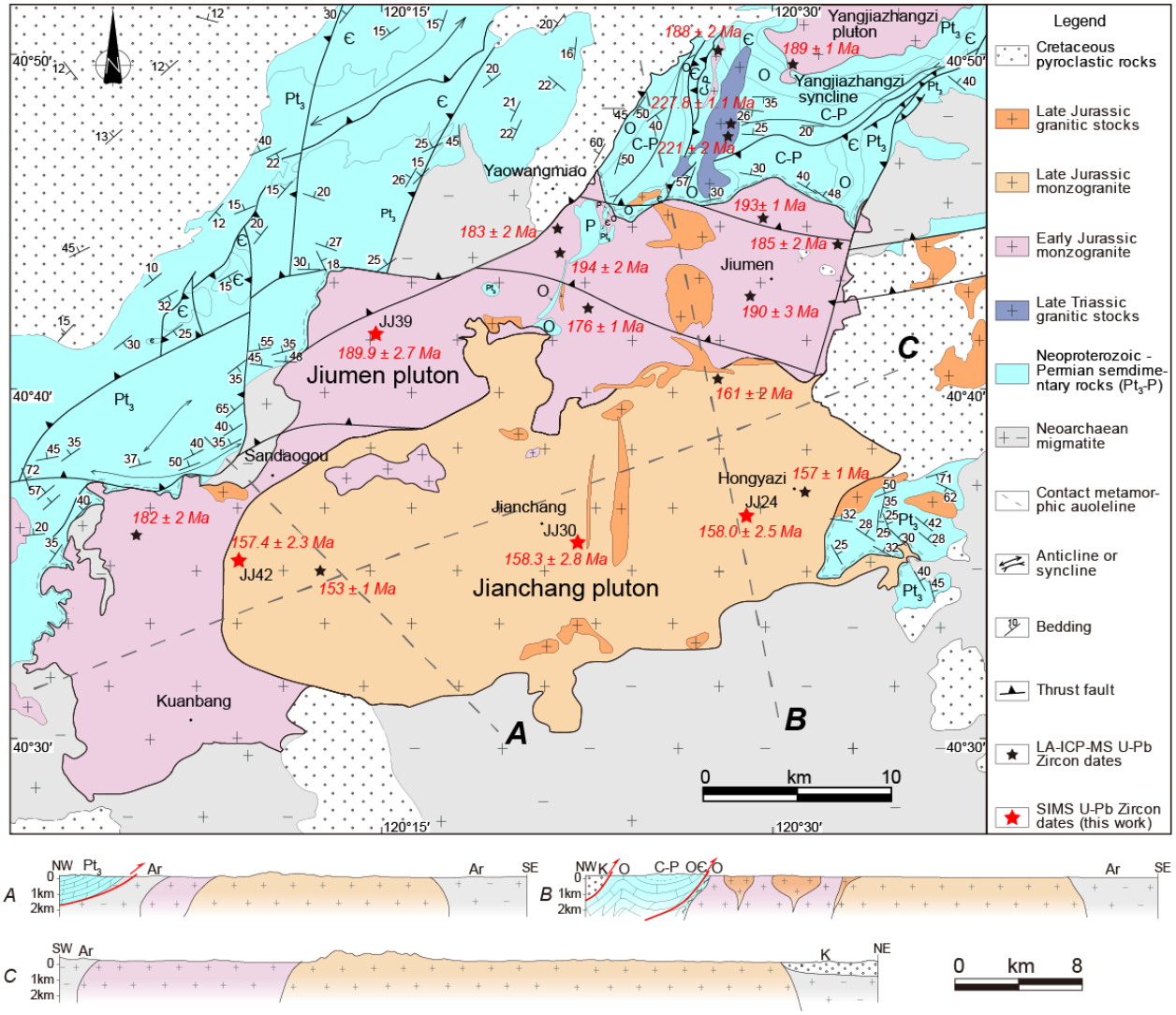

Figure 5.4. Structural geological map of the Jianchang-Jiumen pluton and adjacent areas. U–Pb zircon data are from Wu et al. (2006) and Cui (2015). See Figure 5.2 for locations.

The Jianchang-Jiumen pluton intrudes into Archaean migmatite and Neoproterozoic-Paleozoic sedimentary rocks (Figure 5.4). In the field, both the Jiumen and Jianchang plutons (i.e., pale-red medium- to fine-grained monzogranite and light gray monzogranite) appear isotropic without observable planar and linear fabrics at outcrops (Figures 5.5a and 5.5b). The main rock-forming minerals, namely, quartz, K-feldspar, plagioclase, and biotite, are generally euhedral to subhedral without obvious preferred orientation. The Jianchang pluton intruded into the Jiumen pluton, and some remnants of the Jiumen pluton scatterly remain on the top of the Jianchang pluton. Numerous small stocks or dykes have intruded into the Jianchang-Jiumen

Figure 5.5. Field photographs of the Jianchang-Jiumen pluton and its country rocks. (a) Fine-and medium-grained monzogranite in the Jiumen pluton. (b) Monzogranite in the Jianchang pluton. (c) Hornstone in the northeast of the Jiumen pluton. (d) Marble in the northwest of the Jiumen pluton. (e) Marble in the west of the Jiumen pluton. (f) Migmatite in the south of the Jianchang pluton.

pluton (Figure 5.4).

The country rocks of the Jianchang-Jiumen pluton are mainly composed of Archaean

migmatite in the south and unmetamorphosed Neoproterozoic-Paleozoic carbonate and clastic rocks in the north (Figure 5.4). In the northeast, pre-Triassic strata are folded with nearly E-W striking fold axis, forming the Yangjiazhangzi syncline. This syncline was intruded by Early Jurassic Yangjiazhangzi pluton and Jiumen pluton in its flanks, and Late Triassic granitic stock in its core (Figure 5.4). The nearly E-W trending and NE-SW fold and thrust belts in the northwest cut the Jiumen pluton. The contact between the pluton and the country rocks is irregular. Hornfels and marble can be recognized within hundreds of meters wide zone near the contact in the Neoproterozoic-Paleozoic country rocks. The bedding in the hornfels and marble strike subparallel to the pluton boundary and dip outwards (Figure 5.4). However, both the hornfels and marble in contact zones lack foliations or lineations. Some remnants of the country rocks are preserved above the Jiumen pluton (Figure 5.4). The Jianchang-Jiumen pluton is locally overlain by Cretaceous pyroclastic rocks.

5.3.2. Microscopic Observations

In the Jianchang-Jiumen pluton, microstructures are investigated in 40 sampling sites to determine the relationships between the minerals and magnetic fabrics (Figure 5.6a). Two types of microstructures can be observed. At most sites (68%), magmatic fabrics are developed without any solid-state deformation (Figures 5.6b–5.6c). Quartz grains are anhedral and non-deformed without signs of undulose extinction. The euhedral biotite is neither kinked nor bent with a sharp extinction. The plagioclase exhibits oscillatory zoning. Both the plagioclase and K-feldspars present euhedral crystal habits without any deformation. Besides, submagmatic fabrics can be also observed at some sites (32%). Quartz grains show an undulose extinction and weak dynamic recrystallization with some small subgrains at the border of coarse grains (Figures 5.6d–5.6e). Generally, these fabrics are acquired in magmatic state without significant solid-state deformation.

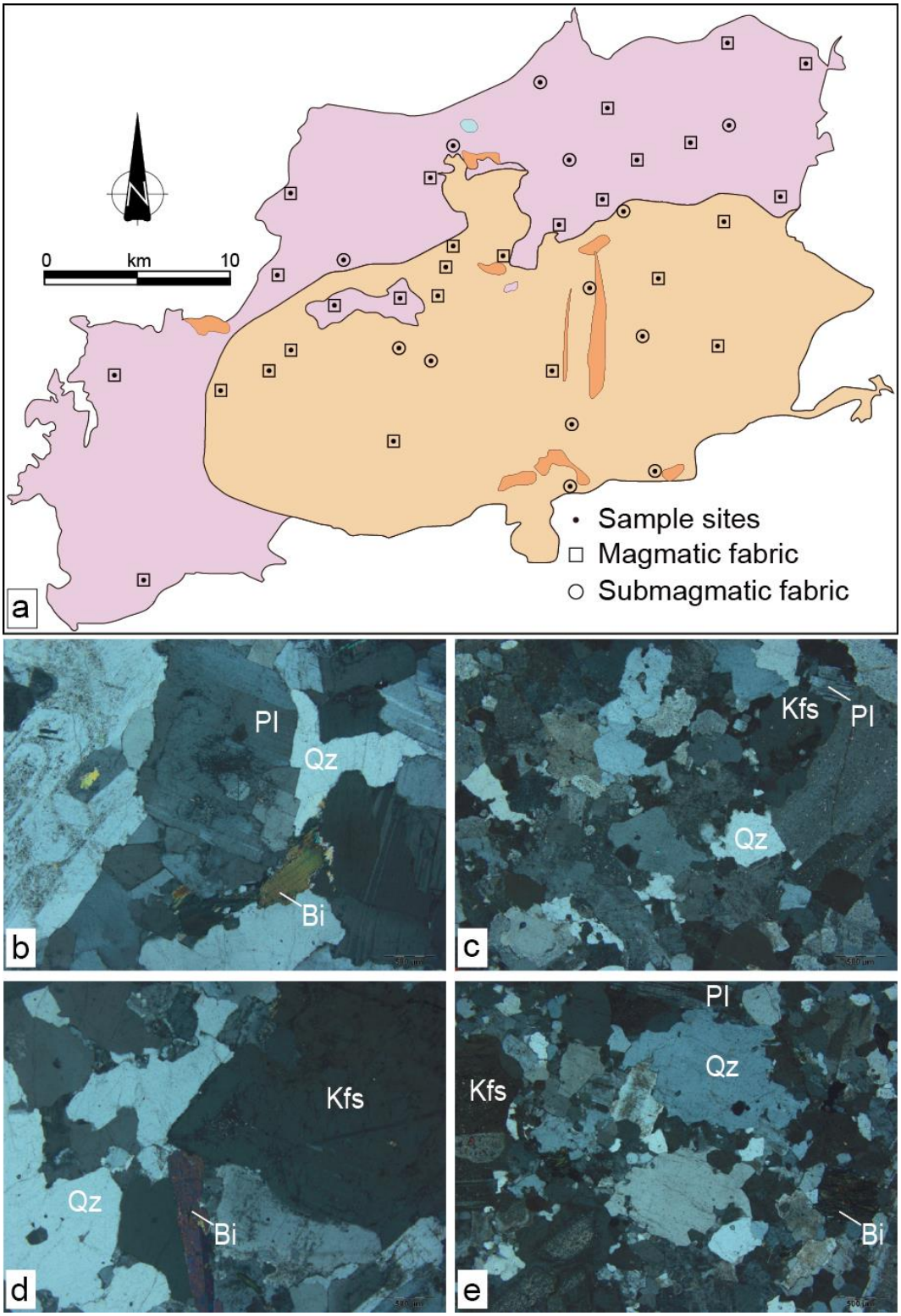

Figure 5.6. Microstructures of typical investigated samples in the Jianchang-Jiumen pluton. (a) Distribution map of the different types of microstructures. (b) and (d) Magmatic fabrics in the Jiumen and Jianchang plutons, respectively. (d) and (e) Submagmatic microstructures in the Jiumen and Jianchang plutons, respectively.

5.4. SIMS zircon U-Pb Dating

Considering the scattered LA-ICP-MS zircon U–Pb dating results (194–176 Ma in the Jiumen pluton and 161–153 Ma in the Jianchang pluton) in previous studies (Wu et al., 2006; Cui, 2015), new SIMS zircon U-Pb dating of four samples was performed to chronologically constrain the magmatism by a Cameca IMS 1280 large-radius SIMS at the Institute of Geology and Geophysics, Chinese Academy of Sciences (IGGCAS), Beijing (Figure 5.4; Table S1). Analytical procedures are the same as those described by Li et al. (2009). Sample JJ39 and other three samples JJ24, JJ30, and JJ42 are collected from the Jiumen pluton and the Jianchang pluton, respectively (Figure 5.4).

Sample JJ39 is a medium-grained monzogranite from the central part of the Jiumen pluton. The zircon grains from these samples are subhedral, transparent, and 100–200 μm in length with aspect ratios between 1:1 and 2:1. CL images show clear oscillatory zoning (Figure 5.7a). Th/U ratios of Sample JJ39 vary from 0.68 to 2.03. Seventeen analyses of the $^{206}Pb/^{238}U$ and $^{207}Pb/^{235}U$ results plotted on a Concordia diagram are relatively consistent, yielding a Concordia age of 189.9 ± 2.7 Ma, interpreted as the Early Jurassic crystallization age of the Jiumen pluton (Figure 5.7b, Table S1). Samples JJ24, JJ30, and JJ42 are collected from the monzogranite in the eastern, central, western parts of the Jianchang pluton, respectively. The zircon grains from these samples are also subhedral, transparent, and 50–200 μm in length with aspect ratios between 1:1 and 3:1. Euhedral concentric zoning is well displayed in CL images (Figure 5.7a). Th/U ratios of Sample JJ24 vary from 0.42 to 1.93. Sixteen analyses of the $^{206}Pb/^{238}U$ and $^{207}Pb/^{235}U$ results plotted on a Concordia diagram are relatively consistent, yielding a Concordia age of 158.6 ± 2.5 Ma. (Figure 5.7b, Table S1). Seventeen analyses of Sample JJ24 were obtained, with Th/U ratios vary from 0.43 to 0.84. All analyses yield a concordia age of 158.3 ± 2.8 Ma. Eighteen analyses of 18 zircons were obtained from Sample JJ24 and Th/U ratios vary from 0.65 to 1.99. The $^{206}Pb/^{238}U$ and $^{207}Pb/^{235}U$ results plotted on a

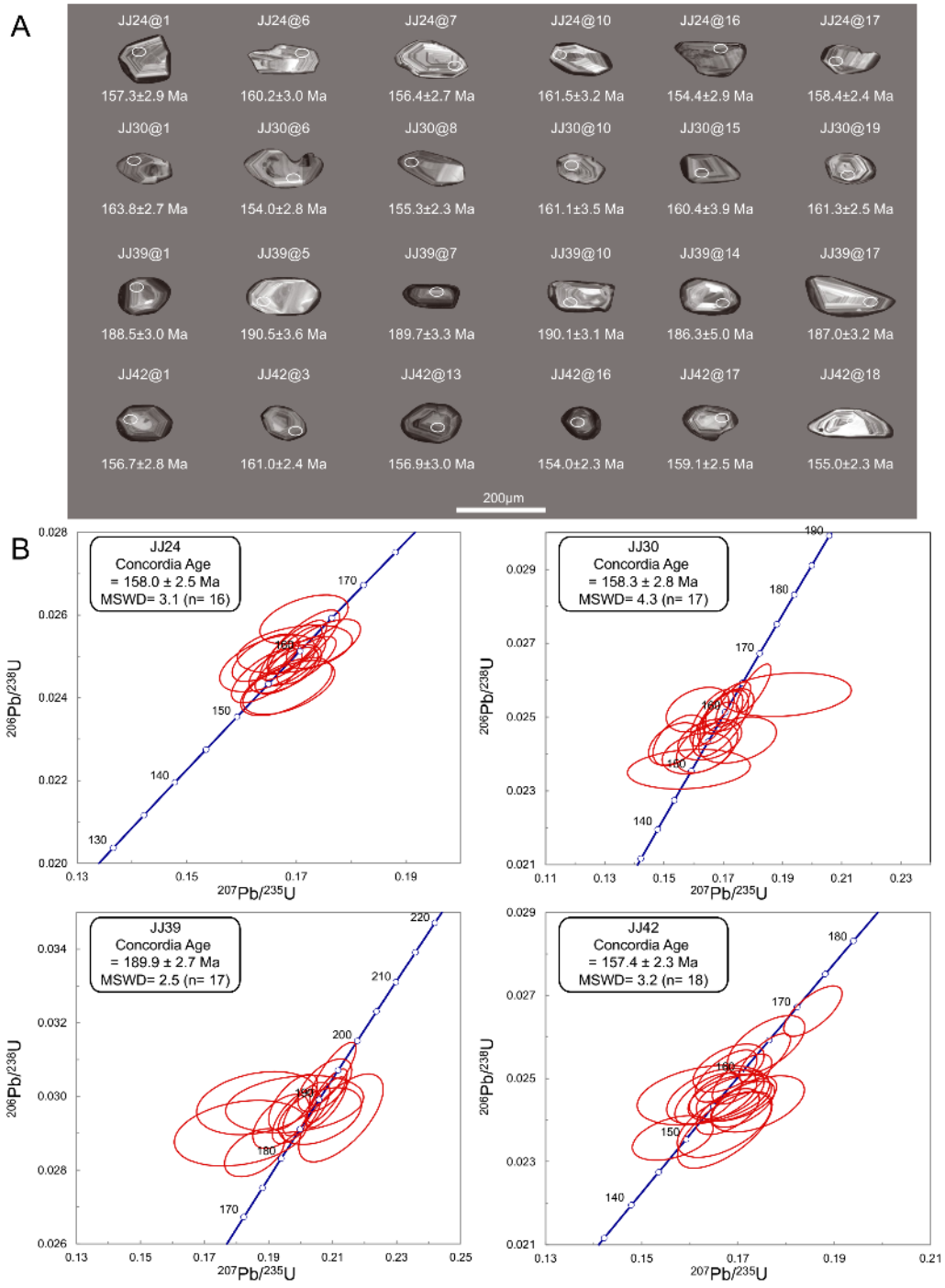

Figure 5.7. Cathodoluminescence (CL) images and U-Pb diagrams of Concordia age of representative zircons from collected samples. White solid ellipses are Secondary Ion Mass Spectrometer (SIMS) U-Pb analysis locations. MSWD: mean square of weighted deviates.

Concordia diagram show a consistent group distribution, yielding a concordia age of 157.4 ±2.3 Ma. These ages correspond to the early Late Jurassic crystallization age of the Jianchang pluton.

Table 5.1 SIMS zircon U-Pb data of the collected samples in the Jianchang-Jiumen pluton.

Sample spot	U (ppm)	Th (ppm)	Th/U	f_{206} (%)	$^{207}Pb/^{206}Pb$	±σ (%)	$^{207}Pb/^{235}U$	±σ (%)	$^{206}Pb/^{238}U$	±σ (%)	$t_{207/206}$(Ma)	±σ (Ma)	$t_{207/235}$(Ma)	±σ (Ma)	$t_{206/238}$(Ma)	±σ (Ma
JJ24@01	241	225	0.933	0.08	0.05004	1.40	0.17185	2.07	0.0249	1.52	196.9	32.1	161.0	3.1	158.6	2.4
JJ24@02	181	139	0.766	0.43	0.04951	1.42	0.16990	2.12	0.0249	1.58	172.2	32.9	159.3	3.1	158.5	2.5
JJ24@03	129	63	0.491	0.49	0.04948	1.67	0.16822	2.25	0.0247	1.51	170.7	38.6	157.9	3.3	157.0	2.3
JJ24@04	98	141	1.442	0.53	0.04775	1.93	0.16438	2.45	0.0250	1.51	86.8	45.1	154.5	3.5	159.0	2.4
JJ24@05	119	106	0.892	0.31	0.04859	2.59	0.14906	3.33	0.0223	2.10	127.9	59.8	141.1	4.4	141.9	2.9
JJ24@06	201	387	1.930	0.18	0.04887	1.40	0.16948	2.35	0.0252	1.89	141.6	32.6	159.0	3.5	160.1	3.0
JJ24@07	246	182	0.742	0.36	0.04866	1.88	0.16461	2.58	0.0245	1.77	131.3	43.6	154.7	3.7	156.3	2.7
JJ24@08	86	81	0.943	0.61	0.05014	2.03	0.17494	2.55	0.0253	1.54	201.4	46.5	163.7	3.9	161.1	2.5
JJ24@09	481	667	1.386	0.18	0.04895	1.13	0.16979	1.91	0.0252	1.54	145.6	26.2	159.2	2.8	160.2	2.4
JJ24@10	134	56	0.421	0.78	0.04899	1.58	0.17127	2.55	0.0254	2.00	147.4	36.6	160.5	3.8	161.4	3.2
JJ24@11	225	217	0.965	0.09	0.04932	2.09	0.16797	2.60	0.0247	1.55	163.3	48.1	157.7	3.8	157.3	2.4
JJ24@12	202	155	0.767	0.43	0.04810	2.97	0.16472	3.49	0.0248	1.83	104.2	68.8	154.8	5.0	158.1	2.9
JJ24@13	123	109	0.887	2.39	0.04801	2.71	0.17141	3.10	0.0259	1.51	99.5	62.9	160.6	4.6	164.8	2.5
JJ24@14	257	237	0.924	3.48	0.04888	3.79	0.16970	4.08	0.0252	1.52	142.3	86.6	159.2	6.0	160.3	2.4
JJ24@15	56	35	0.617	0.78	0.05043	2.76	0.16863	3.28	0.0242	1.78	215.0	62.6	158.2	4.8	154.5	2.7
JJ24@16	182	114	0.628	0.41	0.05026	2.67	0.16818	3.27	0.0243	1.90	206.9	60.7	157.8	4.8	154.6	2.9
JJ30@01	302	152	0.503	0.47	0.05070	1.32	0.18020	2.14	0.0258	1.69	227.1	30.3	168.2	3.3	164.1	2.7
JJ30@02	33	27	0.810	0.45	0.05200	4.66	0.17479	4.95	0.0244	1.69	285.4	103.1	163.6	7.5	155.3	2.6
JJ30@03	201	125	0.621	0.89	0.04613	3.20	0.15499	3.70	0.0244	1.87	0.0	79.5	146.3	5.1	155.2	2.9
JJ30@04	114	57	0.498	0.68	0.04914	2.23	0.16832	2.70	0.0248	1.52	154.6	51.5	158.0	4.0	158.2	2.4
JJ30@05	223	187	0.838	0.46	0.05415	7.45	0.19119	7.61	0.0256	1.52	377.2	159.5	177.6	12.5	163.0	2.5

Table 5.1 Continued.

JJ30@06	169	96	0.571	0.74	0.04934	3.70	0.16448	4.15	0.0242	1.86	164.0	84.4	154.6	6.0	154.0	2.8
JJ30@07	48	34	0.708	0.94	0.04870	8.50	0.15840	8.63	0.0236	1.50	133.5	188.5	149.3	12.1	150.3	2.2
JJ30@08	208	169	0.811	0.71	0.04919	4.02	0.16545	4.30	0.0244	1.50	156.9	91.6	155.5	6.2	155.4	2.3
JJ30@09	207	165	0.798	0.04	0.04826	2.15	0.16620	2.94	0.0250	2.01	111.8	49.9	156.1	4.3	159.1	3.2
JJ30@10	152	103	0.674	0.70	0.04902	2.18	0.16980	2.66	0.0251	1.52	148.6	50.4	159.2	3.9	160.0	2.4
JJ30@11	98	66	0.670	0.94	0.04642	4.04	0.16132	4.34	0.0252	1.58	19.7	94.2	151.9	6.1	160.5	2.5
JJ30@12	219	145	0.662	0.37	0.04938	2.79	0.16907	3.68	0.0248	2.40	165.7	63.9	158.6	5.4	158.1	3.7
JJ30@13	196	125	0.636	1.28	0.04588	3.43	0.15354	3.77	0.0243	1.57	-8.8	80.9	145.0	5.1	154.6	2.4
JJ30@14	166	117	0.705	0.45	0.05128	2.01	0.19452	2.58	0.0275	1.63	253.4	45.5	180.5	4.3	175.0	2.8
JJ30@15	263	202	0.770	0.04	0.04959	1.59	0.17334	2.24	0.0253	1.58	176.0	36.6	162.3	3.4	161.4	2.5
JJ30@16	127	76	0.600	0.45	0.04955	2.73	0.17215	3.12	0.0252	1.51	174.1	62.4	161.3	4.7	160.4	2.4
JJ30@17	57	24	0.426	0.35	0.04863	4.54	0.16104	4.79	0.0240	1.52	130.1	103.5	151.6	6.8	153.0	2.3
JJ39@01	100	105	1.056	0.23	0.04934	1.75	0.20179	2.39	0.0297	1.62	164.2	40.4	186.6	4.1	188.4	3.0
JJ39@02	158	155	0.983	0.25	0.04893	1.91	0.19871	2.51	0.0295	1.63	144.6	44.2	184.0	4.2	187.1	3.0
JJ39@03	160	129	0.806	1.19	0.04533	7.27	0.18128	7.55	0.0290	2.03	-37.8	167.7	169.2	11.8	184.3	3.7
JJ39@04	230	225	0.980	0.07	0.05032	1.15	0.20828	1.98	0.0300	1.60	209.8	26.5	192.1	3.5	190.7	3.0
JJ39@05	151	173	1.145	2.62	0.04535	6.43	0.18645	6.71	0.0298	1.89	-36.9	149.2	173.6	10.8	189.4	3.5
JJ39@06	108	73	0.678	0.29	0.04778	2.31	0.20708	3.30	0.0314	2.35	88.2	53.9	191.1	5.8	199.5	4.6
JJ39@07	108	133	1.228	0.78	0.04823	6.97	0.19813	7.18	0.0298	1.72	110.5	156.8	183.5	12.1	189.3	3.2
JJ39@08	194	174	0.899	0.11	0.04976	1.32	0.21005	2.27	0.0306	1.85	183.7	30.4	193.6	4.0	194.4	3.5
JJ39@09	184	181	0.982	0.07	0.05055	1.33	0.20799	2.02	0.0298	1.52	220.5	30.4	191.9	3.5	189.5	2.8
JJ39@10	148	135	0.910	0.24	0.04801	1.94	0.19762	2.55	0.0299	1.66	99.9	45.2	183.1	4.3	189.6	3.1
JJ39@11	83	122	1.483	0.68	0.04171	6.07	0.17931	7.15	0.0312	3.78	-244.1	146.8	167.5	11.1	197.9	7.4
JJ39@12	146	110	0.750	0.25	0.04612	2.04	0.20132	2.53	0.0317	1.50	0.0	52.3	186.2	4.3	200.9	3.0
JJ39@13	93	142	1.523	0.39	0.04726	2.95	0.18555	3.31	0.0285	1.51	62.6	68.8	172.8	5.3	181.0	2.7

Table 5.1 Continued.

JJ39@14	40	30	0.737	0.60	0.05241	3.09	0.21259	4.09	0.0294	2.68	303.4	69.0	195.7	7.3	186.9	4.9
JJ39@15	199	404	2.026	0.28	0.04794	2.48	0.19383	2.98	0.0293	1.65	96.3	57.7	179.9	4.9	186.3	3.0
JJ39@16	82	67	0.809	0.33	0.04968	2.17	0.20754	2.68	0.0303	1.56	179.9	49.9	191.5	4.7	192.4	3.0
JJ39@17	76	73	0.966	0.35	0.05070	3.78	0.20602	4.16	0.0295	1.72	227.4	85.1	190.2	7.2	187.2	3.2
JJ42@01	104	110	1.061	0.41	0.04855	3.30	0.16453	3.76	0.0246	1.80	126.2	75.8	154.7	5.4	156.5	2.8
JJ42@02	269	250	0.931	0.13	0.05014	2.87	0.16965	3.25	0.0245	1.52	201.3	65.3	159.1	4.8	156.3	2.3
JJ42@03	132	263	1.990	0.65	0.04825	2.48	0.16803	2.90	0.0253	1.51	111.7	57.4	157.7	4.2	160.8	2.4
JJ42@04	88	84	0.951	0.36	0.04975	3.04	0.16827	3.40	0.0245	1.52	183.3	69.4	157.9	5.0	156.2	2.4
JJ42@05	118	153	1.302	1.18	0.04938	2.63	0.16765	3.06	0.0246	1.57	166.1	60.2	157.4	4.5	156.8	2.4
JJ42@06	171	182	1.066	0.25	0.04845	2.23	0.16376	2.78	0.0245	1.66	121.4	51.8	154.0	4.0	156.1	2.6
JJ42@07	158	168	1.061	0.41	0.05073	3.19	0.16712	3.86	0.0239	2.17	228.8	72.0	156.9	5.6	152.2	3.3
JJ42@08	81	62	0.765	0.91	0.05178	3.15	0.17414	3.65	0.0244	1.84	275.8	70.7	163.0	5.5	155.3	2.8
JJ42@09	381	419	1.099	0.03	0.05054	1.53	0.18555	2.15	0.0266	1.50	220.0	35.1	172.8	3.4	169.4	2.5
JJ42@10	156	212	1.359	0.78	0.04941	2.41	0.17583	3.01	0.0258	1.81	167.4	55.3	164.5	4.6	164.3	2.9
JJ42@11	287	207	0.721	0.08	0.05104	2.91	0.16727	3.88	0.0238	2.56	242.8	65.8	157.0	5.7	151.4	3.8
JJ42@12	311	288	0.924	0.56	0.04813	3.20	0.15642	3.53	0.0236	1.50	105.6	73.9	147.6	4.9	150.2	2.2
JJ42@13	190	191	1.003	0.96	0.04798	5.23	0.16277	5.57	0.0246	1.93	98.3	119.2	153.1	8.0	156.7	3.0
JJ42@14	334	229	0.685	0.40	0.04991	1.32	0.17553	2.01	0.0255	1.51	191.0	30.4	164.2	3.0	162.4	2.4
JJ42@15	199	153	0.768	0.63	0.04847	1.92	0.16751	2.53	0.0251	1.65	122.4	44.6	157.3	3.7	159.6	2.6
JJ42@16	139	92	0.657	0.36	0.05030	2.09	0.16788	2.57	0.0242	1.51	208.7	47.6	157.6	3.8	154.2	2.3
JJ42@17	227	183	0.803	0.52	0.04957	1.78	0.17081	2.39	0.0250	1.59	174.9	41.1	160.1	3.5	159.1	2.5
JJ42@18	142	93	0.652	0.93	0.05085	2.09	0.17096	2.57	0.0244	1.50	233.8	47.5	160.2	3.8	155.3	2.3

f_{206} (%) is the percentage of common ^{206}Pb in total ^{206}Pb

5.5. Anisotropy of magnetic susceptibility (AMS)

The AMS study is an effective and practical way to reveal the structural elements of apparently isotropic to weakly deformed granitic plutons (e.g., Archanjo et al., 1994; Bouchez et al., 1997). Field and microscopic observations suggest that the Jianchang-Jiumen pluton does not show any mesoscopic planar and linear fabrics. Therefore, an AMS study has been carried out on the Jianchang-Jiuemn pluton to provide quantitative structural data that cannot be gained in classical field studies. It could provide key information to depict the fabric patterns of the Jianchang-Jiuemn pluton.

5.5.1. Sampling and Measurements

AMS sampling was performed in 76 sites of the Jianchang-Jiumen pluton with a relatively homogeneous spatial distribution (35 sites in the Jiumen pluton and 41 ones in the Jianchang pluton). A total of 467 cores from 76 sites (more than five cores of 2.5 cm in diameter in each site) have been collected with a portable gasoline drill. In the laboratory of Paleomagnetism and Chronology of IGGCAS, each core was cut into cylindrical specimens of 2.2 cm in length. Anisotropy of magnetic susceptibility and bulk susceptibility were measured with a KLY4 susceptometer. The ANISOFT package of programs was used for the statistical analysis of the AMS data that calculates mean orientation of three principal axes of the AMS ellipsoid ($K_1 \geq K_2 \geq K_3$), and the parameters of the AMS ellipsoid features, i.e., anisotropy degree ($P_J = \exp\sqrt{\{2[(\eta_1-\eta)^2 + (\eta_2-\eta)^2 + (\eta_3-\eta)^2]}$), and shape parameter ($T =(2\eta_2-\eta_1-\eta_3)/(\eta_1-\eta_3)$), where $\eta_1 = \ln K_1$, $\eta_2 = \ln K_2$, $\eta_3 = \ln K_3$, and $\eta = (\eta_1 + \eta_2 + \eta_3)/3$ (Jelínek, 1978). The magnetic mineralogy was investigated to identify the magnetic carriers that contribute to the magnetic signal with the following measurements: (1) hysteresis loops; (2) Isothermal Remanent Magnetization (IRM), and (3) thermomagnetic (K-T) curves.

5.5.2. Magnetic Mineralogy

The mean magnetic susceptibility, $K_m = (K_1 + K_2 + K_3)/3$, of 76 sampling sites are higher

than 500 μSI, ranging from 506 to 91,500 μSI (Figure 5.8 and Table S2). The high K_m values in all sampling sites usually attributed to the ferromagnetic contribution (Bouchez, 2000). The hysteresis loops of six representative samples from the Jiumen and Jianchang plutons all display nonlinear variations between the applied magnetic field and the induced magnetization (Figures 5.9a–5.9c). Furthermore, the narrow-waisted loops and the low-coercivity values for all these specimens indicate that the magnetite is the major magnetic susceptibility carrier. All IRM acquisition curves show a rapid increase and a sudden saturation below 200 mT (Figures 5.9d–5.9f), confirming the presence of low-coercivity minerals such as magnetite. All thermomagnetic measurements display sharp drops of magnetic susceptibility at 550-600°C, consistent with the Curie point of magnetite at 580°C (Figures 5.9g–5.9i). Through the above investigations, therefore, we conclude that the magnetic fabrics of the Jianchang-Jiumen pluton are dominated by magnetite. According to the ratios of hysteresis parameters Mr/Ms and Hcr/Hc, the presence of pseudo-single domain (PSD) magnetite has been estimated (Dunlop, 2002; Figure 5.10). Consequently, the principal axis of the magnetic fabrics can be correlated to the petro-fabrics of studied samples (e.g. Hargraves et al., 1991; Tarling & Hrouda, 1993).

More than 82% of sampling sites in the Jianchang-Jiumen pluton have low P_J values ($<$ 1.2; Figure 5.8), indicating that the fabrics have been acquired in magmatic or submagmatic state rather than post-solidus one. Only a few sites (18%) have high P_J values (>1.2), coming mainly from the contact between the two sub-plutons (i.e., Jiumen and Jianchang). It is possible to create a relatively high P_J value due to strain increase near the contact zone of the two plutons. Fifty-four percent of the sites display positive T values, and 46% of the sites show negative T values, indicating no dominant oblate or prolate shape for magnetic fabrics. There are no significant relationships among P_J, T, and Km, implying that AMS varies independently from magnetic minerals (Borradaile and Henry, 1997; Figure 5.8).

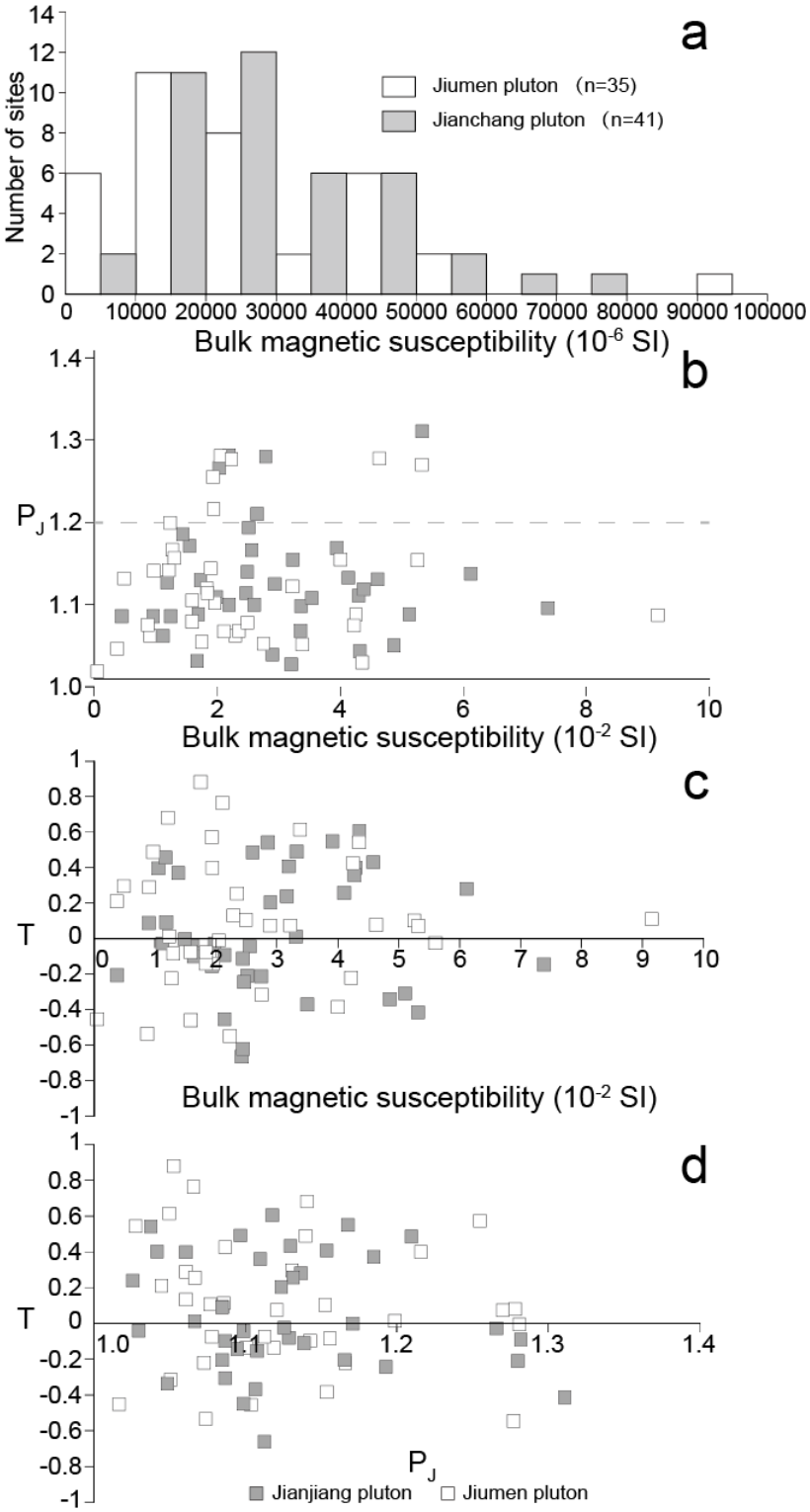

Figure 5.8. AMS scalar parameters of the Jianchang-Jiumen pluton. (a) Histogram of site mean magnetic susceptibility (K_m). (b) Anisotropy degree P_J value vs. Bulk magnetic susceptibility K_m. (c) Shape parameter T vs. Bulk magnetic susceptibility K_m. (d) Shape parameter T vs. anisotropy degree P_J value.

Table 5.2 The results of AMS measurements for the Jiangchang-Jiumen pluton. Lat: latitude, Long: longitude, N: the number of cylinders measured in each site, Km: mean magnetic susceptibility, P_J and T: anisotropy degree and shape parameter, respectively, K_1 and K_3: magnetic lineation and pole of magnetic foliation, respectively, Inc: inclination, and Dec: declination, α_{95max} and α_{95min}: Jelinek's statistic confidence at 95% level (Jelinek, 1981) in degrees, respectively.

site	Coordinates		N	Km	P_J	T	K_1				K_3			
	Long(°E)	Lat(°N)		(10^{-6}SI)			Dec(°)	Inc(°)	α_{95max}(°)	α_{95min}(°)	Dec(°)	Inc(°)	α_{95max}(°)	α_{95min}(°)
JJ1	120.304	40.70106	7	1.27	1.166	-0.222	145.3	83.1	14.4	5.1	301.4	6.3	13.5	6
JJ2	120.298	40.69119	7	9.15	1.086	0.112	276.1	28.1	11.5	2.2	27.1	33.9	13.5	3.3
JJ3	120.3081	40.65613	5	1.18	1.085	0.094	35.2	26.7	23.7	11.9	274.2	45.6	25.5	10.7
JJ4	120.2923	40.65078	8	1.93	1.108	-0.152	234.6	9.5	10.3	3.4	139.3	28.8	13.5	3.4
JJ5	120.3063	40.64473	8	2.42	1.113	-0.659	83.4	7.5	5.4	5.3	353.3	1.4	16.8	5.3
JJ6	120.2993	40.62982	6	2.44	1.446	-0.616	159.4	11	5.9	2.2	273.7	64.6	9.3	3.5
JJ7	120.3438	40.64919	5	0.892	1.085	0.089	24.4	26.9	24.7	9.6	256	50.7	23.2	7.7
JJ8	120.3768	40.66539	6	1.94	1.216	0.399	29	66.3	11.3	4.3	233.5	21.8	13.5	7.4
JJ9	120.4011	40.67584	6	1.21	1.141	0.681	111.6	47.2	25.2	5.8	230.3	24	7.7	1.5
JJ10	120.3627	40.735	6	4.25	1.087	0.426	335.4	76	23.7	4.7	225.1	5	10	7.2
JJ11	120.3833	40.69634	6	1.23	1.199	0.014	123.8	73.2	10.6	8.4	220.2	1.9	16.9	9.9
JJ12	120.4144	40.67383	5	0.487	1.131	0.297	286.6	40.4	28.6	14	113.4	49.4	20.7	9.9
JJ13	120.4239	40.69924	6	3.38	1.05	0.614	321.9	0.6	35	4.2	51.9	1.4	27	9.3
JJ14	120.4095	40.72135	5	2.29	1.061	0.132	167	12	20.8	11.8	65.8	42.5	14.2	9
JJ15	120.3982	40.74951	7	0.0506	1.017	-0.451	275.1	14.7	13.6	5.2	11.3	22.5	25.2	4.3
JJ16	120.438	40.74695	5	4.35	1.028	0.543	155.7	22.2	46.5	9.3	57	20	14.2	14
JJ17	120.4861	40.71395	6	0.908	1.061	0.289	254.4	47.3	34.7	3.9	21.7	29.2	30.7	8.9
JJ18	120.5335	40.74461	8	0.372	1.045	0.211	28.5	32.3	45.8	19.2	187.7	55.9	54.9	17.9
JJ19	120.4867	40.75663	7	0.872	1.074	-0.533	317.3	16.4	19.6	4.6	212.9	40.1	29.6	6.8
JJ20	120.4605	40.70645	7	1.89	1.143	-0.097	117.2	35.8	8.7	4.8	223.8	21.6	26.1	3.6

Table 5.2 Continued.

JJ21	120.5175	40.68194	8	1.96	1.101	-0.137	290.3	47.7	30.7	10.3	191.5	8	15.6	10
JJ22	120.4797	40.66632	7	4.85	1.049	-0.337	44.5	0.6	23.3	11.3	135.5	56.9	47.7	11.3
JJ23	120.4414	40.64155	9	7.38	1.095	-0.143	245.5	3.6	7.6	5.9	336.1	9.6	11.9	5.2
JJ24	120.4814	40.60526	7	6.11	1.137	0.281	10.3	24.7	8	3.4	260.3	36.6	7.9	1.7
JJ25	120.4299	40.61154	6	5.1	1.087	-0.305	41	31.5	6.4	1.9	265.6	49.2	5.8	3.7
JJ26	120.3953	40.60928	6	2.55	1.099	-0.041	61	24.4	24.4	5.5	195.3	57	17.9	6.2
JJ27	120.4147	40.58021	5	1.61	1.03	-0.04	217.7	18.3	28	5.2	313.5	17.1	16.8	4
JJ28	120.3991	40.63708	6	3.16	1.026	0.239	120.1	41.3	15	4.5	236.9	27.2	7.1	4
JJ29	120.3855	40.56721	7	3.31	1.067	0.013	85.6	55.9	13.1	7.4	341.2	9.6	21.4	8.6
JJ30	120.3739	40.59281	6	4.58	1.13	0.431	223.4	15.6	5.8	0.7	324.9	35.4	4	3
JJ31	120.3687	40.606	5	4.29	1.042	0.4	117.6	70.2	50.5	7.4	284.6	19.3	42.3	11.1
JJ32	120.2945	40.6015	8	2.14	1.099	-0.448	62.1	56.3	5.2	4.6	238.2	33.6	13.6	4
JJ33	120.2752	40.60565	6	1.49	1.171	-0.001	94.6	15.4	19.5	3.2	349.9	42.6	9.6	6.8
JJ34	120.2712	40.70888	5	2.75	1.051	-0.313	28.6	77.3	8.8	5.4	290.3	1.9	34.8	6.8
JJ35	120.2398	40.64603	7	1.93	1.255	0.572	278.1	33.5	7.7	4.5	183.1	7.4	5.9	2.3
JJ36	120.0891	40.56966	6	2.49	1.077	0.107	181.7	63.2	22.6	3.8	72.7	9.4	20.6	4.7
JJ37	120.2073	40.60555	6	5.31	1.311	-0.411	280.6	13.4	9	2.3	188.3	9.3	8.7	8
JJ38	120.1964	40.59702	6	1.59	1.104	-0.456	267.7	17.9	9.1	5.4	23.2	53.1	11	6.8
JJ39	120.2406	40.6931	8	4.22	1.073	-0.219	230.4	60.5	14.3	7.8	124.7	8.7	36.3	7.2
JJ40	120.198	40.68195	8	4.63	1.278	0.08	233.3	33	12.4	7.1	133.3	14.9	11.6	7.1
JJ41	120.1006	40.52581	5	1.3	1.156	-0.083	316.4	60.2	9.5	7.8	101.6	25.2	24.5	7.9
JJ42	120.1618	40.58427	6	4	1.154	-0.383	242.3	24.9	7.6	3.2	73.3	64.7	24.3	4.6
JJ43	120.2894	40.57167	5	2.44	1.139	-0.109	70	32.2	9.5	4.7	321.1	27.2	18.3	4.4
JJ44	120.2725	40.56117	5	3.91	1.168	0.548	59.8	18.5	2.7	1.9	315.6	36.1	3.9	2.3
JJ45	120.3848	40.53936	5	3.19	1.154	0.407	227	39.9	36.3	6.7	51.2	50	9.8	6.4
JJ46	120.442	40.5416	5	1.05	1.061	0.396	229.1	6.6	11.6	5.4	136.7	19.6	8.3	5.6
JJ47	120.0951	40.5925	6	1.75	1.053	0.88	316	71.2	31.1	1.2	59.9	4.7	2.4	1.9
JJ48	120.1334	40.55474	7	2.35	1.067	0.255	321.6	56.9	19.2	4.8	144.4	33.1	23.6	2.9
JJ49	120.1736	40.50898	7	2.11	1.066	0.764	41.4	24.5	21.1	8.7	309.4	4.5	9.3	5.4

Table 5.2 Continued.

JJ50	120.1115	40.49232	6	5.25	1.153	0.104	327.6	7.9	11.9	2.5	65.8	45.8	4.9	2.5
JJ51	120.116	40.53346	6	5.32	1.27	0.073	264.6	48.9	13.5	5.6	142.5	24.8	13.3	5.6
JJ52	120.0707	40.49052	7	0.97	1.14	0.488	256.5	76.2	15.6	3.2	8.9	5.4	14.5	4.9
JJ53	120.2043	40.57005	5	1.67	1.129	-0.078	276	10	11.4	6.7	19.6	53.1	17.2	8.1
JJ54	120.1856	40.54051	6	2.05	1.281	-0.007	263.5	9.7	4.6	3.2	1.7	39.8	9	3.9
JJ55	120.2006	40.55278	6	2.51	1.166	-0.205	271.9	9.4	6.2	2.4	6.1	23.6	14.2	5
JJ56	120.2034	40.53397	5	2.23	1.277	-0.546	287.2	13	5.9	1.1	27.5	37.7	8.1	4.3
JJ57	120.2442	40.5599	6	2.6	1.21	0.485	88.6	13.3	9.5	6.3	346.6	41.3	7.2	6
JJ58	120.2458	40.54816	7	1.98	1.266	-0.026	83.7	6.7	4.7	2	348.2	39.3	3.9	2.7
JJ59	120.2463	40.52726	6	2.74	1.28	-0.209	86	6.3	10	1.9	354.2	15.9	12.2	2.3
JJ60	120.2253	40.55003	6	2.14	1.282	-0.089	271.3	0.3	7.6	2.5	1.6	36.5	8.7	6.6
JJ61	120.2673	40.52482	5	2.46	1.193	-0.242	282.7	26.3	5.8	5.2	13.1	0.9	17.3	5.7
JJ62	120.4937	40.64192	5	0.371	1.085	-0.203	248.3	63.7	20.7	6.9	135.9	10.6	20.3	5.4
JJ63	120.52	40.60412	6	4.27	1.11	0.358	24.1	26	13	7	279.9	26.7	9.8	6
JJ64	120.4974	40.57928	7	3.32	1.097	0.49	42	4.2	8	3	307.7	45	6.3	2.2
JJ65	120.4592	40.57044	7	4.1	1.132	0.258	228.4	5.7	10	4.8	323.8	43.6	6.9	2.7
JJ66	120.4457	40.55574	5	4.35	1.118	0.604	191.5	41.8	24.6	5.8	332.7	41.1	9.5	1.7
JJ67	120.3337	40.55508	5	3.5	1.107	-0.367	61.7	3.8	7	3.6	151.9	2.4	19.5	6.6
JJ68	120.3214	40.56776	6	2.89	1.124	0.204	249.7	0.6	7.5	4.2	340	23.8	4.5	3.1
JJ69	120.3138	40.5284	6	2.85	1.038	0.541	202.9	14.3	14.7	6	305.8	41.2	7.2	2.9
JJ70	120.3719	40.63159	6	1.63	1.087	-0.097	297.2	14.3	9.2	3.8	44.7	49.6	10.2	8.6
JJ71	120.3377	40.68353	6	1.17	1.476	0.457	97.2	28.5	9.8	1.8	1.3	10.7	3.9	1.5
JJ72	120.3646	40.67942	6	1.59	1.078	-0.074	42.8	75.4	12.4	5.7	181.6	11.1	17.7	10.3
JJ73	120.3252	40.59231	5	1.38	1.185	0.37	9.3	38.6	19	4.5	252.5	29.5	7.4	5.1
JJ74	120.27	40.65302	5	2.89	1.632	0.075	279.1	13	4.7	0.9	9.7	2.7	4.4	1
JJ75	120.228	40.59559	6	1.12	1.126	-0.024	281.5	3.4	17.2	6	14.3	39.1	32.9	6.1
JJ76	120.2171	40.66088	6	3.22	1.121	0.075	319.9	24.8	16.6	12.9	56.5	13.9	28.8	15.2

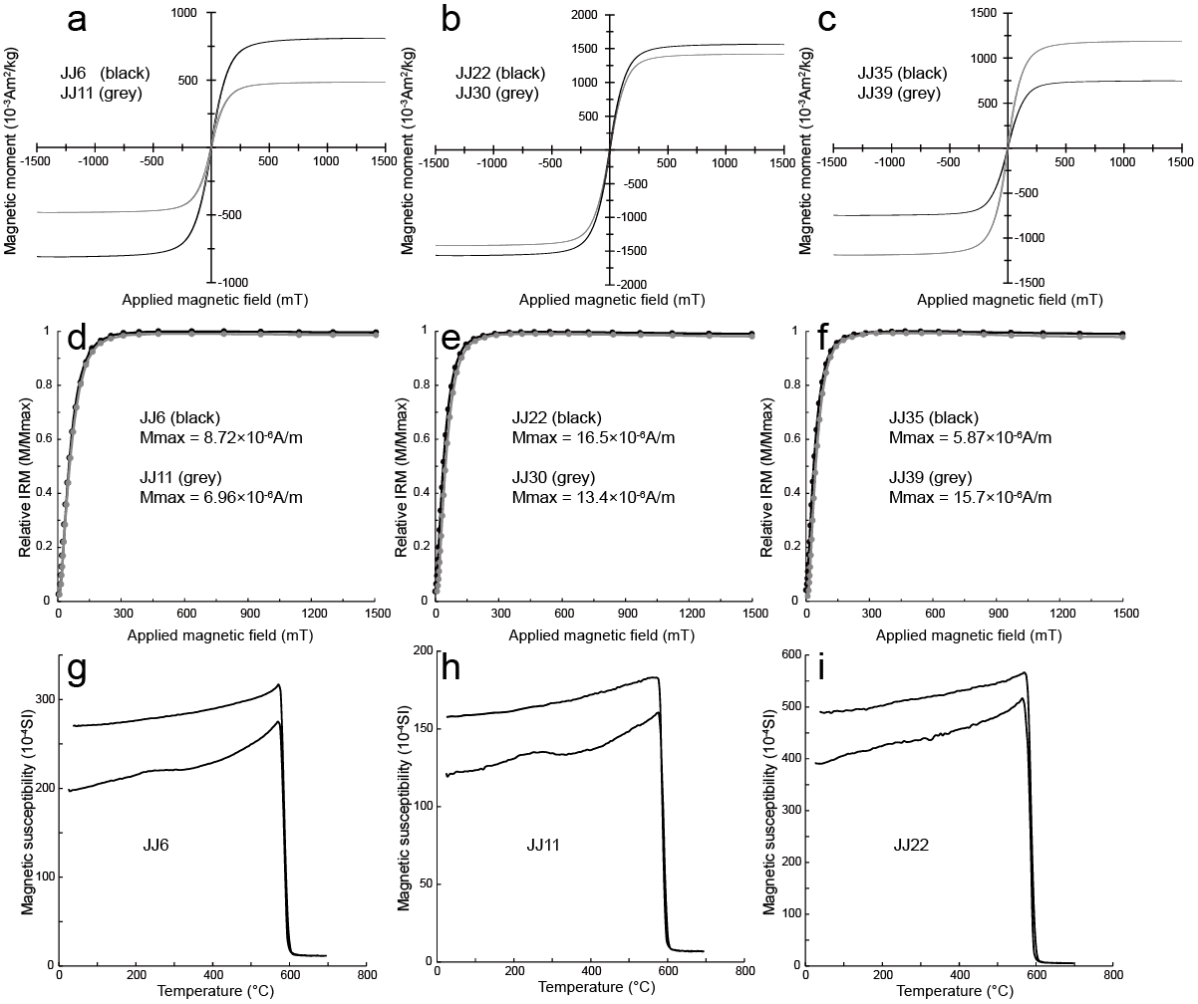

Figure 5.9. Magnetic mineralogy investigations of representative specimens from the Jianchang-Jiumen pluton. (a–c) hysteresis loops, (d–e) acquisition of isothermal remanent magnetization (IRM), and (g–i) thermomagnetic curves (K (T) curves).

5.5.3. Fabric Patterns of the Jianchang-Jiumen pluton

At a given site, the number of samples varies between 5 and 9. For each site, the site-average orientation with confidence intervals at the 95% confidence level (α_{95max} and α_{95min}) was calculated for K_1 and K_3 axes (Jelinek, 1978; Figure 5.11). A confidence level lower than 25° for a magnetic axis, K_1 and/or K_3, is considered as well-defined, otherwise, it is poorly defined and unreliable. In the Jianchang-Jiumen pluton, at least one magnetic principal axis (K_1 or K_3) in more than 96% sites is well defined with low α_{95} values. At map scale, the fabric patterns of the Jianchang-Jiumen pluton are described in details as follows:

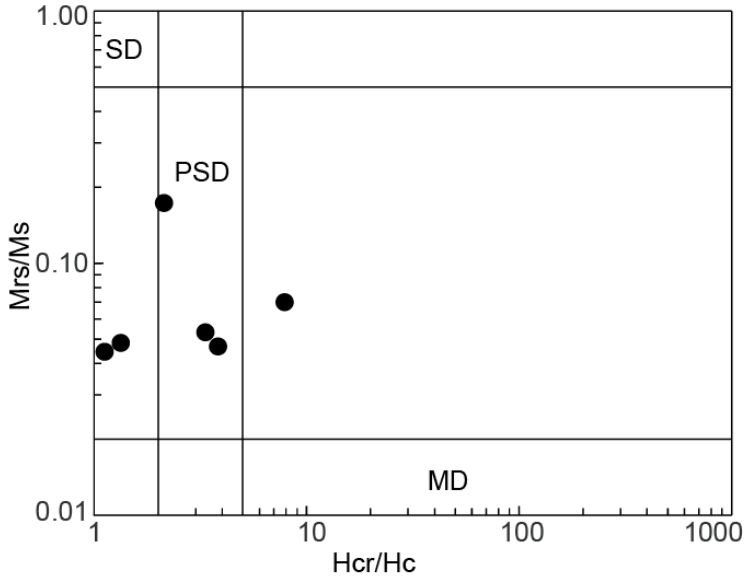

Figure 5.10. Day plot of hysteresis parameters. Mrs: saturation of magnetic remanence, Ms: saturation of induced magnetization, Hcr: magnetic coercivity of magnetic remanence, Hr: magnetic coercivity of the measured sample. SD: single domain, PSD: pseudo-single domain, MD: multidomain.

1. Jiumen pluton. The magnetic foliations throughout the Jiumen pluton generally dip outwards and strike subparallel to the contact with country rocks. Along the NE-SW section, the magnetic foliations dip moderately to the NE close to the northeastern margin, become steeper in the central part, and dip moderately to the SW in the southwestern part of the pluton. However, the magnetic foliations are steep near the contact with the country rocks (e.g., JJ21, JJ36, JJ47, JJ49, and JJ52) and become more scattered near the Jianchang pluton and other stocks or dykes (e.g., JJ2, JJ8, JJ12, JJ35, JJ74; Figure 5.12a). The magnetic lineations generally strike NW-SE with variable plunges; locally, a small family in the NE-SW orientation can be observed near the contact with the Jianchang pluton (Figure 5.12b).
2. Jianchang pluton. There, the margin-parallel magnetic foliations mainly present moderately to highly outward dipping around its northwestern root (see below) and subparallel striking to the contact with the country rocks in its southeastern margin (Figure 5.12a). The magnetic lineations display gentle to moderate NE-SW plunging throughout the

pluton (Figure 5.12b).

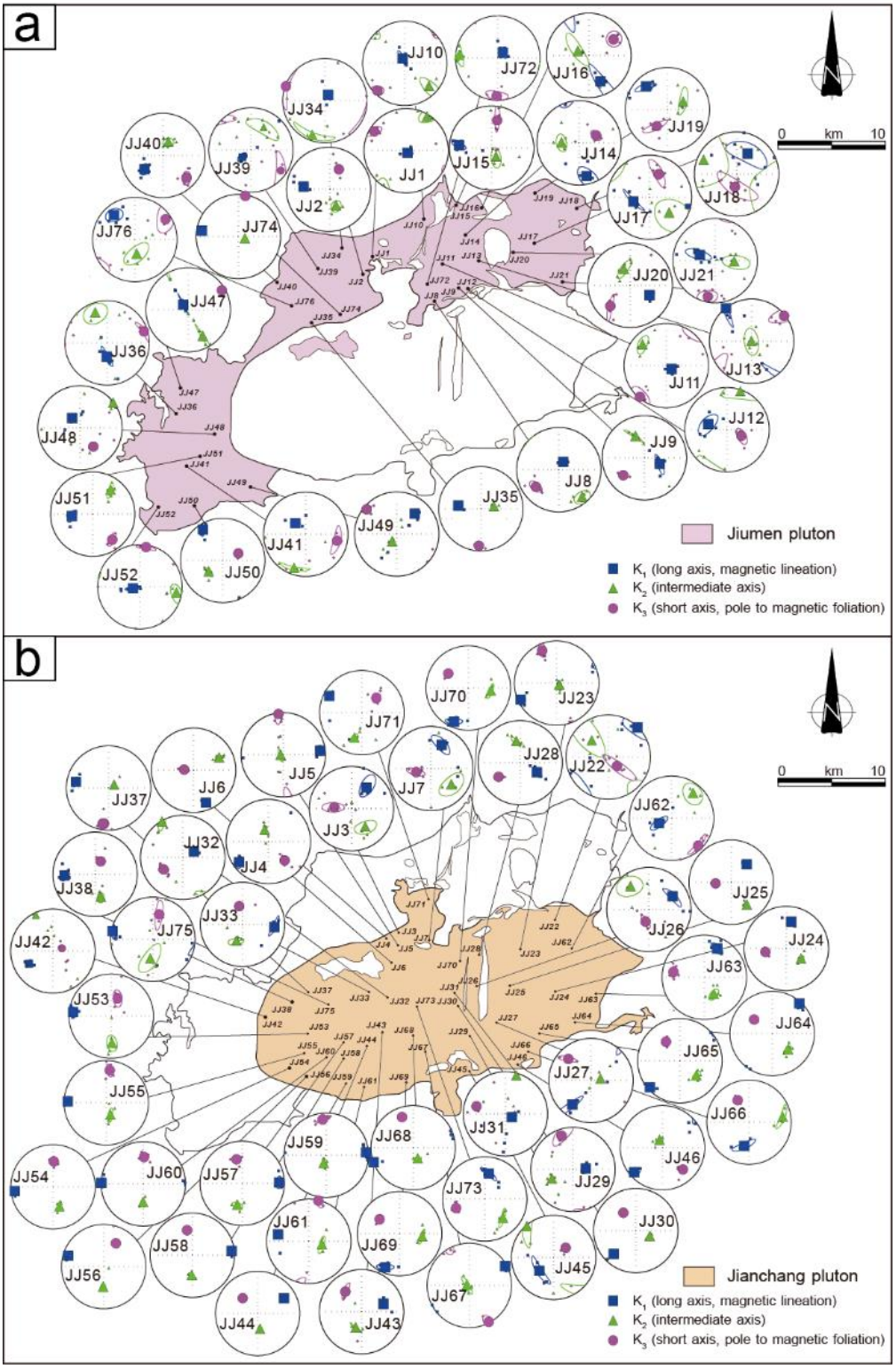

Figure 5.11. Equal-area projections (lower hemisphere) of AMS results for each sampling site. Confidence ellipses at 95% level are drawn around each average orientation direction.

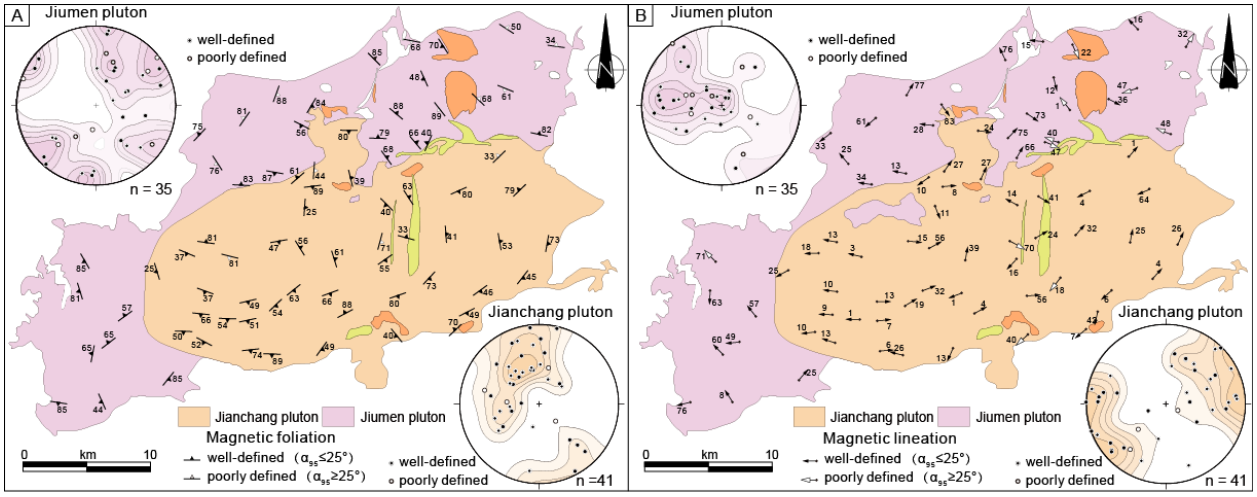

Figure 5.12. Magnetic fabric patterns and orientation diagrams of K_3 and K_1. (a) Foliations. (b) Lineations.

5.6. Gravity Modeling

Gravity modeling has been proven as an efficient method to constrain the geometry and possible feeder zones of pluton (e.g., Améglio & Vigneresse, 1999; Qiu et al., 2020; Vigneresse et al., 1990). To characterize the shape of the Jianchang-Jiumen pluton at depth, a gravity modeling has been performed for the Jiumen-Jianchang pluton.

5.6.1. Residual Bouguer anomaly map

In the Jianchang-Jiumen pluton and its adjacent area, the detailed Bouguer anomaly map (1: 200,000) was derived from the Chinese regional gravity survey, and a lower-resolution (2′×2′) Bouguer grid was acquired from the International Gravimetric Bureau database (Bonvalot et al., 2012). To highlight the Jianchang-Jiumen pluton related short wavelengths anomalies in the upper crust (down to a few kilometers), the long wavelengths of the gravity anomaly from deeper structures must be subtracted from the complete Bouguer anomaly. The long wavelengths of the gravity anomaly were extracted from a lower-resolution (2′×2′) Bouguer grid, using a 200 km low-pass Butterworth filter after several attempts. The residual Bouguer anomaly map was obtained by subtracting the filtered regional Bouguer anomaly that

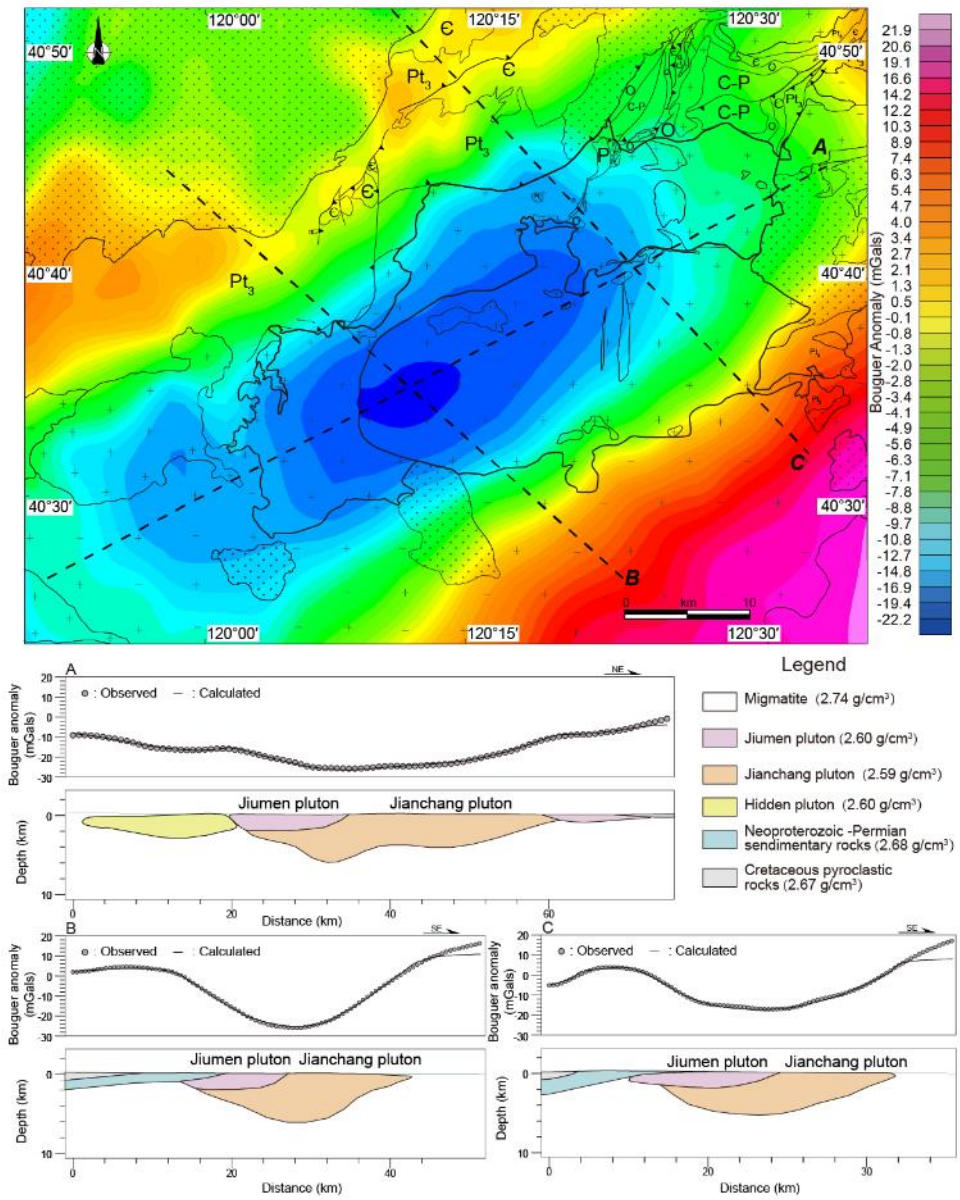

Figure 5.13. Gravity modeling. (a) Residual Bouguer gravity anomaly of the Jianchang-Jiumen pluton and adjacent areas after subtraction of a 200 km wavelength regional trend from the complete Bouguer anomaly. Symbols and captions are the same as in Figure 5.4. (b) 2D gravity modeling across the Jianchang-Jiumen pluton.

represents the long wavelengths of the gravity anomaly (Figure 5.13a).

In the residual Bouguer anomaly map, the Jianchang-Jiumen pluton displays a significant NE–SW trending negative anomaly that more or less correlates with the pluton boundary (Figure 5.13a). Generally, the Jianchang-Jiumen pluton shows a negative anomaly center in the northwestern part of the Jianchang pluton, corresponding to the root of the pluton. The negative

anomalies decrease outwards from the root, even change into positive anomalies in its southeastern border. In its north, the negative anomaly exceeds the pluton boundary, indicating northward extension of the pluton beneath the country rocks. To the southwest, the country rocks show a high negative anomaly, indicating the possible continuity of the pluton to the west below the country rocks.

5.6.2. 2D gravity modeling

In order to image the detailed geometry of the Jianchang-Jiumen at depth, the residual gravity anomaly has been modeled along three cross-sections, subparallel to the long or short axes of the pluton. In this modeling, several constraints have been taken into account for the final models: (1) geological contacts and structural data. These geological data are derived from the available geological map and our field observations. (2) Density of lithological units considered in the modeling. Densities of these units, summarized in Figure 5.13b, are derived from laboratory measurements. (3) Geometrical constraints of considered geological units. During the modeling, the geometry of these geological units with fixed densities has been adjusted to match calculated gravity values with observed ones. The densities of the two plutons (2.60 g/cm^3 for the Jiumen pluton, 2.59 g/cm^3 for the Jianchang pluton) are too close to each other to produce significant gravity variations. The contact between the two plutons has no gravity reliability and only reflects our understanding of the geology with field observation and fabric measurements.

Three 2D modeling profiles image the detailed geometry of the two plutons (Figure 5.13b), indicating (1) the Jianchang-Jiumen pluton exhibits a tabular shape with a maximal thickness of about 6 km, (2) the Jiumen pluton as one stacked sheet overlies the Jianchang pluton, (3) the highest negative anomaly, located in the northwest part of the Jianchang pluton, corresponds to the feeder zone of the Jianchang pluton, and (4) the Jianchang pluton, with shallow to moderately inward-dipping sidewalls, progressively thins outwards.

5.7. Discussion

5.7.1. Significance of Magnetic Fabrics

The Jianchang-Jiumen pluton appears isotropic without obvious mineral preferred orientation in the field (Figures 5.5a-5.5b). Microstructural observations reveal that the fabrics recorded in the Jianchang-Jiumen pluton are mainly magmatic and submagmatic (Figure 5.6), indicating these fabrics were acquired developed during, or just after, the crystallization of the magma. The magnetic fabrics of the Jianchang-Jiumen pluton are dominated by the pseudo-single domain (PSD) magnetite, presenting relatively low P_J value (Figure 5.8), suggesting also a magmatic origin of fabrics in the Jianchang-Jiumen pluton. The preserved magmatic fabrics in the pluton usually represent only the last increment of strain during crystallization, since the fabrics in earlier stages are easily reset by the flowing magma (Yuan and Paterson 1993; Paterson and Vernon 1995; Paterson et al. 1998). Considering the lack of emplacement-related ductile deformation in the country rocks, these fabrics may provide a record of either chamber-related or regional stresses dominated during the final crystallization (Paterson et al. 1998). The Jianchang-Jiumen pluton shows margin-parallel magnetic foliations in these two sub-plutons (Figure 5.12). These margin-parallel magnetic foliations are usually considered as a consequence of magma expansion during the intrusion. Without any regional strain, the magmatic lineation that reflects the magma flow within the pluton would have variable orientations and plunges depending on magma convection (e.g., Paterson, 1989). In the Jianchang-Jiumen pluton, the magnetic lineation patterns define two principle maxima-oriented NW-SE (mean at 300°/29°) and NE-SW (mean at 60°/20°) for these two Jiumen-Jianchang intrusions, respectively (Figure 5.12). These two groups of magnetic lineations seem providing records of the regional stresses during their emplacement.

5.7.2. Emplacement Modes and Their Bearings on the Regional Tectonics

5.7.2.1. Jiumen pluton

Geochronological data suggest that the Jiumen pluton and the Jianchang pluton were emplaced during the Early Jurassic (~190 Ma) and the early Late Jurassic (~158 Ma), respectively (Figure 5.4). Gravity modeling reveals the Jianchang-Jiumen pluton corresponds to two partly overlapping intrusions (Figure 5.13). The Jiumen pluton, as one stacked sheet close to its bottom, overlies the northwestern part of the Jianchang pluton. In the northeast, the pre-existing Yangjiazhangzi syncline were developed before the emplacement of the Jiumen pluton, suggested by the Late Triassic granitic stock intruded into its core (Figure 5.4). Although the Jiumen pluton and its country rocks were cut by the nearly E-W and NE-SW trending fold and thrust belts, all the bedding in the contact metamorphic aureole strikes subparallel to the pluton boundary and dip outwards. It seems that the Jiumen pluton intruded into the core of the anticline adjacent to the Yangjiazhangzi syncline. Considering the steeply outward dipping and margin-parallel foliations and absence of the syn-magmatic ductile shearing in the country rocks, the Jiumen pluton could emplace as a phacolith-like intrusion by the inflation of the magma in the anticlinal core (Figure 5.14).

During the Early to early Middle Jurassic, the small-scale E-W trending extensional basins or normal faults were widely distributed in the western NCB, e.g., the Ordos basin and its periphery (Zhang et al., 2011), the Daqingshan (Darby et al., 2001; Ritts et al., 2001), and the Taihangshan (Li et al., 2015). These structural phenomena suggest that the Early Jurassic to early Middle Jurassic S-N extension occurred in the western NCB (Figure 5.2). In the eastern NCB, the NE trending rift basins were developed, such as the Western Hill of Beijing (Xu and Wu, 1989; Figure 5.2). During this stage, the eruption of basalt (the Nadaling or Xinglonggou Formations) in the eastern NCB and the development of coal-bearing basins have been considered to occur in an extensional setting (Meng et al., 2019; Hao et al., 2020). The granitic and volcanic rocks (including the Jianchang-Jiumen pluton), only distributed in the eastern

Liaoning and Yanshan, were derived from the partial melting of a lower crustal source in a subduction-related setting (Wu et al., 2005). Considering the distribution of the Early Jurassic igneous rocks parallel to the subduction margin of the Paleo-Pacific Plate (Figure 5.2), therefore, we argue that the Jiumen pluton, presenting a NE–SW magnetic lineation, have recorded a NW–SE trending back arc extensional paleostress field related to the subduction of the Paleo-Pacific Plate. Accordingly, the NW–SE extension in the eastern NCB could be in a backarc setting in response to the onset of the Paleo-Pacific Plate subduction beneath the NCB, concur with many studies in petrology and geochemistry (e.g., Wu et al., 2005, 2019; Wang et al., 2019).

5.7.2.2. Jianchang pluton

In the Jianchang pluton, the current exposure is close to the roof of the pluton due to the covering of some remnants of the Jiumen pluton (Figure 5.4). The margin-parallel magnetic foliations define the dome-like roof of the Jianchang pluton (Figure 5.12a). Gravity modeling suggests that the Jianchang pluton has a tabular shape with an unflat bottom and shallow to moderately inward-dipping sidewalls (Figure 5.13). The root of the Jianchang pluton as a feeder zone is located in the northwest of its current exposure. Therefore, the Jianchang pluton with a margin-parallel fabric pattern could emplace by magma inflation from its feeder zone (Figure 5.14).

During the early Late Jurassic, the volcanic and pyroclastic rocks of the Tiaojishan/Lanqi Formation, and concomitant granite plutons (164-155 Ma) are only distributed in the eastern NCB (i.e., the Liaodong and Jiaodong peninsulas and the eastern YFTB; Figure 5.2). These magmatic rocks were also originated from the hybridization between the enriched mantle-derived mafic magma and the thickened lower crust in a subduction-related setting (Wu et al., 2005). An early Late Jurassic extension occurred in the eastern NCB, suggested by the Kalaqin

metamorphic core complex with a top-to-the-NE detachment (156-150 Ma; Lin et al., 2014), and coeval nearly N-S trending grabens or half-grabens, e.g., Diaoe graben and Houcheng half-graben, (Qi et al., 2015); Chengde graben, (Davis et al., 2001); Guojiadian half-graben, (Davis et al., 2009). Therefore, an NE–SW striking magnetic lineation could record an early Late Jurassic extensional paleostress field in the eastern NCB. Similarly, the early Late Jurassic granitoid and coeval volcanic rocks were distributed along the eastern margin of the East Asian continent (Figure 15d). It seems that early Late Jurassic NE-SW backarc extension, related to the Paleo-Pacific Plate subduction beneath the East Asian continent, occurred in the eastern NCB again (Figure 16c).

The emplacement of the Jianchang-Jiumen pluton provides new structural constraints on the Jurassic two-stage extension in the eastern NCB. Furthermore, the Jurassic two-stage extension provides new constraints on multiphase deformation sequences of the NCB during

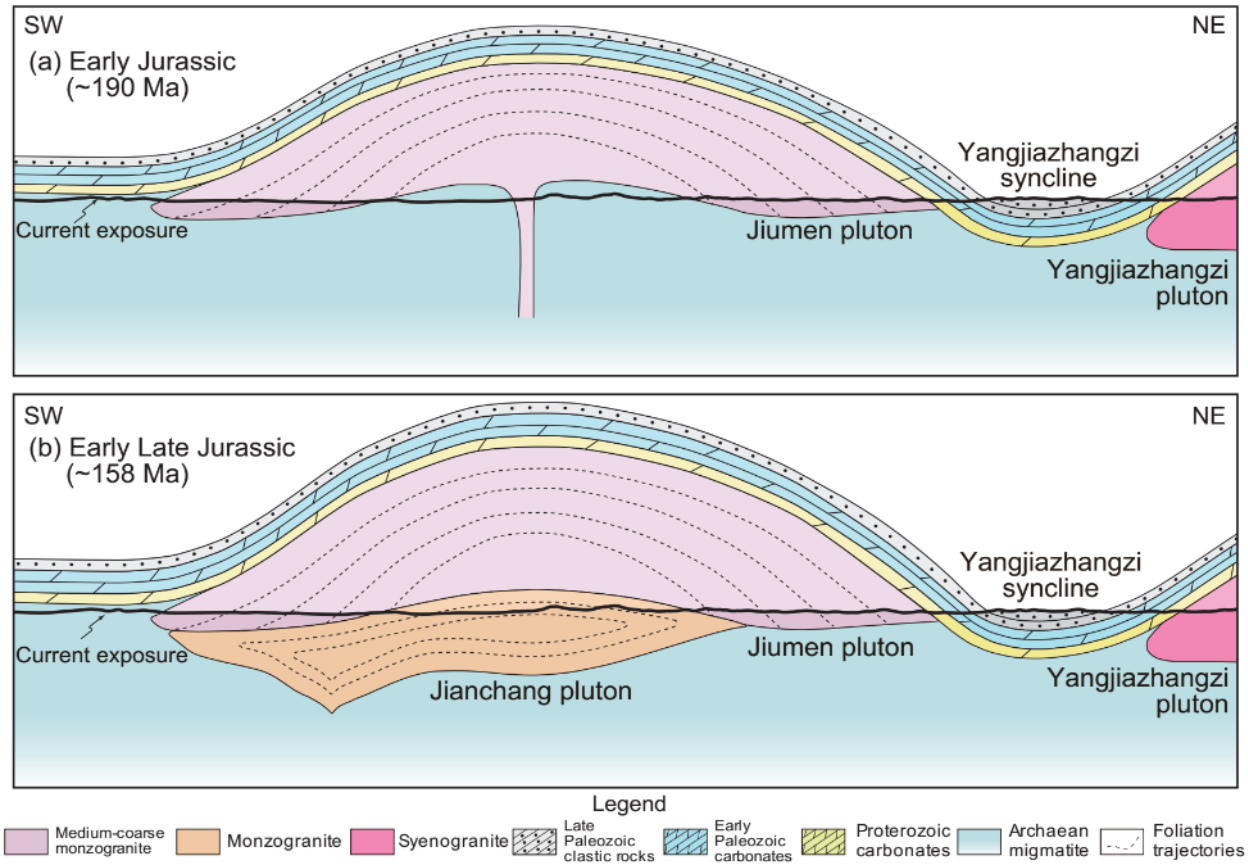

Figure 5.14. Emplacement mode of the Jianchang-Jiumen pluton.

Jurassic-Early Cretaceous. During the Early Jurassic-early Middle Jurassic, post-collisional N-S extension occurred in the western NCB after the collision between the North and South China Blocks, whereas the NW-SE backarc extension occurred in the eastern NCB. The late Middle Jurassic N-S compression, related to the closure of Mongol–Okhotsk Ocean, occurred in the northern NCB. The two-stage extension was interrupted by late Middle Jurassic N-S compression in the northern NCB. During the late Late Jurassic-Early Cretaceous, the NCB underwent large-scale NW-SE compression and extension related to the subduction and rollback of the Paleo-Pacific Plate.

Chapter 6. Early Mesozoic tectonic framework of the northern North China Block and geodynamic mechanism

The stable North China Craton began to transform in the Mesozoic, and decratonization, cratonic destruction, or lithospheric thinning occurred during Early Cretaceous. Due to modification of multi-stage shortening during Yanshannian Movement, only few remnants of Early Mesozoic sedimentary basins were distributed in the NCB. Although some sporadic small grabens and half grabens have been reported in the NCB, the Triassic and Jurassic extensional structures and dynamic mechanism in the NCB have not been well constrained. The emplacement of large-scale granitoid records tectonic information during its emplacement. The structural studies of plutons are an effective way to reveal the coeval regional setting. In this paper, to better understand tectonic setting and dynamic mechanism during Triassic to earliest Cretaceous in the northern NCB, an integrated multidisciplinary investigation, including structural geology, geochronology, geochemistry, AMS, and gravity modeling, has been conducted in Late Triassic Dushan pluton in Eastern Hebei, Late Triassic Wangtufang pluton in northern Hebei and Jurassic Jianchang-Jiumen pluton in western Liaoning. Through the emplacement of three plutons, three extensional stages, including Late Triassic, Early Jurassic-early Middle Jurassic, and early Late Jurassic occurred in the North China Craton. It further constrains regional tectonic framework of the North China Craton during Triassic-earliest Cretaceous and related geodynamic mechanism.

6.1. Early Mesozoic tectonic framework of the northern NCB

Three extensional stages, including Late Triassic, Early Jurassic-early Middle Jurassic, and early Late Jurassic, provide new constraints on multiphase deformation sequences of the NCB during Triassic-Early Cretaceous. Integrating previous studies concerning other structural elements and associated kinematics in different stages of Jurassic-Early Cretaceous, an

improved and more detailed structural framework of the NCB was established for understanding of Jurassic-Early Cretaceous intracontinental orogeny and associated geodynamic mechanism (Figure 6.1).

6.1.1. Early-Middle Triassic N-S compression in the northern NCB

In the NCB, the Triassic strata overlie conformably the Permian strata, while the Upper Triassic strata overlie unconformably the underlying strata (Figure 6.1; Meng et al., 2019). In the northern NCB, the ductile shear zone concerns the E-W trending Chicheng-Fengning, Fengning-Longhua, and Damiao-Niangniangmiao ductile shear zones in the north (Wan, 2012; Wang et al., 2013; Zhang et al., 2014; Figure 6.2), and the E-W trending folds and thrusts include the Unnamed fault, Malanyu anticline, and Jixian thrust fault in the south (Davis et al., 2001; Ma et al., 2007). In the western Liaoning, the Early–Middle Triassic thrusts were covered

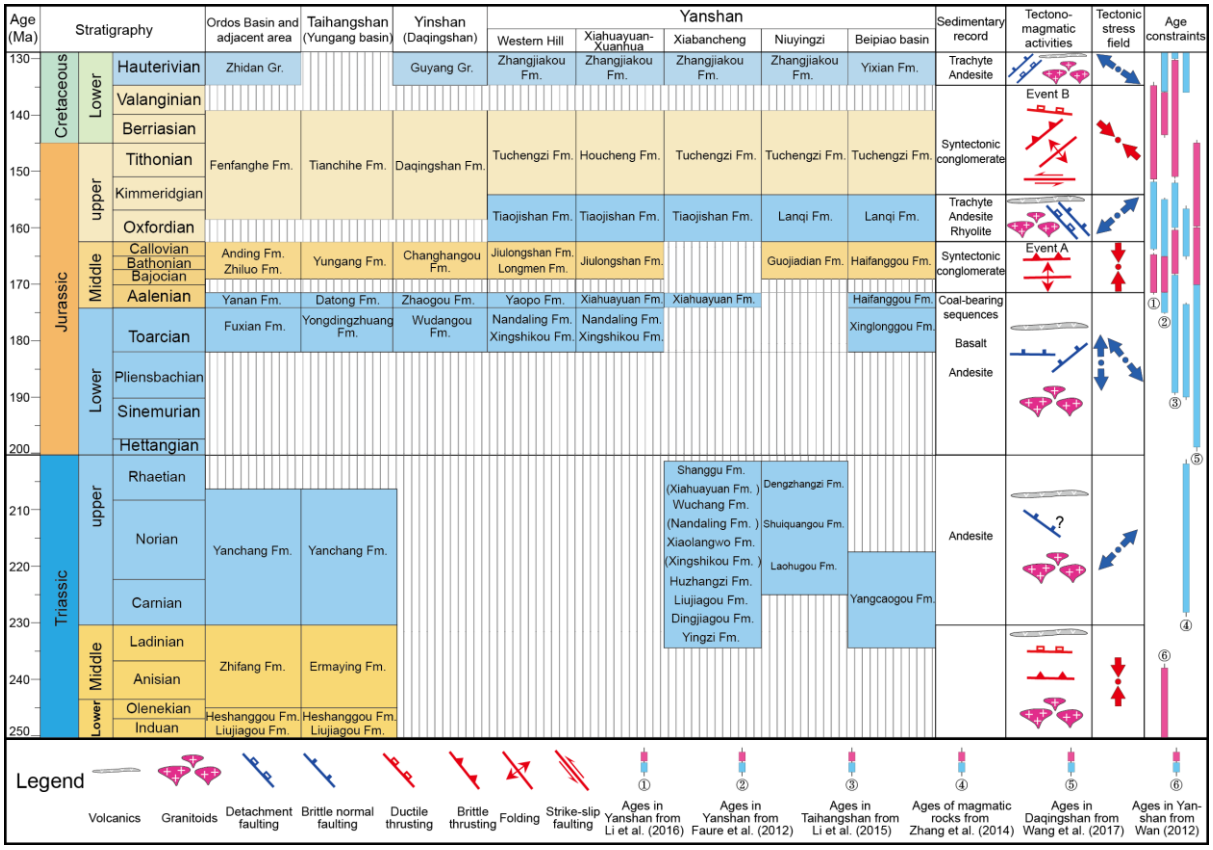

Figure 6.1 Early Mesozoic tectono-stratigraphic summary diagram in the NCB.

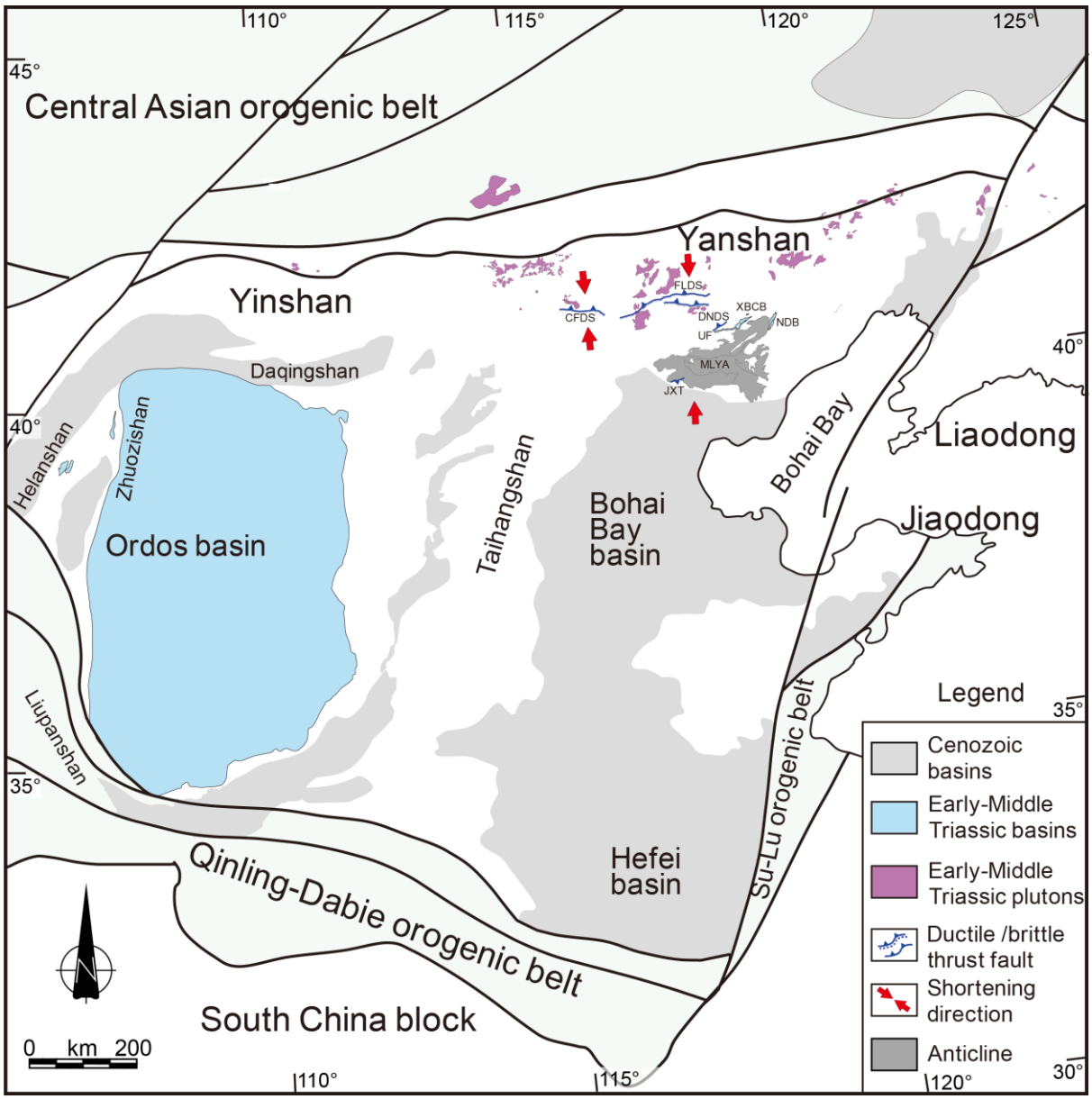

Figure 6.2 Early-Middle Triassic tectonic outline of the NCB. CFSZ: Chicheng-Fengning ductile shear zone, FLSZ: Fengning-Longhua, ductile shear zone, DNSZ: Damiao-Niangniangmiao ductile shear zone, UF: Unnamed fault, JXT: Jixian thrust, MLYA: Malanyu anticline, XBCB: Xiabancheng basin, NDB: Niuying-Dengzhangzi basin.

by the volcanics in the Shuiquangou Formation in the Lingyuan area of the eastern Yanshan belt (Hu et al., 2005, 2010). It suggested that it was in a N-S compressional tectonic setting in the northern NCB (Figures 6.1-6.2).

6.1.2. Late Triassic NE-SW extension in the northern NCB

In the NCB, a Late Triassic extensional setting for the northern NCB has been proposed according to the geochemistry of the E-W trending alkaline intrusive complexes (Yang et al., 2012; Zhang et al., 2012). Fining and deepening upward depositional system and abundant volcaniclastic rocks in the remnant basins suggest a Late Triassic extensional setting in the northern NCB (Davis et al., 2009; Meng et al., 2014; Figure 6.3). In the south of Sonid Zuoqi in the vicinity of the Solonker zone, a NE-SW trending extension has been also documented in a Late Triassic metamorphic core complex (Davis et al., 2004; Figure 6.3). The geochemistry of the Dushan pluton and the Wangtufang pluton, similar to the Late Triassic alkaline intrusive complexes, indicates that it originated from partial melting of the lower crust with a contribution of mantle-derived materials during an extensional setting (Ye et al. 2014; Jiang et al., 2018). Emplacement of the Wangtufang pluton was in an extensional setting, considering: (1) the NE–SW striking magnetic lineation, (2) the NE–SW trending elongated subsurface pluton shape, and (3) the orthogonal NW–SE striking syenogranitic dykes considered as tension gashes during the NE–SW trending extension. Therefore, the Wangtufang pluton provides reliable arguments to the Late Triassic intracontinental extensional setting already suggested in the northern NCB (Figure 6.3).

6.1.3. Early Jurassic-early Middle Jurassic N-S extension in the western NCB and NW-SE extension in the eastern NCB

During the Early Jurassic-early Middle Jurassic, the basin infill contains mafic volcanic rocks in the eastern NCB and widespread coal-bearing sequence in the whole NCB (Figure 6.1), which were considered to take place in an extensional setting (Zhang et al., 2014; Meng et al., 2019; Hao et al., 2020). The N-S extension is well recorded by E-W trending brittle normal faults in the western NCB (Darby et al., 2001; Ritts et al., 2001; Zhang et al., 2011; Li et al., 2015; Figure 6.4). The NNE-SSW and nearly N-S extensional normal faults were identified in the Upper Triassic-Lower Jurassic strata in the central and northeastern Ordos

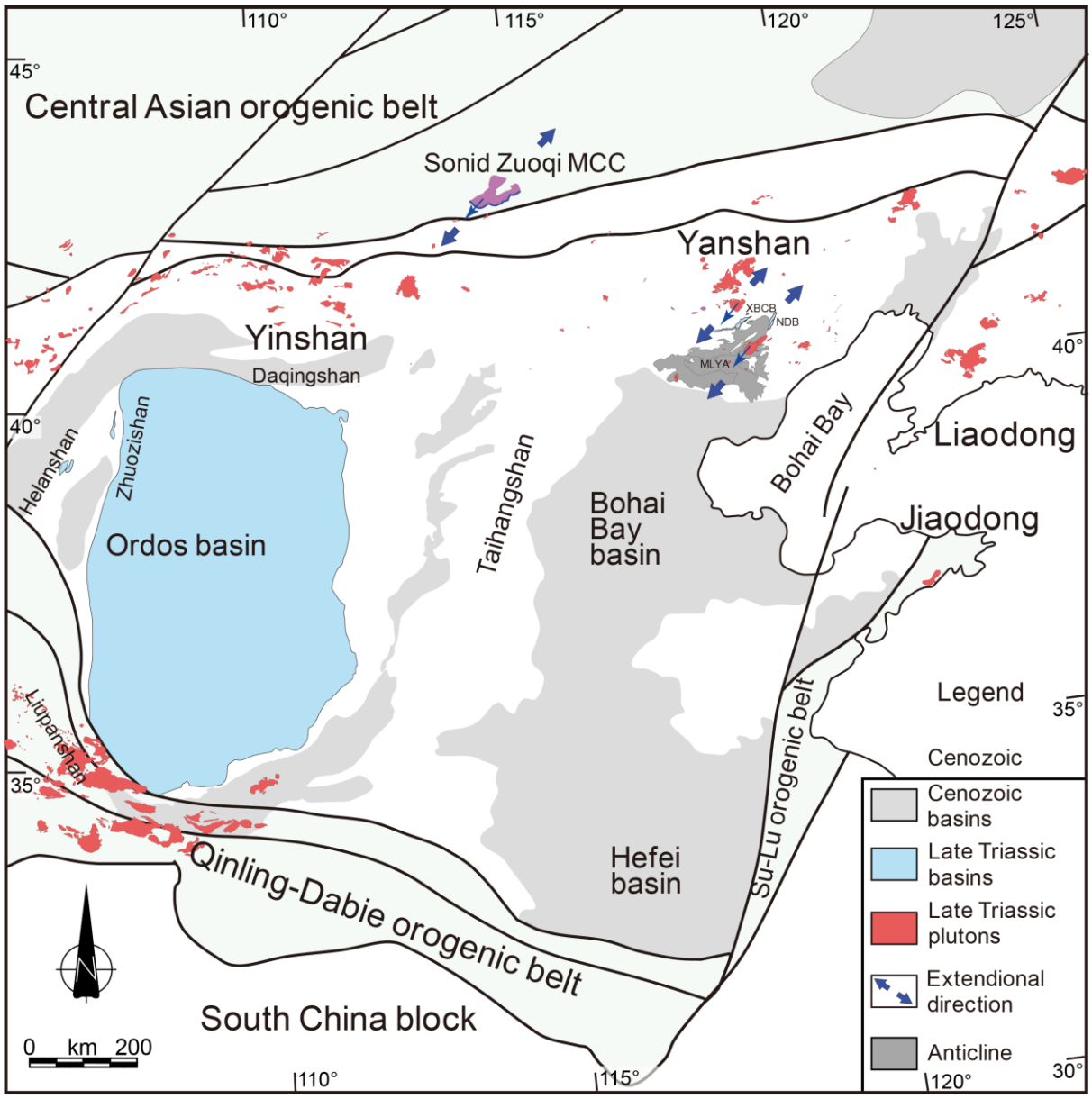

Figure 6.3 Late Triassic tectonic outline of the NCB. MLYA: Malanyu anticline, XBCB: Xiabancheng basin, NDB: Niuying-Dengzhangzi basin.

Basin (Zhang et al., 2011; Figure 6.4). In the Yungang and Guangling Basins, the normal faults cut the conglomerates in the lower Lower Jurassic, covered by the upper Lower Jurassic strata (Li et al., 2015; Figure 6.4). The sedimentary studies showed a fining and deepening upward depositional system from the Upper Triassic to Lower Jurassic strata, suggesting a Late Triassic extensional tectonic setting in the Lingwu-Jingle Basin (Meng et al., 2014; Li et al., 2015). In the southwestern Daqingshan, the E-W trending normal faults cut the unconformity between the Lower Jurassic and Archeozoic (Darby et al., 2001; Figure 6.4). The small-sized grabens

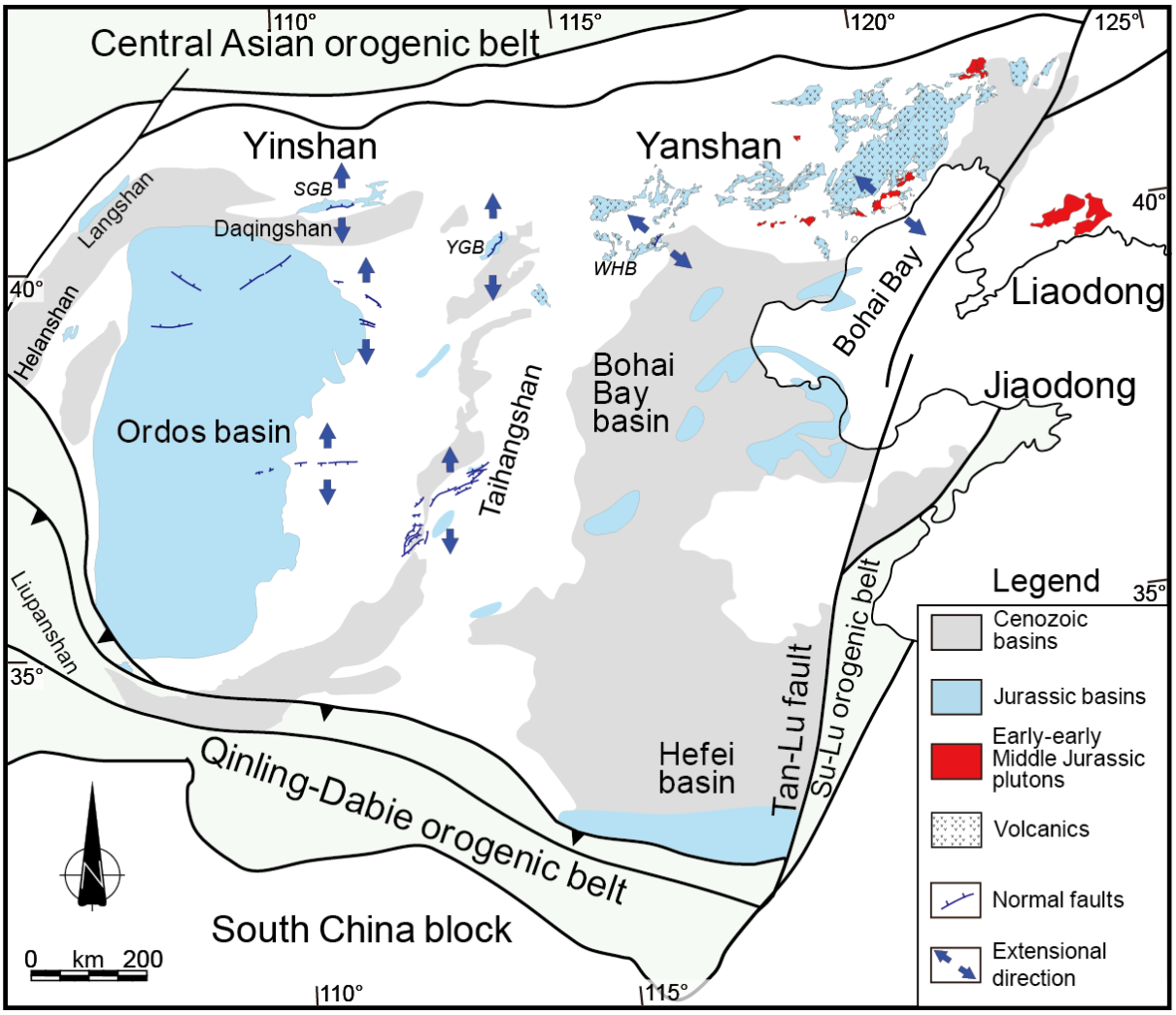

Figure 6.4 Early Jurassic-early Middle Jurassic tectonic outline of the NCB. SGB: Shiguai basin; YGB: Yungang basin; WHB: Western Hill basin.

were developed, dominated by the growth normal faults. In the eastern NCB, the structural and sedimentary studies suggested that the North China Craton was in an extensional setting during the Early-early Middle Jurassic (Meng et al., 2019). Early Jurassic granitoid and coeval volcanic rocks only occurred in the eastern MCB. The Jiumen pluton, together with NE trending rift basin in the Western Hill of Beijing, records a NW–SE extension in the eastern NCB (Figure 6.4).

6.1.4. Late Middle Jurassic N-S compression

The early Middle Jurassic N-S compressional event (i.e., Event A of Yanshanian Orogeny)

is well recorded by the unconformity above the coal-bearing strata and the syntectonic conglomerate and sandstone (Figure 6.1). The Event A was presented as the unconformity between the volcanics in the Tiaojishan Formation and the different underlying strata (Faure et al., 2012). The extensive deformations related to Event A have been overlaid by the volcanics in the Tiaojishan Formation. E-W trending thrusts and fault-related folds mainly localized in the northern NCB (Figure 6.5), e.g., the N–S thrusts covered by the Changhangou and Yungang growth strata in the western Daqingshan and Taihangshan (Li et al., 2014; Wang et al., 2017), E-W trending Miyun-Xifengkou fault and secondary faults in the middle YFTB (Chen, 1998; C. Li et al., 2016), E-W trending Sandaogou fault in the eastern YFTB (Zhao, 2016). In the

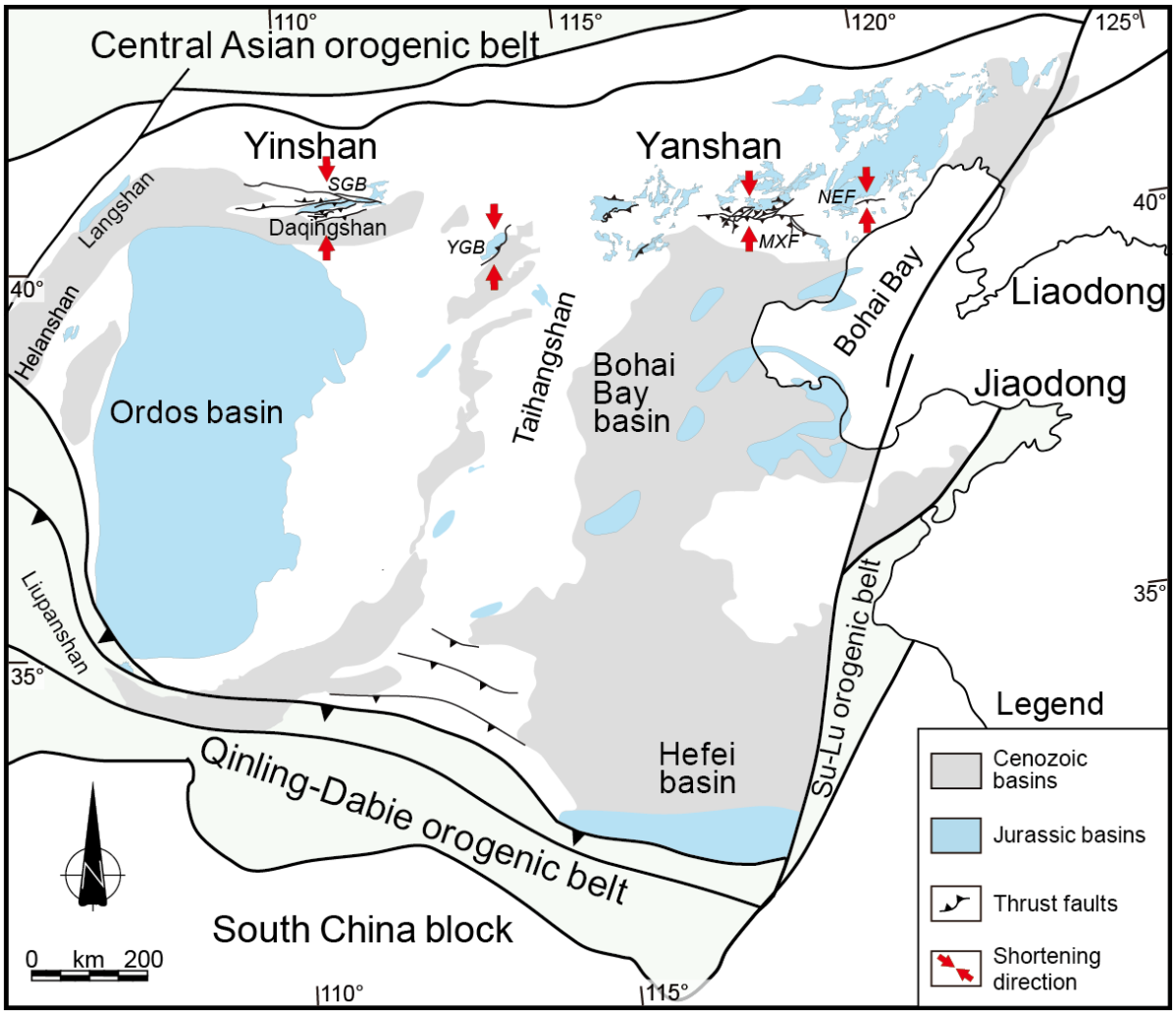

Figure 6.5 late Middle Jurassic tectonic outline of the NCB. SGB: Shiguai basin; YGB: Yungang basin; MXF: Miyun-Xifengkou fault; NEF: Nangou-Erdaogou fault.

Yanshan belt, the fold and thrust belt in the Proterozoic-Paleozoic strata were covered by the he volcanics in the Tiaojishan Formation, e.g., Mengjiazhuang anticline and Duanshuao-Jianbaoshan thrust fault (Li et al., 2016), Miyun-Xifengkou fault, Zhujiagou fault, Qingshuihu fault, Xinglong fault, Gaobanhe fault, Sanpo fault, Banbishan fault, and Lengkou fault (Chen, 1998, Davis et al., 2001; Zhang et al., 2004). The duration of this event has been well constrained between 172 and 164 Ma (Li et al, 2016).

6.1.5. Early Late Jurassic NE-SW extension in the eastern NCB

In the eastern NCB, the early Late Jurassic volcanic and pyroclastic rocks (Tiaojishan/Lanqi Formation) and coeval granite plutons are distributed in the eastern YFTB and the Liaodong and Jiaodong peninsulas (Figures 2.4 and 6.1). The early Late Jurassic NE-SW extension is recorded by the emplacement of the Jianchang pluton, brittle normal faults in the grabens or half-grabens (Davis et al., 2001, 2009; Qi et al., 2015), and the top-to-the-NE shearing detachment fault in the Kalaqin metamorphic core complex (Lin et al., 2014; Figure 6.6). Nevertheless, it is characterized by two sequences of overlapping synorogenic conglomerates in the western NCB (Figure 6.1). Therefore, the early Late Jurassic NE-SW extension only occurred in the eastern NCB (Figures 6.1 and 6.6).

6.1.6. Late Late Jurassic-Early Cretaceous NW-SE large-scale compression and extension

The late Late Jurassic-Earliest Cretaceous mainly NW-SW compressional event (i.e., Event B of Yanshanian Orogeny) is well recorded by the syntectonic conglomerates and the unconformity above them (Figure 6.1). The NE trending thrusts and fault-related folds are well developed throughout the NCB (Figure 6.7). In the mid-eastern YFTB, NE-NNE trending thin- and thick-skinned thrust sheets have accommodated a NW-SE shortening via in- and out-of-

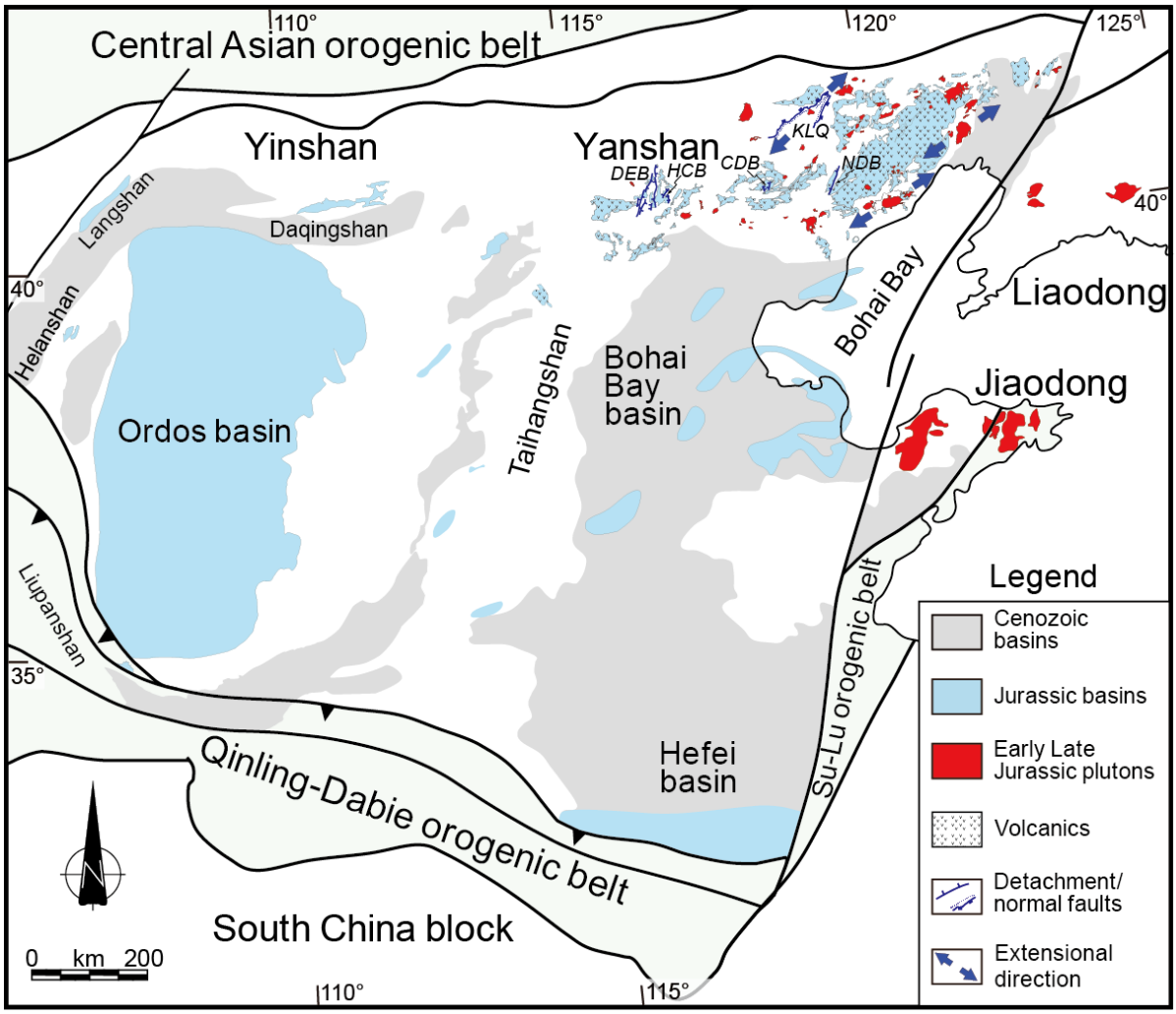

Figure 6.6 early Late Jurassic tectonic outline of the NCB. DEB: Diaoe basin; HCB: Houcheng basin; CDB: Chengde basin; NDB: Niuyingzi-Dengzhangzi basin; KLQ: Kalaqin metamorphic core complex.

sequence thrusting (Davis et al., 2001; C. Li et al., 2016). In the mid-western YFTB, map-scale NE trending thrusts overprint the late Middle Jurassic E-W trending thrusts, accommodated by the dextral strike-slip shear zones (Faure et al., 2012; Lin et al., 2020). The paleostress along the dextral strike-slip faults is NW-SE direction (Lin et al., 2020). The NE trending thrusts and the strike-slip structures are considered to be kinematically coupled, with the E-W trending strike-slip structures as transcurrent fault zones linking the NE trending thrusts along two sides of the dextral strike-slip zones (Faure et al., 2012; Lin et al., 2020). In the Yinshan belt, late Middle Jurassic N–S thrusting was overprinted by the younger Late Jurassic NW-SE thrusting in the western Daqingshan, indicated by the superimposed striations (Wang et al., 2017),

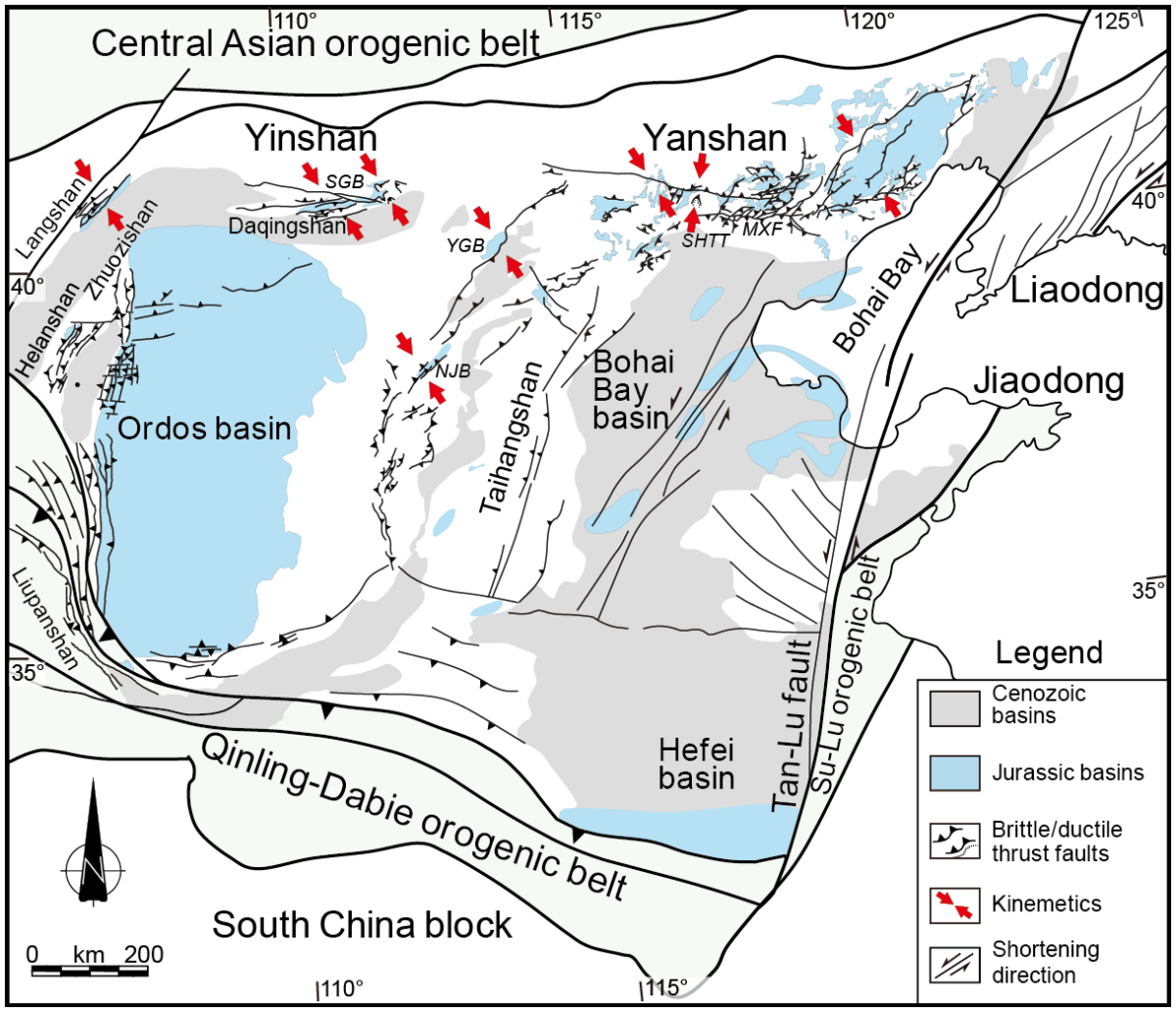

Figure 6.7 late Late Jurassic tectonic outline of the NCB. SGB: Shiguai basin; YGB: Yungang basin; NJB: Ningwu-Jingle basin; MXF: Miyun-Xifengkou fault; SHTT: Sihetang thrust.

whereas large scale low-angle thin-skinned thrusts recorded a NW–SE compression in the eastern Daqingshan (Gong et al., 2015). The NW-SE thrusts are also widely developed in the Taihangshan (Li et al., 2015; Zhang et al., 2020). The NW-SE thrusting dominated multi-directional compression resulted in the shortening deformation during the Late Jurassic along the marginal zones of the Ordos basin (Zhang et al., 2011). The duration of this event (i.e., event B of Yanshanian movement) has also been well constrained around 152–135 Ma (C. Li et al, 2016).

6.2. Discussion of geodynamic mechanism

In the northern NCB, the closure of the Paleo-Asian Ocean is variously interpreted. According to some authors, it occurred in the Late Devonian (Xu et al., 2013; Xu and Chen, 1997; Zhao et al., 2013), afterward, the Central Asian Orogenic Belt experienced an intra-continental rifting, and the formation of small-sized oceanic basins during the Late Carboniferous-Early Permian period. The final event formed the Solonker tectonic zone, partly also accommodated by strike-slip faulting during the Late Permian to Early Triassic (Xu et al., 2014; Zhao et al., 2017). Alternatively, it has been argued that the final closure of the Paleo-Asian Ocean along the Solonker suture zone occurred during the Late Permian to the Early Triassic (Chen et al., 2000, 2009; Eizenhöfer et al., 2014; Jian et al., 2008, 2010; Li et al., 2006; Li et al., 2014; Xiao et al., 2003; Xiao et al., 2015). Whatever the model, during the Late Permian to Early Triassic, the northern part of the NCB was characterized by N-S compression (Figure 6.8a). This deformation featured by E-W trending ductile shear zone and thick- and thin-skinned folds and faults, occurred progressively from the northern margin toward the interior (Wan, 2012, Wang et al., 2013).

An E-W trending Late Triassic alkaline intrusive complexes and the associated mafic rocks occurred at around 231–215 Ma in the northern NCB (Yang, 2012, Zhang et al., 2012, 2014). They were derived from partial melting of lower crust and metasomatized enriched lithospheric mantle with some materials from the depleted asthenospheric mantle (Yang et al., 2012; Zhang et al., 2012; Zhang et al., 2014; Zhu et al., 2012), indicating the upwelling of the asthenospheric mantle and the asthenosphere-lithospheric mantle interaction during the early lithospheric thinning or modification of the North China Craton (e.g., Han et al., 2004). Contemporaneous surface uplift and supracrustal stretching occurred in the northern NCB (Figure 6.1). The Wangtufang pluton recorded the Late Triassic NE–SW intracontinental extension already suggested in the northern NCB. Besides, a Late Triassic metamorphic core complex was developed in the south of Sonid Zuoqi in the vicinity of the Solonker suture zone

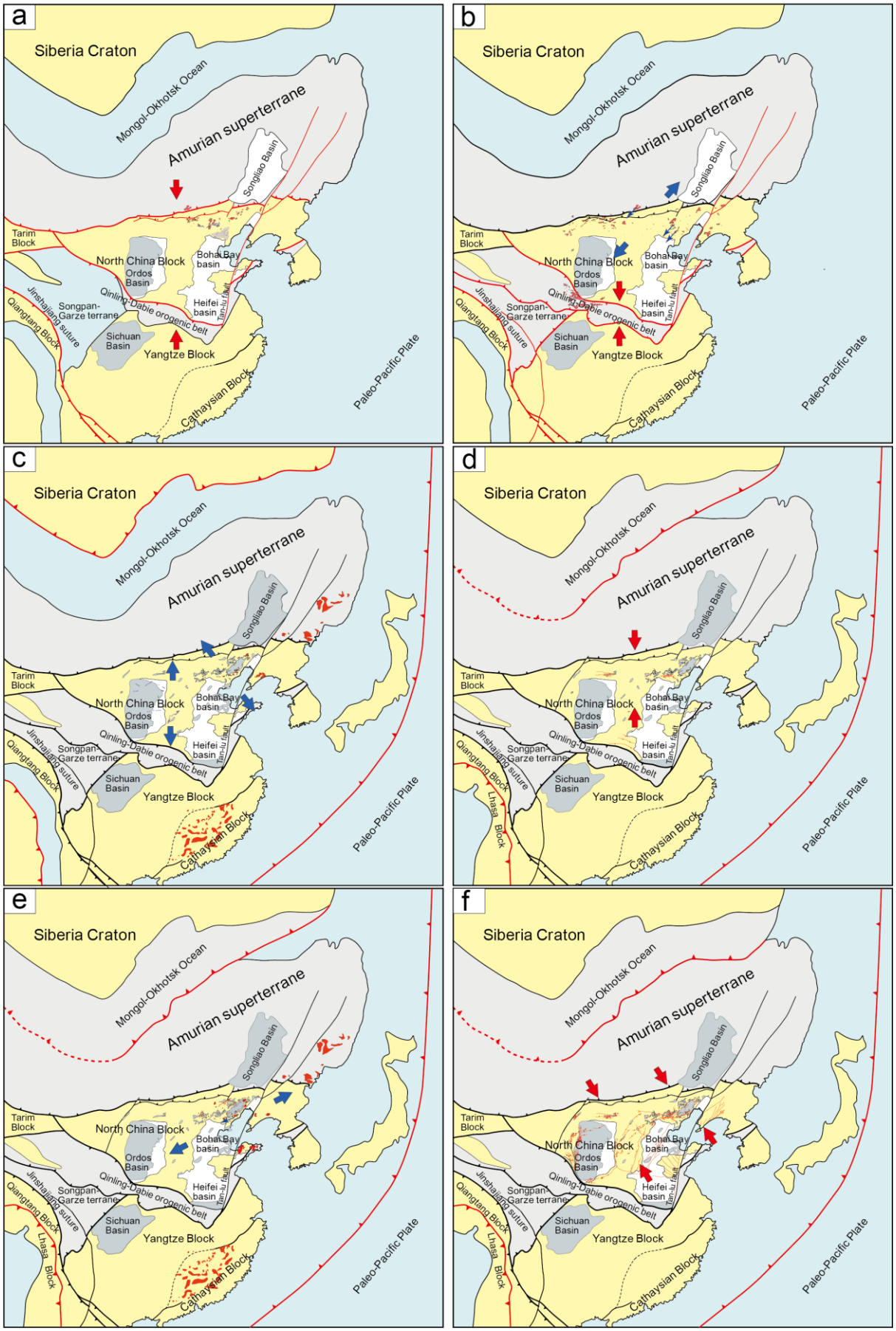
a
Siberia Craton
Mongol-Okhotsk Ocean
Amurian superterrane
Songliao Basin
Tarim Block
North China Block
Ordos Basin
Bohai Bay basin
Qinling-Dabie orogenic belt
Tan-lu fault
Heifei basin
Songpan-Garze terrane
Jinshajiang suture
Qiangtang Block
Sichuan Basin
Yangtze Block
Cathaysian Block
Paleo-Pacific Plate
b
Siberia Craton
Mongol-Okhotsk Ocean
Amurian superterrane
Songliao Basin
Tarim Block
North China Block
Ordos Basin
Bohai Bay basin
Qinling-Dabie orogenic belt
Tan-lu fault
Heifei basin
Songpan-Garze terrane
Jinshajiang suture
Qiangtang Block
Sichuan Basin
Yangtze Block
Cathaysian Block
Paleo-Pacific Plate
c
Siberia Craton
Mongol-Okhotsk Ocean
Amurian superterrane
Songliao Basin
Tarim Block
North China Block
Ordos Basin
Bohai Bay basin
Qinling-Dabie orogenic belt
Tan-lu fault
Heifei basin
Songpan-Garze terrane
Jinshajiang suture
Qiangtang Block
Sichuan Basin
Yangtze Block
Cathaysian Block
Paleo-Pacific Plate
d
Siberia Craton
Mongol-Okhotsk Ocean
Amurian superterrane
Songliao Basin
Tarim Block
North China Block
Ordos Basin
Bohai Bay basin
Qinling-Dabie orogenic belt
Tan-lu fault
Heifei basin
Songpan-Garze terrane
Jinshajiang suture
Qiangtang Block
Lhasa Block
Sichuan Basin
Yangtze Block
Cathaysian Block
Paleo-Pacific Plate
e
Siberia Craton
Mongol-Okhotsk Ocean
Amurian superterrane
Songliao Basin
Tarim Block
North China Block
Ordos Basin
Bohai Bay basin
Qinling-Dabie orogenic belt
Tan-lu fault
Heifei basin
Songpan-Garze terrane
Jinshajiang suture
Qiangtang Block
Lhasa Block
Sichuan Basin
Yangtze Block
Cathaysian Block
Paleo-Pacific Plate
f
Siberia Craton
Mongol-Okhotsk Ocean
Amurian superterrane
Songliao Basin
Tarim Block
North China Block
Ordos Basin
Bohai Bay basin
Qinling-Dabie orogenic belt
Tan-lu fault
Heifei basin
Songpan-Garze terrane
Jinshajiang suture
Qiangtang Block
Lhasa Block
Sichuan Basin
Yangtze Block
Cathaysian Block
Paleo-Pacific Plate

(Davis et al., 2004). It was generally acknowledged that it was related to the deep process after the final amalgamation of the NCB and the Mongolian arc terranes (Figure 6.8b), despite the trigger mechanism remains debated, e.g., intraplate extension (Yang et al., 2012), post-collisional or post-orogenic lithospheric delamination (Zhang et al., 2012), and mantle upwelling in front of the subducting slab of Mongol-Okhotsk plate (Meng et al., 2020).

During the Early Jurassic-early Middle Jurassic, N-S extension occurred in the western NCB, whereas NW-SE trending extension occurred in the eastern NCB. Considering Late Triassic NE-SW extensional setting in the northern NCB (Qiu et al., 2020), the N-S extension in the western NCB should be a result of post-collision following the Triassic collision between the North and South China blocks (Zhang et al., 2011). The Jiumen pluton, together with NE trending rift basin in the Western Hill of Beijing, records a NW–SE extension in the eastern NCB (Figure 6.4). Early Jurassic granitoid and coeval volcanic rocks (including these of the eastern NCB) constitute a NE–SW-trending magmatic belt along the eastern margin of the East Asian continent (Figure 6.4). Accordingly, the NW–SE extension in the eastern NCB could be in a backarc setting in response to the onset of the Paleo-Pacific Plate subduction beneath the NCB (Figure 6.8c), concur with many studies in petrology and geochemistry (e.g., Wu et al., 2005, 2019; Wang et al., 2019).

The early Middle Jurassic N-S compression (i.e., Event A of Yanshanian Orogeny) occurred in the northern NCB (Figure 6.5). The extensive E-W trending thrusts and fault-related folds, related to Event A, mainly localized in the northern NCB (Figure 6.5). In the north of the East Asian continent, it is generally believed that the Mongol–Okhotsk Ocean closed progressively from west to east during the Jurassic-Early Cretaceous (Zorin, 1999; Kravchinsky et al., 2002; Metelkin et al., 2010). The far-field compression, related to the

Figure 6.8 Simplified geological maps showing Triassic-Early Cretaceous structures and magmatic rocks in North China, and geodynamic setting. (a) Early-Middle Triassic. (b) Late Triassic. (c) Early Jurassic-early Middle Jurassic. (d) late Middle Jurassic. (e) early Late Jurassic. (f) late Late Jurassic.

closure of Mongol–Okhotsk Ocean between amalgamated North China–Mongolian terrane and the Siberian Craton, is considered the best explanation for this N-S intraplate compressional event in the northern NCB (Figure 6.8d).

Similar to the Early Jurassic-early Middle Jurassic time, the early Late Jurassic granitoid and coeval volcanic rocks were distributed along the eastern margin of the East Asian continent (Figure 6.8d). The early Late Jurassic NE-SW extension only occurred in the eastern NCB. It is recorded by the emplacement of the Jianchang pluton, brittle normal faults in the grabens or half-grabens (Davis et al., 2001, 2009; Qi et al., 2015), and the top-to-the-NE shearing detachment fault in the Kalaqin metamorphic core complex (Lin et al., 2014; Figure 6.6). It seems that early Late Jurassic NE-SW backarc extension, related to the Paleo-Pacific Plate subduction beneath the East Asian continent, occurred in the eastern NCB again (Figure 6.8e). Therefore, Jurassic Paleo-Pacific Plate subduction-related two-stage backarc extension, interrupted by the far-field N-S compression related to the closure of Mongol–Okhotsk Ocean, occurred in the eastern NCB (Figure 6.8).

Considering that Late Jurassic NW-SE compression characterized by the NE trending thrusts and fault-related folds occurred in South China (J. Li et al., 2016), this large-scale NW-SE compression in the NCB could be a consequence of the Paleo-Pacific plate subduction beneath the East Asian continent (Figure 6.8f). However, the coeval top-to-the-SSW ductile Sihetang thrusting shear zone formed in the middle YFTB (Davis et al., 2001; Zhu et al., 2015; Figure 6.8f). It seems that the far-field compression related to the closure of Mongol–Okhotsk Ocean might have also influenced deep structure in the northern NCB again. During the Early Cretaceous, large-scale NW-SE extension in the East Asian continent is expressed by metamorphic core complexes, graben or half-graben basins, and A-type magmatism (Wang et al., 2011; Lin & Wei, 2018; Wu et al., 2019). The thick (~200 km) Archean lithosphere mantle beneath the eastern NCB was replaced by a thin (<80 km) juvenile one (Fan & Menzies, 1992;

Griffin et al., 1992; Menzies et al., 1993). It was related to the subduction and rollback of the Paleo-Pacific Plate (Wu et al., 2019).

Chapter 7. Conclusions and Perspectives

7.1. Conclusions

The stable North China Craton began to transform in the Mesozoic, and decratonization, cratonic destruction, or lithospheric thinning occurred during Early Cretaceous. Although the destruction of the North China Craton occurred in the Cretaceous, this is controversial with various estimates as to the onset of destruction, i.e., Late Triassic (Han et al., 2004; Yang et al., 2007, 2010b, 2012), or Late Jurassic (Gao et al., 2004). Before the Cretaceous destruction of the North China Craton, the North China Craton has undergone two orogenic cycles, including Paleozoic continental collisions with Mongolian arc terranes and South China Block at block boundaries, and Jurassic-Early Cretaceous intracontinental orogeny (also called Yanshanian Orogeny). It gave rise to a complicated assemblage of folds, thrust and reverse faults, normal faults, and intrusive rocks in the NCB during multiphase deformations. Due to modification of multiphase deformations, only some clues of extensional episodes, coeval with the igneous rocks possibly implying onset of the destruction of the North China Craton, have been found by sporadic small grabens or normal faults (Darby et al., 2001; Davis et al., 2001, 2009; Ritts et al., 2001; Zhang et al., 2011; Meng et al., 2014, 2019; Li et al., 2015; Qi et al., 2015). As such, the extensional tectonics and associated geodynamic mechanism remains poorly constrained due to rare geological records. In this thesis, through the multidisciplinary studies of three plutons, it provides new insights into the emplacement mechanism of the Early Mesozoic granitic pluton and associated extensional tectonic setting, from which we draw four main conclusions.

1. The multidisciplinary study comprising field and microstructural observations, isotope chronology, AMS measurements, and gravity modeling enables us to better understand the emplacement process of the Late Triassic Dushan pluton. The Dushan pluton consists of

monzogranite and biotite-rich marginal facies with a progressive petrographic fabric change between them. The arc-shaped gneissosity with locally mylonitic foliations in the southwestern margin is compatible with the magnetic foliation across the pluton, defining an elliptic dome-like fabric pattern with a NE-SW striking long axis. The NE-SW trending stretching lineations in the mylonitic zones are also concordant with the magnetic lineations measured in the pluton. It presents a continuum of fabric variation from magmatic to solid-state conditions within pluton. The tabular or tongue-like Dushan pluton was probably built through the feeder zone in its northeast, with a first biotite-rich sill-shape intrusion then the inflation of conduit-fed monzogranite magma batches. The progressive and southward magma intrusions might make inflations not only upwards, downwards, but also laterally. The inflation of the successive magma might deform and even recrystallize the former cool-down magma, and form an arc-shaped, gneissic to mylonitic foliation in the southwestern margin of the pluton. Considering that the similar ductile deformation observed in the southern margin of the pluton is absent in the country rocks, the pluton structure recorded rather its emplacement process than the Late Triassic regional tectonics.

2. To better understand Late Triassic tectonic setting in the northern NCB, the emplacement mechanism of the Wangtufang pluton, which recorded the synmagmatic regional tectonic signature, has been investigated. Zircon U-Pb ages, and Hf isotopic data, and whole-rock geochemical analyses suggest that the Late Triassic Wangtufang pluton composed of syenogranite and diorite is derived from partial melting of lower crust with some depleted mantle components. Both the syenogranite and diorite appear isotropic. Anisotropy of magnetic susceptibility and gravity studies have been carried out to characterize internal fabrics and shape of the pluton. The diorite forms just thin remnants above the syenogranite. The syenogranite with a series of NW-SE trending dykes intruded into the diorite and its country rocks. In the syenogranite, the gently dipping magnetic foliations strike nearly parallel to the

pluton border. The shallow plunging magnetic lineations mainly strike NE–SW. Combining NE-SW trending elongated subsurface shape with central root, unflat bottom, and moderate- to high- inward dipping sidewalls, the syenogranite could be considered as a lopolith-like intrusion. The syenogranite was likely emplaced by inflation of magma pulses from its central conduit and built up by floor depression. Emplacement of the syenogranite was in an extensional setting, considering: (1) the NE–SW striking magnetic lineation, (2) the NE–SW trending elongated subsurface pluton shape, and (3) the orthogonal NW–SE striking syenogranitic dykes considered as tension gashes during the NE–SW trending extension. The Wangtufang pluton provides reliable arguments to the Late Triassic intracontinental extensional setting already suggested in the northern NCB.

3. The Jurassic-Early Cretaceous intracontinental orogeny in East Asia is expressed by a complicated structural feature in the NCB with multiphase deformations that timing and kinematics are crucial to decipher the geodynamics of the NCB. Particularly, Jurassic extensional tectonics in North China remains ambiguous due to sporadic geological records. A multidisciplinary investigation on the Jurassic Jianchang-Jiumen pluton has been performed to provide tectonic information for Jurassic extensional episodes. The phacolith-like Jiumen pluton (~190 Ma) reveals margin-parallel foliations produced by magma inflation in the anticlinal core, while the tabular-like Jianchang pluton (~158 Ma) with margin-parallel foliations, intruded by magma inflation, underlay the Jiumen pluton. Two patterns of magnetic lineations recorded Early Jurassic NW-SE extension and early Late Jurassic NE-SW extension in the eastern NCB, respectively.

4. Through the emplacement of three plutons, three extensional stages, including Late Triassic, Early Jurassic-early Middle Jurassic, and early Late Jurassic occurred in the North China Craton. It further constrains regional tectonic framework of the North China Craton during Triassic-earliest Cretaceous. The North China Craton experienced Late Triassic

intracontinental NE-SW extension related to deep-seated tectonic process, following the closure of Paleo-Asian Ocean or subsequent intracontinental compression. Large-scale Late Triassic extensional structures in the northern North China Craton influenced one-third of the craton, indicating the beginning of craton destruction. During the Jurassic, the Early Jurassic-early Middle Jurassic N-S post-collisional extension occurred in the western North China Craton after the amalgamation between North China and South China, whereas Early Jurassic-early Middle Jurassic NW-SE trending and early Late Jurassic ENE-WSW extension and associated magmatism occurred in the eastern North China Craton. The subduction of the Paleo-Pacific plate had an impact on lithosphere of the eastern North China Craton until the cratonic destruction during Early Cretaceous (126 Ma). The two-stage extension was interrupted by late Middle Jurassic N-S compression related to the closure of Mongol–Okhotsk Ocean, followed by large-scale late Late Jurassic-Early Cretaceous NW-SE compression and extension related to the subduction and rollback of the Paleo-Pacific Plate, respectively.

7.2. Perspectives

The Phanerozoic tectonic evolution of the NCB is related to two orogenic cycles, including Paleozoic continental collisions with Mongolian arc terranes and South China Block at block boundaries, and Jurassic-Early Cretaceous intracontinental orogeny (Yanshanian Orogeny). The Early Mesozoic tectonic evolution of the NCB is expressed by a complicated structural feature in the NCB with multiphase deformations that timing and kinematics are crucial to decipher the geodynamics of the NCB. Particularly, Early Mesozoic extensional tectonics in North China remains ambiguous due to sporadic geological records. To understand multiphase evolution of the NCB, it is crucial to clarify Early Mesozoic extensional tectonics and its relationship to the dynamics of plate subduction/collision along active boundaries. Indeed, due to rare geological records, it is difficult to recognize the regional tectonic

framework from few small remnant basins. In this thesis, through the multidisciplinary studies of three plutons, the author provides some arguments for the Early Mesozoic extensional episodes. The structural study of plutons is an effective and practical way to unravel regional tectonic setting coeval with the emplacement process (e.g., Bouchez & Gleizes, 1995; Bouchez, et al., 1997; Sant'Ovaia et al., 2000; De Saint Blanquat et al., 2011; Lin et al., 2013). However, there is not necessary and unique correlation between emplacement mechanism with tectonic setting (i.e. compressive, extensive, strike-slip). Moreover, the link with geodynamic context (i.e. plate convergence, plate divergence, intraplate) is not directly corresponding. Thus, to provide reliable arguments for the Early Mesozoic extensional tectonics, more multidisciplinary studies are needed, such as structural reconstruction of basins and investigations on the magmatic plutons and their adjacent areas.

References

Améglio, L., & Vigneresse, J. L. (1999). Geophysical imaging of the shape of granitic intrusions at depth: a review. Geological Society, London, Special Publications, 168(1), 39–54. https://doi.org/10.1144/GSL.SP.1999.168.01.04

Archanjo, C. J., Launeau, P., & Bouchez, J. L. (1994). Magnetic fabrics vs. magnetite and biotite shape fabrics of the magnetite-bearing granite pluton of Gameleiras (Northeast Brazil). Physics of the Earth and Planetary Interiors, 89(1–2), 63–75. https://doi.org/10.1016/0031- 9201(94)02997-PBerzina, A. P., Berzina, A. N., & Gimon, V. O. (2014). Geochemical and Sr–Pb–Nd isotopic characteristics of the Shakhtama porphyry Mo–Cu system (Eastern Transbaikalia, Russia). Journal of Asian Earth Sciences, 79, 655-665.

Benn, K., Paterson, S. R., Lund, S. P., Pignotta, G. S., & Kruse, S. (2001). Magmatic fabrics in plutons as markers of regional strains and plate kinematics: Example of the Cretaceous Mt. Stuart pluton. Physics and Chemistry of the Earth Part A Solid Earth and Geodesy, 26(4–5), 343–354, https://doi.org/10.1016/S1464-1895(01) 00064-3

Bonvalot, S., Balmino, G., Briais, A., Kuhn, M., Peyrefitte, A., Vales, N., Biancale, R., et al. (2012). World gravity map. (1:50000000 map), BGI-CGMWCNES-IRD, Paris.

Borradaile, G. J., & Henry, B. (1997). Tectonic applications of magnetic susceptibility and its anisotropy. Earth-Science Reviews, 42(1-2), 49-93. https://doi.org/10.1016/S0012-8252(96)00044-X

Bouchez, J. L. (2000). Anisotropie de susceptibilité magnétique et fabrique des granites (Magnetic susceptibility anisotropy and fabrics in granites). Comptes Rendus de l'Académie des Sciences Paris, 330, 1–14Bouchez, J.L., & Gleizes, G. (1995). Two-stage deformation of the Mount-Louis-Andorra granite pluton (Variscan Pyrenees) inferred from magnetic susceptibility anisotropy. Journal of the Geological Society 152 (4), 669–679. https://doi.org/10.1144/gsjgs.152.4.0669

Bouchez, J. L., & Gleizes, G. (1995). Two-stage deformation of the Mount-Louis-Andorra granite pluton (Variscan Pyrenees) inferred from magnetic susceptibility anisotropy. Journal of the Geological Society, 152(4), 669–679. https://doi.org/10.1144/gsjgs.152.4.0669

Bouchez, J. L., Hutton, D., & Stephens, W. E. (1997). Granite is Never Isotropic: An Introduction to AMS Studies of Granitic Rocks. Granite: From Segregation of Melt to Emplacement Fabrics (pp. 95–112). Paris: Springer Science & Business Media. https://doi.org/10.1007/978-94-017-1717-5_6

Brown, E., & Mcclelland, W. C. (2000). Pluton emplacement by sheeting and vertical ballooning in part of the southeast coast plutonic complex, British Columbia. Geological Society of America Bulletin, 112(5), 708–719. https://doi.org/10.1130/0016-7606(2000)112<0708:PEBSAV>2.3.CO;2

Castro, A. (1987). On granitoid emplacement and related structures: A review. Geologische Rundschau, 76(1), 101–124, https://doi:10.1007/BF01820576

Chen, A. (1998). Geometric and kinematic evolution of basement-cored structures: intraplate orogenesis within the Yanshan Orogen, northern China: Tectonophysics, v. 292, no. 1, p. 17-42.

Chen, B., Jahn, B. M., & Tian, W. (2009). Evolution of the Solonker suture zone: Constraints from zircon U–Pb ages, Hf isotopic ratios and whole-rock Nd–Sr isotope compositions of subduction- and collision-related magmas and forearc sediments. Journal of Asian Earth Sciences, 34(3), 245–257. https://doi.org/10.1016/j.jseaes.2008.05.007

Chen, B., Jahn, B. M., Wilde, S., & Xu, B. (2000). Two contrasting Paleozoic magmatic belts in northern Inner Mongolia, China: Petrogenesis and tectonic implications. Tectonophysics, 328(1), 157–182. https://doi.org/10.1016/S0040-1951(00)00182-7

Cogné, J. P., Kravchinsky, V. A., Halim, N., & Hankard, F. (2005). Late Jurassic-Early Cretaceous closure of the Mongol-Okhotsk Ocean demonstrated by new Mesozoic palaeomagnetic results from the Trans-Baikal area (SE Siberia). Geophysical Journal International, 163(2), 813-832.

Cope, T. D., Shultz, M. R., & Graham, S. A. (2007). Detrital record of Mesozoic shortening in the Yanshan belt, NE China: testing structural interpretations with basin analysis. Basin Research, 19(2), 253-272.

Cruden, A. R., Tobisch, O. T., & Launeau, P. (1999). Magnetic fabric evidence for conduit-fed emplacement of a tabular intrusion: Dinkey Creek Pluton, central Sierra Nevada batholith, California. Journal of Geophysical Research: Solid Earth, 104(B5), 10511–10530. doi:10.1029/1998jb900093

Cui, F. H. Petrogenesis of Mesozoic granitoids and crustal evolution in Xingcheng area, western Liaoning Province. Ph. D Thesis, Jilin University, 2015, pp. 1-152.

Daoudene, Y., Ruffet, G., Cocherie, A., Ledru, P., & Gapais, D. (2013). Timing of exhumation of the Ereendavaa metamorphic core complex (north-eastern Mongolia)–U–Pb and $^{40}Ar/^{39}Ar$ constraints. Journal of Asian Earth Sciences, 62, 98-116.

Darby, B.J., Davis, G.A., & Yadong Z. (2001). Structural evolution of the southwestern Daqing Shan,

Yinshan belt, Inner Mongolia, China, in Hendrix, M.S., and Davis, G.A., eds., Paleozoic and Mesozoic tectonic evolution of central Asia: From continental assembly to intracontinental deformation: Boulder, Colorado, Geological Society of America Memoir 194, 199–214.

Darby, B. J., & Ritts, B. D. (2002). Mesozoic contractional deformation in the middle of the Asian tectonic collage: the intraplate Western Ordos fold–thrust belt, China. Earth and Planetary Science Letters, 205(1-2), 13-24.

Davis, G. A. (2003). The Yanshan belt of North China: tectonics, adakitic magmatism, and crustal evolution. Earth Science Frontiers, 10(4), 373-384.

Davis, G.A., Meng, J.F., & Cao, W.R. (2009). Triassic and Jurassic tectonics in the eastern Yanshan belt, North China: insights from the controversial Dengzhangzi Formation and its neighboring units. Earth Science Frontiers 16 (3), 69–86. https://doi.org/10.1016/S1872-5791(08)60090-1

Davis, G.A., Wang, C., Zheng, Y., Zhang, J., Zhang, C., & Gehrels, G.E. (1998). The enigmatic Yinshan fold-and-thrust belt of northern China: new views on its intraplate contractional styles. Geology, 26, 43–46.

Davis, G.A., Xu, B., Zheng, Y.D., & Zhang, W.J. (2004). Indosinian extension in the Solonker suture zone: the Sonid Zuoqi metamorphiccore complex, Inner Mongolia, China. Earth Science Frontiers 11 (3), 135–144. https://doi.org/ 10.1007/BF02873097

Davis, G.A., Zheng, Y.D., & Wang, C. (2001). Mesozoic tectonic evolution of the Yanshan fold and thrust belt, with emphasis on Hebei and Liaoning provinces, northern China. In: Hendrix, M.S., Davis, G.A. (Eds.), Paleozoic and Mesozoic tectonic evolution of central Asia: From continental assembly to intracontinental deformation, Boulder, Colorado. Geological Society of America Memoir 194, 171–197.

De Saint Blanquat, M., Horsman, E., Habert, G., Morgan, S., Vanderhaeghe, O., Law, R., & Tikoff, B. (2011). Multiscale magmatic cyclicity, duration of pluton construction, and the paradoxical relationship between tectonism and plutonism in continental arcs. Tectonophysics, 500(1–4), 20–33. https://doi.org/10.1016/j.tecto.2009.12.009

Deng, S. H., & Li, D. L. (1998). New knowledge of Triassic in Liupanshan Basin, Ningxia and its significance. Chinese Science Bulletin, 43, 425-431.

Dong, S., Zhang, Y., Zhang, F., Cui, J., Chen, X., Zhang, S., Miao, L., Li, J., Shi, W., Li, Z., Huang, S., & Li, H. (2015). Late Jurassic–Early Cretaceous continental convergence and intracontinental orogenesis in

East Asia: a synthesis of the Yanshan revolution. Journal of Asian Earth Sciences 114, 750–770. https://doi.org/10.1016/j.jseaes.2015.08.011

Dong, Y., & Santosh, M. (2016). Tectonic architecture and multiple orogeny of the Qinling Orogenic Belt, Central China. Gondwana Research, 29(1), 1-40.

Dong, Y., Zhang, G., Neubauer, F., Liu, X., Genser, J., & Hauzenberger, C. (2011). Tectonic evolution of the Qinling orogen, China: review and synthesis. Journal of Asian Earth Sciences, 41(3), 213-237.

Donskaya, T.V., Gladkochub, D.P., Mazukabzov, A.M., & Ivanov, A.V. (2013). Late Paleozoic–Mesozoic subduction-related magmatism at the southern margin of the Siberian continent and the 150 million-year history of the Mongol-Okhotsk Ocean. Journal of Asian Earth Sciences, 62, 79-97.

Ding, L.X., Ma, C.Q., Li, J.W., Robinson, P.T., Deng, X.D., Zhang, C., & Xu, W.C. (2011). Timing and genesis of the adakitic and shoshonitic intrusions in the Laoniushan complex, southern margin of the North China Craton: implications for post-collisional magmatism associated with the Qinling Orogen. Lithos, 126, 212–232.

Dunlop, D. J. (2002). Theory and application of the day plot (Mrs/Ms versus Hcr/Hc) 1. Theoretical curves and tests using titanomagnetite data. Journal of Geophysical Research, 107(B3), 2056. https://doi.org/10.1029/2001JB000487

Eizenhöfer, P. R., Zhao, G., Zhang, J., & Sun, M. (2014). Final closure of the Paleo-Asian Ocean along the Solonker Suture Zone: Constraints from geochronological and geochemical data of Permian volcanic and sedimentary rocks. Tectonics, 33, 441–463, https://doi.org/10.1002/2013TC003357

Enkin, R. J., Yang, Z., Chen, Y., & Courtillot, V. (1992). Paleomagnetic constraints on the geodynamic history of the major blocks of China from the Permian to the present. Journal of Geophysical Research: Solid Earth, 97(B10), 13953-13989.

Fan, W. M., & Menzies, M. A. (1992). Destruction of aged lower lithosphere and accretion of asthenosphere mantle beneath eastern China. Geotectonica Metallogenia, 16, 171-180.

Faure, M., Lin, W., Shu, L., Sun, Y., & Scharer, U. (1999). Tectonics of the Dabieshan (eastern China) and possible exhumation mechanism of ultra high-pressure rocks. Terra Nova, 11(6), 251-258.

Faure, M., Lin, W., Scharer, U., Shu, L., Sun, Y., & Arnaud, N. (2003). Continental subduction and exhumation of UHP rocks. Structural and geochronological insights from the Dabieshan (East China). Lithos, 70(3), 213-241.

Faure, M., Trap, P., Lin, W., Monié, P., & Bruguier, O. (2007). Polyorogenic evolution of the Paleoproterozoic Trans-North China Belt, new insights from the in Lüliangshan-Hengshan-Wutaishan and Fuping massifs. Episodes Journal of International Geoscience, Seoul National University 30 (2), 95–106.

Faure, M., Lin, W., & Chen, Y. (2012). Is the Jurassic (Yanshanian) intraplate tectonics of North China due to westward indentation of the NCC? Terra Nova 24 (6), 456–466. https://doi.org/10.1111/ter.12002

Fu, Z. B., Zhao, Y., Liu, J. L., Zhang, S. H., & Gao, H. L. (2018). Revisiting of the Yanshanian basins in western and northern Beijing, North China. Journal of Asian Earth Sciences, 163, 90-107.

Gao, S., Rudnick, R. L., Yuan, H. L., Liu, X. M., Liu, Y. S., Xu, W. L., & Ling, W. L., et al. (2004). Recycling lower continental crust in the North China Craton. Nature, 432, 892–897. https://doi.org/10.1038/nature03162

Gleizes, G., Leblanc, D., & Bouchez, J.L. (1997). Variscan granites of the Pyrenees revisited: their role as syntectonic markers of the orogen. Terra Nova, 9, 38–41.

Gong, W., Hu, J., Chen, H., Li, Z., Qu, H., & Yang, Y. (2015). Late Mesozoic tectonic evolution and kinematic mechanisms in the Daqing shan at the northern margin of the North China Craton. Journal of Asian Earth Sciences, 114, 103-114. http://dx.doi.org/10.1016/j.jseaes.2015.07.016

Griffin, W. L., O'Reilly, S. Y., & Ryan, C. G. (1992). Composition and thermal structure of the lithosphere beneath South Africa, Siberia and China: porton microprobe studies. Abstract of the International Symposium on Cenozoic Volcanic Rocks and Deep-seated Xenoliths of China and its Environs. Beijing, 65-66.

Guo, F., Li, H.X., Fan, W.M., Li, J.Y., Zhao, L., Huang, M.W., & Xu W.L. (2015). Early Jurassic subduction of the Paleo-Pacific Ocean in NE China: Petrologic and geochemical evidence from the Tumen mafic intrusive complex. Lithos, 244–245, 46–60.

Guo, Z.X., Yang, Y,T., Zyabrev, S., & Hou, Z.H. (2017). Tectonostratigraphic evolution of the Mohe-Upper Amur Basin reflects the final closure of the Mongol–Okhotsk Ocean in the latest Jurassic–earliest Cretaceous. Journal of Asian Earth Sciences, 145, 495–511.

Griffin, W. L., Zhang A. D., O'Reilly, S. Y., & Ryan, C. G. (1998). Phanerozoic evolution of the lithosphere

beneath the Sino-Korean craton. In Mantle Dynamics and Plate Interactions in East Asia (eds. M. F. J, Flower, S. -L., Chung, C. -H. Lo and T. -Y. Lee). Am. Geophy. Union, Washington, D. C., Geodynamic Series. 27: 107-126.

Hacker, B. R., Ratschbacher, L., Webb, L., & Shuwen, D. (1995). What brought them up? exhuming the dabie shan ultrahigh-pressure rocks. Geology, 23(8).

Hacker, B.R., Ratschbacher, L., Webb, L., McWilliams, M.O., Ireland, T., Calvert, A., Dong, S., Wenk, H., & Chateigner, D. (2000). Exhumation of ultrahigh-pressure continental crust in east central China: Late Triassic-Early Jurassic tectonic unroofing. Journal of Geophysical Research: Solid Earth, 105 (B6), 13339–13364. https://doi.org/10.1029/2000JB900039

Hacker, B. R., Ratschbacher, L., Webb, L., Ireland, T., Walker, D., & Shuwen, D. (1998). U/pb zircon ages constrain the architecture of the ultrahigh-pressure qinling–dabie orogen, china. Earth & Planetary Science Letters, 161(1-4), 0-230.

Hacker, B. R., Wang, X., Eide, E. A., & Ratschbacher, L. (1996). “Qinling-Dabie ultrahigh-pressure collisional orogen”. In The tectonic evolution of Asia, Edited by: Yin, A. and Harrison, T. M. 345–370. Cambridge, UK: Cambridge University Press.

Han, B. F., Kagami, H., & Li, H. M. (2004). Age and Nd–Sr isotopic geochemistry of the Guangtoushan alkaline granite, Hebei Province, China: implications for early Mesozoic crust–mantle interaction in North China Block (in Chinese with English abstract). Acta Petrologica Sinica, 20, 1375–1388.

Han, G.Q., Liu, Y.J., Neubauer, F., Genser, J., Zhao, Y.L., Wen, Q.B., Li, W.M., Wu, L.N., Jiang, X., & Zhao, L.M. (2012). Provenance analysis of Permian sandstones in the central and southern Da Xing'an Mountains, China: Constraints on the evolution of the eastern segment of the Central Asian Orogenic Belt. Tectonophysics 580, 100-113.

Han, R., Ree, J. H., Cho, D. L., Kwon, S. T., & Armstrong, R. (2006). SHRIMP U–Pb zircon ages of pyroclastic rocks in the Bansong Group, Taebaeksan Basin, South Korea and their implication for the Mesozoic tectonics. Gondwana Research, 9(1-2), 106-117.

Hao, W., Zhu, G., & Zhu, R. (2019). Timing of the Yanshan Movement: evidence from the Jingxi Basin in the Yanshan fold-and-thrust belt, eastern China. International Journal of Earth Sciences, 108(6), 1961-1978.

Hao, W., Zhu, R., & Zhu, G. (2020). Jurassic tectonics of the eastern North China Craton: Response to initial

subduction of the Paleo-Pacific Plate. Geological Society of America.

Hargraves, R. B., Johnson, D., & Chan, C. Y. (1991). Distribution anisotropy: the cause of AMS in igneous rocks? Geophysical Research Letters, 18(12), 2193–2196. https://doi.org/10.1029/91GL01777

He, Z., Wang Z., & Ren, J. (1999). A preliminary research on sedimentary features and genetic mechanism of frontal basins before Jurassic large-scale nappe in the northern region of North China (in Chinese). Chinese Journal of Geology, 2, 186-195.

Horsman, E., Morgan, S., de Saint-Blanquat, M., Habert, G., Nugent, A., Hunter, R. A., & Tikoff, B. (2009). Emplacement and assembly of shallow intrusions from multiple magma pulses, Henry Mountains, Utah. Earth and Environmental Science Transactions of the Royal Society of Edinburgh, 100(1-2), 117-132. https://doi.org/10.1017/S1755691009016089

Hu, J., Zhao, Y., Liu, X., & Xu, G. (2010). Early Mesozoic deformations of the eastern Yanshan thrust belt, northern China. International Journal of Earth Sciences, 99(4), 785-800.

Jelinek, V. (1978). Statistical processing of anisotropy of magnetic susceptibility measured on groups of specimens. Studia Geophysica et Geodaetica, 22(1), 50–62. https://doi.org/10.1007/BF01613632

Jelinek, V. (1981). Characterization of the magnetic fabric of rocks. Tectonophysics, 79(3–4), T63–T67. https://doi.org/10.1016/0040-1951(81)90110-4

Jian, P., Liu, D., & Kröner, A. (2010). Evolution of a Permian intraoceanic arc-trench system in the Solonker suture zone, Central Asian Orogenic Belt, China and Mongolia. Lithos, 118, 169–190. https://doi.org/ 10.1016/j.lithos.2010.04.014

Jian, P., Liu, D., Kröner, A., Windley, B. F., Shi, Y., Zhang, F., Shi, G., et al. (2008). Time scale of an Early to Mid-Paleozoic orogenic cycle of the long-lived Central Asian Orogenic Belt, Inner Mongolia of China: implications for continental growth. Lithos, 101, 233–259. https://doi.org/ 10.1016/j.lithos.2007.07.005

Jiang, S. H., Bagas, L., Liu, Y. F., & Zhang, L. L. (2018). Geochronology and petrogenesis of the granites in Malanyu anticline in eastern North China Block. Lithos, 312, 21–37. https://doi.org/10.1016/j.lithos.2018.04.028

Kim, J., Yi, K., Jeong, Y. J., & Cheong, C. S. (2011). Geochronological and geochemical constraints on the petrogenesis of Mesozoic high-K granitoids in the central Korean peninsula. Gondwana Research, 20(2-

3), 608-620.

Kravchinsky, V. A., Cogné, J. P., Harbert, W. P., & Kuzmin, M. I. (2002). Evolution of the Mongol-Okhotsk Ocean as constrained by new palaeomagnetic data from the Mongol-Okhotsk suture zone, Siberia. Geophysical Journal International, 148(1), 34-57.

Li, C., Zhang, C., Cope, T. D., & Lin, Y. (2016). Out-of-sequence thrusting in polycyclic thrust belts: an example from the Mesozoic Yanshan belt, North China Craton. Tectonics 35, 2082–2116. https://doi.org/10.1002/2016TC004187

Li, H., Zhang, H., Qu, H., Cai, X., & Wang, M. (2014). Initiation, the First Stage of the Yanshan (Yenshan) in Western Hills. Constraints from Zircon U–Pb Movement Dating (in Chinese). Geological Review, 60(5), 1026-1042.

Li, J., Dong, S., Cawood, P. A., Zhao, G., Johnston, S. T., Zhang, Y., & Xin, Y. (2018). An Andean-type retro-arc foreland system beneath northwest South China revealed by SINOPROBE profiling. Earth and Planetary Science Letters, 490, 170-179.

Li, J. Y. (2006). Permian geodynamic setting of Northeast China and adjacent regions: closure of the Paleo-Asian Ocean and subduction of the Paleo-Pacific Plate. Journal of Asian Earth Sciences, 26(3), 207–224. https://doi.org/10.1016/j.jseaes.2005.09.001

Li, S., Wilde, S., He, Z., Jiang, X., Liu, R., & Zhao, L. (2014). Triassic sedimentation and postaccretionary crustal evolution along the Solonker suture zone in Inner Mongolia, China. Tectonics, 33(6), 960–981. https://doi.org/10.1002/2013TC003444

Li, S. Z., Kusky, T. M., Zhao, G., Wu, F., Liu, J. Z., & Sun, M., et al. (2007). Mesozoic tectonics in the Eastern Block of the North China Craton: implications for subduction of the Pacific plate beneath the Eurasian plate. Geological Society London Special Publications, 280(1), 171-188.

Li, S.Z., Jahn, B.M., Zhao, S.J., Dai, L.M., Li, X.Y., Suo, Y.H., Guo, L.L., Wang, Y.M., Liu, X.C., Lan, H.Y., Zhou, Z.Z., Zheng, Q.L., & Wang, P.C. (2017). Triassic southeastward subduction of North China Block to South China Block: insights from new geological, geophysical and geochemical data. Earth-Science Reviews, 166, 270-285.

Li, S.Z., Zhao, G.C., Santosh, M., Liu, X., Dai, L.M., Suo, Y.H., Tam, P.Y., Song, M.C., & Wang, P.C. (2012). Paleoproterozoic structural evolution of the southern segment of the Jiao-Liao-Ji Belt, North China Craton.

Precambrian Research, 200-203, 59-73. https://doi.org/10.1016/j.precamres.2012.01.007

Li, S.Z., Zhao, S.J., Liu, X., Cao, H.H., Yu, S., Li, X.Y., Somerville, I., Yu, S.Y., Suo, Y.H., 2018. Closure of the Proto-Tethys Ocean and Early Paleozoic amalgamation of microcontinental blocks in East Asia. Earth-Science Reviews, 186, 37-75.Li, Z. H., Qu, H. J., & Gong, W. B. (2015). Late Mesozoic basin development and tectonic setting of the northern North China Craton. Journal of Asian Earth Sciences, 114, 115-139.

Li, X.H., Liu, Y., Li, Q.L., Guo, C.H., & Chamberlain, K.R. (2009). Precise determination of Phanerozoic zircon Pb/Pb age by multicollector SIMS without external standardization. Geochemistry Geophysics Geosystems, 10, Q04010. http://dx.doi.org/10.1029/2009GC002400.

Li, Z. H., Dong, S. W., & Qu, H. J. (2014). Timing of the initiation of the Jurassic Yanshan movement on the North China Craton: evidence from sedimentary cycles, heavy minerals, geochemistry, and zircon U–Pb geochronology. International Geology Review, 56(3), 288-312. https://doi.org/10.1080/00206814.2013.855013

Li, Z. H., Qu, H. J., & Gong, W. B. (2015). Late Mesozoic basin development and tectonic setting of the northern North China Craton. Journal of Asian Earth Sciences, 114, 115-139. https://doi.org/10.1016/j.jseaes.2015.05.029

Li, Z.X., & Li, X.H. (2007). Formation of the 1300-km-wide intracontinental orogen and postorogenic magmatic province in Mesozoic South China: a flat-slab subduction model. Geology, 35(2), 179-182.

Lin, S. Z., Zhu, G., Zhao, T., Song, L., & Liu, B. (2014) Structural characteristics and formation mechanism of the Kalaqin metamorphic core complex in the Yanshan area, China (in Chinese). Chinese Science Bulletin, 59, 3174–3189, https://doi.org/10.1360/N972014-00100

Lin, W., Charles, N., Chen, K., Chen, Y., Faure, M., Wu, L., & Wang, F. (2013). Late Mesozoic compressional to extensional tectonics in theYiwulüshan massif, NE China and its bearing on the evolution of the Yinshan–Yanshan orogenic belt part II: Anisotropy of magnetic susceptibility and gravity modeling. Gondwana Research, 23 (1) 78–94. https://doi.org/10.1016/j.gr.2012.02.012

Lin, W., Faure, M., Nomade, S., Shang, Q., & Renne, P. R. (2008). Permian–Triassic amalgamation of Asia: insights from Northeast China sutures and their place in the final collision of North China and Siberia.

Comptes Rendus Geoscience, 340(2-3), 190-201.

Lin, W., Shi, Y. H., Wang, Q. C. (2009). Exhumation tectonics of the HP-UHP orogenic belt in Eastern China: new structural–petrological insights from the Tongcheng massif, Eastern Dabieshan. Lithos, 109, 285–303.

Lin, W., Wang, Q. C., Faure, M., Arnaud, N. (2005). Tectonic evolution of Dabie orogen: in the view from polyphase deformation of the Beihuaiyang metamorphic zone. Science China Series D, 48(7), 886-899.

Lin, W., & Wei, W. (2018). Late Mesozoic extensional tectonics in the North China Craton and its adjacent regions: a review and synthesis: International Geology Review, 1–29, https://doi.org/10.1080/00206814.2018.1477073.

Lin, Y., Zhang, C., Li, C., & Deng, H. (2020). From dextral contraction to sinistral extension of intracontinental transform structures in the Yanshan and northern Taihang Mountain belts during Early Cretaceous: Implications to the destruction of the North China Craton. Journal of Asian Earth Sciences, 189, 104139. https://doi.org/10.1016/j.jseaes.2019.104139

Liu, H., Martelet, G., Wang, B., Erdmann, S., Chen, Y., Faure, M., Huang, F. et al. (2018). Incremental emplacement of the Late Jurassic midcrustal, lopolith-like Qitianling pluton, South China, revealed by AMS and Bouguer gravity data. Journal of Geophysical Research: Solid Earth, 123. https://doi.org/10.1029/2018JB015761

Liu, J., Zhao, Y., Liu, X., Wang, Y., & Liu, X. (2012). Rapid exhumation of basement rocks along the northern margin of the North China craton in the early Jurassic: Evidence from the Xiabancheng Basin, Yanshan Tectonic Belt. Basin Research, 24(5), 544-558.

Liu, S. F., Lin, C. F., Liu, X. B., & Zhuang, Q. T. (2018). Syn-tectonic sedimentation and its linkage to fold-thrusting in the region of Zhangjiakou, North Hebei, China. Science China Earth Sciences, 61(6), 681-710. https://doi.org/10.1007/s11430-017-9175-3

Liu, Y.J., Li, W.M., Feng, Z.Q., Wen, Q.B., Neubauer, F., & Liang, C.Y. (2017). A review of the Paleozoic tectonics in the eastern part of Central Asian Orogenic Belt. Gondwana Research, 43, 123–148. https://doi.org/10.1016/j.gr.2016.03.013

Luo, Z. K., Miao, L. C., Guan, K., Qiu, Y. S., Qiu, Y. M., Mcnaughton, N. J., & Groves, D. I. (2003). SHRIMP U-Pb zircon dating of the Dushan granitic pluton and related granite-porphyry dyke, eastern Hebei province,

China, and their geological significance. Geochimica, 32(2), 173–180.

Ma, Y.S., Zeng, Q.L., Song, B., Du, J.J., Yang, F.Q., & Zhao, Y. (2007). SHRIMP U–Pb dating of zircon from Panshan granitoid pluton in Yanshan orogenic belt and its tectonic implications (in Chinese with English abstract). Acta Petrologica Sinica, 23, 547–556.

Martín-Hernández, F., & Hirt, A. M. (2003). Paramagnetic anisotropy of magnetic susceptibility in biotite, muscovite and chlorite single crystals. Tectonophysics, 367(1–2), 13–28. https://doi.org/10.1016/S0040-1951(03)00127-6

Mattauer, M., Matte, P., Malavieille, J., Tapponnier, P., Maluski, H., Qin, X.Z., Lu, Y.L., & Tang, Y.Q. (1985). Tectonics of the Qinling belt: build-up and evolution of eastern Asia. Nature, 317 (6037), 496–500. https://doi.org/10.1038/317496a0

McNulty, B. A., Tobisch, O. T., Cruden, A. R., & Gilder, S. (2000). Multistage emplacement of the mount givens pluton, central Sierra Nevada batholith, California. Geological Society of America Bulletin, 112(1), 119–135. https://doi.org/10.1130/0016-7606(2000)1122.3.CO;2

Menzies, M. A., Fan, W. M. & Zhang, M. (1993). Palaeozoic and Cenozoic lithoprobe and the loss of >120km of Archean lithosphere, Sino-Korean craton, China. In Magmatic Processes and Plate Tectonic (eds. H. M. Prichard, T. Alabaster, N. B. W. Harris and C. R. Neary). Geological Society Special Publication. 76, 71-81.

Meng, Q. R., Wei, H. H., Wu, G. L., & Duan, L. (2014). Early Mesozoic tectonic settings of the northern North China craton. Tectonophysics, 611, 155-166.

Meng, Q. R., Wu, G. L., Fan, L. G., & Wei, H. H. (2019). Tectonic evolution of early Mesozoic sedimentary basins in the North China block. Earth Science Review, 190, 416–438. https://doi.org/10.1016/j.earscirev.2018.12.003

Meng, Q.R., Wu, G.L., Fan, L.G., Wei, H.H., & Wang, E. (2020). Late Triassic uplift, magmatism and extension of the northern North China block: Mantle signatures in the surface. Earth and Planetary Science Letters, 547, 116451. doi:10.1016/j.epsl.2020.116451

Meng, Q.R., & Zhang, G.W. (1999). Timing of collision of the North and South China blocks: controversy and reconciliation. Geology 27 (2), 123–126. https://doi.org/10.1130/0091-7613(1999)027<0123:TOCOTN>2.3.CO;2

Metelkin, D. V., Vernikovsky, V. A., Kazansky, A. Y., & Wingate, M. T. (2010). Late Mesozoic tectonics of Central Asia based on paleomagnetic evidence. Gondwana Research, 18(2-3), 400-419.

Okay, A. I., Xu, S., & Sengor, A. C. (1989). Coesite from the Dabie Shan eclogites, central China. European Journal of Mineralogy, 1(4), 595-598.

Parfenov, L. M., Popeko, L. I., & Tomurtogoo, O. (2001). Problems of tectonics of the Mongol-Okhotsk orogenic belt. Russian Journal of Pacific Geology, 16(5), 797-830.

Passchier, C. W., & Trouw, R. A. J. (2005). Microtectonics. Berlin-Heidelberg-New York: Springer.

Paterson, S. R., & Vernon, R. H. (1995). Bursting the bubble of ballooning plutons: A return to nested diapirs emplaced by multiple processes. Geological Society of America Bulletin, 107(11), 1356–1380. https://doi.org/10.1130/0016-7606(1995)107<1356:BTBOBP>2.3.CO;2

Paterson, S. R., Vernon, R. H., & Tobisch, O. T. (1989). A review of criteria for the identification of magmatic and tectonic foliations in granitoids. Journal of Structural Geology, 11(3), 349–363.

Pei, J., Sun, Z., Liu, J., Liu, J., Wang, X., Yang, Z., Zhao, Y., & Li, H. (2011). A paleomagnetic study from the Late Jurassic volcanics (155 Ma), North China: implications for the width of Mongol–Okhotsk Ocean. Tectonophysics, 510(3-4), 370-380.

Qi, G. W., Zhang, J. J., & Wang, M. (2015). Mesozoic tectonic setting of rift basins in eastern North China and implications for destruction of the North China Craton. Journal of Asian Earth Sciences, 111, 414-427.

Qiu, H., Lin, W., Faure, M., Chen, Y., Meng, L., Zeng, J., Ren, Z., & Li, Q. (2020). Late Triassic extensional tectonics in the northern North China Craton, insights from a multidisciplinary study of the Wangtufang pluton. Journal of Asian Earth Sciences, 200, 104462. 10.1016/j.jseaes.2020.104462

Ratschbacher, L., Hacker, B. R., Calvert, A., Webb, L. E., & Hu, J. (2003). Tectonics of the Qinling (Central China): tectonostratigraphy, geochronology, and deformation history. Tectonophysics, 1-53.

Ratschbacher, L., Franz, L., Enkelmann, E., Jonckheere, R., Porschke, A., Hacker, B. R. & Zhang, Y. (2006). The Sino-Korean-Yangtze suture, the Huwan detachment, and the Paleozoic-Tertiary exhumation of (ultra) high-pressure rocks along the Tongbai-Xinxian-Dabie Mountains. Special Papers-Geological Society of America, 403, 45.

Ritts, B. D., Darby, B. J., & Cope, T. (2001). Early Jurassic extensional basin formation in the Daqing Shan segment of the Yinshan belt, northern North China Block, Inner Mongolia. Tectonophysics, 339(3-4), 239-258.

Ritts, B. D., Hanson, A. D., Darby, B. J., Nanson, L., & Berry, A. (2004). Sedimentary record of Triassic intraplate extension in North China: evidence from the nonmarine NW Ordos Basin, Helan Shan and Zhuozi Shan. Tectonophysics, 386(3-4), 177-202.

Sagong, H., Kwon, S.T., & Ree, J.H. (2005). Mesozoic episodic magmatism in South Korea and its tectonic implication. Tectonics, 24.

Sant'Ovaia, H., Bouchez, J.L., Noronha, F., Leblanc, D., & Vigneresse, J.L. (2000). Composite-laccolith emplacement of the post-tectonic Vila Pouca de Aguiar granite pluton (northern Portugal): a combined AMS and gravity study. Transactions of the Royal Society of Edinburgh: Earth Sciences, 91 (1-2), 123-137.

Şengör, A. M. C., Natal'In, B. A., & Burtman, V. S. (1993). Evolution of the Altaid tectonic collage and Palaeozoic crustal growth in Eurasia. Nature, 364(6435), 299-307.

Şengör, A. M. C., & Natal'In, B. A. (1996). Paleotectonics of Asia: fragments of a synthesis, in: Yin A, Harrison M Eds, The Tectonic Evolution of Asia. Cambridge University Press, Cambridge, 486-640.

Shang, Q. (2004). Occurrences of Permian radiolarians in central and eastern Nei Mongol (Inner Mongolia) and their geological significance to the northern China Orogen. Chinese Science Bulletin, 49(24), 2613-2619.

Sun, D. Y., Gou, J., Wang, T. H., Ren, Y. S., Liu, Y. J., Guo, H. Y., & Hu, Z. C. (2013). Geochronological and geochemical constraints on the Erguna massif basement, NE China–subduction history of the Mongol–Okhotsk oceanic crust. International Geology Review, 55(14), 1801-1816.

Talbot, J. Y., Martelet, G., Courrioux, G., Chen, Y., & Faure, M. (2004). Emplacement in an extensional setting of the Mont Lozère–Borne granitic complex (SE France) inferred from comprehensive AMS, structural and gravity studies. Journal of Structural Geology, 26(1), 11–28. https://doi.org/10.1016/S0191-8141(03)00083-X

Tarling, D. H., & Hrouda, F. (1993). Magnetic Anisotropy of Rocks. London, U. K.: Chapman and Hall.

Tomurtogoo, O., Windley, B. F., Kröner, A., Badarch, G., & Liu, D. Y. (2005). Zircon age and occurrence of the Adaatsag ophiolite and Muron shear zone, central Mongolia: constraints on the evolution of the Mongol–Okhotsk ocean, suture and orogen. Journal of the Geological Society, 162(1), 125-134.

Trap, P., Faure, M., Lin, W., Le Breton, N., Monié, P., 2012. Paleoproterozoic tectonic evolution of the Trans-North China Orogen: toward a comprehensive model. Precambrian Research 222, 191–211. https://doi.org/10.1016/j.precamres.2011.09.008

Vander Voo, R., Spakman, W., & Bijwaard, H. (1999). Mesozoic subducted slabs under Siberia. Nature, 397(6716), 246-249.

Vigneresse, J. L. (1990). Use and misuse of geophysical data to determine the shape at depth of granitic intrusions. Geological Journal, 25(3–4), 249–260. https://doi.org/10.1002/gj.3350250308

Wang, F., Xu, W.L., Xing, K.C., Wang, Y.N., Zhang, H.H., Wu, W., Sun, C.Y., & Ge, W.C. (2019). Final closure of the Paleo–Asian Ocean and Onset of Subduction of Paleo–Pacific Ocean: Constraints from Early Mesozoic magmatism in Central southern Jilin Province, NE China. Journal of Geophysical Research: Solid Earth, 124, 2601–2622.

Wang, Q., & Liu, X. (1986). Paleoplate tectonics between Cathaysia and Angaraland in Inner Mongolia of China. Tectonics, 5, 1073–1088.

Wang, Q. C., Liu, X. H., Maruyama, S., & Cong, B. L. (1995). Top boundary of the Dabie UHPM rocks, central China. Journal of Southeast Asian Earth Sciences, 11(4), 295-300.

Wang, T., Zheng, Y., Zhang, J., Zeng, L., Donskaya, T., Guo, L., & Li, J. (2011). Pattern and kinematic polarity of late Mesozoic extension in continental NE Asia: Perspectives from metamorphic core complexes. Tectonics, 30(6), TC6007, https://doi.org/10.1029/2011TC002896

Wang, X., Liou, J. G., & Mao, H. K. (1989). Coesite-bearing eclogite from the Dabie Mountains in central China. Geology, 17(12), 1085-1088.

Wang, Y., Dong, S., Shi, W., Chen, X., & Jia, L. (2017). The Jurassic structural evolution of the western Daqingshan area, eastern Yinshan belt, North China. International Geology Review, 59(15), 1885-1907.

Wang, Y., Dong, S., Shi, W., Chen, X., & Li, J. (2016). An Analysis of Late Mesozoic Tectonic Evolution Process in Northern China: Based on Basin Sedimentary Records in Northern Taihang Mountains (in

Chinese). Acta Geoscientica Sinica, 37(1), 35-45.

Wang, Y., Zhou, L., & Zhao, L. (2013). Cratonic reactivation and orogeny: an example from the northern margin of the North China Craton. Gondwana Research, 24(3–4), 1203–1222. https://doi.org/10.1016/j.gr.2013.02.011

Windley, B.F., Alexeiev, D., Xiao, W., Kröner, A., & Badarch, G. (2007). Tectonic models for accretion of the Central Asian Orogenic Belt. Journal of the Geological Society 164 (1), 31–47. https://doi.org/10.1144/0016-76492006-022

Wong, W. H. (1927). Crustal movements and igneous activities in Eastern China since Mesozoic time. Geological Society of China Bulletin, 6, 9–37.

Wong, W. H. (1928). Study on geological structure near Beipiao and Rehe (in Chinese). Geological report, 11, 1-23.

Wong, W.H. (1929). The Mesozoic orogenic movement in eastern China. Geological Society of China Bulletin, 8, 33–44.

Wu, F. Y., Sun, D. Y., Ge, W. C., Zhang, Y. B., Grant, M. L., Wilde, S. A., & Jahn, B. M. (2011). Geochronology of the Phanerozoic granitoids in northeastern China. Journal of Asian Earth Sciences, 41(1), 1-30.

Wu, F. Y., Yang, J. H., Wilde, S. A., & Zhang, X. O. (2005). Geochronology, petrogenesis and tectonic implications of Jurassic granites in the Liaodong Peninsula, NE China. Chemical geology, 221(1-2), 127-156.

Wu, F. Y., Yang, J. H., Xu, Y. G., Wilde, S. A., & Walker, R. J. (2019). Destruction of the North China Craton in the Mesozoic. Annual Review of Earth and Planetary Sciences, 47(1), 73–95. https://doi.org/10.1146/annurev-earth-053018-060342

Wu, F. Y., Yang, J. H., Zhang, Y. B., & Liu, X. M. (2006). Emplacement ages of the Mesozoic granites in southeastern part of the Western Liaoning Province. Acta Petrologica Sinica, 22(2), 315–325.

Wu, F.Y., Zhao, G.C., Sun, D.Y., Wilde, S.A., & Zhang, J.H. (2007). The Hulan Group: its role in the evolution of the Central Asian Orogenic Belt of NE China. Journal of Asian Earth Sciences, 30, 542–556.

Wu, Y. B., & Zheng, Y. F. (2013). Tectonic evolution of a composite collision orogen: an overview on the Qinling–Tongbai–Hong'an–Dabie–Sulu orogenic belt in central China. Gondwana Research, 23(4),

1402-1428.

Xiao, W.J., & Kusky, T. (2009). Geodynamic processes and metallogenesis of the Central Asian and related orogenic belts: introduction. Gondwana Research. 16, 167–169.

Xiao, W. J., Windley, B., Hao, J., & Zhai, M. G. (2003). Accretion leading to collision and the Permian Solonker suture, Inner Mongolia, China: termination of the Central Asian Orogenic Belt. Tectonics, 22, 1069–1089. http://doi.org/10.1029/ 2002TC001484.

Xiao, W., Windley, B.F., Sun, S., Li, J., Huang, B., Han, C., Yuan, C., Sun, M., & Chen, H. (2015). A tale of amalgamation of three Permo-Triassic collage systems in Central Asia: oroclines, sutures, and terminal accretion. Annual Review of Earth and Planetary Sciences 43 (1), 477–501. https://doi.org/10.1146/annurev-earth-060614-105254

Xiong, L., Wei, J., Shi, W., Fu, L., Li, H., Zhou, H., & Chen, M. (2017). Geochronology, petrology and geochemistry of the Mesozoic Dashizhu granites and lamprophyre dykes in eastern Hebei – western Liaoning: implications for lithospheric evolution beneath the North China Craton. Geological Magazine, 1–24. https://doi.org/ 10.1017/S0016756817000437

Xu, B., Charvet, J., Chen, Y., Zhao, P., & Shi, G. (2013). Middle Paleozoic convergent orogenic belts in western Inner Mongolia (China): framework, kinematics, geochronology and implications for tectonic evolution of the Central Asian Orogenic Belt. Gondwana Research, 23(4), 1342–1364. https://doi.org/10.1016/j.gr.2012.05.015Xu, B., Charvet, J., Chen, Y., Zhao, P., & Shi, G. (2013). Middle Paleozoic convergent orogenic belts in western Inner Mongolia (China): framework, kinematics, geochronology and implications for tectonic evolution of the Central Asian Orogenic Belt. Gondwana Research, 23 (4), 1342–1364. https://doi.org/10.1016/j.gr.2012.05.015

Xu, B., & Chen, B. (1997). Framework and evolution of the middle Paleozoic orogenic belt between Siberian and North China Plates in northern Inner Mongolia. Science in China: Series D, 40, 463–469.

Xu, C., Zhang, L., Shi, H., Brix, M. R., Huhma, H., Chen, L., ... & Zhou, Z. (2017). Tracing an early Jurassic magmatic arc from South to East China Seas. Tectonics, 36(3), 466-492.

Xu, W. L., Ji, W. Q., Pei, F. P., Meng, E., Yu, Y., Yang, D. B., & Zhang, X. (2009). Triassic volcanism in eastern Heilongjiang and Jilin provinces, NE China: chronology, geochemistry, and tectonic implications. Journal of Asian Earth Sciences, 34(3), 392-402.

Xu, X., Jiang, N., Fan, W., Hu, J., & Zong, K. (2016). Petrogenesis and geological implications for the Mesozoic granites in Qinglong area, eastern Hebei Province. Acta Petrologica Sinica, 32(1), 212–232.

Xu, Z., Lu, Y., Tang, Y., Mattauer, M., Matte, P., Malavieille, J., Tapponnier, P., & Maluski, H. (1986). Deformation characteristics and Tectonic evolution of the eastern Qinling orogenic belt. Acta Geologica Sinica, 60(3), 23–35. https://doi.org/10.1111/j.1755-6724.1986.mp60003003.x

Xu, Z.B., & Wu, Y.Z. (1989). The characteristics of Mesozoic rift in Western Hill of Beijing [in Chinese]. Coal Geology of China, 1(3), 1-8.

Xu, Z.C., & Wang, Z.M. (1983). Geotectonic features of Yanshan area in Hebei province [in Chinese]. Regional Geology of China, 3, 39–55.

Yang, H., Ge, W.C., Zhao, G.C., Yu, J.J., & Zhang, Y.L. (2015). Early Permian-Late Triassic granitic magmatism in the Jiamusi–Khanka Massif, eastern segment of the Central Asian Orogenic Belt and its implications. Gondwana Research, 27(4), 1509–1533.

Yang, J. H., O'Reilly, S. Y., Walker, R. J., Griffin, W. L., Wu, F. Y., Zhang, M., & Pearson, N. (2010). Diachronous decratonization of the Sino-Korean craton: geochemistry of mantle xenoliths from North Korea. Geology, 38, 799–802. 10.1130/G30944.1

Yang, J. H., Sun, J. F., Zhang, M., Wu, F. Y., & Wilde, S. A. (2012). Petrogenesis of silica-saturated and silica-undersaturated syenites in the northern North China Craton related to post-collisional and intraplate extension. Chemical Geology, 328(11), 149–167. https://doi.org/10.1016/j.chemgeo.2011.09.011Zhao, G.C., Wilde, S.A., Cawood, P.A., & Lu, L.Z. (1998). Thermal evolution of the Archean basement rocks from the eastern part of the North China Craton and its bearing on tectonic setting. International Geology Review, 40, 706–721.

Yang, J., Wu, F., Wilde, S.A., Xie, L.W., Yang Y.H., & Liu X.M. (2007). Tracing magma mixing in granite genesis: in situ U–Pb dating and Hf-isotope analysis of zircons. Contrib Mineral Petrol 153, 177–190. https://doi.org/10.1007/s00410-006-0139-7

Yang, M., Li, L., Zhou, J., Jia, H., Sun, X., Qu, X., ... & Ding, C. (2015). Mesozoic structural evolution of the Hangjinqi area in the northern Ordos Basin, North China. Marine and Petroleum Geology, 66, 695-710.

Yarmolyuk, V. V., Kovalenko, V. I., Vorontsov, A. A., Ivanov, V. G., Baikin, D. N., & Sandimirova, G. P.

(2000). Stages of bimodal and alkaline granite magmatism in the western Transbaikal region: geochronological data on rocks from the Tugnui Depression. In Doklady Earth Sciences, . 373, 811-815.

Ye, H., Zhang, S. H., Zhao, Y., & Wu, F. (2014). Petrogenesis and emplacement deformation of the Late Triassic Dushan composite pluton in the Yanshan fold and thrust belt: Implications for the tectonic settings of the northern margin of the North China Craton during the Early Mesozoic (in Chinese with English abstract). Earth Science frontiers, 21 (4), 275–292.

Yin, A., & Nie, S. (1996). A Phanerozoic palinspastic reconstruction of China and its neighboring regions. In: Yin, A., Harrison, T.A. (Eds.), The Tectonic Evolution of Asia. Cambridge University Press, New York, 442–485.

Yuan, E.S., & Paterson, S.R. (1993). Evaluating flow from structures in plutons. GSA Abstract with Progress, 25, 305.

Žák, J., Kratinová, Z., Trubač, J., Janoušek, V., Sláma, J., & Mrlina, J. (2011). Structure, emplacement, and tectonic setting of Late Devonian granitoid plutons in the Teplá–Barrandian unit, Bohemian Massif. International Journal of Earth Sciences, 100(7), 1477–1495. https://doi.org/10.1007/s00531-010-0565-7

Žák, J., Verner, K., Holub, F. V., Kabele, P., Chlupáčová, M., & Halodová, P. (2012). Magmatic to solid state fabrics in syntectonic granitoids recording early Carboniferous orogenic collapse in the Bohemian Massif. Journal of Structural Geology, 36, 27–42. https://doi.org/10.1016/j.jsg.2011.12.011

Žák, J., Verner, K., Sláma, J., Kachlík, V., & Chlupáčová, M. (2013). Multistage magma emplacement and progressive strain accumulation in the shallow-level Krkonoše-Jizera plutonic complex, Bohemian Massif. Tectonics, 32(5), 1493–1512. https://doi.org/10.1002/tect.20088

Zak, J., Verner, K., & Tycova, P. (2008). Multiple magmatic fabrics in plutons: an overlooked tool for exploring interactions between magmatic processes and regional deformation? Geological Magazine, 145(4), 537–551. https://doi.org/10.1017/S0016756808004573

Zhang, A., Liu, S., Lin, C., & Zhang, B. (2019). Timing of deposition in the Dengzhangzi and Guojiadian Basins of the Yanshan fold-thrust belt, North China. International Geology Review, 1-22.

Zhang, C., Wang, G., Wang, G., Wu, Z., Zhang, L., & Sun, W. (2002). Thrust tectonics in the eastern segment of the intraplate Yanshan Orogenic belt, western Liaoning, North China (in Chinese). Acta Geologica

Sinica, 76(1), 64-76.

Zhang, C. H., Wu, G. G., Xu, D. B., Wang, G. H., & Sun, W. H. (2004). Mesozoic tectonic framework of the intraplate and evolution in the central segment Yanshan orogenic belt (in Chinese). Geological Bulletin of China, 23(9–10), 864-875.

Zhang, J., Qu, J., Zhang, B., Zhao, H., Niu, P., Zhao, S., Hui, J., Yun, L., Nie, F., & Wang, Y. (2020). Mesozoic intraplate deformation of the central North China Craton: Mechanism and tectonic setting. Journal of Asian Earth Sciences, 192, 104269. https://doi.org/10.1016/j.jseaes.2020.104269

Zhang, Y., Shi, W., & Dong, S. (2011). Changes of Late Mesozoic tectonic regimes around the Ordos Basin (North China) and their geodynamic implications. Acta Geologica Sinica, 85(6), 1254-1276.

Zhang, Y., Shi, W., Dong, S., Wang, T., & Yang, Q. (2020). Jurassic intracontinental deformation of the central North China Plate: Insights from syn-tectonic sedimentation, structural geology, and U-Pb geochronology of the Yungang Basin, North China. Tectonophysics, 778, 228371.

Zhao, G., Wilde, S.A., Cawood, P.A., & Sun, M. (2001). Archean blocks and their boundaries in the North China Craton: lithological, geochemical, structural and P–T, path constraints and tectonic evolution. Precambrian Research, 107 (1), 45–73. https://doi.org/10.1016/S0301-9268(00)00154-6

Zhang, S.H., Zhao, Y., Davis, G.A., Ye, H., & Wu, F. (2014). Temporal and spatial variations of Mesozoic magmatism and deformation in the North China Craton: implications for lithospheric thinning and decratonization. Earth-Science Reviews, 131 (4), 49–87. https://doi.org/10.1016/j.earscirev.2013.12.004

Zhang, S.H., Zhao, Y., Ye, H., Hou, K.J., & Li, C.F. (2012). Early Mesozoic alkaline complexes in the northern North China Craton: implications for cratonic lithospheric destruction. Lithos, 155, 1–18. https://doi.org/10.1016/j.lithos.2012.08.009

Zhang, S. H., Zhao, Y., Song, B., Hu, J. M., Liu, S. W., Yang, Y. H., & Chen, F. K., et al. (2009). Contrasting Late Carboniferous and Late Permian-Middle Triassic intrusive suites from the northern margin of the North China Craton: geochronology, petrogenesis, and tectonic implications. Geological Society of America Bulletin, 121, 181–200. https://doi.org/10.1130/B26157.1

Zhang, S. H., Zhao, Y., Song, B., Yang, Z., Hu, J. M., & Wu, H. (2007). Carboniferous granitic plutons from the northern margin of the North China block: implications for a late Paleozoic active continental margin. Journal of the Geological Society. 164(2), 451-463.

Zhao, G., Wilde, S. A., Cawood, P. A., & Sun, M. (2001). Archean blocks and their boundaries in the North China Craton: lithological, geochemical, structural and P-T, path constraints and tectonic evolution. Precambrian Research, 107(1), 45–73. https://doi.org/10.1016/S0301-9268(00)00154-6

Zhao, P., Chen, Y., Xu, B., Faure, M., Shi, G., & Choulet, F. (2013). Did the Paleo-Asian Ocean between North China Block and Mongolia Block exist during the late Paleozoic? first paleomagnetic evidence from central-eastern Inner Mongolia, China. Journal of Geophysical Research: Solid Earth, 118(5), 1873–1894. https://doi.org/10.1002/jgrb.50198

Zhao, P., Faure, M., Chen, Y., Shi, G., & Xu, B. (2015). A new Triassic shortening-extrusion tectonic model for Central-Eastern Asia: Structural, geochronological and paleomagnetic investigations in the Xilamulun Fault (North China). Earth and Planetary Science Letters, 426, 46-57. https://doi.org/10.1016/j.epsl.2015.06.011

Zhao, W. C. The Mesozoic tectonic deformation sequence around Yaowangmiao area of Jianchang county, Southwest Liaoning Province. M. S. Thesis, China University of Geosciences (Beijing), 2016, pp. 1-53.

Zhao, Y., (1990). The Mesozoic orogenesis and tectonic evolution of the Yanshan area (in Chinese). Geology Review. 36 (1), 1–13.

Zhao, Y., (2006). Mesozoic Thrust tectonics around Cenozoic Yanqing-Huailai Basin and their geological implications, Northwest of Beijing Municipality (in Chinese). Master of Dissertation of China University of Geosciences (Beijing), 1-79.

Zhou, J.B., Wilde, S.A., Zhao, G.C., Han, J., 2018. Nature and assembly of microcontinental blocks within the Paleo-Asian Ocean. Earth-Science Reviews, 186, 76–93. https://doi.org/10.1016/j.earscirev.2017.01.012

Zhou, X. M., & Li, W. X. (2000). Origin of Late Mesozoic igneous rocks in Southeastern China: implications for lithosphere subduction and underplating of mafic magmas. Tectonophysics, 326(3-4), 269-287.

Zhu, G., Jiang, D., Zhang, B., & Chen, Y. (2011). Destruction of the eastern North China Craton in a backarc setting: evidence from crustal deformation kinematics. Gondwana Research, 22(1), 86-103. https://doi.org/10.1016/j.gr.2011.08.005

Zhu, R. X., Yang, J. H., & Wu, F. Y. (2012). Timing of destruction of the North China craton. Lithos, 149(4), 51–60. https://doi.org/10.1016/j.lithos.2012.05.013

Zorin, Y. A. (1999). Geodynamics of the western part of the Mongolia–Okhotsk collisional belt, Trans-Baikal region (Russia) and Mongolia. Tectonophysics, 306(1), 33-56.

Zonenshain, L. P., Kuzmin, M. I., Natapov, L. M., & Page, B. M. (1990). Geology of the USSR: A Plate-Tectonic Synthesis, Am. Geophys. Union Geodyn. 21, 242.

Publications

1. **Qiu, H.**, Lin, W., Faure, M. Chen, Y., Meng, L., & Ren, Z., et al. (2020). Late Triassic extensional tectonics in the northern North China Craton, insights from a multidisciplinary study of the Wangtufang pluton. Journal of Asian Earth Sciences, 104462. https://doi.org/10.1016/j.jseaes.2020.104462.
2. **Qiu, H.**, Deng, S., Cao, Z., Yin, T., & Zhang, Z. (2019). The evolution of the complex anticlinal belt with crosscutting strike-slip faults in the central Tarim Basin, NW China. Tectonics, 38, 2087-2113. https://doi.org/10.1029/2018TC005229.
3. **Qiu, H.**, Lin, W., Chen, Y., Faure, M., Meng, L., & Ren, Z., et al. Emplacement mechanism of the Late Triassic granitic Dushan pluton (North China), insights from structural geology, geochronology, AMS and gravity modeling. Journal of Geophysical Research: Solid Earth (Under review).
4. **Qiu, H.**, Lin, W., Chen, Y., & Faure, M., et al. Jurassic two-stage extension in North China and implications for Jurassic-Early Cretaceous intracontinental orogeny in East Asia: insights from a multidisciplinary study of the Jianchang-Jiumen pluton (Submitting).
5. **Qiu, H.**, Lin, W., Deng, S., Lin, H., Zhang, Z., Cao, Z., & Huang, C., et al. The evolution of the early Paleozoic carbonate platform in the Central Uplift and adjacent areas, Tarim Basin, NW China, and hydrocarbon accumulation. AAPG bulletin (Under review).

Huabiao QIU

Tectonique extensive du Mésozoïque inférieur dans le nord du Craton de Chine du Nord et ses implications géodynamiques

Le craton de Chine du Nord est resté stable du Mésoprotérozoïque au Paléozoïque, après sa formation au Paléoprotérozoïque. Le craton stable de Chine du Nord a commencé à se transformer au Mésozoïque, et la destruction du craton ou l'amincissement lithosphérique ont eu lieu au cours du Crétacé inférieur. Avant la destruction du Crétacé, le craton de Chine du Nord a subi deux cycles orogéniques, y compris les collisions continentales d'âge Paléozoïque avec les arcs magmatiques mongols et le bloc de Chine du Sud, et l'orogenèse intracontinentale d'âge Jurassique-Crétacé précoce (également appelée orogenèse Yanshanienne). Certains indices d'épisodes d'extension au début du Mésozoïque ont été identifiés dans les petites reliques des bassins sédimentaires ou des failles normales. En tant que telle, la tectonique extensive pendant la déformation polyphasée et le mécanisme géodynamique associé restent mal contraint en raison de rares enregistrements géologiques. Pour mieux comprendre le contexte tectonique et le mécanisme géodynamique du Mésozoïque dans le bloc de Chine du Nord, une étude pluridisciplinaire, comprenant la géologie structurale, la géochronologie, la géochimie, l'AMS et la modélisation gravimétrique, a été menée dans les plutons de Dushan du Trias supérieur dans l'est de Hebei, de Wangtufang du Trias supérieur au nord de Hebei et de Jianchang-Jiumen du Jurassique à l'ouest du Liaoning.

Notre étude montre que: (i) les structures mésoscopiques et magnétiques du pluton de Dushan étaient plutôt liées à sa construction et non à la tectonique régionale du Trias supérieur; (ii) Le pluton de Wangtufang était mis en place au cours d'une extension intracontinentale orientée NE-SW au Trias supérieur; (iii) Le pluton jurassique de Jianchang-Jiumen a enregistré une extension au Jurassique inférieur orientée NW-SE et une extension d'âge Jurassique supérieur orientée NE-SW dans l'est du bloc de Chine du Nord; (iv) Trois stades d'extension contraignent davantage le cadre tectonique régional du craton de Chine du Nord et le mécanisme géodynamique associé au cours du Mésozoïque inférieur. Le Trias tardif était une période d'extension intracontinentale après la formation finale de la Ceinture de l'Asie Centrale Orogénique (CAOB) ou la compression intracontinentale ultérieure. L'extension avait lieu en deux étapes au cours du Jurassique inférieur-Jurassique moyen et du Jurassique supérieur, et la compression et l'extension NW-SE au Jurassique tardif-–Crétacé inférieur étaient probablement liées à la subduction de la plaque Paléo-Pacifique. L'extension a été interrompue par la compression N-S à la fin du Jurassique moyen probablement due à la fermeture de l'océan Mongol-Okhotsk.

Mots clés: Craton de Chine du Nord, Pluton granitique, Mésozoïque inférieur, Tectonique extensive, Mécanisme géodynamique

Early Mesozoic extensional tectonics in the northern North China Craton and its geodynamic implications

The North China Craton formed a stable craton from Mesoproterozoic to Paleozoic, after its assembly during the Paleoproterozoic. The stable North China Craton began to transform in the Mesozoic, and decratonization, cratonic destruction, or lithospheric thinning occurred during the Early Cretaceous. Before the Cretaceous destruction, the North China Craton has undergone two orogenic cycles, including Paleozoic-Triassic continental collisions with Mongolian arc terranes and South China Block at block boundaries, and the Jurassic-Early Cretaceous intracontinental orogeny (also called Yanshanian Orogeny). Some clues of extensional episodes during the Early Mesozoic have been found in sporadic small grabens or normal faults. As such, the extensional tectonics during the multiphase deformation and associated geodynamic mechanism remains poorly constrained due to rare geological records. To better understand the Mesozoic tectonic setting and dynamic mechanism in the North China Craton, an integrated multidisciplinary investigation, including structural geology, geochronology, geochemistry, AMS, and gravity modeling, has been conducted in the Late Triassic Dushan pluton in Eastern Hebei, Late Triassic Wangtufang pluton in northern Hebei and Jurassic Jianchang-Jiumen pluton in western Liaoning.

Our study shows that: (i) Both mesoscopic and magnetic fabrics in the Late Triassic Dushan pluton were rather related to its building than to the Late Triassic regional tectonics; (ii) The Wangtufang pluton emplaced during a Late Triassic NE-SW trending intracontinental extensional setting; (iii) The Jurassic Jianchang-Jiumen pluton recorded Early Jurassic NW-SE extension and early Late Jurassic NE-SW extension in the eastern NCB; (iv) Three extensional stages further constrain the regional tectonic framework of the NCB and associated geodynamic mechanism during the Early Mesozoic. The Late Triassic was an intracontinental extensional setting after the final formation of the Central Asian Orogenic Belt (CAOB) or subsequent intracontinental compression. Two-stage extension during the Early Jurassic-early Middle Jurassic and early Late Jurassic, and the late Late Jurassic-Early Cretaceous NW-SE compression and extension were probably related to the subduction of the Paleo-Pacific Plate. It was interrupted by the late Middle Jurassic N-S compression probably related to the closure of Mongol–Okhotsk Ocean.

Keywords: North China Block, Granitic pluton, Early Mesozoic, Extensional tectonics, Dynamic mechanism

Institut des Sciences de la Terre d'Orléans

1A, rue de la Férollerie – 45071 Orléans Cedex 2, France

Institute of Geology and Geophysics, Chinese Academy of Sciences

No. 19, Beitucheng Western Road, Chaoyang District, 100029, Beijing, P.R.China